DANISH
TECHNOLOGICAL
INSTITUTE

# EUDP17-11: Future Ammonia Refrigeration Systems Evaporators (FARSEvap)

## - Final report

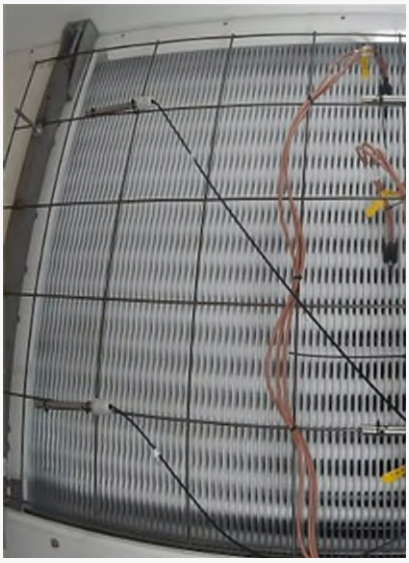

**Title:**
Future Ammonia Refrigeration Systems Evaporators (FARSEvap).

**Prepared for:**
EUDP, project no. 64017-05128.

**Prepared by:**
Danish Technological Institute
Gregersensvej 2, DK-2630 Taastrup
Refrigeration and Heat Pump Technology

Technical University of Denmark
Niels Koppels Allé, Bygning 403, DK-2800 Kongens Lyngby
Department of Mechanical Engineering

**Project consortium:**
Danfoss A/S
Aluventa A/S
Scanico A/S
Claus Sørensen A/S
Innoterm A/S
Technical University of Denmark
Danish Technological Institute (project leader)

November 2021

**Authors:**
Danish Technological Institute:
Jóhannes Kristófersson
Lars Overvad Rasmussen
Kenneth Rugholm Kramer

Technical University of Denmark:
Martin Ryhl Kærn

---

# Table of Contents

# 1. Preface

This is the final report of the study: "Future Ammonia Refrigeration Systems Evaporators (FARSEvap)". The objective of the project is to develop new system solutions that reduce energy consumption in industrial refrigeration and freezing equipment significantly. The systems can be used on both existing and new industrial evaporators for ammonia, which through active control will minimize or eliminate the considerable extra energy losses that exist in the system designs used today (so-called pump circulated systems). This has been done by investigating three concepts:

1. Controlled Circulation Ratio (CCR)
2. Wet Direct Expansion (WDX)
3. Micro channel evaporators.

The CCR is aimed at existing industrial ammonia systems which ensures the largest immediate impact of the three developed solutions. The WDX is aimed at new systems and extensions to older systems and will further increase the efficiency, reduce system cost, and the charge. In the last concept, the Micro channel, it is intended to do a proof of concept of a new evaporator design based on micro channel. This will increase the efficiency and drive the charge further down.

Furthermore, the results of the CCR in the laboratory is demonstrated in a full-scale heat pump system where two evaporators are equipped with a data acquisition system to compare the state-of-the-art to the new technology developed in the project to verify the high efficiency of the evaporator and the lower refrigerant charge.

This research project is financially supported by the Danish Energy Agency's EUDP programme (Energy Technology Development and Demonstration). Project number: 64017-05128.

The project is carried out in cooperation with Technical University of Denmark and the following industrial cooperating partners: Danfoss, Aluventa, Scanico, Claus Sørensen and Innoterm A/S.

The following persons have participated in the project:

- Niels P. Vestergaard, Danfoss A/S
- Morten Juel Skovrup, Danfoss A/S
- Jesper Bech-Madsen, Aluventa A/S
- Søren K. Andersen, Scanico A/S
- Michael Glering, Claus Sørensen A/S
- Palle B. Lemminger, Innoterm A/S
- Martin Ryhl Kærn, Technical University of Denmark
- Johannes Kristofersson, Danish Technological Institute
- Alexander Rosenvinge Lindholm Bork, Danish Technological Institute
- Lars Overvad Rasmussen, Danish Technological Institute
- Kenneth Rugholm Kramer, Danish Technological Institute.

The project team would like to thank the EUPD programme (Danish Energy Agency) for supporting the project.

## 1.1. Project details

| | |
|---|---|
| **Project title** | Future Ammonia Refrigeration Systems Evaporators (FARSEvap) |
| **Project identification (program abbrev. and file)** | EUDP 2017, Project no.: 64017-05128 |
| **Name of the programme which has funded the project** | Energiteknologisk Udviklings- og Demonstrationsprogram (EUDP) |
| **Project managing company/institution (name and address)** | Danish Technological Institute, Gregersensvej 1, DK-2630 Taastrup |
| **Project partners** | Danfoss A/S<br>Aluventa A/S<br>Scanico A/S<br>Claus Sørensen A/S<br>Innoterm A/S<br>Technical University of Denmark |
| **CVR** (central business register) | 56976116 |
| **Date for submission** | 30. November 2021 |

## 1.2. Summary

*English version*

The objective of the project is to develop new system solutions for evaporators in industrial ammonia systems that reduce energy consumption by reducing the liquid refrigerant flowing in the wet return suction pipes. The systems can be used on both existing and new industrial evaporators for ammonia, which through active control will minimize or eliminate the considerable extra energy losses that exist in the system designs used today (so-called pump circulated systems). This has been done by investigating three concepts:

1. Controlled Circulation Ratio (CCR)
2. Wet Direct Expansion (WDX)
3. Micro channel evaporators.

The CCR is aimed at existing industrial ammonia systems which ensures the largest immediate impact of the developed solutions. The WDX is aimed at new systems and extensions to older systems and will further increase the efficiency, reduce system cost,

and reduce the charge. The last concept, the Micro channel, is intended to do a proof of concept of a new evaporator design based on micro channel design. This will further increase the efficiency and drive the charge further down.

Furthermore, the results of the CCR in the laboratory is demonstrated in a full-scale heat pump system where two of the evaporators are equipped with a data acquisition system to compare the state-of-the-art to the new technology developed in the project to verify the high efficiency of the evaporator and the lower refrigerant charge.

For the CCR and WDX solution, design and measurements have led to a design of a new heated sensor from Danfoss capable of measuring the quality of the refrigerant leaving the coil. A new control strategy is also developed to use the signal from this sensor to control a pulse modulating valve.

A functional micro channel evaporator was designed, built and placed in the climate chamber. A proof-of-concept test of this evaporator has shown positive results. The water drainages during defrost was of great concern and was found not to be a problem. The available ice amount to accumulate on the evaporator was lower than for the traditional evaporators, but the defrosting time was shorter. To develop this concept into a market ready product, there is a need for further development and measurements to minimize the charge and find optimal fin spacing.

*Danish version*

Formålet med projektet er at udvikle nye systemløsninger til fordampere i industrielle ammoniaksystemer, der reducerer energiforbruget ved at reducere det flydende kølemiddel, der strømmer i de våde sugerør. Systemerne kan anvendes på både eksisterende og nye industrielle fordampere til ammoniak, som gennem aktiv styring vil minimere eller eliminere de betydelige ekstra energitab, der findes i de systemdesign, der anvendes i dag (såkaldte pumpecirkulationssystemer). Dette er sket ved at undersøge tre koncepter:

1. Controlled Circulation Ratio (CCR)
2. Wet Direct Expansion (WDX)
3. Mikrokanalfordampere.

CCR er rettet mod eksisterende industrielle ammoniaksystemer, som sikrer den største umiddelbare effekt af de udviklede løsninger. WDX er rettet mod nye systemer og udvidelser til ældre systemer og vil yderligere øge effektiviteten, reducere systemomkostningerne og reducere afgiften. Det sidste koncept, mikrokanalen, er beregnet til at lave et "proof of concept" af et nyt fordamperdesign baseret på mikrokanaldesign. Dette vil øge effektiviteten yderligere og drive fyldningerne længere ned.

Resultaterne af CCR i laboratoriet er demonstreret i et fuldskala varmepumpesystem, hvor to af fordamperne er udstyret med et dataopsamlingssystem for at sammenligne state-of-the-art med den nye teknologi udviklet i projektet for at verificere den høje effektivitet af fordamperen og den lavere kølemiddelfyldning.

For CCR- og WDX-løsningen har design og målinger ført til et design af en ny sensor fra Danfoss (heatet sensor), der er i stand til at måle kvaliteten af det kølemiddel, der forlader fordamperen. En ny styringsstrategi er udviklet til at bruge signalet fra denne sensor til at styre en pulsmodulerende indsprøjtningsventil.

En funktionel mikrokanalfordamper blev designet, bygget og placeret i klimakammeret. En proof-of-concept-test af denne fordamper har vist positive resultater. Vanddrænet fra fordamperen under afrimning var en bekymring før projektet men viste sig ikke at være et problem. Den tilgængelige ismængde, der kunne ophobes på fordamperen, var lavere end for de traditionelle fordampere, men afrimningstiden var kortere. For at udvikle dette koncept til et markedsklart produkt, er der behov for yderligere udvikling og målinger for at minimere fyldningen og finde frem til en optimal finneafstand.

## 1.3. Project objectives

The objectives for the project can be divided into three parts:

1. Solution for already existing industrial systems.
2. Solution for the future industrial systems based on fin and tube evaporators.
3. Solution for the future industrial systems based on finned-microchannel coils.

To realize first objective in the project a new method of controlling the already existing industrial evaporators was developed. This method has been called CCR which stands for Controlled Circulation Ratio. Here the circulation ratio through the evaporator is controlled by a control valve and a newly developed type of sensor called the Heated Sensor. A control strategy for the solution has also been developed in the project.

To address objective number 2 the same sensor technology i.e., the heated sensor from objective 1 was used to control a specially designed fin and tube evaporator. Here an evaporator was specially designed to be able to reduce the flooding of the evaporator without reducing efficiency to very close to a circulation ration of one.

For objective three a new prototype of so-called Microchannel evaporators was developed to increase efficiency, reduce the charge and footprint. This evaporator was tested in the project regarding icing up and defrost.

## 1.4. Project implementation

The project evolved according to the plan laid out to start with through with one year of delay. The project was delayed twice for a period of 6 months each time. First due to difficulties in developing the heated sensor. Through measurements and simulations, the task of being able to measure the state of the refrigerant leaving the evaporator was more challenging than anticipated at start. The second delay was due to the covid 19 pandemic which delayed the installation of a new climate chamber where the measurements on the microchannel evaporator should take place.

Originally the field test was planned at Claus Sørensen but it turned out to be too expensive and troublesome to install the test setup there to be able to get a reliable measurements. Instead, the developed technology was installed on a new large evaporator in a new heat pump installation that Innoterm installed at Brædstrup district heating. Here two

evaporators were equipped with measuring equipment. One as a comparison and the other with the technology developed in the project.

## 1.5. Project results, dissemination

The original objectives of the project were obtained. There were developed components and control strategies to control the circulation ratio for existing evaporators. The same sensor and control technology was also developed for the future WDX (wet direct expansion) systems. At last, a prototype of the microchannel evaporator was designed, built, and tested.

Apart from the attended usage the developed WDX evaporator was also tested for pumped circulation systems i.e., CCR. The evaporator showed great performance because of low maldistribution.

The commercial outcome of the project are sensor, valve, and control strategies that Danfoss is bringing to the market. When these products will be available the system builder can start to use them to build highly efficient and low charge industrial ammonia systems. Another unexpected but important user turned up during the project. This is in air to water heat pump applications where the charge is large because of the large air fin and tube evaporators. The large heat pumps quickly come above the 5000kg limit which is the system limit for more regulatory burden that results in more expensive systems. The system builders of these applications have shown interest in using the technology to reduce the charge and increase efficiency.

The target group for the project is the system builders of industrial ammonia systems. Their benefit is a more efficient systems with less charge.

The project results have been disseminated through conferences and papers plus articles in refrigeration magazines.

The conferences where the project has been and will be presented are:

1. 7th IIR conference: Ammonia and CO2 Refrigeration Technologies, Ohrid, 2017.
2. 8th IIR conference: Ammonia and CO2 Refrigeration Technologies, Ohrid, 2019.
3. 13th IIR Gustav Lorentzen Conference, Valencia, 2018.
4. 14th IIR Gustav Lorentzen Conference, Kyoto, 2020.
5. ECOS 2020: 33rd International Conference on Efficiency, Cost, Optimization, Simulation and Environmental Impact of Energy Systems.
6. 15th IIR Gustav Lorentzen Conference, Kyoto, 2022.

The papers written have been:

1. Ammonia charge reduction potential in recirculating systems – Calculations.
2. Ammonia charge reduction potential in recirculating systems – System benefits.
3. Charge reduction in pump circulating ammonia systems.
4. Defrost efficiency for ammonia air cooled evaporator systems.
5. Numerical analysis of flow maldistribution in large-scale liquid overfed finned-tube ammonia evaporators.

6. Multi-objective optimization of low charge liquid overfeed ammonia evaporators for industrial refrigeration.
7. Numerical Investigation of Air-Side Heat Transfer and Pressure Drop Characteristics of a New Triangular Finned Microchannel Evaporator with Water Drainage Slits.
8. Numerical investigation of fin geometry on the air-side heat transfer and pressure drop characteristics of heat exchangers using in-line rectangular microchannels.

The magazines where the project has been presented are:

1. Fluids 2019; 4; 205.
2. Kulde og Varmepumper.
3. Maskinmesteren.

## 1.6. Utilization of project results

The results obtained in the project have led to the development of a new sensor and controller that is now being developed into a market ready product by Danfoss. This product is essential to be able to harvest the benefits shown in the project and will lead the way into future industrial ammonia systems.

A new type of evaporator was designed in the project for a new efficient low charge industrial ammonia system. This evaporator design evens out the maldistribution on the refrigerant side which leads to systems able to control the circulation ratio to a lower value and thereby increasing efficiency and at the same time with lower charge.

These products will able the designers of industrial ammonia systems to maintain the efficiency of the systems and at the same time reduce charge. These products also give the system builder opportunity to reconstruct older systems to increase their efficiency.

Competitive solutions are described in section 3. All of those is intended for new installation and does not address the existing installed industrial system base. Many of them are also very specific to the companies providing them. The solution developed in the project will give the ordinary system builder components to put into their conventional design to accomplish higher efficiency and lower charge and thereby widening the uptake of these new system solution.

The proof of concept for the micro channel evaporator has been verified, and the next step is to design the concept for a lower refrigerant charge.

## 1.7. Project overall conclusion and perspective

The project has revealed many of the challenges concerning future ammonia systems and especially the low charge ammonia systems. The effort has been on reducing the liquid out of the evaporator to reduce the pressure drop in wet suction lines and thereby increase the suction temperature which at the same time increases the efficiency.

The project showed the importance of keeping the new system types clean and without air and water. This requires a new approach for the service technicians when evacuating the system after repair and at start up. This includes to evacuate the systems more thoroughly compared to traditional systems.

To be able to run the evaporators with very low circulation ratio, a new method of measuring and controlling the quality of the refrigerant out of the evaporator is needed. The product developed in the project to control the quality out of the evaporator consists of a new type of sensor and a new control strategy. Both of those products have been developed by Danfoss in the project.

A new concept for the industrial evaporators based on micro channel profiles has been investigated. A new evaporator was designed and built-in comparable size to the fin and tube evaporators tested in the project. The measurements revealed that the micro channel can be used as an industrial evaporator, and the defrost issue was not a problem. The measurements also revealed the issues to be addressed in further design of the concept.

# 2. Introduction

In the project, a solution to control the circulation number for evaporators in industrial ammonia systems is developed and tested. This is done to increase the efficiency of the system and to reduce the ammonia charge in the system. The increased efficiency is of vital importance in the transition to a carbon neutral future, and the lower charge is important to increase the safety of industrial ammonia systems.

## 2.1. State-of-the-art solutions for evaporator control

For traditional state-of-the-art industrial ammonia systems, the evaporator is controlled on and off for both cold and freezing stores. The temperature in the storage is measured in strategic locations, and when it has risen certain degrees above the setpoint, the liquid injection to the evaporator is opened and the fan is turned on full speed. The fan is normally kept on lower speed in off periods to ensure mixing in the storage. When the temperature in the storage has dropped certain degrees below the setpoint, the liquid injection valve is closed, and the fan is controlled down to lower speed. In this way, the capacity on the evaporator fluctuates during operation. When ice accumulates on the evaporator, the capacity drops, and the running time of the evaporator extends.

The traditional solution is to use manual liquid control valves that are adjusted at start up according to maximum load and a certain circulation ratio, often 3 to 5 for cold and freezing stores. The valves are left unattended unless there are problems. During operation, the capacity of the evaporator changes according to the load from the cold store and according to the ice formation on the evaporator as explained above. When the capacity drops from the maximum capacity, the circulation number increases. As the pressure drop in risers and wet return lines are dependent on the circulation number, the pressure drop increases with an increasing circulation number. The increasing pressure drop means lower saturated suction temperatures at the compressors to maintain the same suction temperature in the evaporator and thereby a lower efficiency. A typical rule of thumb is a 3 % better COP per °C higher saturated suction temperature.

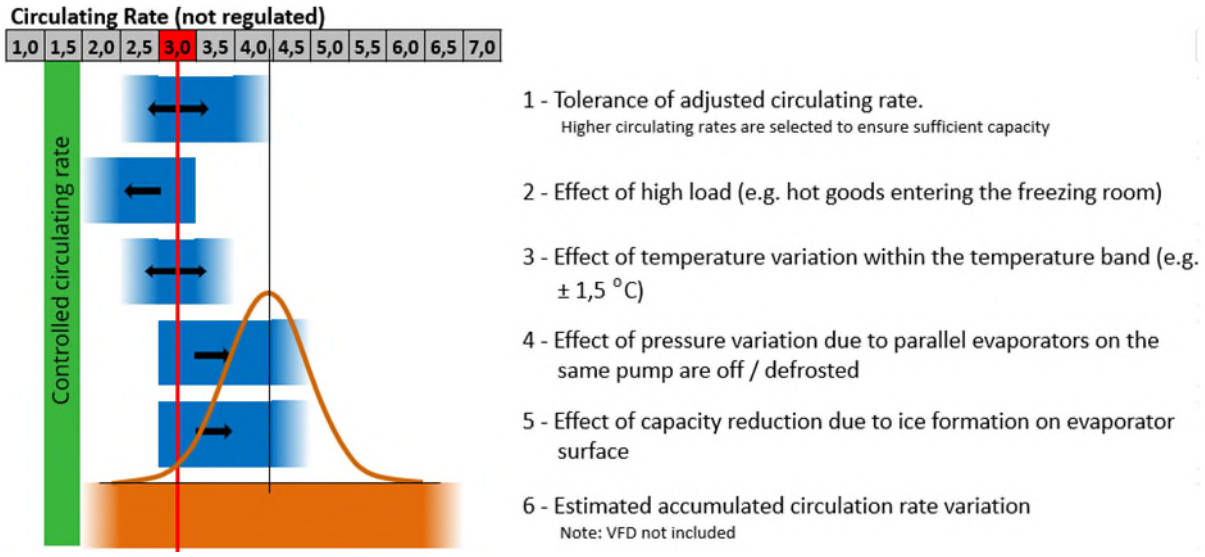


**Figure 1: Effect of changes in the system on circulation number.**

Figure 1 explains the influence of changes in the system on circulation number. In the figure, the design circulation number 3 has been selected to ensure flooded operation during operation. When the load increases on the cold storage above design load, the circulation ratio drops. And vice versa – when the load drops, the circulation ratio increases. The circulation ratio increases as some of the evaporators are turned off and the refrigeration pump is not VSD controlled leading to higher pressure in the liquid pipeline and thereby more flow through the evaporator. All in all, the average circulation ratio, when the design one is on 3, could thereby end up being around 4 under normal running conditions with increasing pressure drop in the wet suction line.

## 2.2. Project objectives

In this project, the aim is to develop a new solution for evaporators in industrial refrigeration systems using ammonia as a refrigerant. The main goal is to increase efficiency by eliminating or minimizing the liquid recirculated in the wet return lines from the evaporators by controlling the circulation number to a fixed number under all load conditions. Three concepts are lined up and investigated in the project. These are:

1. Controlled Circulation Ratio (CCR)
2. Wet Direct Expansion (WDX)
3. Micro channel evaporators.

In the first concept, the CCR (Controlled Circulation Ratio), the aim is to control the circulation ratio through the evaporator to the lowest sensible value without effecting the evaporator performance. This solution is intended to be applied to the already existing industrial systems in the field to be able to lower their charge and increase their efficiency. For systems that are close to the national charge limit, an extension to these systems could be done by using the technique developed in the project.

The second developed concept, the WDX, is intended to be used for new installations and extensions to existing systems. Here, the high-pressure liquid from the receiver is led directly to the evaporators which decreases the charge and the installation price and at the same time increases the efficiency of the total system. WDX is different from traditional DX since the allowed superheat is much lower, and since the small amount of liquid exiting the evaporators must be dealt with before entering the compressors. Normal DX for ammonia systems requires a superheat of 8 to 12K which reduces the efficiency of these systems considerable. The WDX lies on the limit of wet return from the evaporator and thereby increases the efficiency compared to the liquid overfeed systems used today.

In the third concept (Micro Channel evaporator), a proof of concept for a preliminary design of a full-size micro channel evaporator is done and an evaporator built. With this evaporator, the charge and footprint are further reduced, and at the same time the efficiency is increased compared to traditional design.

To be able to accomplish these objectives, a new type of controlling concept has been developed. This includes a new control strategy, and a new sensor type so called Heated Sensor. This has been tested and verified in the project.

Traditional state-of-the-art evaporators have been investigated as well as design and testing of advanced evaporator design.

The most promising candidates have been tested in a laboratory environment to verify the simulations.

The CCR concept was also verified in the project on a full-scale industrial heat pump evaporator.

## 2.3. The project framework

The project is divided into five work packages in addition to the one containing project management and administration. These include a knowledge gathering where the newest research in the field was assembled and reviewed, and the solutions found in the field were listed up.

This led to a work package containing research of new evaporator design where new control ideas and evaporator design were listed up, and the most promising ones were selected for further evaluation. As a result, the most promising ideas were laid out and developed into a solution to be verified in a climate chamber in the laboratory.

A verification of the selected solutions was conducted in the following work package. Here, a test setup was developed and build, and a series of test were conducted. These tests along with simulations assisted in the development of the components and control strategies to be finally tested and used.

Finally, a field test setup was developed on a large heat pump installation at Brædstrup District Heating to test the CCR solution. Here, two large, air-cooled evaporators were equipped with measuring equipment and a data acquisition system to be able to test the developed equipment. One of these evaporators were a reference and the other included the newly designed equipment. Here, a test was conducted, and the two evaporators were compared under normal running conditions.

Dissemination of the project results was conducted in a separate work package.

## 2.4. The project implementation

The original plan for the project was to start on 01-10-2017 and end on 30-09-2020. However, during the execution, some complications appeared caused by the Corona pandemic, and the project had to delay by one year to be able to finish the developed sensor and to test the micro channel evaporator. The project finished on 30-09-2021.

The project started after the start up meeting and after signing the cooperation agreement. It started with a search in the scientific community for the latest research in the field. The various papers and reports were read to draw up a picture of the current situation and the challenges to be solved. This was included in "WP01: Knowledge gathering".

Then a work on identifying the ideas to solve the challenges at hand was conducted in "WP02: Research of new evaporator systems". Here, various solutions were lined up and evaluated, and the most promising solution was selected for further investigation.

In "WP03: Verification of solution at DTI", the test setup for testing the selected solution was designed and built. Then a series of test was made to verify the designed solution, and through the testing, changes to the design were done to meet the challenges found.

When the final CCR solution was close to ready, a field test setup was designed and installed on a heat pump installation at Brædstrup District Heating company where two evaporators were dedicated for the testing. One of the evaporators was installed with the designed solution and the other was equipped as normal for the state-of-the-art industrial solution. There the running conditions for the newly designed system were compared to the state-of-the-art solution.

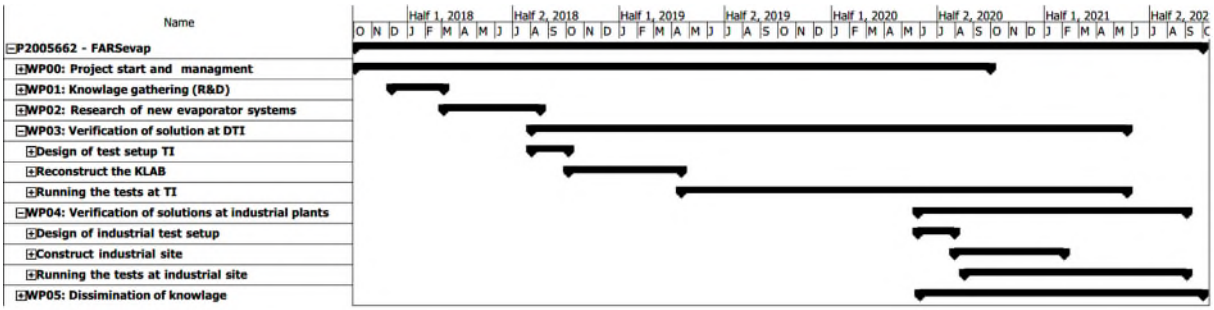


**Figure 2: Time schedule for the project.**

# 3. Knowledge gathering

## 3.1. Introduction

In this part, the new trend in ammonia refrigeration systems - the so called "low charge ammonia systems" - found on the market is described. First, a definition of low charge is established, and then the companies making these systems are listed up, and their solutions described. At last, some of the identified challenges in running with low circulation number (CCR) and wet direct expansion (WDX) are identified.

## 3.2. Low charge definition

The specific charge of an industrial ammonia system is a number that indicates the charge for each kW of cooling capacity, and it is calculated by taking the total charge and divide it with the cooling capacity.

$$Specific\ charge\ \left[\frac{kg}{kW}\right] = \frac{Charge\ [kg]}{Cooling\ capacity\ [kW]}$$

Traditional existing ammonia systems today are normally with specific charge of about 4 to 5 kg NH3/kW. For state-of-the-art properly designed systems, the charge can be brought down to maybe 3.5 kg NH3/kW. A low charge limit has not been defined in the industry, but a reasonable limit could be argued to be on 1.5 kg NH3/kW, i.e., systems with that charge or lower could be defined as low charge.

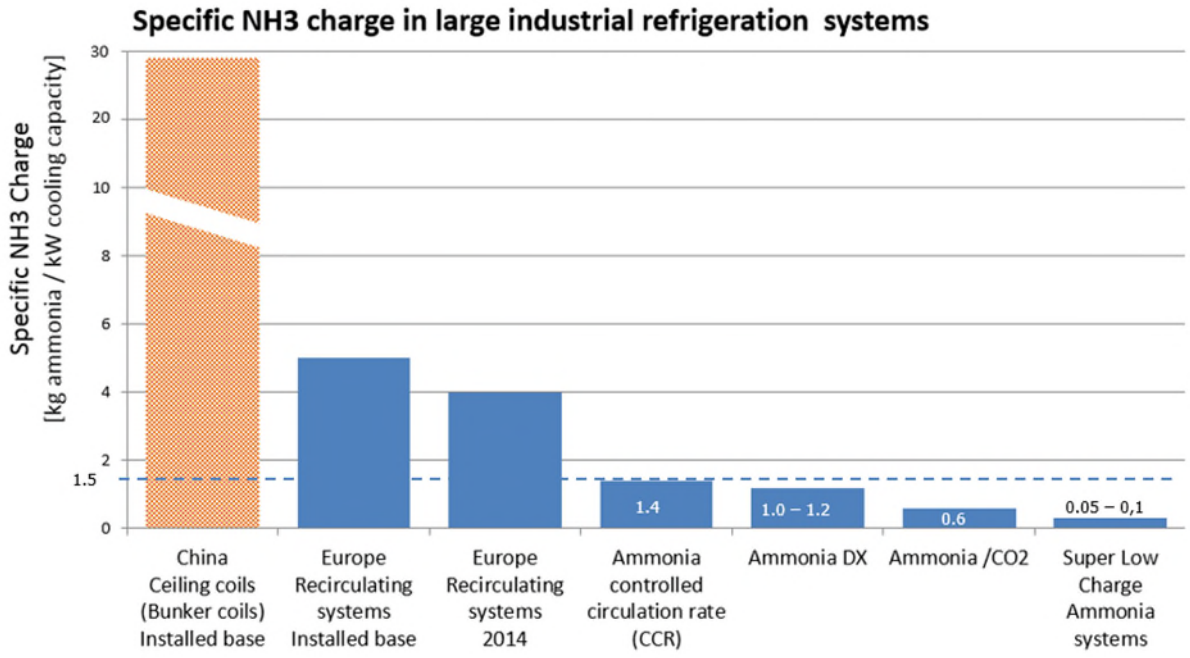


**Figure 3: The charge of ammoniac systems.**

The limit of 1.5 kg NH3/kW is the level that traditional systems modified with controlled circulation rate (CCR) can be expected to reach. For DX and WDX ammonia systems, the charge could lie around 1.0 to 1.2 kg NH3/kW. For cascade systems of ammonia and CO2, the charge can lie around 0.6 kg NH3/kW, and for super low charge, i.e., chiller solutions

with water or brine on both condenser and evaporator, the charge is in the range 0.05 to 1.0 kg NH3/kW.

## 3.3. Companies in low charge solutions

There are now increasing focus on the low charge ammonia systems. Only a few system providers are found which supply low charge solutions. The companies can be divided into three categories, i.e., centralised, localised, and cascade systems.

### 3.3.1. Centralized systems

The first category is central systems where the system has a centralized machine room with the refrigerating compressors and the refrigerant distributed from there to the evaporators.

#### 3.3.1.1. Scantec – Stefan Jensen

Scantec is an Australian company lead by a Dane, Stefan Jensen. He is one of the pioneers in low charge ammonia and has been active in the low charge business and promoted his solutions since 2005.

Scantec claims to be able to reach a charge of 1.2 to 2.2 kg NH3/kW.

Scantec has built several plants with ammonia using DX. Stefan Jensen started with using traditional DX without liquid distributor. He has later changed the design to use HB Products quality sensor and superheat control to control the expansion valve, and he uses a liquid distributor based on a patent from KUBA. The reason for both quality sensor and traditional superheat control is that after defrosting the quality sensor is submerged in liquid ammonia. While the liquid ammonia around the quality sensor is evaporated, the traditional controlled superheat is used. The quality sensor can be seen in Figure 4 to the left in the outlet of the suction header.

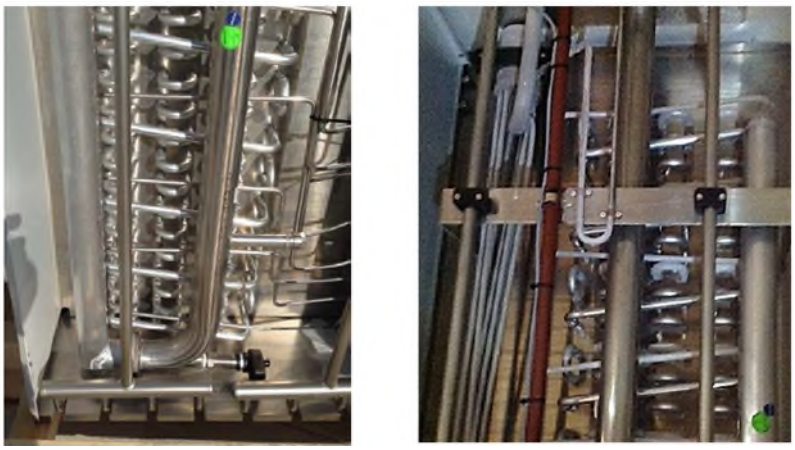

**Figure 4: The quality sensor in the suction pipe to the left and the liquid inlet distributor to the right.**

The liquid distributor is a tank distributor shown in Figure 5 on the left. It is based on an old patent from KUBA filed in 1993. The patent period is 20 years if the patent fee has been paid, which means that the patens should expire in 2023.

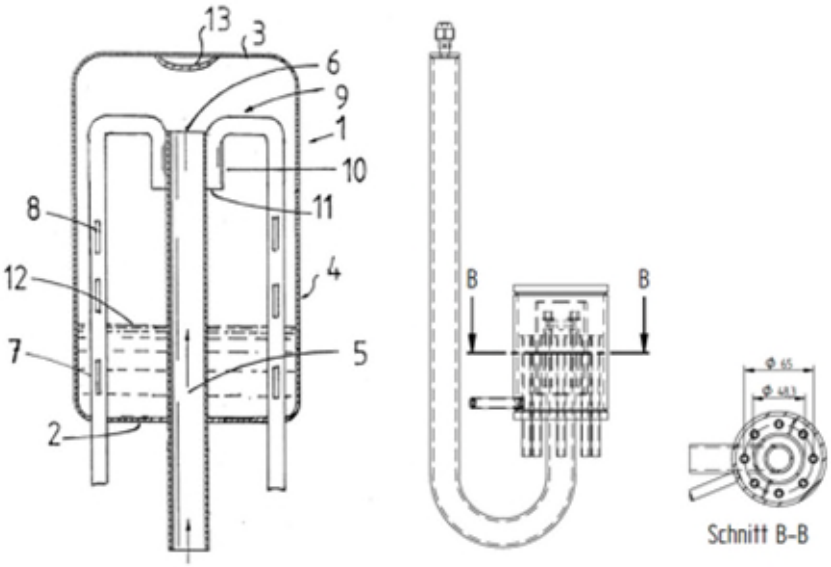


**Figure 5: Tank distributor - To the left KUBA patent, on the right from Scantec paper.**

The liquid/gas mixture flows into the tank distributor through the middle pipe and is distributed to each pass in the coil through smaller sized pipes. There is a liquid level in the vessel, and a mixture of liquid and gas is evenly distributed to each pass. The tank distributor act as an oil separator as well and the oil collected in the bottom of the tank is drained away through the oil drain.

The evaporators used by Scantec are side-bottom fed as shown in Figure 6 where the liquid refrigerant enters the coil from the side and flows countercurrent to the air flow and then up to the next pipe row where it flows co-current with the air flow. Through the last pipe row, the flow is countercurrent again and enter the suction header at last. The material in the evaporator pipes is aluminum.

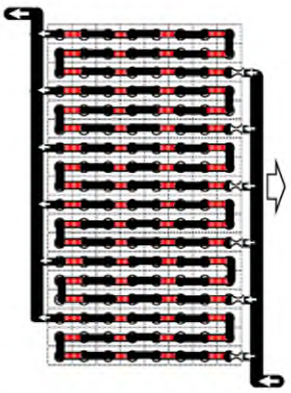

**Figure 6: Feeding of the evaporator.**

The piping around the evaporator can be seen from the PI diagram in Figure 7 which is taken from Scantec's recent defrost patent. It is a two stage system with two temperature levels.

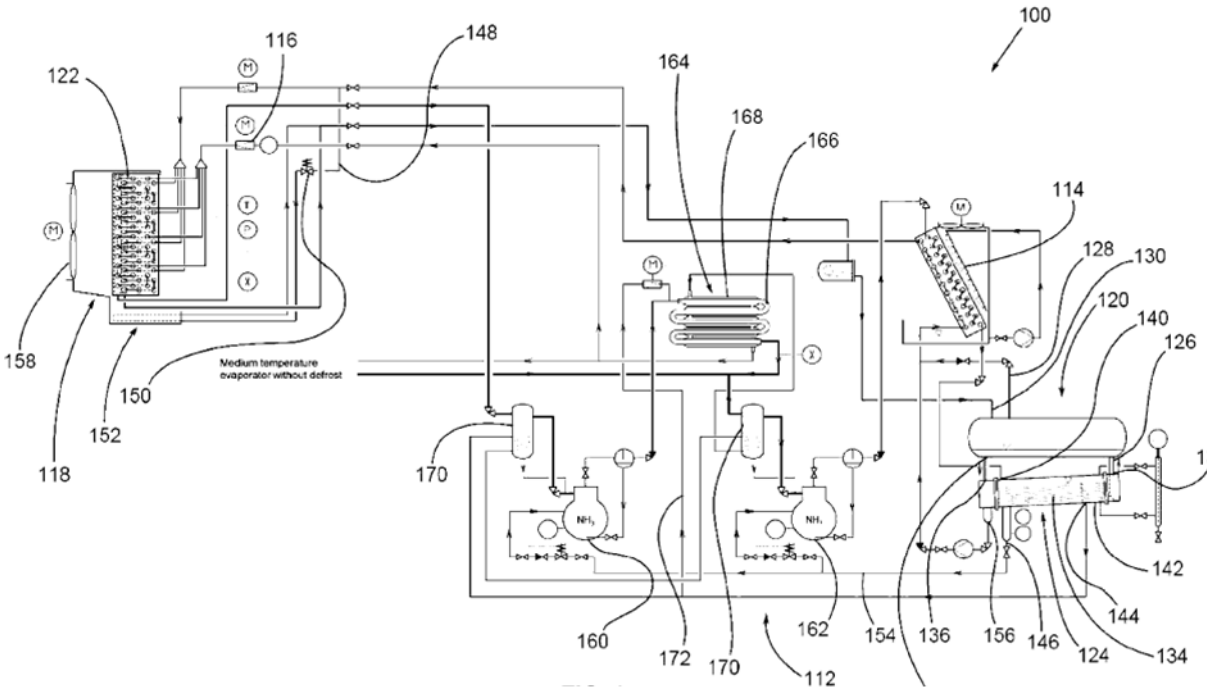


**Figure 7: PI diagram of the Scantec solution.**

Here, the liquid tank distributor is shown in-between the liquid valve (116) and the coil (122). Here, the defrost is shown taken to the coil through the distributor and returned to the liquid receiver through a drain line. There is a separate defrost to the drain pan.

The liquid refrigerant to the evaporators is first directed to the coil in the suction accumulator (170) for the low stage, where it boils off any liquid refrigerant coming from the low stage evaporators. Thereafter, it goes to the coil in the suction accumulator for the medium stage. From there it goes to an internal heat exchanger to be cooled down to the intermedium temperature before reaching the coils. The discharge gas from the low stage is cooled down to the intermedium temperature before reaching the heat exchanger. The liquid from defrost is directed to the receiver through a float valve.

### 3.3.1.2. Colmac Coil – Bruce Nelson

Another pioneer in low charge ammonia refrigeration is Bruce Nelson, CEO of Colmac Coil. Their methods are quite similar to Scantec's. Colmac Coil is a producer of evaporators, and they produce their own coils with aluminium pipes with enhanced internal surface. Colmac Coil has published a handbook on DX ammonia to address the challenges and benefits of using a low charge DX ammonia solution.

Colmac Coil claims to be able to reach a charge of 0.9 kg NH3/kW.

Colmac Coil uses DX on the evaporator and controls the expansion valve by using a suction superheat signal in the outlet of the evaporator or by using a quality sensor. They state that for higher suction temperatures, one can use normal distributors, but for low temperature applications, the need for tank distributors arises.


**Figure 8: To the left a tank distributor and to the right a traditional distributor.**

The tank distributor which Colmac Coil uses is similar to the KUBA principle. The tank distributor is shown in Figure 9. The liquid/gas mixture from the expansion valve comes into the distributor at 304 and is divided into gas and liquid in the first tee-junction. The liquid is sampled in the bottom where oil is separated. The liquid flows further into vessel 11 where the liquid flows are distributed evenly into the pipes 82&85 connected to each evaporator pass, through small holes in the side of each pipe. The flash gas flows into the pipes at the top and is distributed evenly to each pass.

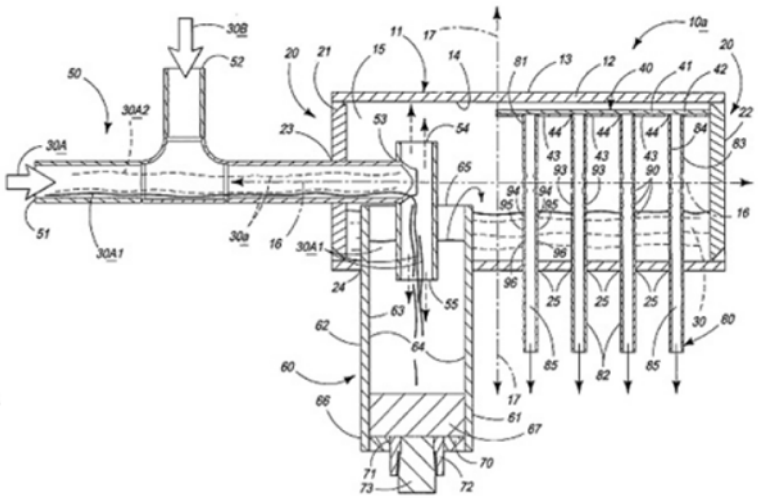

**Figure 9: Colmac Coil tank distributor.**

The PI diagram of the system can be seen in Figure 10 where a solution for a two-stage system with two temperature levels is shown.

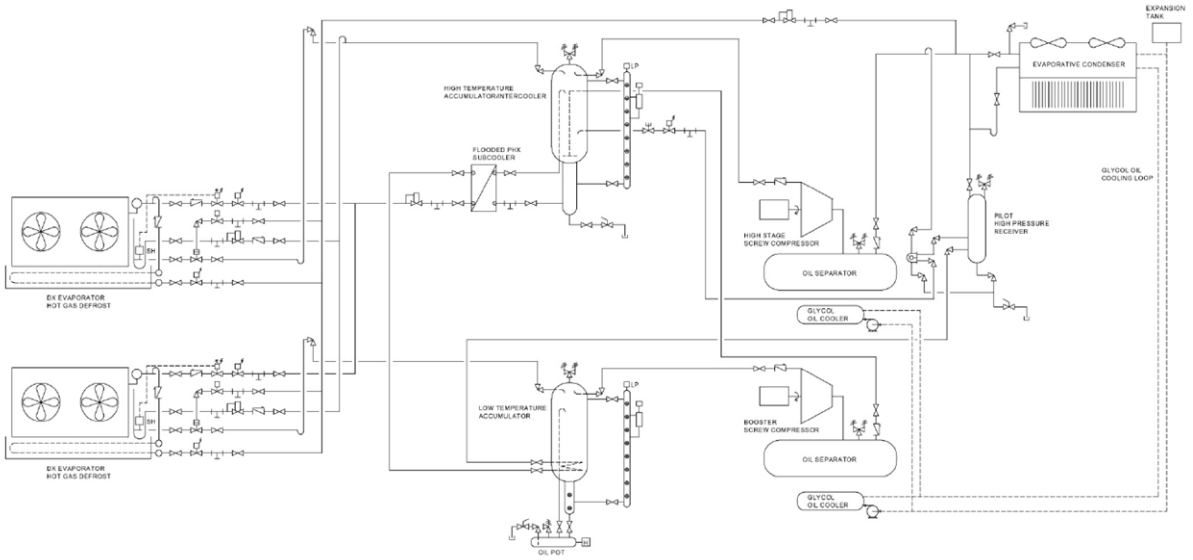


**Figure 10: PI diagram of the recommended system from Colmac Coil.**

In the PI diagram, the condenser is an evaporative condenser which is normal for larger industrial systems. The liquid from the condenser flows to a pilot receiver. From there, it flows to the low-pressure accumulator where it is used to evaporate liquid coming from the low stage system. From there, the liquid flows to a subcooler before entering the expansion valves. This is done to subcool liquid refrigerant going to the expansions valves which eliminates flash gas in the pipe due to pressure drop and reduces the flash gas in the liquid distributor after the expansion valve. The liquid charge that cannot be in the pilot receiver is directed to the intermediate accumulator that works as a receiver for the system. The subcooling is done with liquid from the intermedium stage through a plate heat exchanger. The liquid from hot gas defrosting is taken up by the suction accumulators.

### 3.3.1.3. Frick

Frick uses another strategy which they call Low Charge Central Systems (LCCS). They claim to have a patent pending. Their approach is to build remote distributed condensing units placed closed to each evaporator. The refrigerant compressors are placed in a centrally located machine room. The refrigerant pipelines to and from the machine room are dry i.e., suction and discharge pipes. The system is shown in Figure 11.

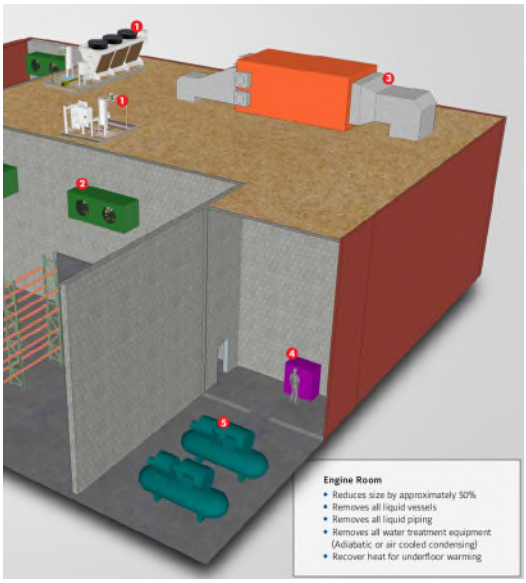


**Figure 11: Johnson LCCS system.**

The machine room containing the refrigeration compressors is shown as 4&5. The remote distributed condensing units (RDC) are shown as 1 and the DX evaporators as 2.

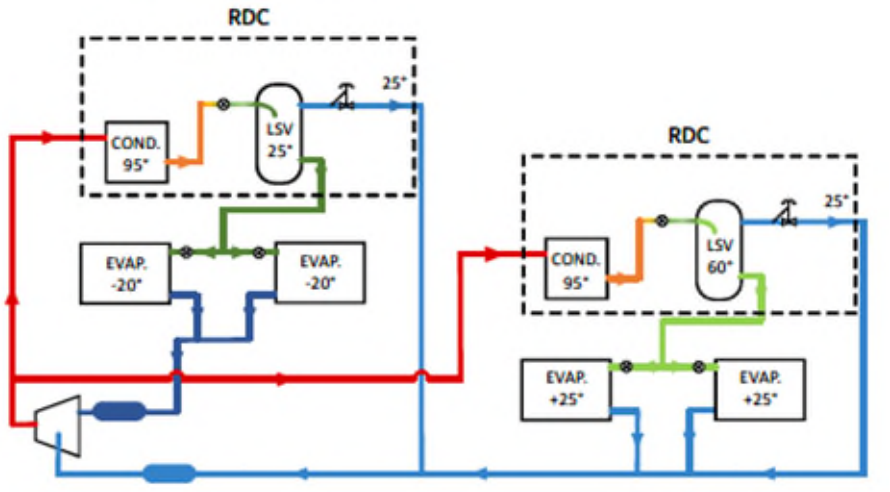


**Figure 12: PI diagram from Johnson LCCS**

As can be seen from the PI diagram in Figure 12, their liquid charge is distributed to the RDC units. The RDC units have their own condenser and receiver and serve the nearby placed evaporators. The evaporators use DX technology and return the gas through a suction gas accumulator on their way to the compressors.

Johnson claims a specific charge of the systems of 0.2 to 0.4 kg NH3/kW.

### 3.3.1.4. Star – LPR (Low Pressure Receiver)

The solution from Star which they patented many years ago uses a low-pressure receiver where the liquid charge of the system is stored. A PI diagram of the system is shown in Figure 13.

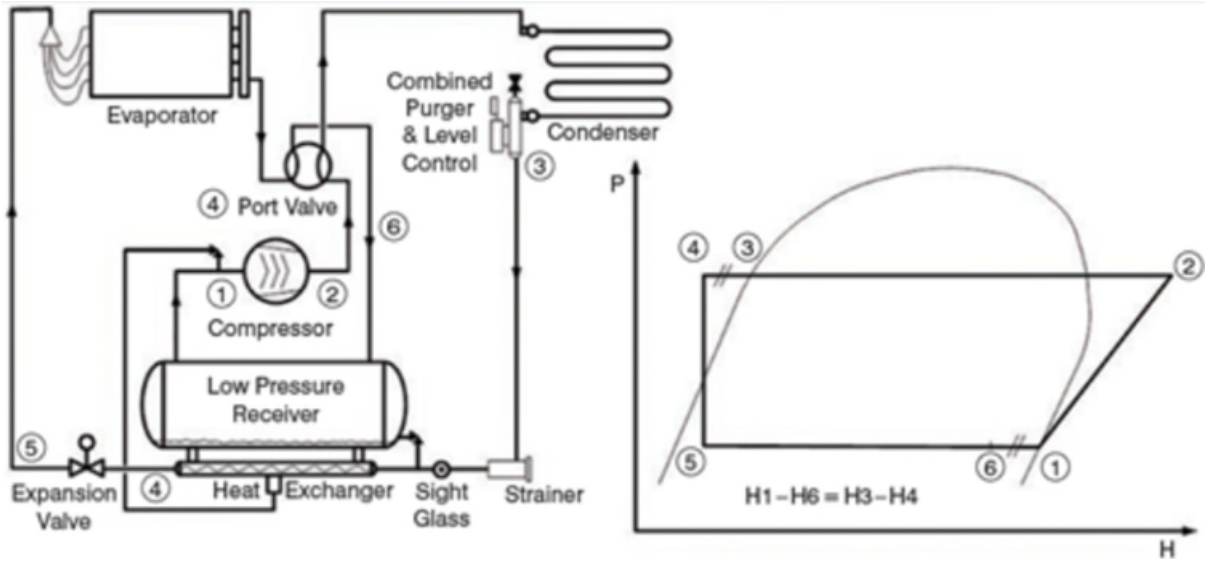


**Figure 13: Star Refrigeration LPR solution.**

The liquid refrigerant leaves the condenser through a combined purger & level controller on its way to the evaporators. The excess liquid in the system is stored in the low-pressure receiver (LPR). The liquid in the LPR cools the high pressure (HP) liquid on its way to the expansion valves in front of the heat exchangers. The liquid leaving the evaporators which is wet, returns to the LPR where the liquid is separated, and the gas leaves the vessel to enter the compressors. The excess liquid from the evaporators is evaporated in the heat exchanger by subcooling the HP liquid flowing to the expansion valves. In the system, there is a four-way valve which is used to divert the flow when defrosting the evaporator. Then the gas from the compressor is diverted to the evaporator, and the condensed liquid is evaporated in the condenser.

### 3.3.1.5. Frigoscandia

Frigoscandia has a patent on a method to separate the liquid coming from the evaporator from the gas before entering the suction gas pipes. This patent was filed in 1997. The concept is explained in Figure 14.

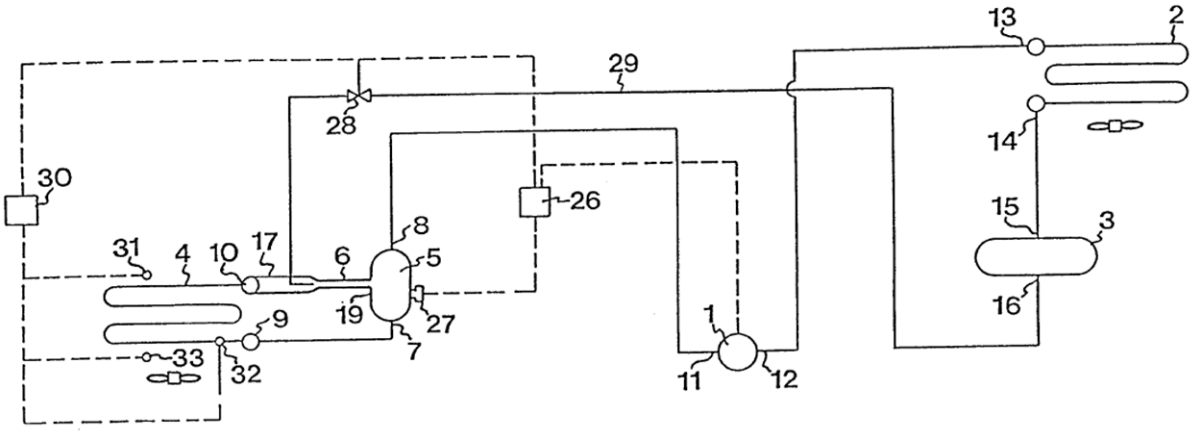


**Figure 14: Frigoscandia method of separating liquid and gas.**

The discharge gas leaving the compressor (1) enters the condenser (2) on its way to the receiver (3). From the receiver (3), the high-pressure liquid flows to the expansion valve (28). From the expansion valve (28), the mixture of gas and liquid flows to the evaporator outlet. The injected gas/liquid mixture from the expansion valve draws a gas/liquid mixture from the evaporator and delivers it along with the incoming gas/liquid mixture to the separator. A controller (26) in the liquid separator controls the expansion valve.

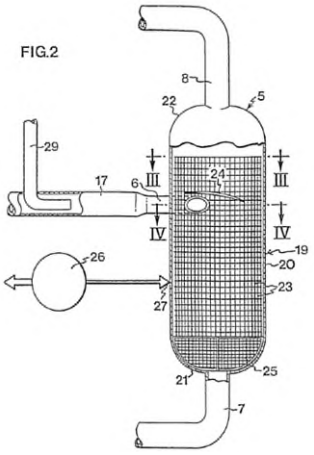


**Figure 15: Separation unit**

The inlet of the separator (6) in Figure 15 is tangential, and together with the demister (23) in the separator it separates the liquid from the gas. The gas flows through the exit pipe (8) to the compressor, and the separated liquid flows to the evaporator by gravity through the pipe (7).

### 3.3.2. Local systems

The next category are the local systems where the machine room is built together with the condenser and evaporator locally where the refrigeration is needed. This contributes to many locally placed units to supply the refrigeration capacity needed. By doing this, the liquid lines to the evaporators and the wet suction lines back to the machine room are eliminated. The total charge in the system is also divided into many distributed smaller charges.

#### 3.3.2.1. Evapco - Evapcold

Evapco has with their Evapcold solution addressed the challenge by building units of various sizes for high, medium, and low temperature applications. The user byes the number of units needed and places them on top of the cold storage. In Figure 16, the solution is shown where four units are placed on top of the cold store.


**Figure 16: Evapcold air cooled unit placed on top of the building to the left, and unit lowered in place to the right.**

Each unit consists of a machine room section and two evaporator sections. The division in two evaporation sections is due to defrost requirements.

**Figure 17: Unit from Evapcold on the left, and machine room on the right.**

The evaporators use DX technology to reduce the charge.

The claimed specific charge for these units is 0.4 to 0.8 kg NH3/kW.

### 3.3.2.2. NXTCOLD

Another local system solution is the one from NXTCOLD. It is like the Evapcold solution from Evapco. As can be seen from Figure 18, the unit is divided into an evaporator section and a machine room section.


**Figure 18: A drawing of the NXTCOLD unit to the left, and a picture of the unit on the right.**

The evaporators are controlled by direct expansion using two quality sensors. The one in the middle of the evaporator and the other in the outlet. According to NXTCOLD this is done to be able to control the superheat to a low value. NXTCOLD calls this new control strategy for ERIC, and it is shown in Figure 19.

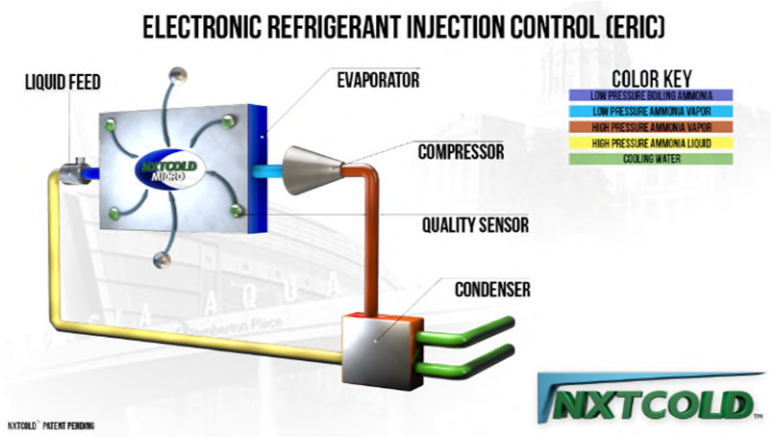


**Figure 19: NXTCOLD electronic refrigerant injection control (ERIC) system.**

NXTCOLD claims specific charge for these units to be 0.06 kg NH3/kW.

### 3.3.3. Cascade systems

The third category is the cascade system where the ammonia is on the high stage, and another refrigerant is on the low stage with a cascade heat exchanger in between. Normally, the high stage refrigerant is ammonia, and the low stage refrigerant is CO2. The high stage and the cascade heat exchanger plus the compressors for the CO2 are placed in a machinery room built onto a frame with CO2 piping distributing the refrigeration to the evaporators.

#### 3.3.3.1. Mayekava - NewTon

One of the solution providers in cascade NH3/CO2 systems is Mayekava with their NewTon units. This units have water cooled condensers which reduce the charge but also

the efficiency. The concept can be seen in Figure 20. The CO2 is on the cold side where CO2 refrigerant is distributed to the users.

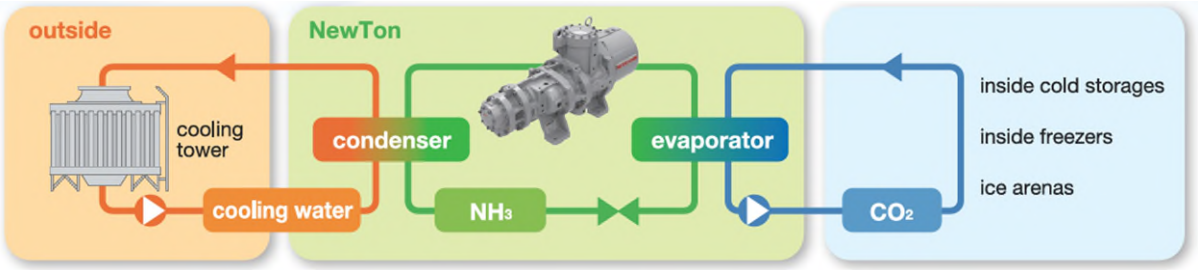


**Figure 20: Princip diagram of cascade system from Mayekava.**

The system from Mayekava is the so-called volatile CO2 system where no CO2 compressors are used. In this way, the CO2 is used as an evaporating brine. The CO2 is pumped to the evaporators (see Figure 19) where it partly evaporates and returns to the CO2 separator as liquid and gas. There the gas is separated from the liquid and flows to the cascade cooler to be condensed to liquid again. On the other side of the cascade cooler, there is a two-stage ammonia system used to cool down the CO2 gas.

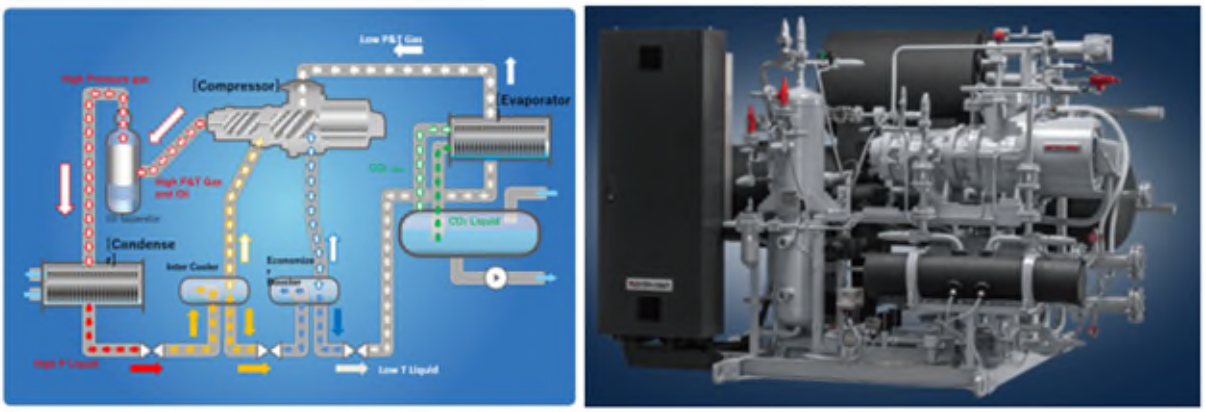


**Figure 21: Diagram and picture of the Mayekava NewTon concept.**

Mayekava claims the specific charge of their systems to be 0.2 kg NH3/kW.

### 3.3.3.2. M&M Refrigeration

M&M Refrigeration in the USA has since 2004 built custom made and in-place-built cascade systems using NH3 and CO2. They also build the smaller unit on a frame that is shipped to the customers.

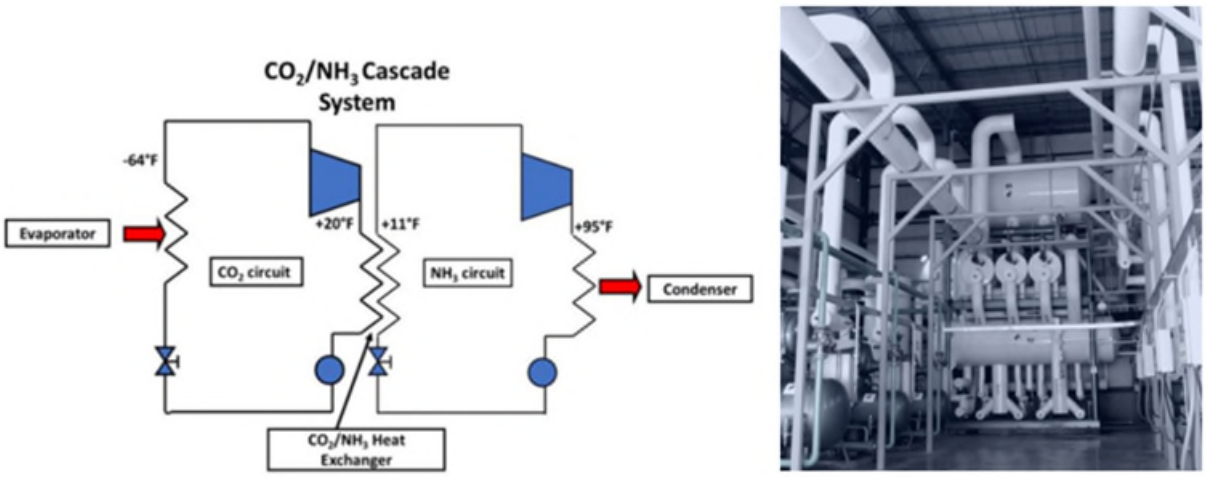


**Figure 22: The M&M refrigeration concept to the left, and a picture of the system to the right.**

M&M Refrigeration, unlike Mayekava, uses a two-stage cascade system (see Figure 22) with CO2 compressors on the low stage. This gives a better efficiency for the total system compared to the volatile system from Mayekava.

### 3.3.3.3. Johnson Controls

Johnson Controls also sells a NH3/CO2 cascade solution built on a frame – the so-called CAFP unit. They use the same concept as M&M Refrigeration using a two-stage system with CO2 compressors on the low stage.

**Figure 23: The Johnson Controls CAFP unit.**

Figure 23 is a picture of their CAFP unit with CO2 compressors seen on the left and an NH3 compressor on the right.

Johnsons Controls claims the specific charge of their systems to be 0.2 to 0.4 kg NH3/kW.

## 3.4. Challenges in the CCR and WDX systems

Traditional pumped overfeed systems are less sensitive to pollution of the refrigerant compared to the systems where the circulation ratio is controlled to the lowest possible one. It is specially the water content in the ammonia that is critical for the CCR and WDX systems. In this section, there is a description of the main pollutants water, oil and air and their influence on the system.

### 3.4.1. Water

Water mixes perfectly with ammonia and is circulated together with ammonia in traditional pumped circulated systems. By mixing water with ammonia, the evaporation temperature starts to deviate when the ammonia in the mixture starts to evaporate. The ammonia has lower evaporation pressure and thereby evaporates first. This entails that the liquid mixture changes during evaporation with a changing evaporation temperature as a result. This can be seen in Figure 24 which is taken from [14] where the water content in the ammonia is 3 % and the evaporation temperature is -40 °C.

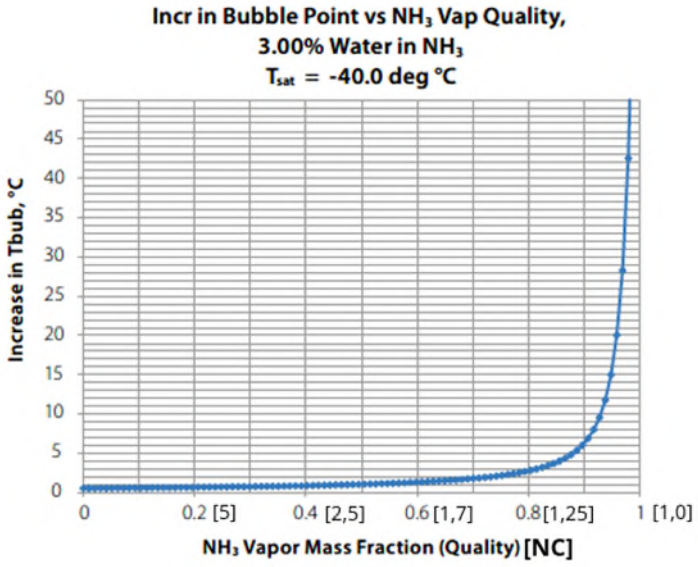


**Figure 24: The effect of water on the boiling point of ammonia water mixture.**

The influence of the water is an increased evaporation temperature to be able to dry out the ammonia. The increase depends on the circulation number. For most pumped circulated systems running on 3 or higher, this increase is low or around 1K. For the CCR or WDX systems the influence is large. For CCR adjusted to hold the circulation number on 1.2, the increase is around 5K. For WDX, where the quality is around 1, the increase is over 50K which is impossible to obtain for a normal evaporator which results in liquid ammonia out of the evaporator even if the measured superheat is 12 K.

To explain what happens a temperature mass fraction diagram as shown in Figure 25 can be used. The diagram on the right is taken for a pressure that corresponds to a -35 °C

suction temperature for pure ammonia. The lower line is the boiling point, and the upper line is the dew point line. The area under the boiling point is represented by liquid and above the dew point as gas. The area in between is a mixture of gas and liquid in a composition given by the level rule. The horizontal axes present the mass fraction of ammonia, i.e., pure water on 0 and pure ammonia on 1.

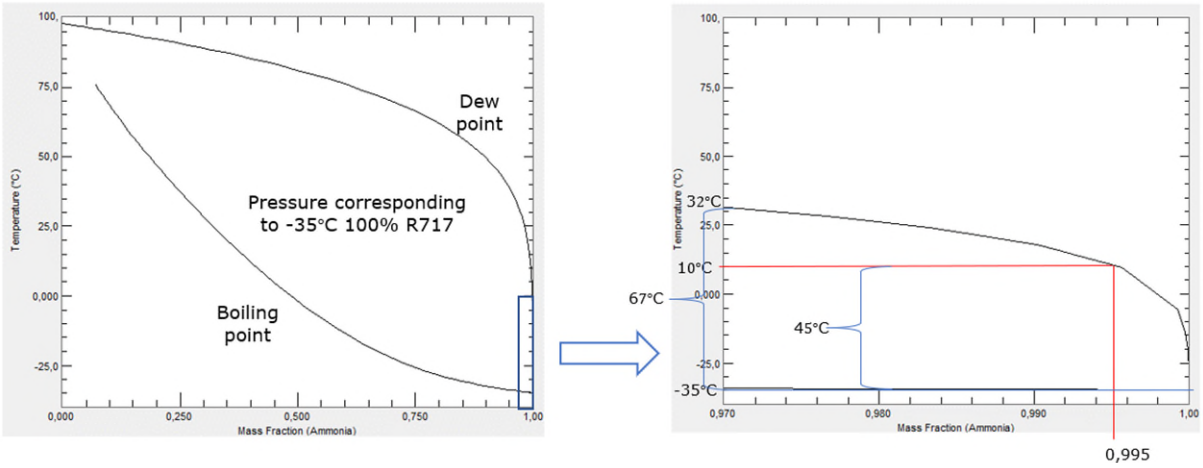


**Figure 25: Temperature mass fraction diagram for water ammonia mixture.**

On the right, the area marked by the blue box on the picture to the right is blown up. In the right picture a water content from 3 % and down to 0 is presented. As an example, an ammonia content of 99,5 % is taken (red line), i.e., there is a water content of 0,5 %. This is considered as a max level in pumped recirculated systems. When coming from the liquid phase i.e., the bottom part of the graph, the mixture starts to boil at close to -35 °C. When into the two-phase area the composition of the liquid changes rapidly as the evaporation temperature increases i.e., moving upward in the graph. As can be seen from the graph, a temperature increase of 45 °C is needed to completely dry out the mixture. For a 3 % water content, the superheat would need to be 67 K. This is impossible to reach in normal systems with dry expansion control as this superheating is not available from the air side. For the DX controlled systems with a small amount of water, the leaving mixture from the evaporator is thereby always wet, i.e., DX for ammonia with water is impossible if dry gas phase is required out of the evaporator.

To explain what happens in an evaporator, the log-PH diagram can be used.

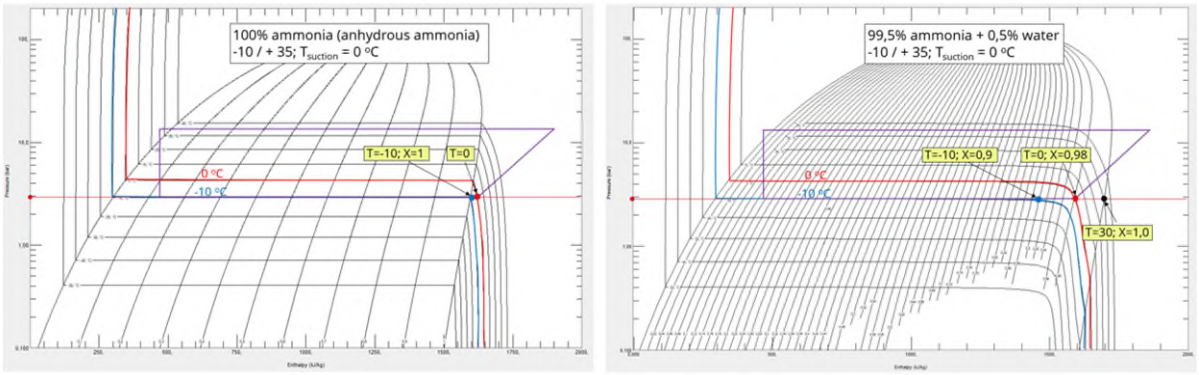


**Figure 26: Log-PH diagram for pure ammonia on the left and for ammonia with 0,5 % water on the right for -10 °C suction temperature.**

In Figure 26 on the left, the temperature/pressure lines inside the clock are straight i.e., there is a direct relationship between temperature and pressure. As soon as water enters the ammonia as seen in the picture on the left the temperature/pressure lines inside the clock are no longer coincident. Higher water content brings more deviation. With 10K superheat, the vapour in the evaporator outlet is superheated for pure ammonia, but for ammonia with 0,5 % water, the quality of the vapour is 0,98, i.e., slightly overflooded. To get the vapour totally evaporated, the superheat must be 40K as shown by the black dot in the picture on the right in Figure 26. This liquid leaving the evaporator will hit the temperature sensor on a normal superheat-controlled evaporator and disturb the control.

For lower evaporation temperatures, the situation is the same. In Figure 27, the evaporation temperature of -35 °C is shown in a log-PH diagram for 0,5 % and 0,2 % water content, respectively.

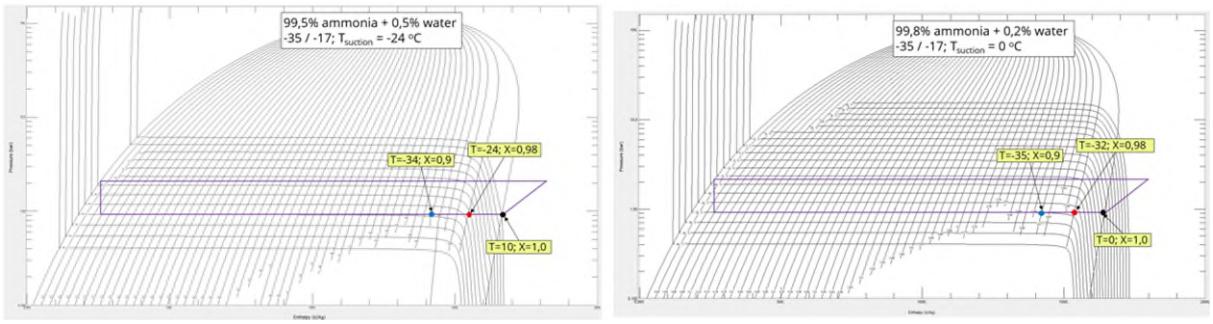


**Figure 27: Log-PH diagram for ammonia with 0,5 % on the left and with 0,2 % water on the right for -35 °C suction temperature.**

The figure shows the same tendency for a -35 °C evaporation temperature as for -10 °C, i.e., it is not possible to have dry vapour out of the evaporator if there is water in the ammonia.

In the new refrigeration standard EN 378, part 2, article H.4.5, a new concern is raised regarding the oxygen and water content in ammonia systems. Here it is stated that some research has shown that to eliminate the risk of stress corrosion in vessels, where oxygen can be contained, it is necessary to have at least 0,2 % of water in the ammonia. As shown before, this water content gives challenges in CCR and WDX systems. Thereby it is

necessary to exclude air and water from these systems by installing equipment to remove continuously air and water out of the system.

### 3.4.2. Air

Air is another pollutant in the system and has the same decrement on efficiency for both pumped circulation systems as for CCR and WDX systems. It tends to assemble on the high-pressure side and finally increase the condensing pressure and thereby reducing efficiency. Stress corrosion is also an issue when no water is present as mentioned earlier. This air needs to be removed during operation. The evacuation of new installations before adding ammonia and after maintenance of older systems needs to be done thoroughly.

### 3.4.3. Oil

Oil in ammonia systems has no or a very low miscibility in the ammonia. This leads to a separate oil phase in both liquid and vapor ammonia. For liquid overfeed systems with large circulation ratio this is less of a problem since the oil entering the refrigeration system is captured in the liquid separator vessel and in the entrance to the evaporator. The oil still entering the evaporators is washed out of the evaporator with the ammonia defrost and returned to the liquid separator. For WDX systems the refrigerant liquid flow goes directly to the evaporators and the oil from the leaving the compressors oil separator enters the evaporator through the expansion valve. The oil will then first be washed out during defrost. It is thereby important in these types of systems to have a very good oil separation after the compressors. It is also important to try to catch the oil after the expansion valve before the evaporator and to ensure that the defrost gas is with as low oil content as possible.

## 3.5. Summary and conclusions

A definition on low charge is not found in the industry today and depends on the system configuration and application. For the industrial ammonia systems considered in the project, a low charge definition of 1.5 kg/kW has been used. This is the goal for the project. This is a reduction from typically 4 to 5 kg/kW for state-of-the-art industrial ammonia systems. By reaching this or a lower number, the liquid carried through the wet suction lines and back to the pumped liquid separator is reduced tremendously. This brings a lower pressure drop for the same piping sizes which gives the opportunity to raise the suction pressure correspondingly.

There are a few companies worldwide that market a low charge solution. The available solutions are divided into three categories, i.e., centralized systems, local systems, and cascade systems.

Centralized systems are closest to the state-of-the-art industrial ammonia systems designed today but run with direct expansion (DX). All those solutions are mainly usable for new systems and do not address the older type of systems. The fin and tube of the evaporators are made of aluminum, and they use a specific liquid distributor, the so-called gravity liquid distributor, to distribute the liquid into the coil. One of the companies, Frick, use a distributed system design where the condenser and evaporator are located close to the point of use, and the evaporators are overflooded. Another company, Star, uses a

configuration that is just applicable for smaller units and that cannot be used for larger systems.

Cascade systems are systems with ammonia on the top and another refrigerant on the bottom circuit, e.g., CO2. These systems reduce the ammonia refrigerant charge considerably but come with an efficiency penalty because of the temperature difference over the cascade heat exchanger. These solutions are also for new system design.

The third category is the distributed system where the refrigeration system is built up by a lot of smaller systems installed close to where the cooling will be used. These systems are built into a machinery room combined with a room for the evaporators. These systems require a roof construction that can bear the weight of the combined unit and air ducts down to the cold store. These systems are also for new applications.

The pollutant in the refrigeration system that has the largest influence on the solutions developed in this project is water. A moderate amount of water does not have a large impact on normal pumped circulated systems. For the low charge systems developed in the project it is, however, of vital importance to remove the water from the system.

# 4. Research of new evaporator systems

## 4.1. Introduction

In this work package, a solution for the three concepts in the project was developed.

## 4.2. Controlled Circulation Ratio (CCR) solutions

The CCR solution is intended to be able to increase the efficiency and lower the charge of existing industrial refrigeration systems. By CCR, the liquid flow into the evaporator in conventional industrial refrigeration systems is controlled to a specific circulation number all the time instead of using a manually adjusted valve and let the circulation number be uncontrolled.

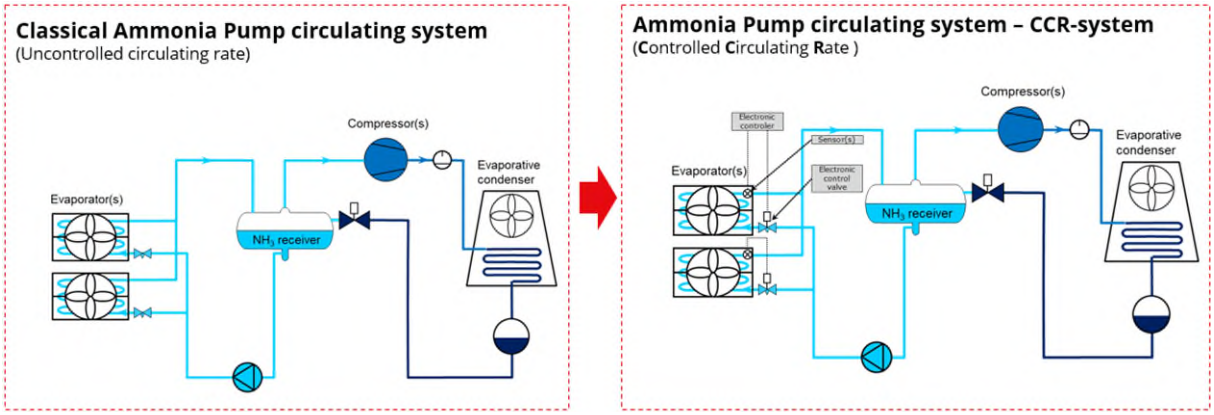


**Figure 28: Classical vs. CCR controlled evaporators.**

To explain what happens in the state-of-the-art on the one hand compared to CCR on the other hand, Figure 29 can be used.

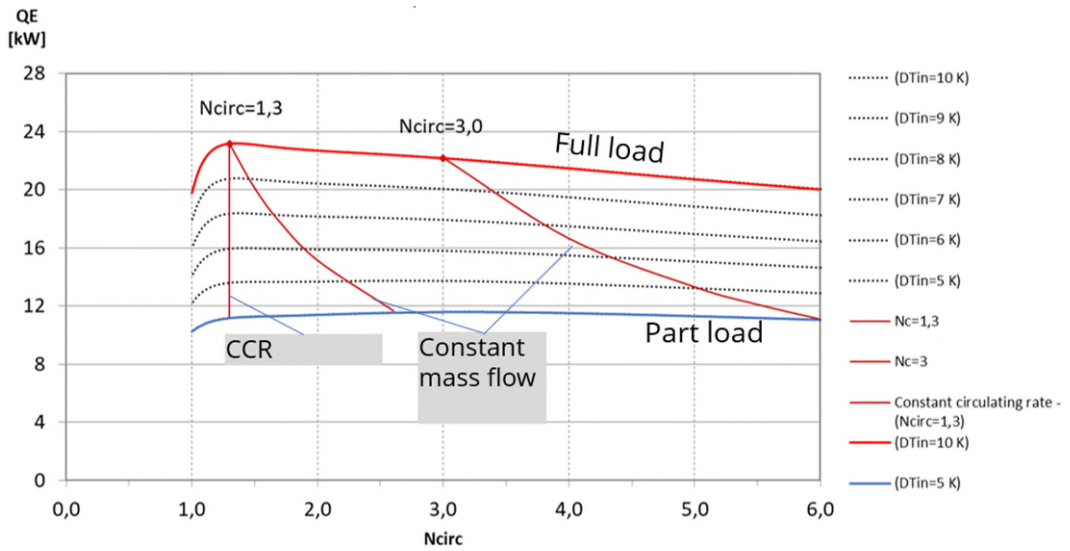


**Figure 29: The influence of evaporator load on the circulation number.**

Figure 29 shows how the capacity changes for an evaporator at full load (red line on top) and at part load (dotted lines and the blue line). For the CCR the circulation number is held

constant at around 1.3 as seen by the vertical red line i.e., constant for all load cases. Then two scenarios are shown for the uncontrolled case. One where the evaporator is at full load adjusted manually to a circulation number of 1.3 and then another where it is adjusted to 3 which is the normal design rule of thumb to compensate for various uncertainties in the system. When the load decreased because of icing up of the coil or other load changes, the circulation number increases. This increases, both the charge of the evaporator and the pressure loss in the wet return line and thereby decreases the efficiency of the system.

To realize the CCR, two concepts are to be addressed. One is the evaporator where a new type of circuiting is laid out to both minimize the charge and at the same time to reduce the maldistribution in the evaporator. The other concept needed is a control system for the liquid flow to the evaporator consisting of a valve, a sensor, and a control strategy.

### 4.2.1. The evaporator

The state-of-the-art evaporator mostly used in Europe is a bottom feed evaporator as shown in Figure 30.

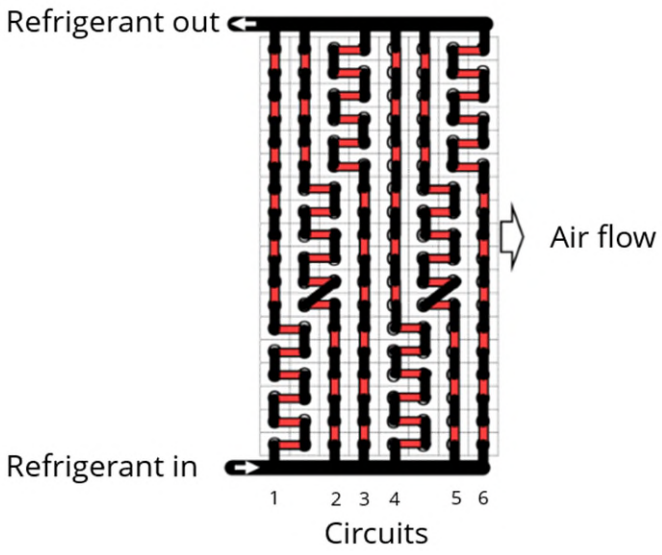


**Figure 30: Bottom feed evaporator - side view.**

Here, the air enters the evaporator from the left and travels through the evaporator from left to right. The refrigerant enters in the bottom as shown, and it is divided into circuits entering the coil from the bottom and flowing through the coil to exit at the top. For this configuration, the warmest air meets the first circuit, i.e., circuit number 1, and the last circuit meets the coldest air. This entails that the fist coil has a higher load than the last one which will result in a higher quality of the refrigerant out of the coil compared to the last circuit for the same refrigerant flow through all circuits and the same circuit length. This will lead to a maldistribution on the refrigerant side.

In a commercial project made for Danfoss (674503-Danfoss Low Charge Ammonia LCA), a state-of-the-art design of three types of evaporators (bottom-, side- and top feed), shown in Figure 31, were tested for various circulation rates (1.1 to 5) at two temperature levels -10 °C and -30°C). These tests showed a lot of maldistribution of the refrigerant out

of the evaporator which resulted in a capacity reduction with relatively high circulation numbers.

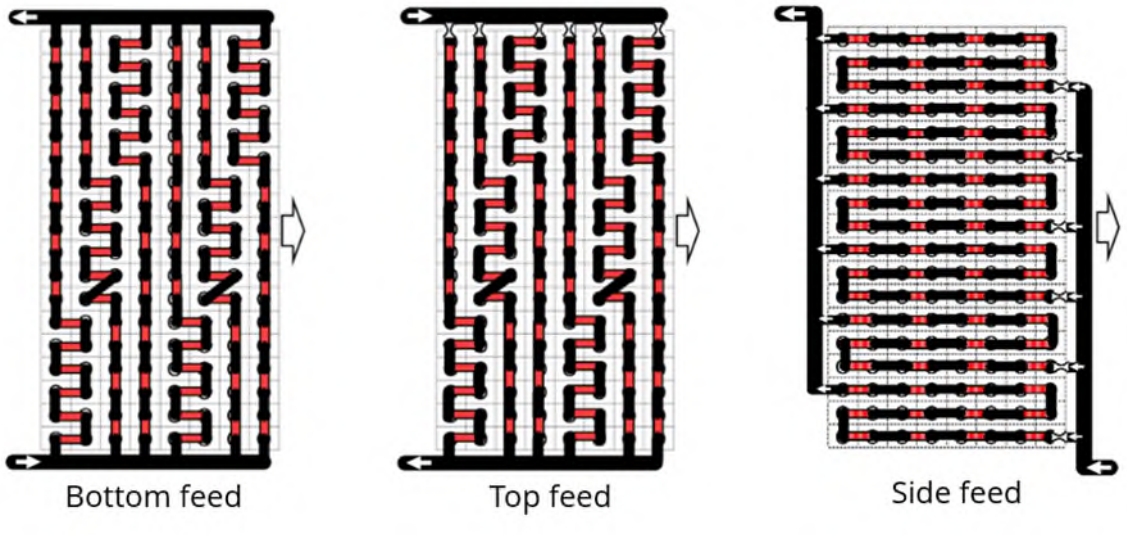


**Figure 31: Three types of the state-of-the-art evaporators.**

To be able to run with lower circulation numbers and thereby increase the efficiency and reduce the charge, a new evaporator design is preferred.

Through simulation, two types of evaporator circuiting are found to be able to increase the efficiency and reduce the charge of an industrial evaporators.

One is a bottom feed interlaced evaporator shown in Figure 32, and the other is a side-fed co-current evaporator shown in Figure 34.

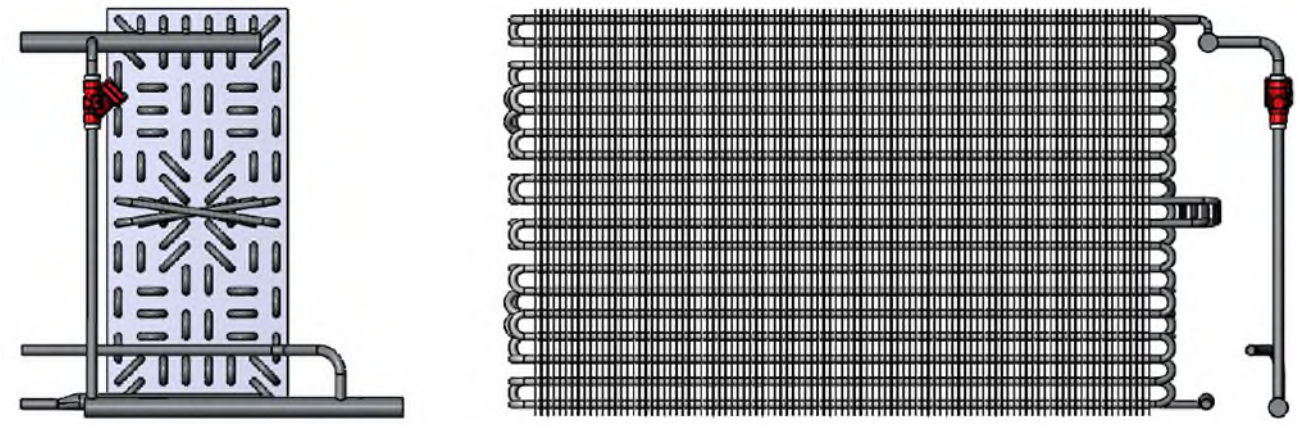

**Figure 32: Interlaced bottom feed evaporator.**

Normally, the evaporators have orifices in the refrigeration inlet to the coil to even out the refrigerant flow, but these can give problems. They can affect the defrosting of the coil by restraining the liquid flow out of the coil. They can also be clogged by both oil and impurities circulating in the system which will change the pressure drop through them and can contribute to increase maldistribution. It is therefore preferred to do without the orifices. Thereby, the evaporator was ordered without the orifices.

The intention of the interlace midway in the coil is to even out the load on the circuits from the air side and thereby even out the capacity of each pass which results in less maldistribution in the refrigerant circuits.

The technical data of the evaporator is shown in Table 1 and the circuiting in Figure 32 and Figure 33.

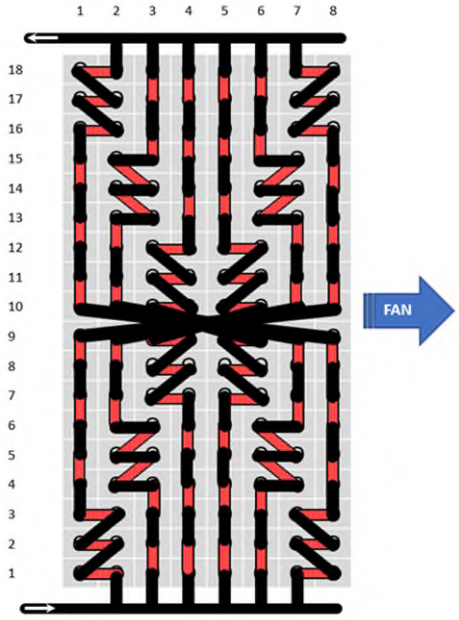


**Figure 33: Circuiting of the bottom feed cross over evaporator.**

**Table 1: Technical data for bottom feed cross over evaporator**

| | | | | | | |
|---|---|---|---|---|---|---|
| Tube arrangement | Inline | | | Refrigerant | R717 | |
| Tube columns | 8 | | | Capacity | 24,6 | kW |
| Tube rows | 18 | | | Evaporation temperature | -30 | °C |
| Number of circuits | 6 | | | Feed rate pump | 1,2 | |
| Tube length | 1360 | mm | | Air flow | 15146 | $m^3/h$ |
| Pipe outer diameter | 15,6 | mm | | Air face velocity | 3,5 | m/s |
| Pipe inner diameter | 14,6 | mm | | Air inlet temperature | -20 | °C |
| Tube spacing | 50x50 | mm | | Air inlet humidity | 95 | % |
| Fin spacing | 12 | mm | | Air outlet temperature | -23,7 | °C |
| Fin thickness | 0,5 | mm | | Air outlet humidity | 100 | % |
| Pipe material | AISI 304 | | | Sensible heat rate | 90,3 | % |
| Fin material | Aluminium | | | | | |
| Surface area | 84,7 | $m^2$ | | | | |

The side feed evaporator is circuited with co-current refrigerant flow, i.e., the refrigerant comes into the coil on the same side as the air enters. The circuiting is side-bottom fed, i.e., the refrigerant enters in each pass at the bottom left and flows upwards when going from one row to the next. The pipes in each pass travel horizontally through the coil from

air inlet to air outlet. When reaching the last pipe column in each row, the refrigerant is piped to the first column again in the row above and takes three runs through the coil before leaving to the suction header. The side fed evaporators tested in the previous commercial project for Danfoss were also side-bottom fed, but in mixed co- and countercurrent configuration.

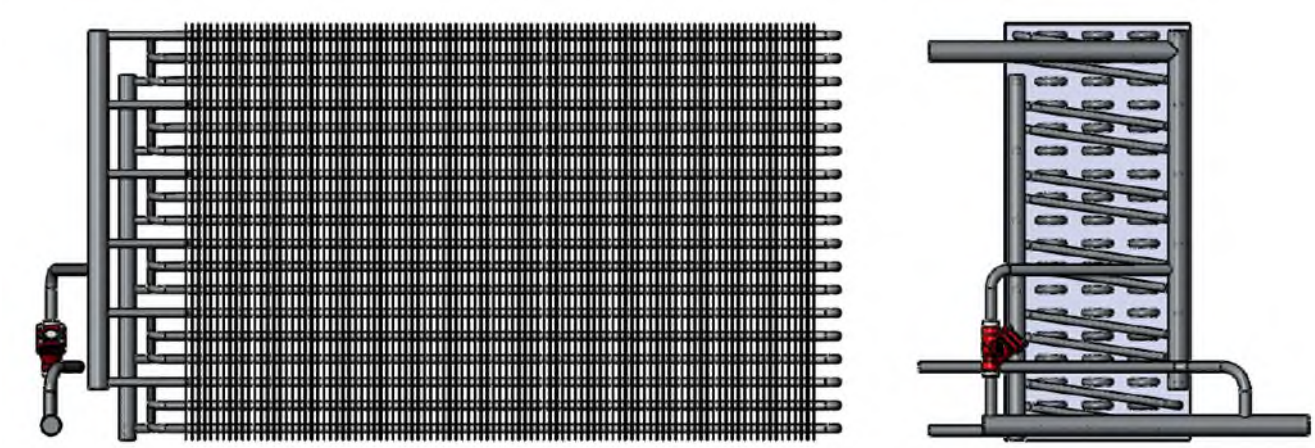

**Figure 34: Sidefeed evaporator.**

The idea behind the co-current flow is to increase the effectivity of the evaporator. The refrigerant liquid content in the start of each refrigerant pass is high with low speed and slightly subcooled which results in a low heat transfer coefficient. To kickstart the boiling, the low heat transfer is compensated with a high temperature difference by letting the refrigerant meet the warmest air.

The technical data of the evaporator is shown in Table 2 and the circuiting in Figure 34 and Figure 35.

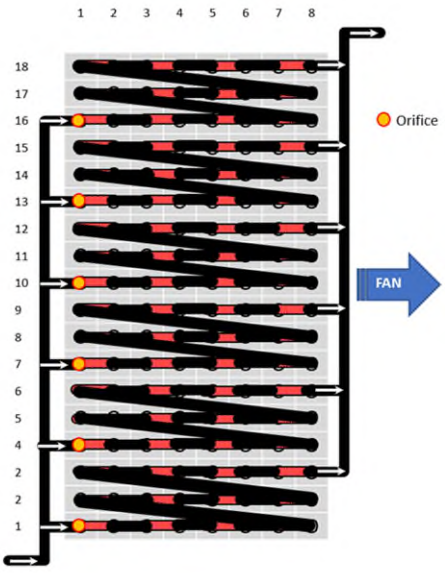


**Figure 35: Circuiting for side bottom feed evaporator.**

**Table 2: Technical data for the side bottom feed evaporator**

| | | | | | | |
|---|---|---|---|---|---|---|
| Tube arrangement | Inline | | | Refrigerant | R717 | |
| Tube columns | 8 | | | Capacity | 24,6 | kW |
| Tube rows | 18 | | | Evaporation temperature | -30 | °C |
| Number of circuits | 6 | | | Feed rate pump | 1,2 | |
| Tube length | 1360 | mm | | Air flow | 15146 | $m^3/h$ |
| Pipe outer diameter | 15,6 | mm | | Air face velocity | 3,5 | m/s |
| Pipe inner diameter | 14,6 | mm | | Air inlet temperature | -20 | °C |
| Tube spacing | 50x50 | mm | | Air inlet humidity | 95 | % |
| Fin spacing | 12 | mm | | Air outlet temperature | -23,7 | °C |
| Fin thickness | 0,5 | mm | | Air outlet humidity | 100 | % |
| Pipe material | AISI 304 | | | Sensible heat rate | 90,3 | % |
| Fin material | Aluminium | | | | | |
| Surface area | 84,7 | $m^2$ | | | | |

### 4.2.2. The sensor, the valve, and the control strategy

To be able to control the circulation ratio, a new type of sensor is needed that can measure the quality of the refrigerant flow out of the evaporator. This is a difficult task in ammonia systems since the liquid and gas tend to separate in the pipe and the liquid flows as a river in the bottom of the pipe unless a high superficial gas velocity is established. This high velocity contributes to a high pressure drop and thereby the temperature drops through the coil on the refrigerant side. This drop in temperature decreases the efficiency of the coil.

Two measuring principles are found. One is where the dielectric constant of the fluid mixture is measured, and another is where the heat conductivity of the fluid mixture is measured. Both methods face the same challenges with liquid separation in the pipe. The selected method in the project is the heat conductivity method where Danfoss through the project has developed a sensor to accomplish this.

The gas quality is a measure of the dryness of the refrigerant and states how many kg of the refrigerant is gas compared to the total mass of the mixture and is given as:

$$x = \frac{m_{gas}}{m_{total}}$$

Another measure often used in industrial refrigeration is the circulation number and is defined as:

$$n_c = \frac{m_{total}}{m_{gas}}$$

The circulation number is a measure of how much extra refrigerant flows through the evaporator compared to what is needed. As can be seen, the quality is the reciprocal of the circulation number.

The evaporation through the evaporator circuit changes quality from 0 in the start of the circuit and ends at a certain quality depending on the extra flow of refrigerant through the circuit i.e., the circulation number. This is shown in Figure 36.

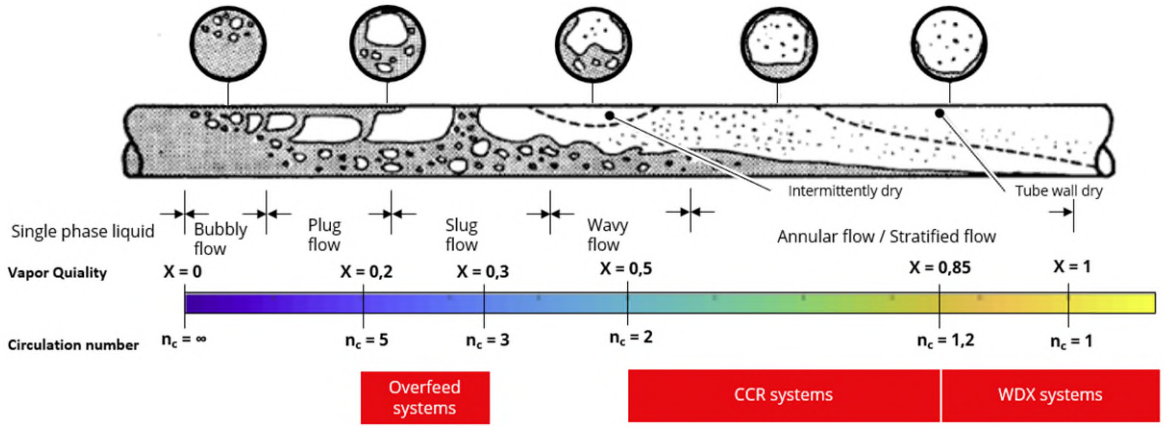


**Figure 36: Flow pattern inside a coil circuit.**

State-of-the-art overfeed systems for evaporators are typically designed to a circulation number of 3 which in real operation and part load the circulation number will lie between 3 and 5 or even higher. By controlling the circulation number as in the CCR system, the circulation number can be maintained on a much lower number reducing the charge and the liquid carryover through the wet suction lines with reduction in pressure drop as a result contributing to higher energy efficiency. The pressure drop penalty is most severe in liquid risers, i.e., the pipe going from the evaporators and up to the main wet suction line.

The flow pattern inside the pipe is dependent on the gas speed in the pipe as shown in Figure 37.

- **Fully annular flow** (uniformed liquid film thickness)
- Evaporator with **very high superficial gas velocity (Ugas > 15 m/s)**

- **Partly annular flow** (uneven liquid film thickness)
- Evaporator with **high superficial gas velocity (Ugas ~ 10-15 m/s)**

- **Stratified flow** ("separated" gas and liquid flow.
- Very **low superficial gas velocity (Ugas 5-10 m/s)**

**Figure 37: Flow pattern inside pipe vs. gas velocity.**

As liquid ammonia has a high specific weight compared to the gas phase, a high speed is necessary to introduce the annual flow. Another property of the ammonia is its high latent heat of evaporation which means that the mass flow will be low for a certain capacity compared to other refrigerants. This requires small pipe diameters to get the gas speed up to be able to get a high heat transfer and maintain an annual flow in the outlet. To restrict the pressure drop for this high superficial gas speed the circuit has to be short. The annual

flow is preferred where the sensor is sitting to be able to be independent on the sensor placement.

The pipe sizes used in state-of-the-art evaporators today is Ø15mm. This pipe size normally places the flow in the outlet in the partly annual to stratified flow. To be able to cope with that, the sensor must be placed in a certain position, and the control strategy must be able to calibrate the sensor at start up.

The sensor to be developed is based on the heat conductivity method and will be clamped on the pipe as shown in Figure 38.

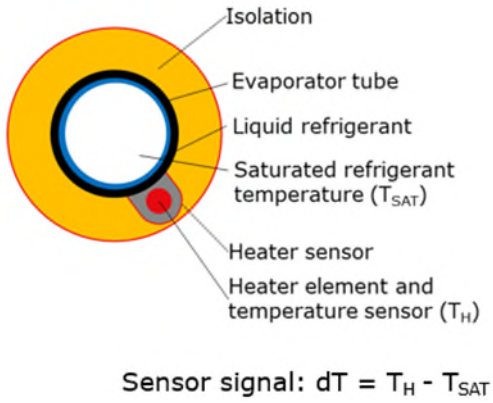


**Figure 38: The heated sensor clamped on a pipe.**

The valves used to control the refrigerant flow must be adjustable and able to control a small refrigerant flow without too small orifices that could be clogged by dirt or oil in the system. The valves to be use is pulse modulating AKVA valves from Danfoss. These valves change between fully open and closed where the opening time versus closing time in each cycle is changed to control the average flow. By using this valve, the opening degree of the valve is the same for all load conditions and thereby the risk of clogging reduced.

The control system is developed specifically to the industrial refrigeration systems and built into the existing control platform from Danfoss.

### 4.2.3. Summary and conclusions

The controlled circulation ratio (CCR) reduces the circulation ratio in the system be controlling the liquid flow to the evaporators by measuring on the quality of the refrigerant on the outlet of the evaporator.

A good liquid refrigerant distribution in the evaporator is vital to be able to control the liquid flow. In the project, two types of evaporators were designed and tested to reduce the maldistribution on the refrigerant side through the evaporator. These were the interlaced or cross over type and the side-fed type. These new evaporator types are then compared to state-of-the-art evaporators measured in another project.

In the interlaced type, the most loaded circuit, which is the first circuit that meats the warm air flow, is directed midways to the least loaded circuit, i.e., the last circuit in the

evaporator. The other circuits are also directed from a higher load to a lower load or vice versa to try to even out the maldistribution.

In the side-fed evaporators, the refrigerant enters from the side and is directed through the evaporator coil in the same row of pipes. When the last pipe at the outlet of the air flow is reached, the flow is directed up to the first pipe in the next pipe row and through the evaporator again. This continuous three times for each pass. Hence, the name side-upwards feed. The idea behind the configuration is that the liquid entering the coil meets the warmest air to start the boiling as soon as possible. To even the liquid distribution through the coil, the orifices are placed at the inlet to compensate for the height of the header. For ammonia these orifices are normally with a small diameter hole which can cause problems if dirt or oil enters and can introduce difficulties under defrosting because of various pressure drops through each pass.

A new sensor based on a heated censor principle is developed and tested in the project. This is a clamp-on sensor that uses a heating element and a temperature sensor to measure the quality in the pipe.

Since ammonia has a very high latent heat and the circulation ratio will be low, the liquid valves must have a small orifice to be able to control the liquid injection. Here, various types of valves will be tested.

A test setup and a data acquisition system for the CCR tests were designed.

## 4.3. Wet direct expansion (WDX) solutions

The purpose of the WDX solution is to be able to increase the efficiency and lower the charge of a new industrial refrigeration system by reducing or eliminating the liquid ammonia in the suction lines from the evaporators and in the pumped liquid vessels. In this solution, the high-pressure liquid is fed directly to the expansion valves (see Figure 39). This will reduce or eliminate the need for a pumped liquid vessel and thereby considerably reduce the system refrigerant charge.

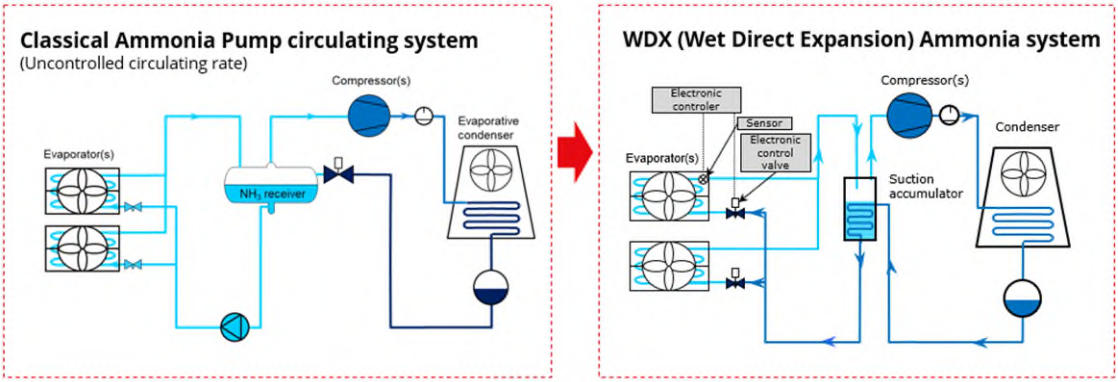


**Figure 39: One stage classical pumped ammonia system vs. new WDX system.**

By eliminating the pumped liquid vessel on both the low stage and the intermediate stage of a two-stage system and replace it with a smaller liquid accumulator, the price of the system can be reduced. The suction line from the evaporators will also be smaller for the same pressure drop reducing the pipe and insulation cost.

The important efficiency difference in a traditional DX solution and the WDX is illustrated in Figure 40.

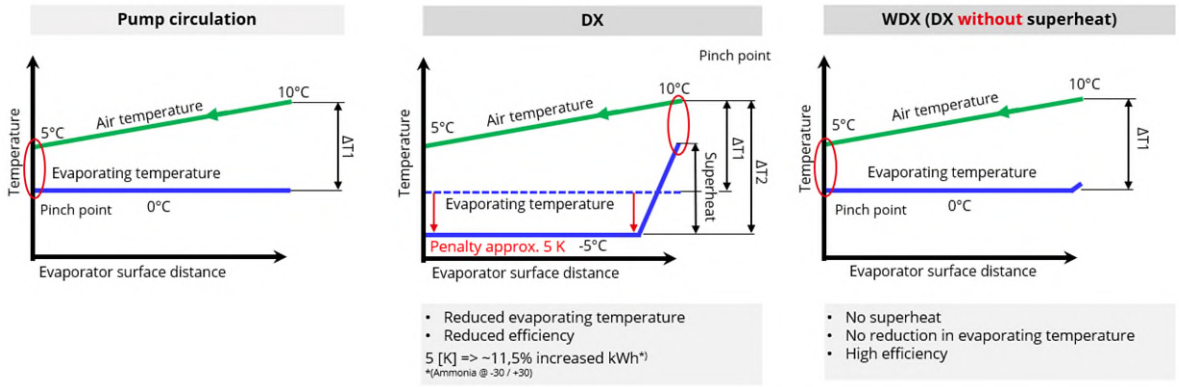


**Figure 40: Air and refrigeration temperature profiles in pumped circulation, DX and WDX.**

The green line in the picture is the air temperature drop through the evaporator. This is typically around 5K for industrial ammonia evaporators. The blue line represents the refrigerant temperature in the coil.

When looking at the profile for the pumped circulation, it is seen that the pinch point is in the air evaporator outlet. The pinch point is where the closest approach between the air and the refrigerant temperature is found in the evaporator.

For normal controlled superheat (DX), where the needed superheat must be around 10K for ammonia to secure dry gas to the compressors, the pinch point is found in the air inlet of the evaporator. Using the same pinch point approach as for pumped circulation of 5K, the suction temperature must be dropped by 5 K down to -5 °C to be able to reach the superheat signal for the expansion valve.

For the WDX developed in the project, the low or no SH results in the same suction temperature as for the pumped circulated though without the liquid overfeed to the suction line and thereby higher efficiency than for the pumped circulated.

To be able to harvest these benefits of the WDX systems, a new way of controlling the evaporators must be developed where the expansion valve is controlled on the limit between flooded and dry.

### 4.3.1. Solutions for the WDX

As the solution for the WDX is not found as a commercially available product, a viable solution for the WDX to be tested had to be found. The project group came up with seven ideas to how this could be done. The ideas were divided into two groups.

- Dry gas out of the evaporator.
- Wet gas out of the evaporator.

For the first group, the liquid separation and drying out of the gas were thought of as being an integrated part of the evaporator.

For the second group, the small amount of liquid escaping the evaporator would be collected in a central suction accumulator to be boiled off before entering the compressors.

The project group ended up with six ideas for the first group and one for the second group.

#### 4.3.1.1. Dry gas out of the evaporator

The first of the six ideas in this group were based on a patent from Zimmermann where the liquid entering the evaporator was first expanded to an intermediate pressure self-controlled by the capacity of the suction gas heat exchanger (SGHX) (see a in Figure 41).

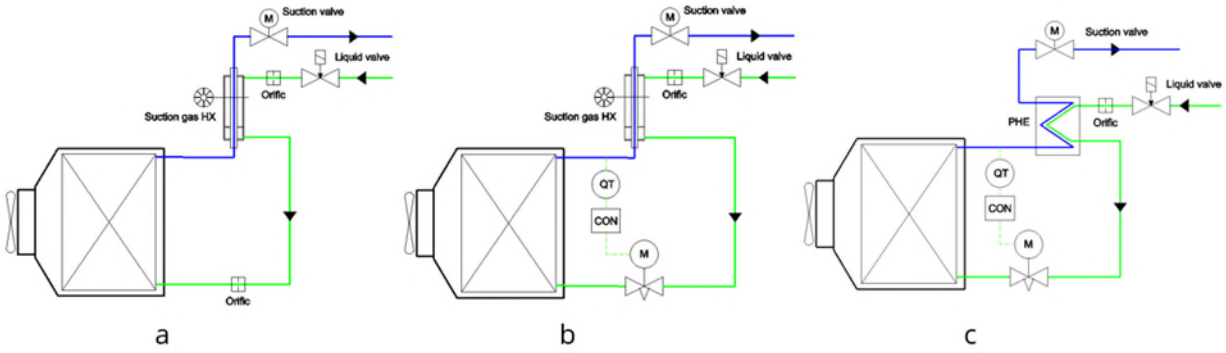


**Figure 41: Idea group 1 in WDX solutions based on Zimmermann patent. First on the left is uncontrolled and the two others controlled.**

The other two solutions b and c were based on the same idea with controlled feed to the evaporator based on the quality out of the evaporator and into the SGHX. Solution b with coaxial SGHX and c with plate heat exchanger.

Another idea was to have an intermediate pressure controlled by a pressure-controlled valve.

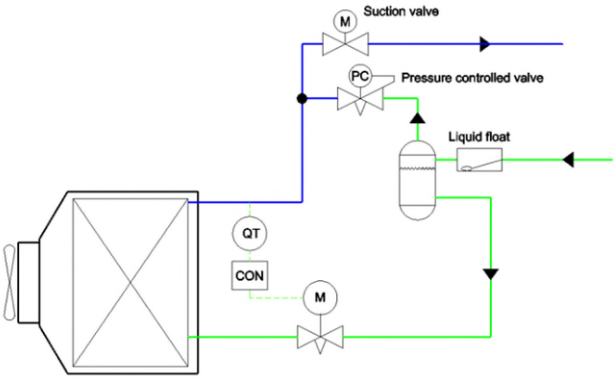


**Figure 42: Idea group 2 in WDX.**

The flash gas from the intermediate vessel is then led to the suction line and used to boil off the liquid exiting the evaporator.

The third group of ideas in Figure 43 was to use a normal superheat or quality to control the liquid to the evaporators and then burn off the leaving liquid before entering the suction line.

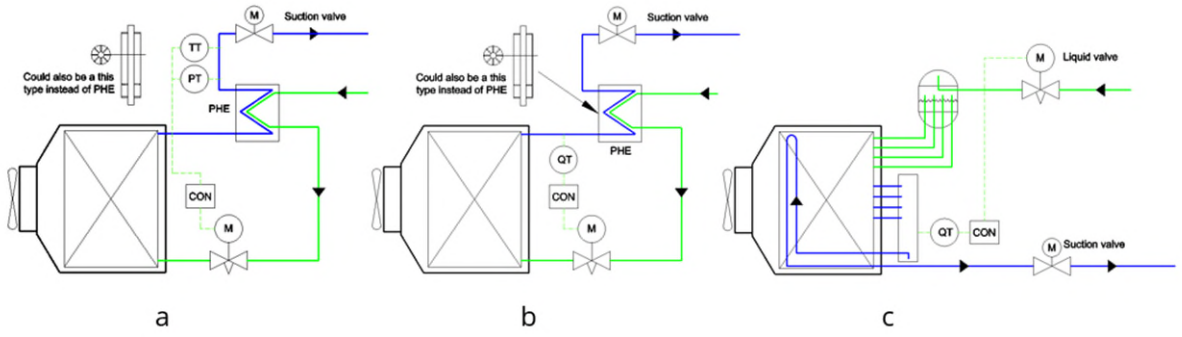


**Figure 43: Idea group 3 in WDX.**

The first idea (a) in Figure 43 was to use a normal SH controller with the sensors placed downwards of the SGHX. The SGHX could be either coaxial or PHE. This will be very hard to control since the SGHX adds to the instability of controlling the expansion valve. In solution b, the liquid into the evaporator is controlled by the quality out of the evaporator, and the liquid in the suction gas is burned off in the SHGX before entering the suction line. In the last solution, a special circuit in the evaporator is used to burn off the liquid from the quality-controlled expansions valve.

The fourth group of ideas was to recirculate the excess liquid from the evaporator back to the evaporator inlet. It is shown in Figure 44.

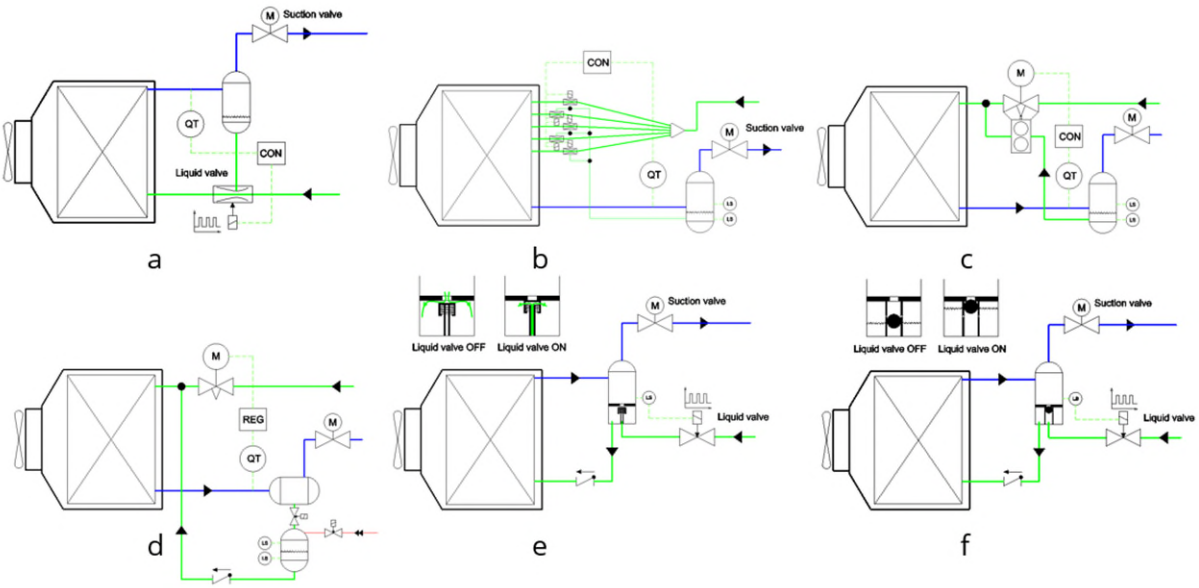


**Figure 44: Idea group 4 in WDX.**

In part a and b, ejectors are used to feed the liquid back to the inlet of the evaporator. In part c, a pump is used to circulate the surplus liquid back to the inlet. The pump is driven

by the expansion energy from the expansion valve. In d, the pump is replaced by a hot gas driven liquid injection. In e and f, the surplus liquid is pumped back to the inlet by a special designed combined liquid separator and a pump.

The fifth group of ideas was based on developing a new type of expansion valve as shown in a in Figure 45 and using a dedicated expansion valve for each circuit of the evaporator.

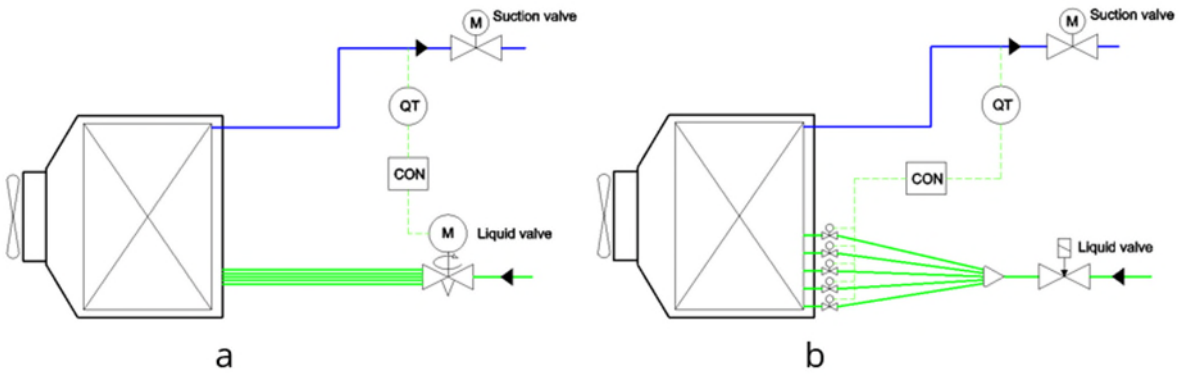


**Figure 45: Idea group 5 of WDX.**

The last idea that was investigated and included dry gas to the system is shown in Figure 46.

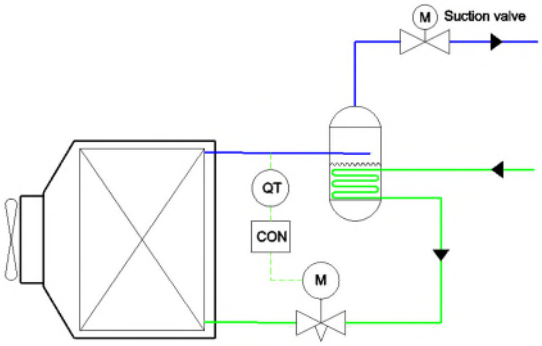


**Figure 46: Idea group 6 of WDX.**

Here, a liquid separator with integrated heating coil where the high-pressure liquid boiled off the liquid exiting in the evaporator.

### 4.3.1.2. Wet gas out of the evaporator

By accepting a small amount of liquid in the gas exiting in the evaporator, a centralized liquid accumulator is needed downstream of the evaporator to separate the liquid from the gas before entering the compressor.

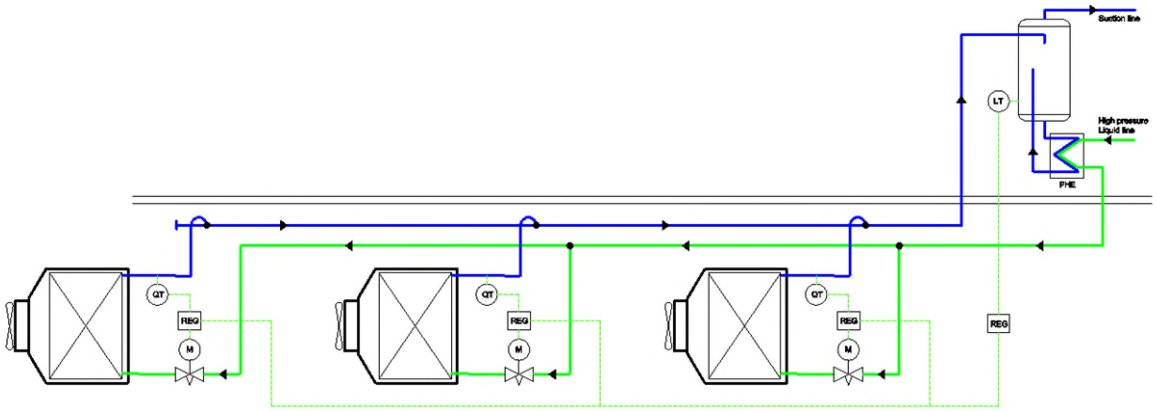


**Figure 47: Idea group 7 of WDX.**

In this idea, the evaporators are controlled with a quality-controlled expansion valve to each evaporator. The excess liquid is assembled in the suction accumulator and burned off by the high-pressure liquid to the evaporators.

## 4.3.2. The evaporator

The evaporator for the WDX solution was especially designed for the project by Guentner.

In Figure 48, the technical data for the WDX evaporator from Guentner is given.

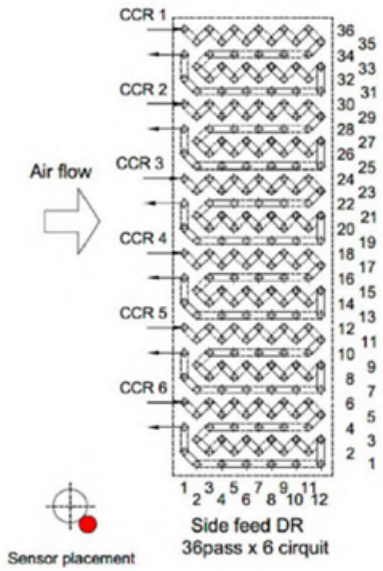


| | | | | | |
|---|---|---|---|---|---|
| Tube arrangement | Staggered | | Capacity | 18 | kW |
| Tubes columns | 12 | | Evaporation temp. | -10 | °C |
| Tube rows | 18 | | Liquid temp. | 34 | °C |
| Tube length | 1360 | mm | Superheat | 7 | K |
| Pipe outer diameter | 12 | mm | Air flow | 14692 | m³/h |
| Pipe inner diameter | 11 | mm | Air face velocity | 3,4 | m/s |
| Tube spacing | 50x25 | mm | Air inlet temp. | 0,0 | °C |
| Fin spacing | 9 | mm | Air outlet temp. | -3,3 | °C |
| Fin thickness | 0,5 | mm | | | |
| Pipe material | AISI 304 | | | | |
| Fins | Aluminium | | | | |

**Figure 48: Technical data for the WDX evaporator.**

In Figure 49, a picture taken from each end of the evaporator is shown. The picture on the left shows the end where the ammonia enters and leaves the evaporator, and the picture on the right shows a close-up of the coil circuiting taken from the other end.

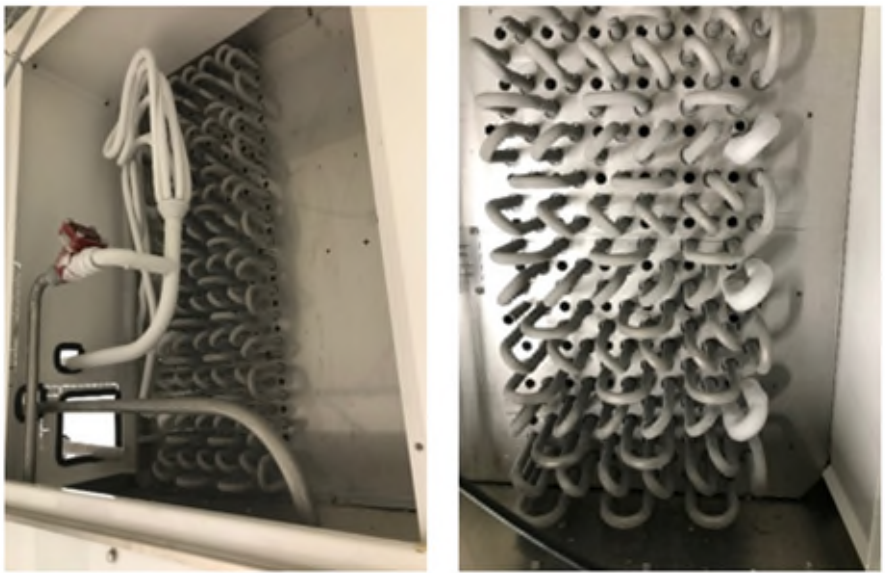

**Figure 49: The ends of the DR evaporator. To the left refrigerant inlet.**

It is a general believe that a special liquid distributor is needed to distribute the ammonia liquid into the evaporator coil. It was decided in cooperation with Guentner to start with using a traditional venturi distributor to see how it worked and thereafter change to the more expensive and complicated distributor if it turned out to be necessary.

### 4.3.3. The sensor, the valve, and the control strategy

To be able to control the liquid entrance to the evaporator, a new type of control strategy is needed. A new sensor to control the quality is also needed and is based on the one used for the CCR solution. A suitable valve to control the flow is also needed to succeed.

### 4.3.4. The suction gas heat exchanger (SGHX)

To be able to test some of the selected ideas from 4.3.1.1, a suction gas heat exchanger was designed and built. Restricted by the available material, it was necessary to divide the SGHX into four parallel coupled SGHXs. One of those sections is shown in Figure 50. Here, the liquid refrigerant flows in the space between the external and internal pipe and the wet return gas from the evaporators inside the internal pipe.

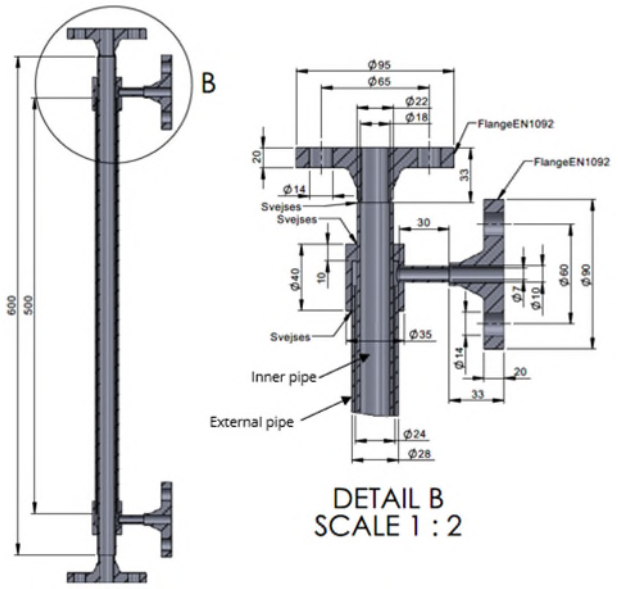


**Figure 50: Suction gas heat exchanger (SGHX).**

Those four pipes are assembled into the complete SGHX as seen in Figure 51. The liquid refrigerant and the wet suction gas flows in co-current in each SGHX.

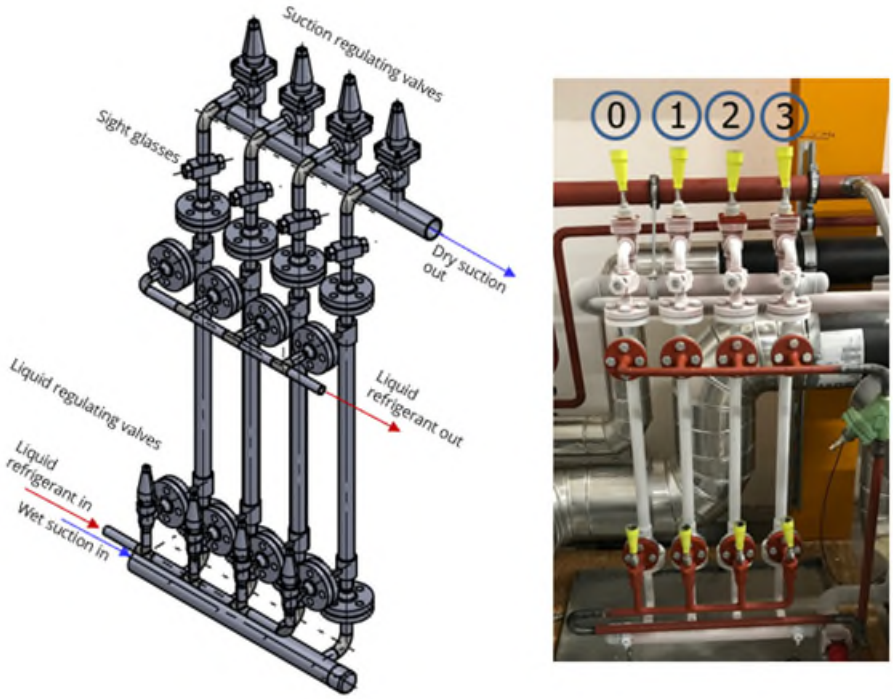


**Figure 51: SGHX assembly drawing on the left side and picture of the installed SGHX on the right.**

There are regulating valves on both the wet suction gas out of the SGHX and on the refrigerant liquid into the SGHX to adjust the flow though the SGHX.

### 4.3.5. Summary and conclusions

The wet direct expansion solution is developed to reduce the complexity of industrial ammonia systems where high-pressure liquid from the condenser is fed directly into the evaporator.

A lot of ideas about how to solve the issue were investigated, and the most viable ones integrated into the test setup.

A new evaporator with a smaller pipe diameter was designed and built into the test setup. This evaporator was side feed with a long circuit to start with through the coil in the same direction as the air flow to use the benefit of warm air to start the boiling process. Then, at the end of each circuit, two pipes in the front facing the warm incoming air are used to superheat the refrigerant before the evaporator exit.

A suction gas heat exchanger (SHGX) was designed to try out the idea of burning the liquid exiting the evaporator. In this way the evaporator would run slightly over-fed with maximum efficiency.

A test setup and data acquisition system for the WDX tests was designed.

## 4.4. The micro channel solutions

To increase the efficiency and reduce the charge further, a new type of evaporator was designed. The design was made in cooperation between Aluventa, DTU and DTI.

The design was based on an extruded aluminum profile, the so-called micro channel, where the refrigerant flows through the small channels as seen in Figure 52.


**Figure 52: Micro channel WEB-MPE profile.**

These micro channel profiles are placed side by side with fin material in between as shown in Figure 53.

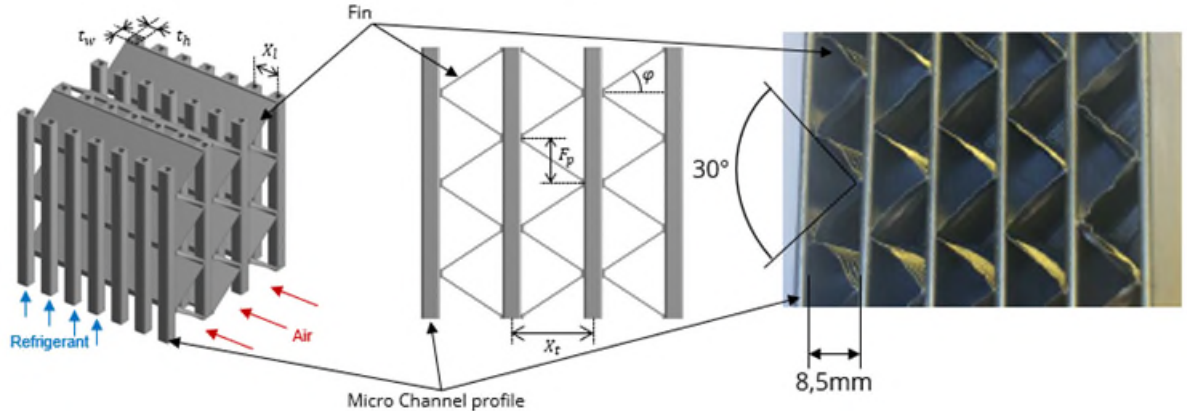


**Figure 53: Micro Channel profiles with fin in between.**

The micro channel profiles and the fins in Figure 53 are then soldered to the liquid and suction headers as shown in Figure 54.

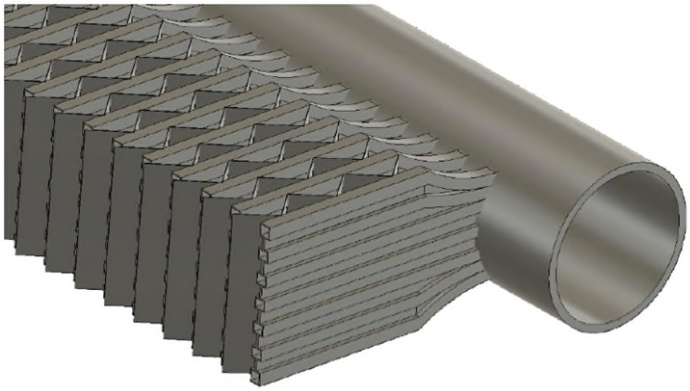

**Figure 54: Micro Channel profiles soldered to the headers.**

62 of these micro channel profiles with fins in between soldered to a suction and liquid header make up one section as shown in Figure 55 on the left. Two of those sections make up one face element as shown on the right.

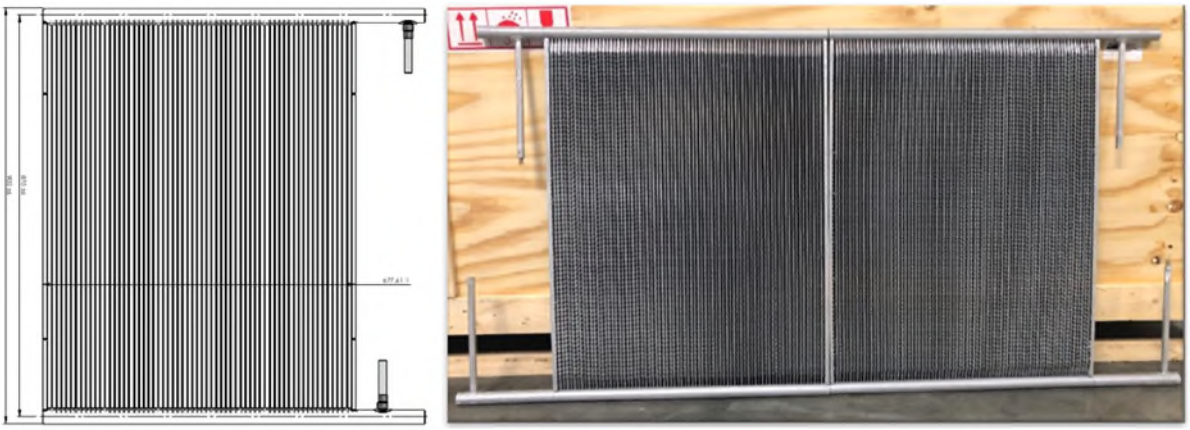

**Figure 55: On the left a micro channel section and to the right one face with two sections.**

These sections make up the final evaporator as shown in Figure 56. The built evaporator consists of eight sections assembled as shown in the picture. The evaporator build in the project was intended to test the function of the micro channel profiles in both icing up and during defrost and was not thought as a final design. In the final design, a smarter solution for the headers must be developed both to reduce the number of headers and their refrigerant charge.

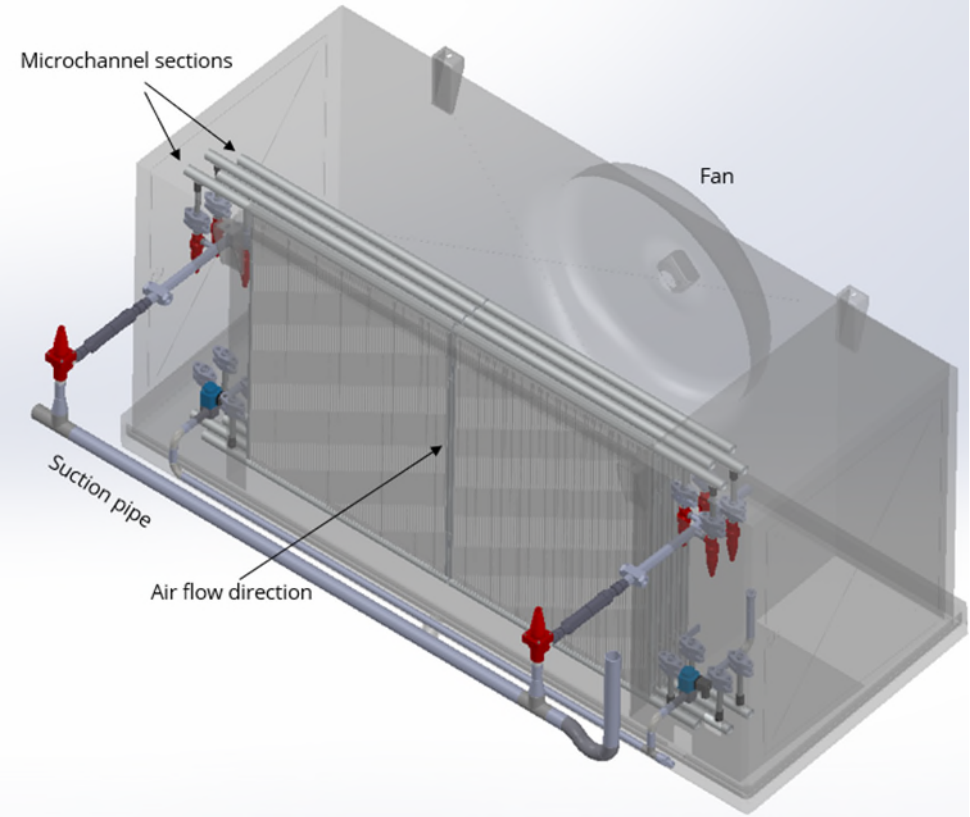


**Figure 56: Final micro channel evaporator.**

# 5. Simulations and verification

## 5.1. Introduction

The simulations to support the development in the project were divided into two paths. The first path was regarding the CCR and WDX solution where different designs were evaluated. The second one was around the micro channel solution where the initial design of the test evaporator was conducted.

## 5.2. The CCR and WDX solution

The state-of-the-art pumped liquid overfed evaporators are fin and tube coils and designed to circulate about three to six times more refrigerant than is necessary for full evaporation. Consequently, the pressure drop induced temperature drop is substantial in these systems, especially at very low evaporation temperatures (e.g. -30 °C), and results in a poor heat transfer driving potential as well as a high pumping power.

The project has shown that there is a significant potential for energy savings by optimizing the tube circuiting, especially making them more robust towards flow maldistribution on both the refrigerant side and the airside. It is crucial to size the inlet orifice correctly for side-fed evaporators and they are largely dependent on the designed recirculation rate. The bottom-fed evaporator with crossover circuits performs the best and is very robust towards flow maldistribution.

The project also revealed that some important design parameters such as the tube pitches, tube diameters and numbers of tube rows could be largely optimized for better heat transfer performance and lower refrigerant charge.

Two papers were published on this subject (Kærn et al., 2020, 2019) during the project, and another paper on the numerical results is pending for the Gustav Lorentzen International Conference in 2022.

### 5.2.1. Investigation on flow maldistribution in finned-tube evaporators

The aim of the research is to analyse the effect of flow maldistribution in different evaporators for industrial refrigeration systems with ammonia. As the minimization of refrigerant charge has become increasingly important in these systems, refrigeration engineers and equipment manufacturers are developing new ways to control the evaporator overfeeding or circulation ratio close to unity. These efforts bring along challenges regarding flow maldistribution and possibly large superheated or unused heat exchanger areas in the evaporators. In the current research, we simulated the refrigerant flow distribution numerically in order to understand the consequences in terms of cooling capacity for different tube circuitries as the recirculation ratio was reduced towards unity. The different tube circuitries involved two bottom-fed evaporators (a traditional straight through and a crossover or interlaced circuitry) and one side-fed evaporator with and without inlet orifices to outbalance the liquid column in the inlet header, see Figure 57.

The objective is to study the penalties in terms of cooling capacity associated with flow maldistribution as the recirculation ratio approaches unity. The different evaporators are

exposed to non-uniform airflow profiles at various recirculation ratios. Furthermore, the effect of inlet orifices is investigated for the side-fed evaporator, where they are employed. The evaporators are specified in Kristófersson et al., (2017a). The inlet liquid temperature and the outlet saturation temperature are fixed at -30 °C, corresponding to a pumped recirculation system at the same receiver temperature. Furthermore, the total air volume flow rate is kept constant.

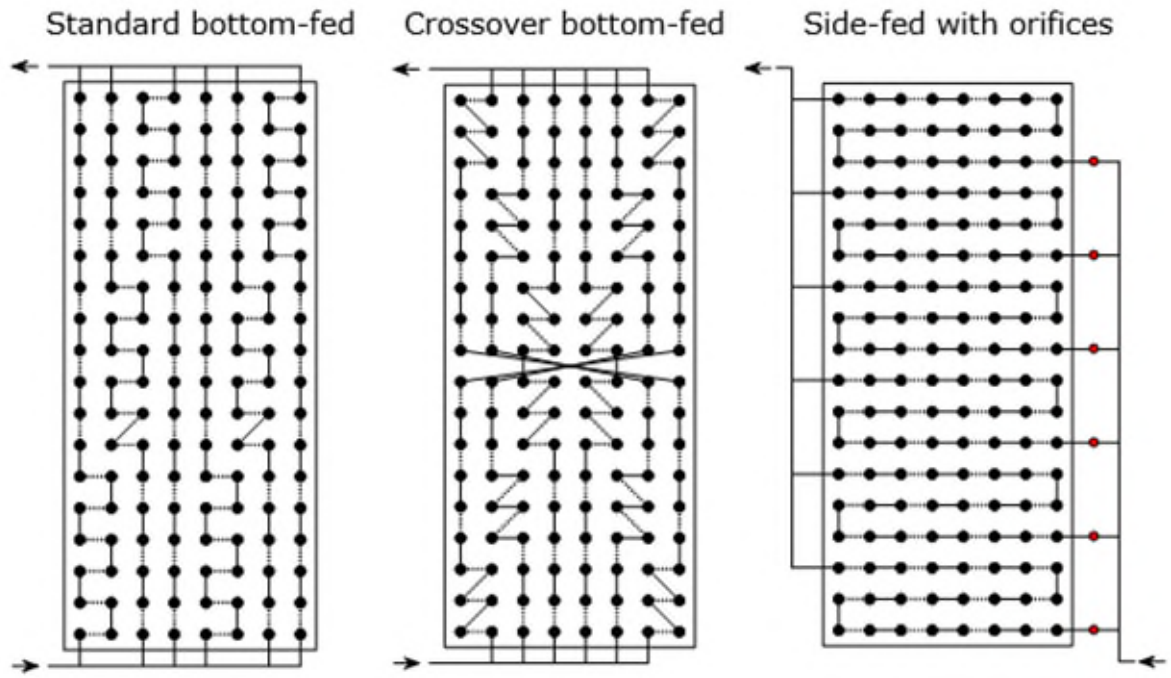


**Figure 57: Sketch of the evaporator circuitries, airflow from left, red symbols indicate orifices.**

## 5.2.2. Numerical model

The model of the evaporator circuiting was originally implemented in Dymola 7.4 as presented in Kærn (2011), but has been rewritten in Matlab2017a in order to control and speed-up the solution methodology. Thermophysical properties of R717 were obtained from CoolProp 4.2, while air properties were obtained using the ideal gas equation and polynomials based on CoolProp 4.2 at 1 atm. Each finned tube was divided into a number of cells for both the refrigerant and the air, where one-dimensional cross flow was assumed on both sides. The air and refrigerant cells were then connected and solved by tracking first the airflow paths and second the refrigerant flow paths (see Figure 57), while successively substituting the wall temperature until the energy balances converged for each tube cell:

$$\begin{aligned}\dot{Q}^{(j,k)} &= \dot{m}_r^{(i)}\left(h_r^{(j,k+1)} - h_r^{(j,k)}\right) = \alpha_r^{(j,k)} A_{r,s}^{(j,k)}\left(T_w^{(j,k)} - \tilde{T}_r^{(j,k)}\right) \\ &= C_{min}^{(j,k)}\left(T_{a,in}^{(j,k)} - T_{a,out}^{(j,k)}\right) = \varepsilon_a^{(j,k)} C_{min}^{(j,k)}\left(T_{a,in}^{(j,k)} - T_w^{(j,k)}\right)\end{aligned} \quad (1)$$

Here "*i*" denotes the number of circuits, "*j*" denotes the number of tubes, and "*k*" denotes the number of cells per tube. $\varepsilon_a^{(j,k)}$ denotes the effectiveness and was computed by the effectiveness-NTU relation for evaporators with $\mathrm{NTU}^{(j,k)} = \alpha_a^{(j,k)}\eta_{a,o}^{(j,k)}A_{a,s}^{(j,k)}/C_{\min}^{(j,k)}$, where $\alpha_a$ and

$\eta_{a,o}$ denote the heat transfer coefficient and overall surface efficiency on the airside, respectively. The model neglects heat transfer resistance in the tube wall as well as fouling on the fluid surfaces. Additionally, upwinded approximations of cell center/average variables ($\tilde{\psi}_i$) were used. The local heat transfer and pressure drop were computed for the refrigerant flow in tubes and bends including friction and gravitational pressure drop. Gravitational pressure drop was also computed at the inlet and outlet headers for the side-fed evaporator as well as the pressure drop caused by the inlet orifices. We used general well-known or dedicated correlations for ammonia where applicable as indicated in Table 3. An outer iteration loop was constructed to solve for each circuit outlet pressures (corresponding to fixed outlet saturation temperature) and recirculation ratio by adjusting each circuit mass flow rate and inlet pressure, respectively. Furthermore, the model has been validated with experimental results presented in Kristófersson et al. (2017a), assuming uniform airflow.

**Table 3. Employed correlations for air and refrigerant**

| | | |
|---|---|---|
| Air | Heat transfer coefficient | Kim and Kim, 2005 |
| Refrigerant single-phase | Heat transfer coefficient | Gnielinski, 1976 |
| | Tube friction | Blasius, 1913 |
| | Bend friction | Ito (1960) |
| | Orifice friction | Idel'chik (1966) |
| Refrigerant two-phase | Heat transfer coefficient | Fenton, 1999 |
| | Tube friction | Müller-Steinhagen and Heck, 1986 |
| | Bend friction | Geary (1975) |
| | Void fraction | Zivi, 1964 |

### 5.2.3. Conditions and imposed maldistribution

The refrigerant outlet pressure boundary was fixed by the outlet saturation temperature of -30 °C. Furthermore, the inlet enthalpy was fixed at the bubble point corresponding to the outlet saturation temperature, and the total mass flow rate was fixed by the recirculation ratio $N_{RR} = {x_{\text{out}}}^{-1}$. These refrigerant boundary conditions correspond to pumped circulation systems with a small amount of inlet liquid subcooling due to refrigerant pressure drop. The inlet air temperature and volume flow rate were always -20 °C and 19390 $m^3$/hr, the latter estimated by using the energy balance obtained from the measurements. Moreover, the flow was distributed across the evaporator using a one-dimensional velocity profile in the transverse direction $y$:

$$u_a(y) = \bar{u}_a F - y\frac{2\bar{u}_a(1-F)}{L_t} \tag{2}$$

When the $F$ factor is unity, the air flow is distributed evenly across the evaporators. When $F = 0$, the velocity tends to zero at the top and $2\bar{u}_a$ at the bottom, and vice versa at $F = 2$. In this work, F was varied from 0.5 to 1.5.

### 5.2.4. Main geometry

The main geometry of the evaporators is given in Table 4. The tube and fin materials are AISI 304 and aluminum, respectively, and the fins are wavy. All the geometric parameters are identical except for the tube circuiting and header/orifice arrangement. The orifices were only necessary for the side-fed evaporator, where the liquid column is sought to be compensated to ensure a good distribution. Two different orifice diameters were simulated:

$$d_{o,v1}^{(i)} = [2.40, 2.20, 2.20, 2.00, 2.00, 2.00]$$
$$d_{o,v2}^{(i)} = [1.90, 1.68, 1.53, 1.41, 1.31, 1.23] \quad (3)$$

Where i denotes the circuit number from top to bottom. These orifice diameters were based on a manufacturers calculation for optimal orifice diameters at a recirculation ratio of 3. In the first set, a minimum orifice diameter was chosen to be 2 mm, while the second set had no size limitations. The smallest orifice diameters are placed in the bottom of the inlet header. The header tube diameter was assumed to be 28.5 mm. Furthermore, the fin spacing was 12 mm to accomodate freezing conditions, however, the model assumed dry air conditions always for simplicity. No particular consideration was addressed towards the frost build-up throughout the investigation and may be addressed once the dry conditions results have been obtained.

**Table 4. Baseline heat exchanger specifications**

| | | | |
|---|---|---|---|
| Tube arrangement | Inline | Tube outer diameter | 15.6 mm |
| Tube rows | 8 | Longitudinal tube pitch | 50 mm |
| Tubes per row | 18 | Transverse tube pitch | 50 mm |
| Tube circuits | 6 | Fin spacing | 12 mm |
| Tube length | 1360 mm | Fin thickness | 0.35 mm |
| Tube inner diameter | 14.6 mm | Tube coil volume | 34.5 L |
| Fin spacing | 12 mm | | |

### 5.2.5. Results

Figure 58 shows the results of the simulations of the three evaporators and includes also the side-fed evaporators with the 2 sets of orifices as given in Equation 3. At recirculation ratios larger than 1.5, the evaporators perform rather similar, since all the refrigerant circuits are within the two-phase domain. The two bottom-fed evaporators perform slightly better at higher $F$ factor than one. This is because the bottom tube layer, where the refrigerant is in a subcooled state having a low heat transfer coefficient, is less affected by a lower airflow passing, resulting in less penalty on the cooling capacity.

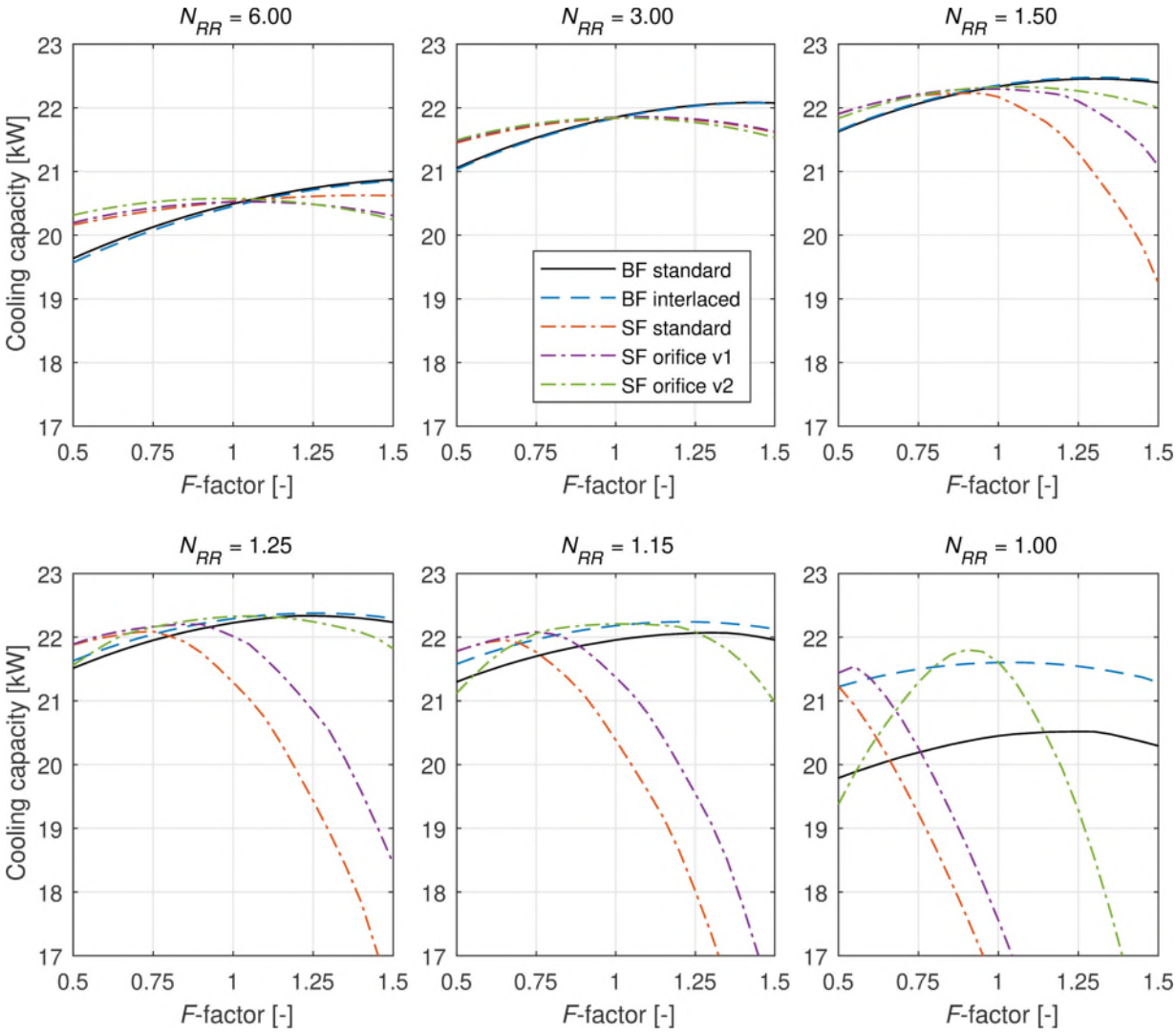


**Figure 58: Cooling capacity vs. $F$-factor for different recirculation ratios.**

As the recirculation ratio was decreased, the side-fed evaportor, with and without the 2 sets of orifices, starts to decrease in cooling capacity. This decrease is due to superheated areas starting to appear in the top part of the evaporator, see Figure 59b. The penalty is worse for the side-fed evaporator without inlet header orifices to balance the flow. In fact, the liquid column is causing a higher inlet pressure in the bottom circuit and a lower inlet pressure in the top circuit, which means that more refrigerant mass flows through the bottom circuit rather than the top circuit. Thus, the top circuits become superheated and even more as the *F* factor increases and more air flows through the top of the evaporator. On the other hand, as the *F* factor decreases, the higher air flow is balancing the higher refrigerant mass flow rate at the bottom of the evaporator, see Figure 59a.

Refering to Figure 58, the standard side-fed evaporator (SF standard) results in cooling capacity penalties even at uniform airflow due to refrigerant maldistribution as the recirculation ratio decreases below 1.5. Likewise, the side-fed evaporator with largest orifice diameters (SF orifice v1) experience a drop in capacity as the recirculation ratio decreases below 1.25. It is only the side-fed evaporator with the smallest set of orifices (SF orifice v2) that appears to work properly as the recirculation ratio approaches the unity. However, the balancing of the liquid column at these low refrigerant flow rates as well as

operating close to the vapor region seems to make this evaporator vulnerable to airflow maldistribution as indicated by the rather narrow peak in Figure 58 at $N_{RR}$ = 1. The bottom-fed evaporators appear more robust to airflow maldistribution and perform evenly at most recirculation ratios. However, as the recirculation ratio approaches the unity, the standard bottom-fed evaporator experiences a large superheated area in the top front. This superheated area is practically speaking eliminated by using the bottom-fed crossover circuitry, which results in a balancing of the temperature approah for each circuit as well as a balancing of any airflow maldistribution.

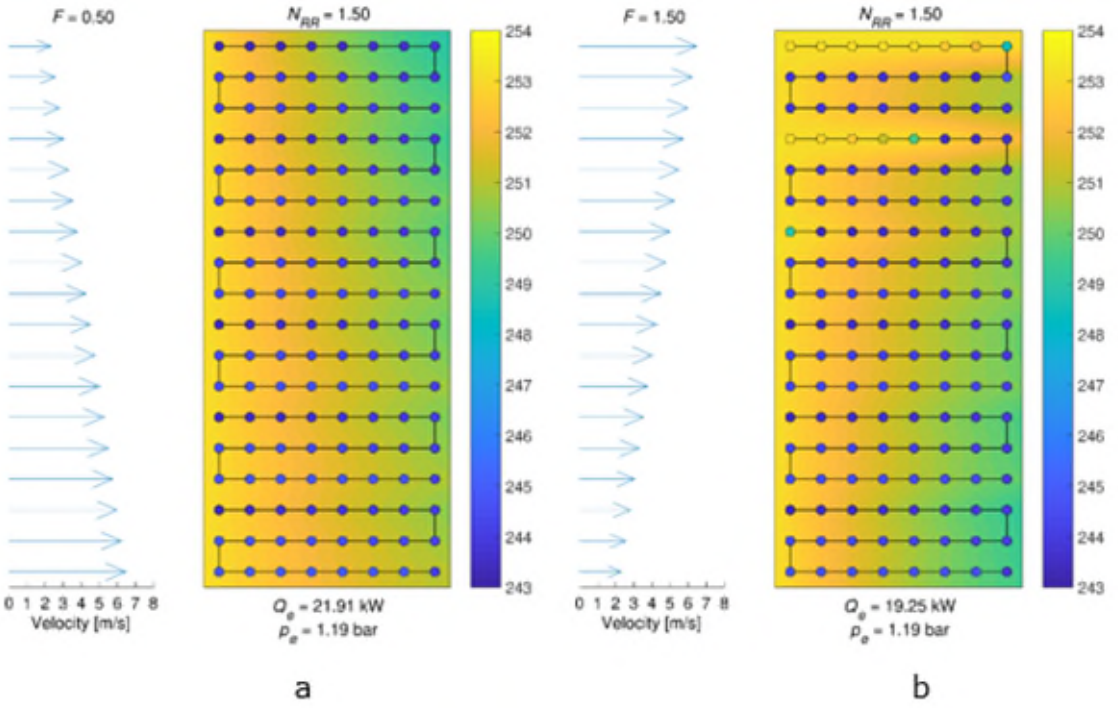


**Figure 59: Air and refrigerant temperature maps (K) through middle of side-fed evaporator without orifices.**

## 5.2.6. Discussion

The presented results serve as guidelines for evaporator manufacturers and control equipment suppliers. The results show how the cooling performance of three different evaporator types is affected by air and refrigerant flow maldistribution as the recirculation rate is decreased towards unity. It appears that the side-fed evaporators are difficult to operate properly at very low recirculation rates and mass flow rates. Moreover, the orifice sizes required to balance the liquid column at these low mass flow rates decrease to approach impractical small sizes and create a risk of orifice clogging as well as difficulties to handle hot gas defrosts.

On the other hand, the bottom-fed evaporator with crossover circuiting performs very well, even at a recirculation ratio of unity and non-uniform airflow distribution. It is imperative to have a refrigerant distribution that does not result in large superheated areas at the outlet of the evaporator, which has been the main reason for penalties in terms of cooling capacity for all our simulations.

The simulations showed that the bottom-fed evaporators performed the best considering the reductions in recirculation ratios and imposed airflow maldistribution. The crossover tube circuiting resulted in high cooling capacities at all imposed airflow maldistribution and recirculation ratios. The side-fed evaporators revealed some difficulties to handle the balancing of the refrigerant flow distribution, especially as the recirculation ratio decreased and turned out to be vulnerable to the imposed airflow maldistribution here too. Moreover, the size of the inlet header orifices appear to be a crucial point for balancing the liquid column in vertical inlet headers for side-fed evaporators.

### 5.2.7. Multi-objective optimization (heat transfer area vs. charge)

Multi-objective optimization of the traditional finned-tube evaporator design was also carried out. The work focussed on the charge minimization in liquid overfeed systems by exploring the effect of key evaporator design parameters numerically. The considered parameters were transverse tube pitch, longitudinal tube pitch, tube diameter and number of tube circuits as well as recirculation ratio. The main research question was whether the optimal design of the evaporator changes as recirculation ratio decreases?

The objective was to minimize the ammonia charge as well as the evaporator cost, here exemplified by heat transfer area, by employing a multi-objective genetic algorithm to optimize a numerical model of the evaporator. The bottom-fed evaporator was used as the baseline for the optimization. The cooling capacity, air-volume flow, and frontal area were fixed to the baseline values and provide the same cooling load and air throw length in a given cold store for each solution of the optimization. Moreover, the required heat transfer area was solved for at each combination of heat exchanger design parameters (transverse tube pitch, longitudinal tube pitch, tube diameter), and the optimization was carried out at several recirculation ratios and number of tube circuits. Furthermore, the airside pressure drop was constraint to less than 55 Pa, and the fin spacing was fixed at 12 mm to accommodate freezing conditions.

The model was very similar to the previous model detailed in Section 5.2.2. The main difference was that the tube circuiting was idealized for the purpose of numerical speed for the optimization procedure.

### 5.2.8. Optimization procedure

The multi-objective genetic algorithm in Matlab2017a is employed. This algorithm uses a controlled, elitist genetic algorithm that favors individuals that can help increase the diversity of the population even if they have a lower fitness value. We used default options and recommended values for the population size etc. The multi-objective functions, decision variables, lower and upper bounds were:

$$F(x) = min[Area(x), charge(x)]$$
$$x = [X_l, X_t, d_o]$$
$$lb = [0.034\ mm, 0.034\ mm, 0.012\ mm]$$
$$ub = [0.060\ mm, 0.060\ mm, 0.018\ mm]$$

Notice that we fixed the recirculation ratio ($N_{rc}$) to 1.25, 2, 3 and 6 and the number of tube circuits ($N_{tc}$) to 6, 9 and 12, respectively, to better observe and visualize the optimal

geometry as function of recirculation ratio and number of tube circuits. This resulted in 4x3 optimization runs. Again, the airside pressure drop was constraint to less than 55 Pa, as the baseline airside pressure drop was calculated to be 54 Pa.

### 5.2.9. Results

Figure 60 and Figure 61 show the pareto fronts of the optimizations (minimizations) of area and charge for each recirculation ratio ($N_{rc} = 1.25, 2, 3 \text{ and } 6$) and the number of tube circuits ($N_{tc} = 6, 9 \text{ and } 12$), respectively. The results were obtained at a fixed cooling capacity of 22.5 kW, saturation temperature of -30 °C and inlet air temperature of -20 °C. The capacity corresponds to the maximum value of the baseline capacity curve. The colors of the pareto fronts in Figure 60 and Figure 61 indicate airside pressure drop (a), tube outer diameter (b), longitudinal tube pitch (c) and transverse tube pitch (d). Furthermore, the baseline calculation is indicated by a red filled circle. Figure 62 and Figure 63 show corresponding pareto fronts, where colors indicate longitudinal heat exchanger length (a), number of total tubes (b), gas velocity (c), and liquid velocity (d).

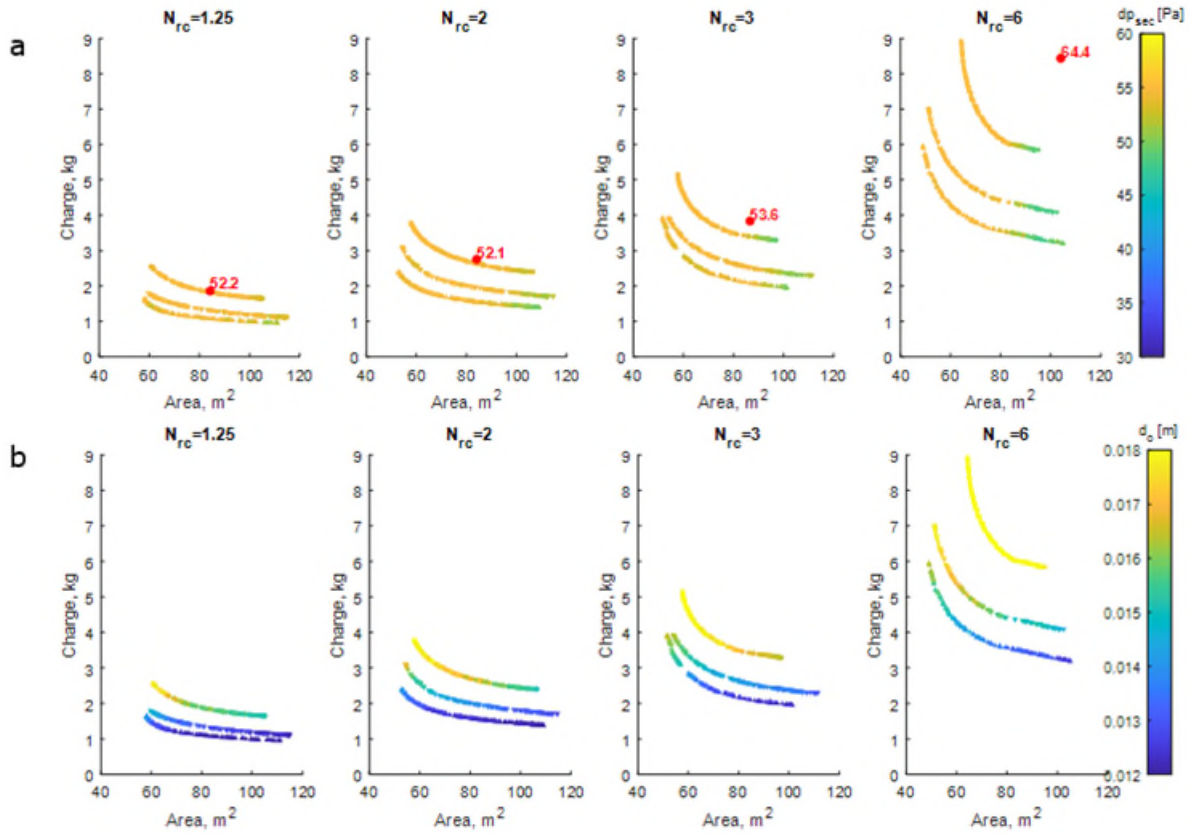


**Figure 60: Charge vs. area pareto fronts at 4 recirculation ratios and 3 numbers of tube circuits. Colors represent airside pressure drop (a) and tube diameter (b).**

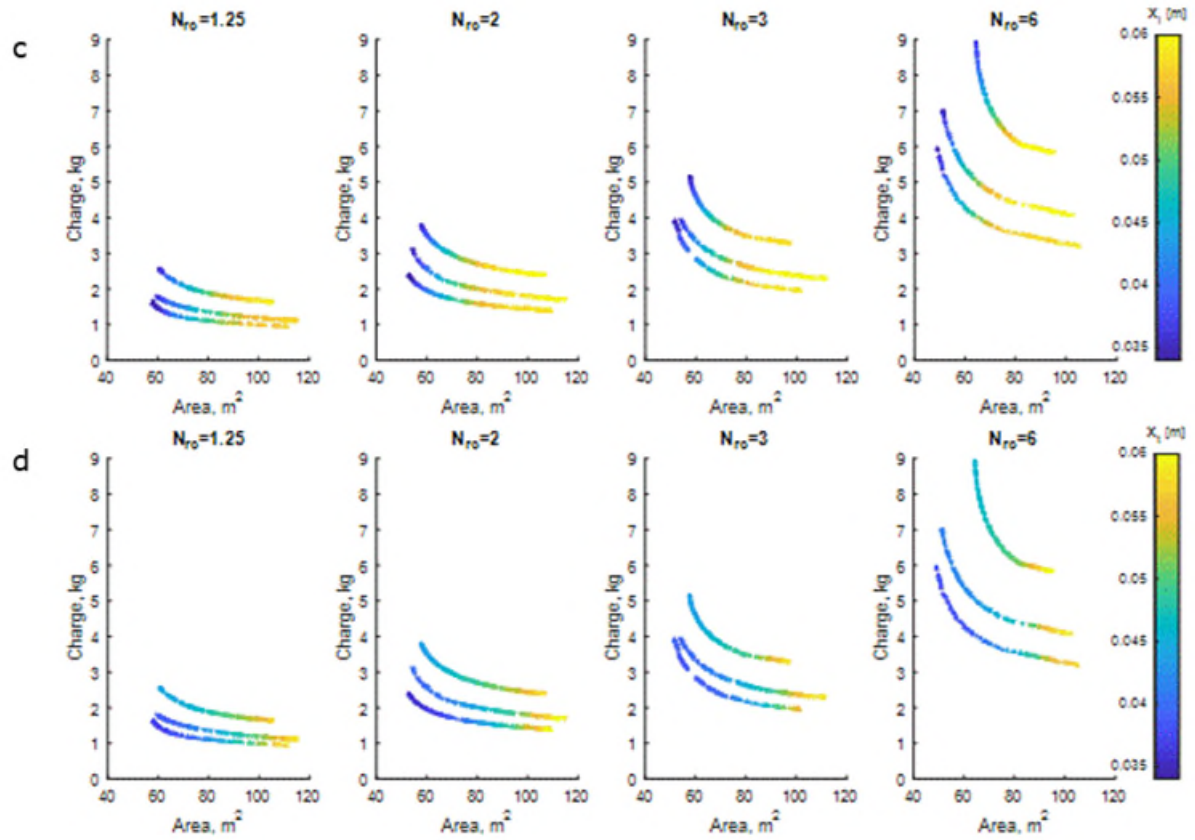


**Figure 61: Charge vs. area pareto fronts at 4 recirculation ratios and 3 numbers of tube circuits. Colors represent longitudinal tube pitch (c) and transverse tube pitch (d).**

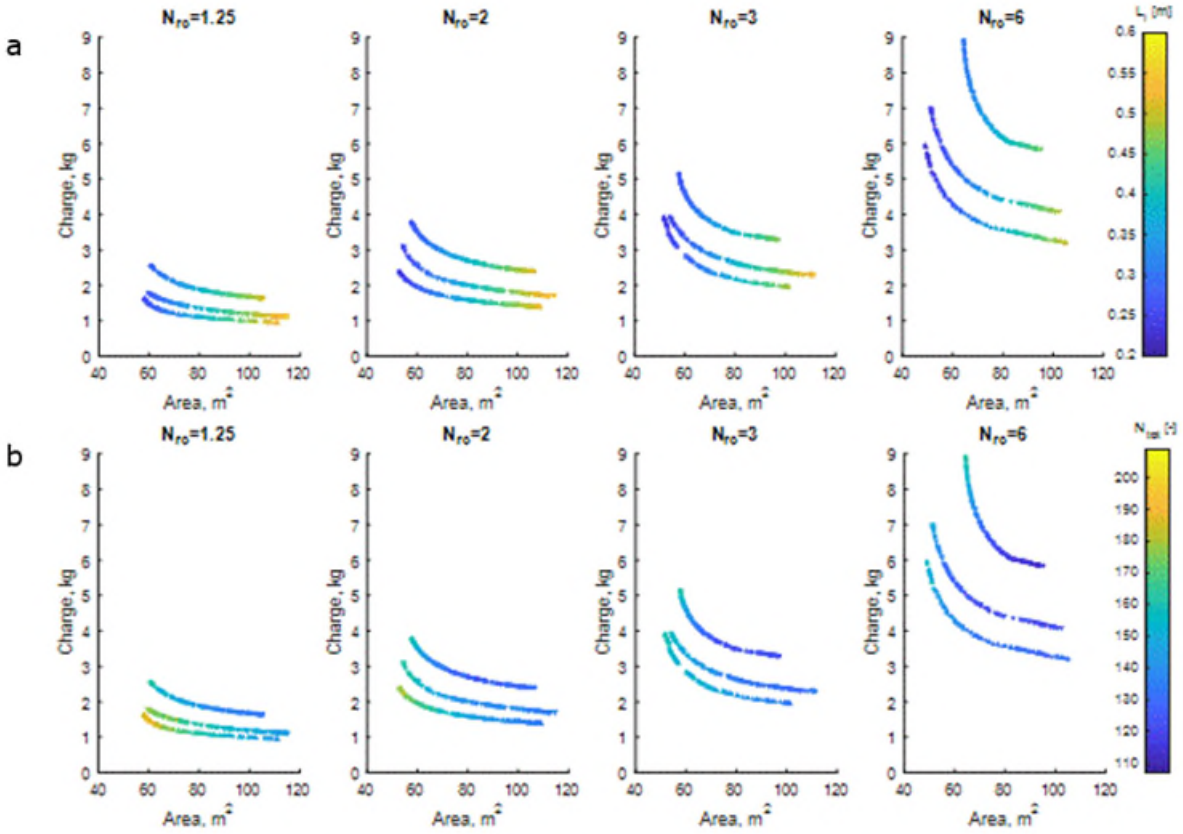


**Figure 62: Charge vs. area pareto fronts at 4 different recirculation ratios and 3 numbers of tube circuits. Colors represent longitudinal HX length (a) and number of total tubes (b).**

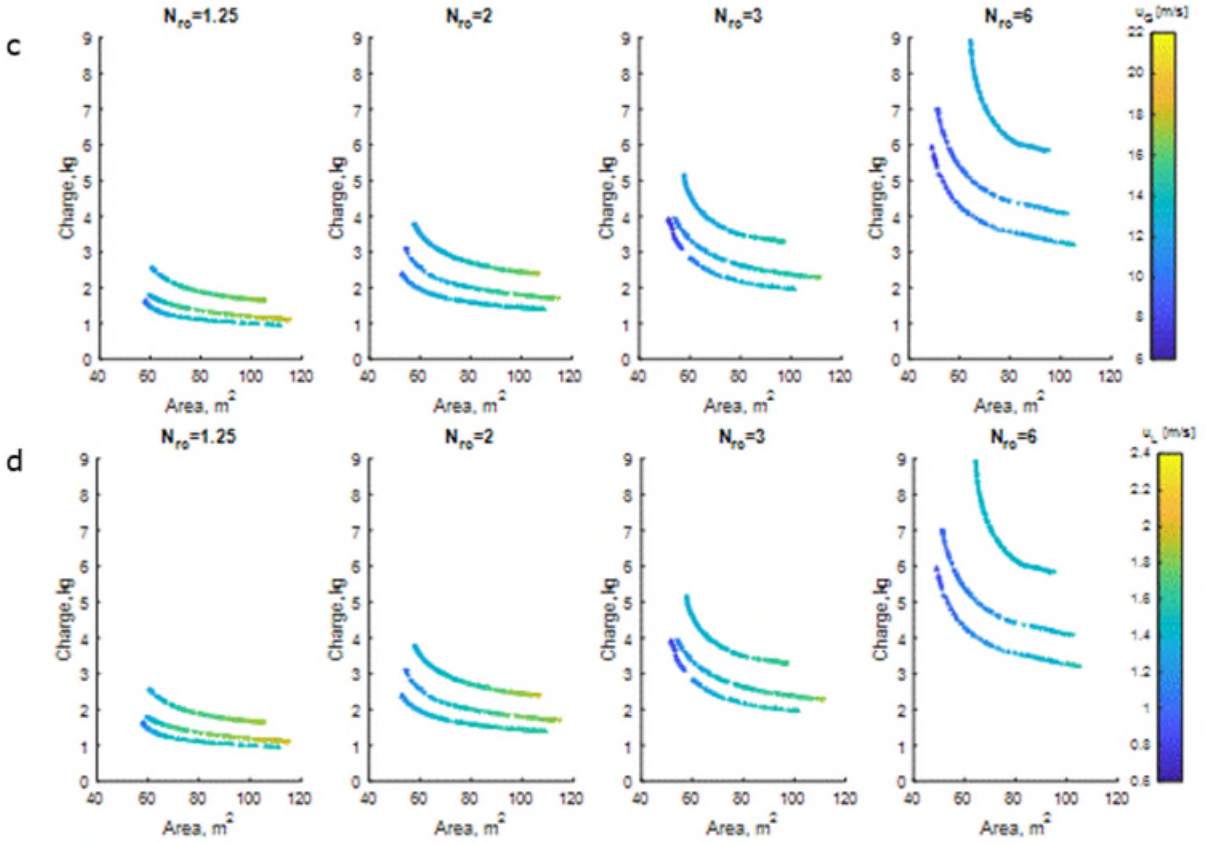


**Figure 63:Charge vs. area pareto fronts at 4 different recirculation ratios and 3 numbers of tube circuits. Colors represent gas velocity (c) and liquid velocity (d).**

The results show that a decrease in recirculation ratio from 6 to 1.25 decreases the charge significantly. A further reduction is possible, if the tube diameter is reduced (following the pareto front, Figure 60b), but comes with an increasing heat exchanger area (longitudinal length increase, Figure 62a), and the transverse tube pitch (Figure 61d) increases as well. If both the diameter is decreased toward 12 mm and the number of tube circuits is increased from 6 to 12, a further reduction of the charge is possible even with a smaller heat exchanger area. This is especially an important result because it indicates that the charge and the cost of the heat exchanger, assuming that the heat transfer area is proportional to the heat exchanger cost, can be reduced simultaneously, although the total number of tubes increases (see Figure 62b).

The pareto fronts tend to become flat as the recirculation ratio decreases, but it is likely due to the lower bound of the longitudinal tube pitch and tube diameter (Figure 60b and Figure 61c), which in principle could have been lower and, thereby given, rise to even lower heat transfer areas or lower refrigerant charge.

Interestingly, the baseline geometry is optimal at a low recirculation ratio and 6 tube circuits and falls directly on top of the pareto front. However, as the recirculation ratio increases, the baseline geometry gets further away from the pareto front. It should be noted that the model solves for the required longitudinal length of the heat exchanger in order to deliver the required cooling capacity. This is why the airside pressure drop increases as the recirculation ratio increases too (Figure 60a, text in red).

Two very important evaporator design parameters are the gas and liquid velocities, respectively, as shown in Figure 63c and Figure 63d and calculated at the evaporator outlet with the slip ratio correlation by Zivi. Because Zivi assumes a constant slip ratio, the values in these two figures differ by the slip ratio directly, calculated to be 9. These values (Figure 63c and Figure 63d) do not seem to decrease significantly as the recirculation ratio decreases, and it ensures that oil is not retained inside the evaporator as well as a reasonable heat transfer coefficient. Moreover, general rule of thumb indicate on the order 10 m/s for gaseous ammonia (Granryd et al., 2009).

## 5.2.10. Discussion

The presented results serve as guidelines for evaporator manufacturers and control equipment suppliers. The results show how the main geometry (tube outer diameter, longitudinal tube pitch and transverse tube pitch) changes with the recirculation ratio as well as the number of tube circuits. It is difficult to point directly at a specific optimal point on the pareto front, and this is likely a subjective choice depending on a choice of trade-off between charge and heat exchanger area.

Some tools exist to analytically calculate knee points of pareto fronts, which provides a compromise between the two objective functions. In the current study, the knee does not reveal exactly at the lowest recirculation ratio (1.25) and highest number of tube circuits (12), because the lower bound of the longitudinal tube pitch is reached. Choosing a point close to an imaginable knee, say a 70 m$^2$ area, corresponds to 1.20 kg charge, and $X_t$ = 38.5 mm, $X_l$ = 43.4 mm, $d_o$ = 12.3 mm, $N_l$ = 7.4 (7), $N_t$ = 23.4 (23) and $\Delta p_{\text{air}}$ =54.7 Pa. This result shows that the optimized evaporator is more compact compared to the baseline evaporator. However, it should also be noted that the proposed evaporator is more prone to have refrigerant mal-distribution. A close tube circuiting based on this geometry is illustrated in Figure 64.

The methodology used herein provides 12 pareto fronts for several recirculation ratios and number of tube circuits. If these values were included in a single optimization, and the genetic algorithm would converge at the lowest recirculation and the highest number of tube circuit constraints, it would not indicate a reasonable overview of the effect of these important parameters.

The multi-objective optimization showed that a large reduction of refrigerant charge is possible by considering solely the recirculation ratio. If a further reduction of charge is favoured, a simultaneous reduction of the tube diameter as well as an increase of tube circuits are necessary, and it is even possible with a decreased heat exchanger size and volume. Furthermore, the gas and liquid velocities at the outlet of the evaporator do not raise concerns about possible oil retention or weak two-phase heat transfer.

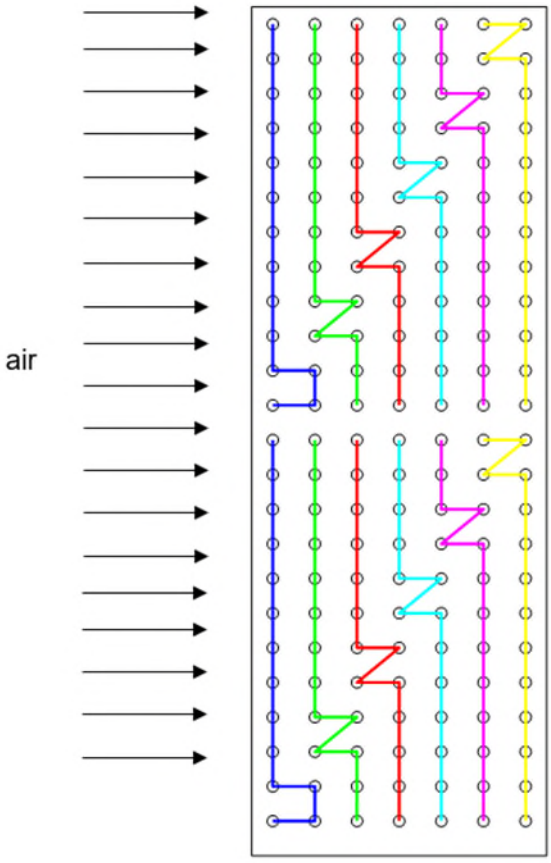


**Figure 64: Optimized tube circuiting. X_t= 38.5 mm, X_l= 43.4 mm, d_o= 12.3 mm, N_l= 7, N_t= 24.**

## 5.3. The micro channel solution

Micro channel heat exchangers are attractive due to their high heat transfer area vs. internal volume ratio. In recent years, they have gained increased market shares in many small-scale refrigeration applications as air-cooled condensers, because of better thermo-hydraulic performance compared with traditional finned-tube heat exchangers. However, their use as evaporators is challenged by (1) airside water condensate retention with weak water drainage during defrost and (2) poor refrigerant distribution. The research aims to solve these challenges while maintaining high heat transfer performance and cost-competitiveness. A recent development by Sapa Precision Tubing offers a compromise between compactness and condensate retention, claiming a reduction of 90 % water retained using a webbed micro channel profile evaporator design (WEB-MPE™) with water drain passages between each port. The design is novel, which means that airside correlations for heat transfer and pressure drop do not exist in the open literature. Numerical modeling and fin design investigations were carried out to optimize the thermal-hydraulic design.

Two papers were published on this subject (Rogie et al., 2019; Rogié et al., 2020) during the project, and a paper on the experimental results is pending for the Gustav Lorentzen International Conference in 2022.

### 5.3.1. Target design

The microchannel design is made from extruded aluminum profiles (WEB-MPE, see Figure 65) and pressed sheets (extended surfaces, fins) to balance the poor heat transfer of the airside and the good heat transfer of the boiling refrigerant. Based on CFD simulations of the airside thermo-hydraulic performance and reduced order models of the heat transfer and pressure drop, total heat exchanger calculations were carried out to obtain the most suitable design for the experimental investigation. Triangular fins were chosen in the end as indicated in Figure 66.

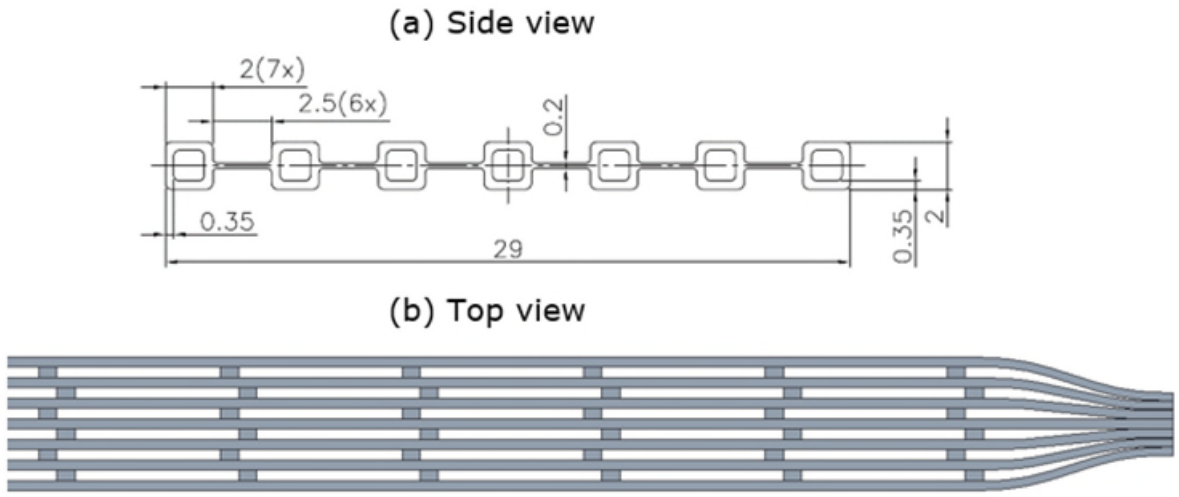


**Figure 65: Extruded aluminium profile before punching (a) and after punching (b).**

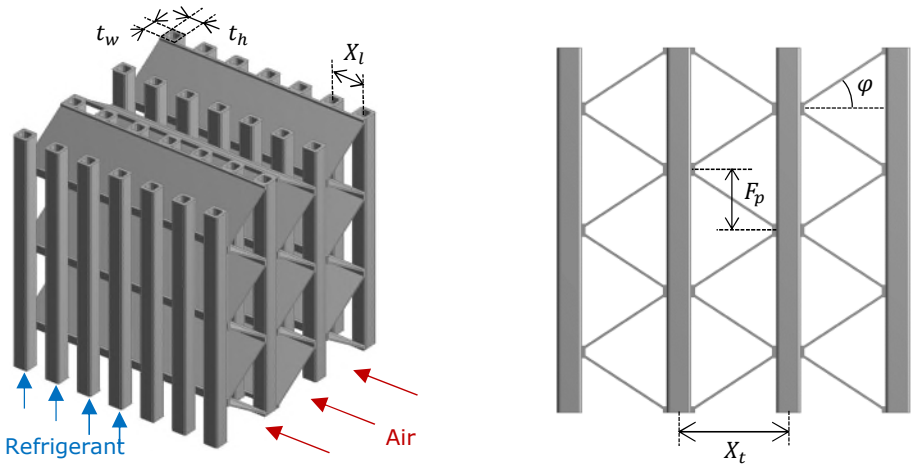


**Figure 66: 3D model of the micro channel heat exchanger (7 channels, 4 rows).**

### 5.3.2. CFD simulation results

The CFD simulations bring extensive knowledge of the flow behavior inside the micro channel evaporator and provides local data, which is challenging and possibly subject to high uncertainties with an experimental setup. The CFD simulations were carried out using the commercial software ANSYS 19.1 with the CFX solver. In order to keep a reasonable simulation time, only a small part of the microchannel was modelled in the CFD simulations.

Symmetries were used where the geometry allowed for it. The 3D CFD model is shown in Figure 67. Moreover, only a single fin was included in the computational domain.

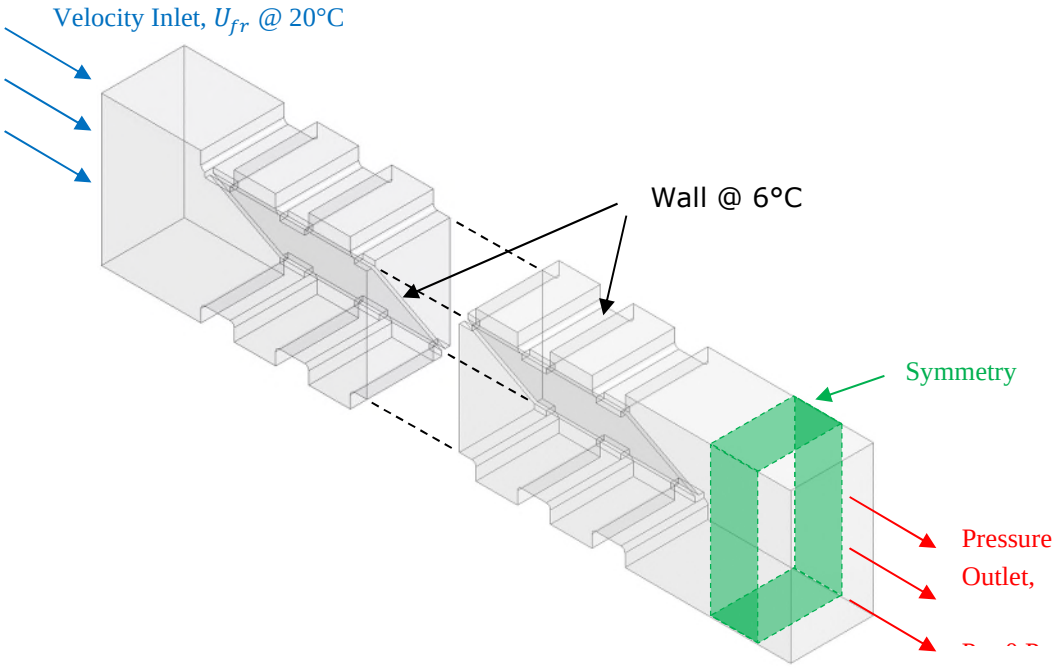


**Figure 67: 3D model of the simulated geometry (X_t = 9.00 mm, F_p = 5.00 mm, N_l = 35).**

The longitudinal velocity, the temperature and the static pressure contours are shown in Figure 68 and Figure 69, respectively, for the simulation: $X_t$ = 9.00 mm, $F_p$ = 5.00 mm, $U_{fr}$ = 4.40 m.s$^{-1}$. Figure 68 shows the contours at different locations of the heat exchanger, i.e., the two first tubes (entrance region), the 17$^{th}$ and 18$^{th}$ tubes (center) and the last two tubes (exit region), respectively. Figure 69 shows the contours at different minimum cross sections normal to the airflow, i.e., the first tube (entrance region), the 17$^{th}$ tube (center) and the last tube (exit region), respectively.

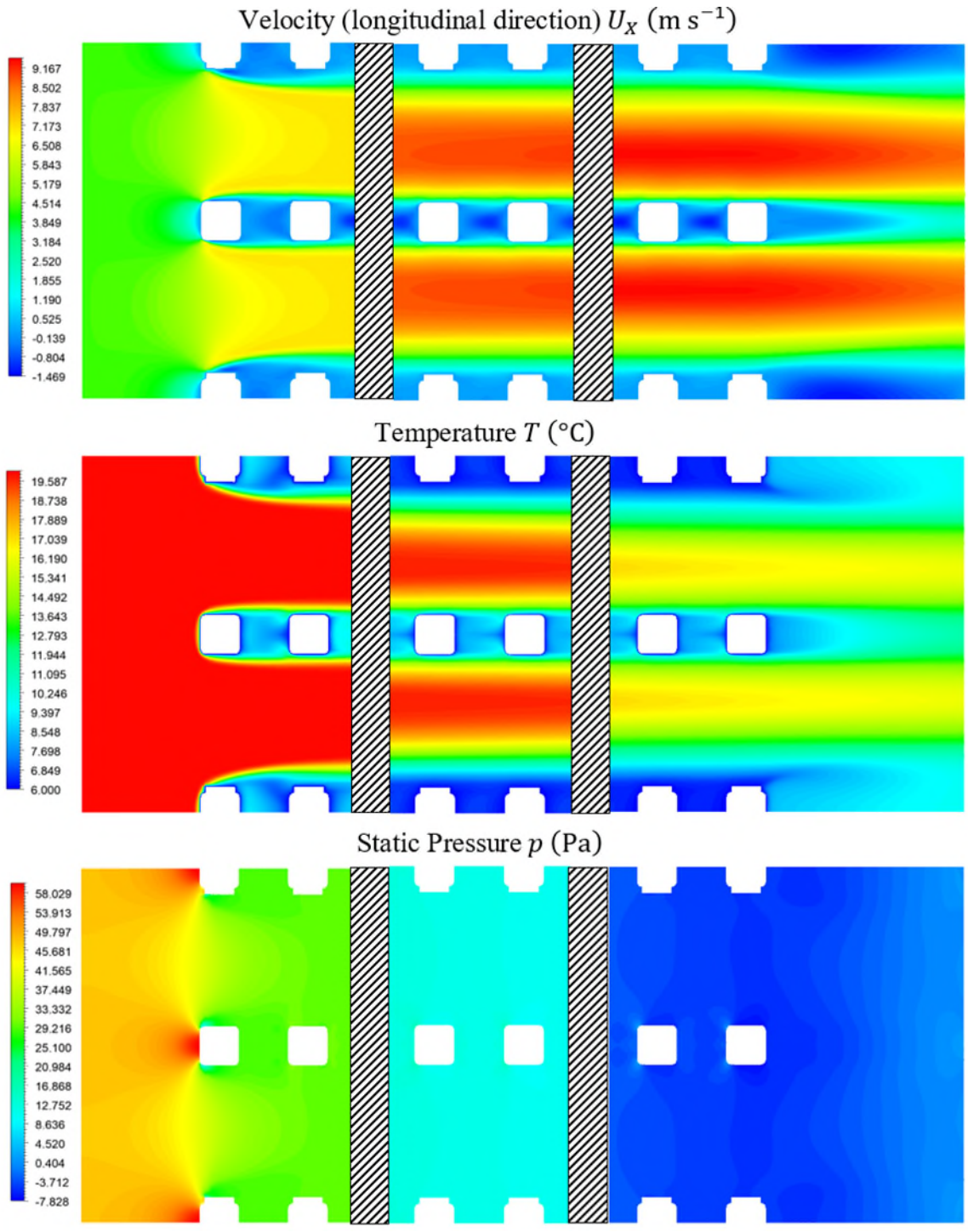


**Figure 68: Longitudinal velocity, temperature and static pressure contours at the entrance (left), middle (center) and exit (right); (side view); X_t = 9.00 mm, F_p = 5.00 mm, U_fr = 4.40 m.s-1.**

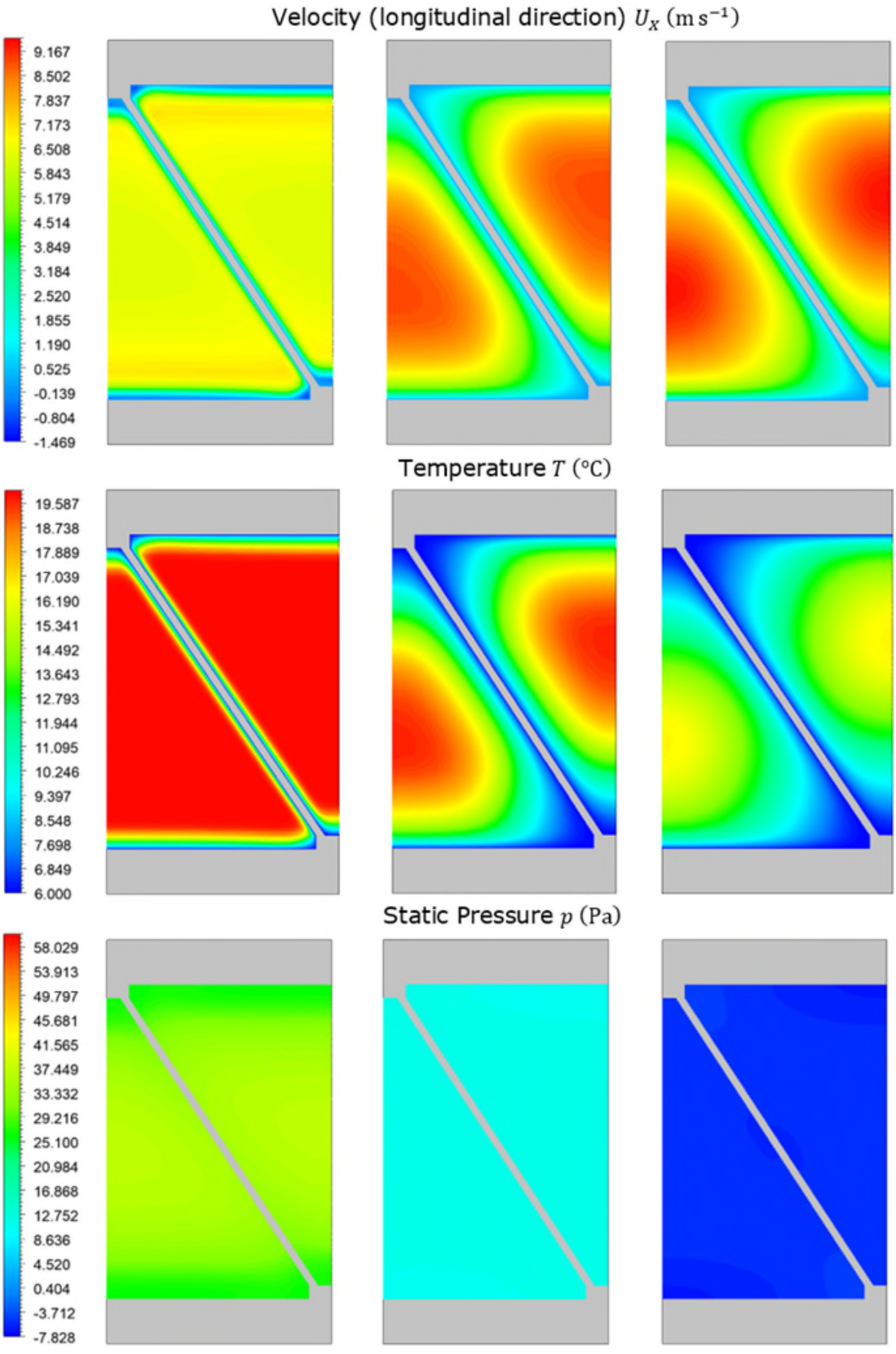


**Figure 69: Longitudinal velocity, temperature and static pressure contours at the entrance (left), middle (center) and exit (right); (frontal view); X_t = 9.00 mm, F_p = 5.00 mm, U_fr = 4.40 m.s-1.**

The velocity contours on Figure 68 and Figure 69 indicate that the flow develops and reaches an almost fully developed velocity contour at the center region compared with the exit region. The temperature contours indicate similarity at the center and the exit region, which also confirms that the flow becomes fully developed. Additionally, the pressure change during the inlet contraction and outlet expansion are easily observable in Figure 68.

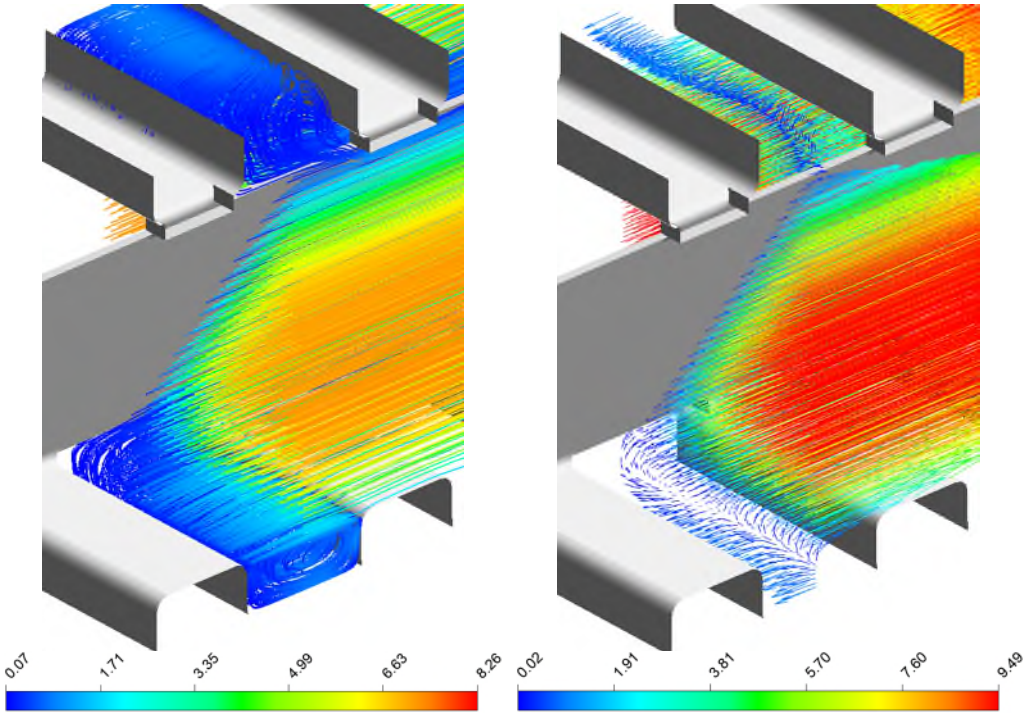


**Figure 70: Velocity streamlines (left), velocity vectors (right); X_t = 9.00 mm, F_p = 5.00 mm, U_fr = 4.40 m.s-1.**

Figure 70 indicates recirculation in the wake of the channels with a locally low heat transfer coefficient.

### 5.3.3. Reduced order models

The reduced CFD results in terms of Colburn j-factor and Fanning friction f-factor were regressed using multiple linear and non-linear regression techniques. Moreover, the asymptotic model was used to model the transition between the entrance region ($ent$) and the fully developed ($fd$) region, respectively,

$$y^n = {y_{ent}}^n + {y_{fd}}^n \tag{4}$$

where $y$ denote the Colburn j-factor or Fanning f-factor, respectively. Four non-dimensional parameters based on the hydraulic diameter were used to model the entrance and fully developed regions,

$$y_{ent} = b_1 \cdot {Re_{d_h}}^{b2} \cdot \left(\frac{L_l}{d_h}\right)^{b3} \cdot \left(\frac{X_t}{d_h}\right)^{b4} \cdot \left(\frac{F_p}{d_h}\right)^{b5} \tag{5}$$

$$y_{fd} = b_6 \cdot {Re_{d_h}}^{b7} \cdot \left(\frac{X_t}{d_h}\right)^{b8} \cdot \left(\frac{F_p}{d_h}\right)^{b9} \tag{6}$$

where $Re$ is the Reynolds number, $b_{1,2\ldots}$ regression coefficients and $d_h$ the hydraulic diameter given by,

$$d_h = \frac{4 \cdot A_c \cdot L_l}{A_{tot}} \tag{7}$$

Notice that the fully developed equation was independent longitudinally, in contrast to the entrance equation.

The regression procedure followed the four steps:

1. Linear regression of $y_{ent}$ based on the first 5 consecutive points longitudinally (the choice of 5 points was based on visual interpretation of the results),
2. Linear regression of $y_{fd}$,
3. Non-linear regression of $y$,
4. A repeated non-linear regression of the coefficients $b_1, b_2, b_3, b_4, b_5$ and $n$ in order to alleviate errors related to the visual interpretation in step 1.

Figure 71 illustrates the regression methodology for the j- and f-factor, respectively.

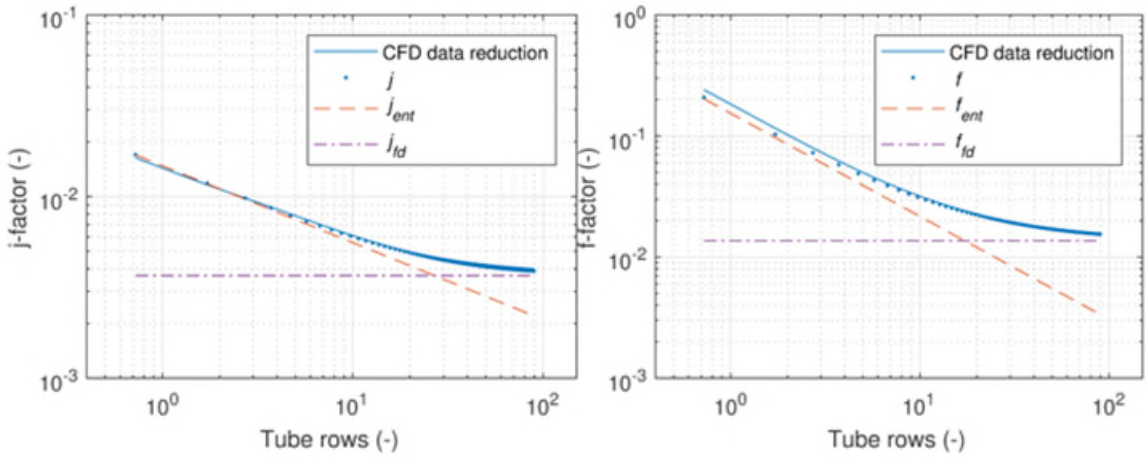


**Figure 71: Regression methodology for j-factor (left) and friction factor (right).**

Equations 15-17 resulted in very accurate correlations compared with the CFD simulation results. Table 5 indicates the coefficients to be used for the j- and f-factor correlations.

Table 5. Coefficients for the heat transfer and friction correlations

| Coefficient | j-factor | f-factor |
|---|---|---|
| $b_1$ | 0.8539 | 0.8665 |
| $b_2$ | -0.5433 | -0.2804 |
| $b_3$ | -0.4234 | -0.8512 |
| $b_4$ | 0.0424 | 0.1777 |
| $b_5$ | -0.0966 | 0.9961 |

| | | |
|---|---|---|
| $b_6$ | 0.0303 | 1.4393 |
| $b_7$ | -0.2697 | -0.5795 |
| $b_8$ | 0.1015 | -0.1196 |
| $b_9$ | 0.1095 | -0.2454 |
| $n$ | 3.1784 | 1.2611 |

The accuracy of the correlations cannot be guaranteed when the correlations are applied beyond the ranges of the simulation points. The ranges of the simulation points were as follows:

- $d_h = 3.45\ \text{mm} - 12.33\ \text{mm}$
- $Re_{d_h} = 481 - 4084$
- $X_t/d_h = 1.4 - 5.0$
- $F_p/d_h = 0.6 - 1.1.$

### 5.3.4. Evaluation

The volume goodness factor, defined for extended surfaces by Shah and Sekulic (Shah and Sekulic, 2003), is used to compare the micro channel geometries with the baseline finned-tube evaporator for industrial refrigeration. The volume goodness factor compares the heat transfer rate per unit temperature difference and unit core volume versus the friction power expenditure per unit core volume, both defined by:

$$\eta_o h\beta = \frac{c_p \mu}{Pr^{2/3}} \eta_o \frac{4\sigma}{{d_h}^2} j \cdot Re \tag{8}$$

$$E\beta = \frac{\mu^3}{2\rho^2} \frac{4\sigma}{{d_h}^4} f \cdot Re^3 \tag{9}$$

where $\eta_o$ is the overall surface efficiency calculated using the fin efficiency for rectangular fins, $\mu$ is the viscosity, and $E$ is the friction power per unit surface area.

Most correlations for finned-tube evaporators in the literature are developed for staggered tube layouts as pointed out by Webb and Kim (Webb and Kim, 2005). The correlations are typically developed for designs with lower fin pitch and a lower number of tube rows compared with the baseline finned-tube evaporator for industrial refrigeration. This complicates the choice of correlations to compare with our results. In the following comparison, the plain finned-tube correlations by Kaminski and Groß (Kaminski, S. Groß, 2000) are used to calculate the j- and f- factors and the overall surface efficiency, as outlined by Fraß et al. (F. Fraß, R. Hofmann, 2015). Figure 72 shows the comparisons of the microchannel evaporator having 35 tube rows and the baseline finned-tube evaporator having 8 tube rows.

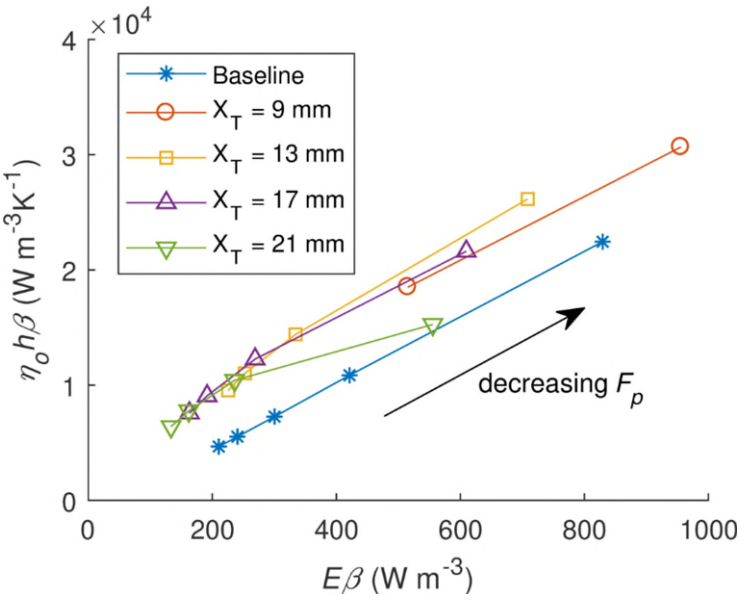


**Figure 72: Volume goodness factors for the micro channel evaporator geometries and the baseline finned-tube industrial refrigeration evaporator. (U_fr = 2.93 m s-1, N_l = 35 and 8, respectively).**

The volume goodness factors reveal that the micro channel evaporator is indeed more attractive than the baseline finned-tube evaporator, transferring more heat per unit volume at the same fluid flow power, and vice versa. In other words, the micro channel performs the best from the viewpoint of heat exchanger volume. There is, however, a single point ($X_t$ = 21 mm, $F_p$ = 2.5 mm) where the pressure drop of the micro channel evaporator increases more than the heat transfer and results in similar performance as the baseline finned-tube evaporator. This is mainly due to the low fin angle effects for this geometry. Furthermore, the variation of the number of tube rows had an insignificant effect on the volume goodness factor.

### 5.3.5. Other fin geometries

The above analysis on triangular fins was reported in Rogie et al. (2019). Other geometries were investigated in Rogié et al. (2020), i.e., straight fins, wavy fins, and offset fins. The straight fins and wavy fins do not offer extra pathways for the water to drain, unlike the other fin designs due to their discontinued geometry for the offset fins and inclination for the triangle fins. A portion of the evaporator is shown in Figure 73, including the triangular fin geometry.

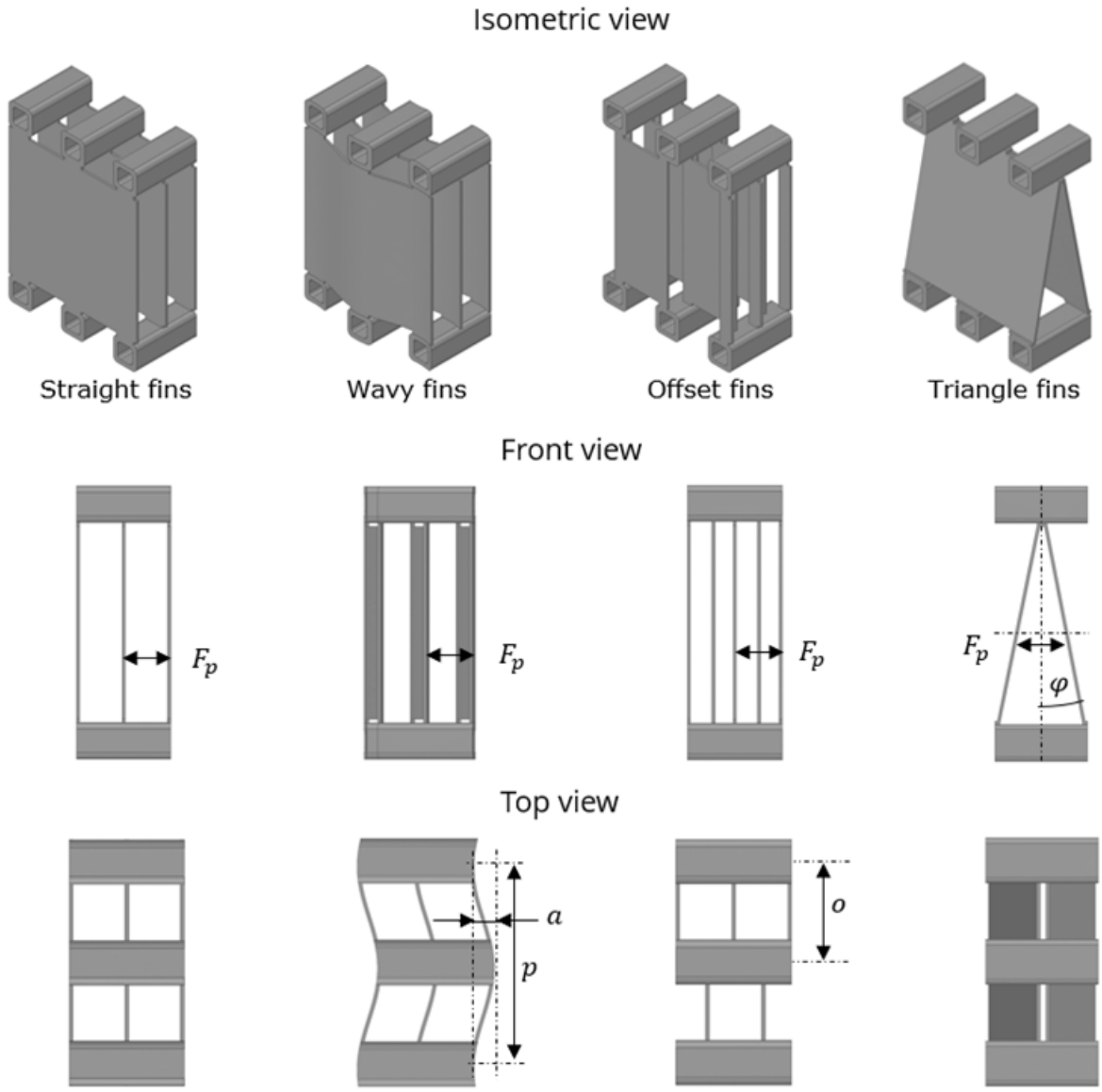


**Figure 73: Partial representation of the 3D models of the straight fins, wavy fins, offset fins, and triangle fins (X_p= 13 mm, X_p = 2.5 mm).**

The temperature profiles are shown in Figure 74 for all fin designs. The figure represents a partial view of the temperature field of the airside of the evaporator at row 17$^{th}$ and 18$^{th}$ (centre of the evaporator), where the flow is fully developed.

For the straight fins and the triangle fins, the temperature is uniform along the flow direction. This means that the heat is carried away from the channels and the fins by natural convection in the transverse and vertical directions. It results in lower heat transfer capability compared to fin geometries where obstacles or swirl generators are implemented, such as the wavy fins and the offset fins. The presence of obstacles or corrugations, which locally increase velocity and thermal gradients, causes change of direction of the flow, as it can be seen in Figure 74 and Figure 75, and therefore causes a change in the heat transfer coefficient. It is the reason why the average temperatures of the contour plots in Figure 74 are lower for wavy fins and offset fins, meaning that for the same conditions these fin designs offer a higher heat transfer rate. However, the

enhancement of local heat transfer coefficients results in higher friction factor and pressure drop, which counterbalances the benefits of these fin designs. Large recirculation zones can be observed in Figure 75 for the wavy fins due to the corrugations. Recirculation can also be observed in the wake of the channels due to the sudden change in cross section area for all fin designs.

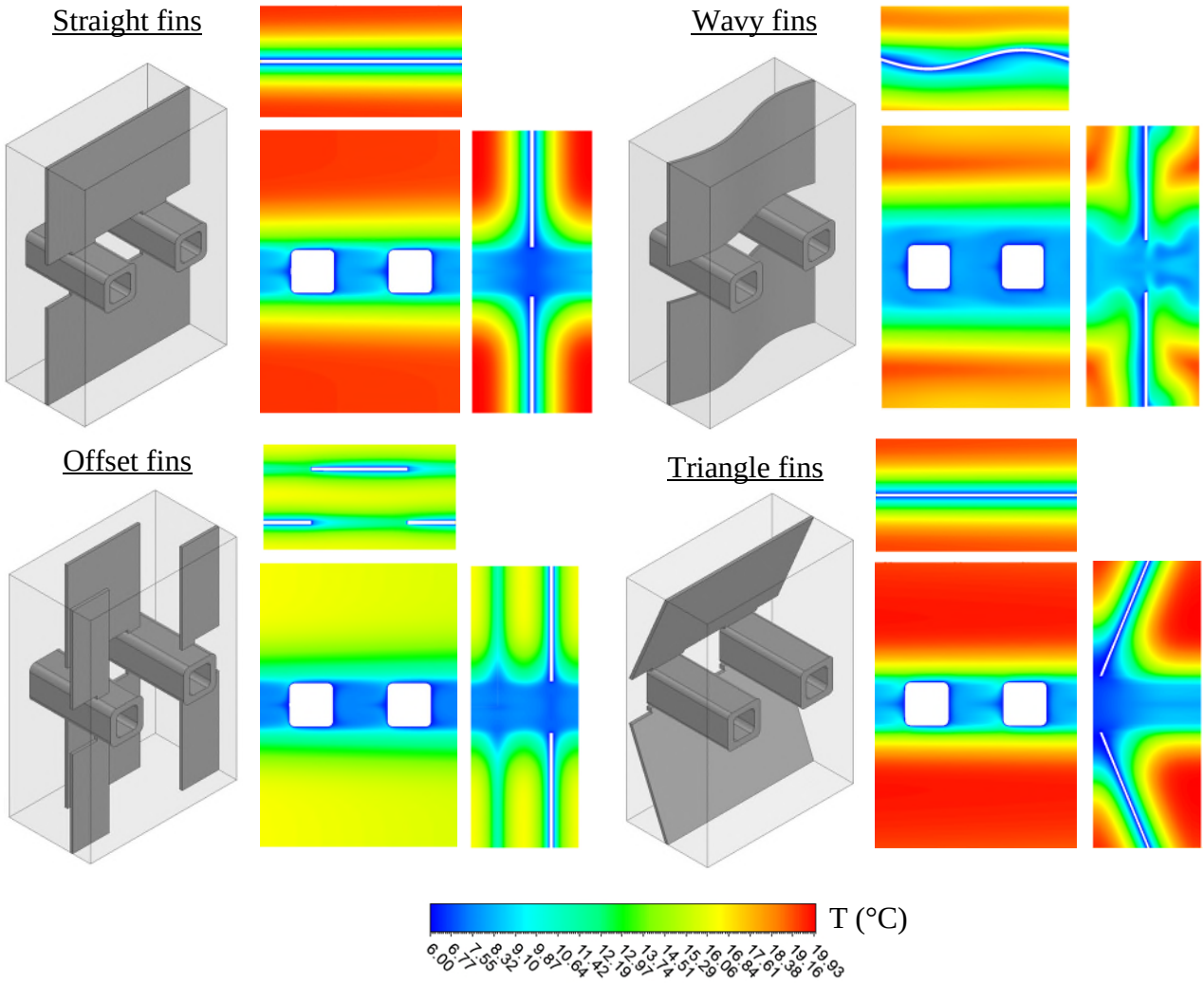


**Figure 74: Temperature contours for all fin designs at row 17 and row 18 (X_p= 13 mm, F_p = 5 mm).**

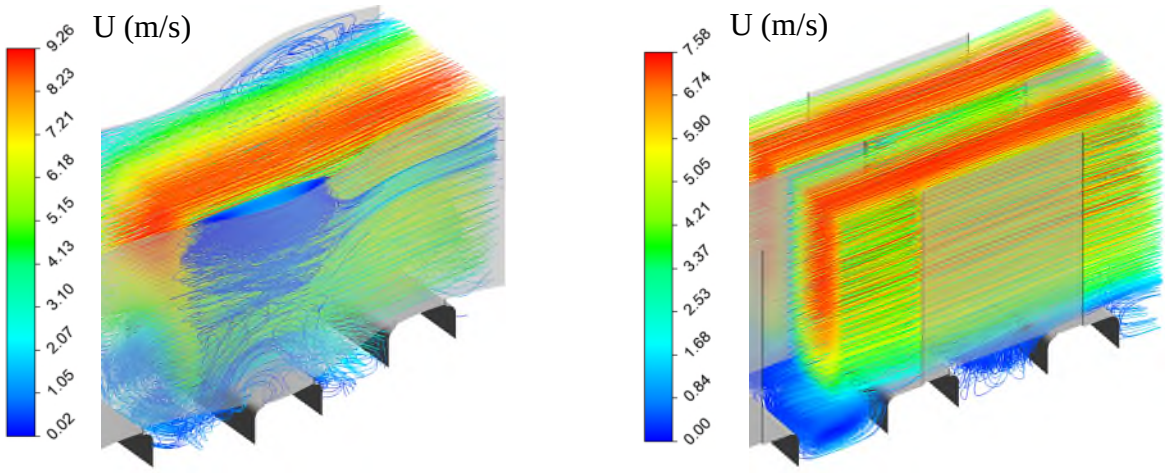


**Figure 75: Velocity streamlines for wavy and offset fins at row 17 and row 18 (X_p= 13mm, F_p = 5mm)**

### 5.3.6. Heat exchanger calculations

The reduced order models of the WEP-MPE with triangular fins were used in a numerical code developed in the past 10 years at the Technical University of Denmark. The idea was to exchange the cabinet of an existing finned-tube evaporator with that of the micro channel heat exchanger, assembled by Aluventa (project partner), see Figure 76.

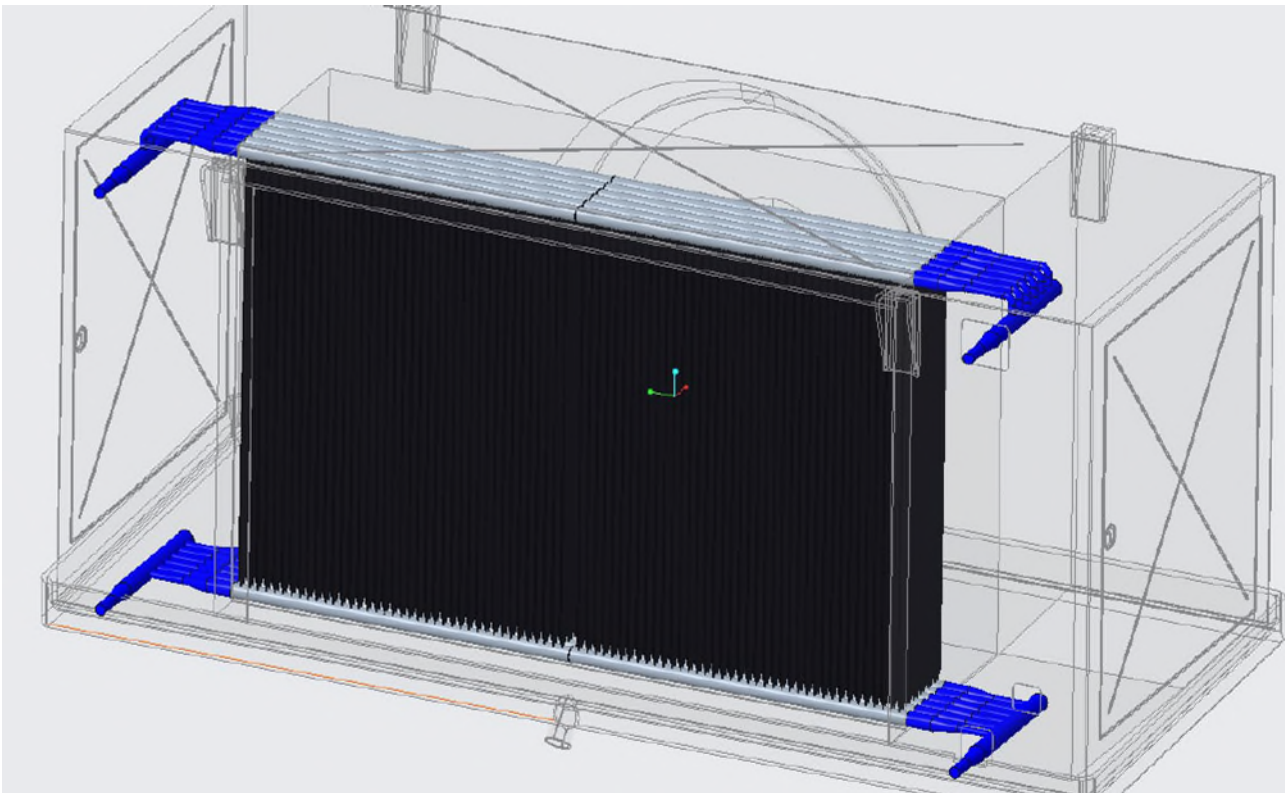

**Figure 76: Novel WEB-MPE heat exchanger, 2 x 6 evaporators (2 x 4 was the final design).**

The choice involved constraints on the face area (height and width). Similarly, constraints were bound to the fin machine, so that the hypotenuse was fixed at 10 mm and the angle could change, as indicated in Figure 77.

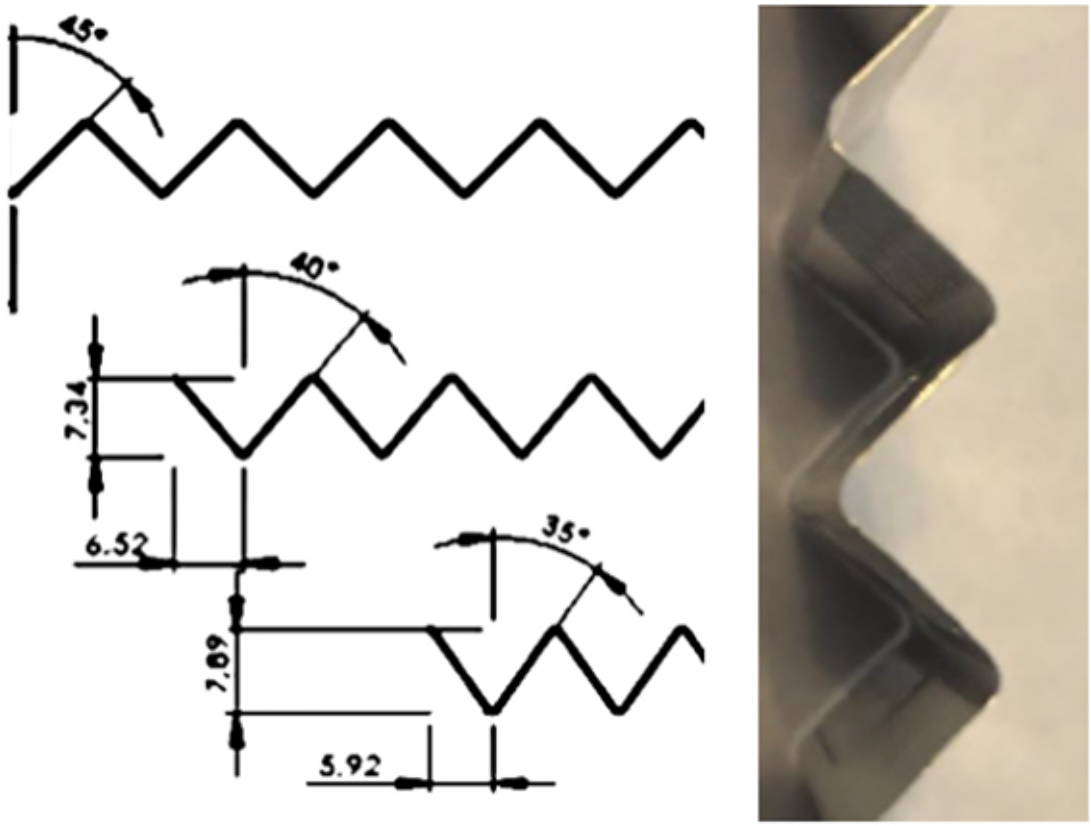


**Figure 77: Fin dimensions: a final angle was 30º.**

Simulations were performed by parameter variation of the circulation ratio, the fin angle, and the heat exchanger depth. In the end, 2 x 4 coils were chosen and a fin angle of 30º, which resulted in equal-sided triangles. Figure 78 indicates the heat exchanger simulations, in which the choice of the fin angle was sought to have a small pressure drop, heat exchanger area (less WEB-MPE profiles), and compactness. In terms of cooling capacity and charge, the fin angle and recirculation rate had little influence due to the small internal volume.

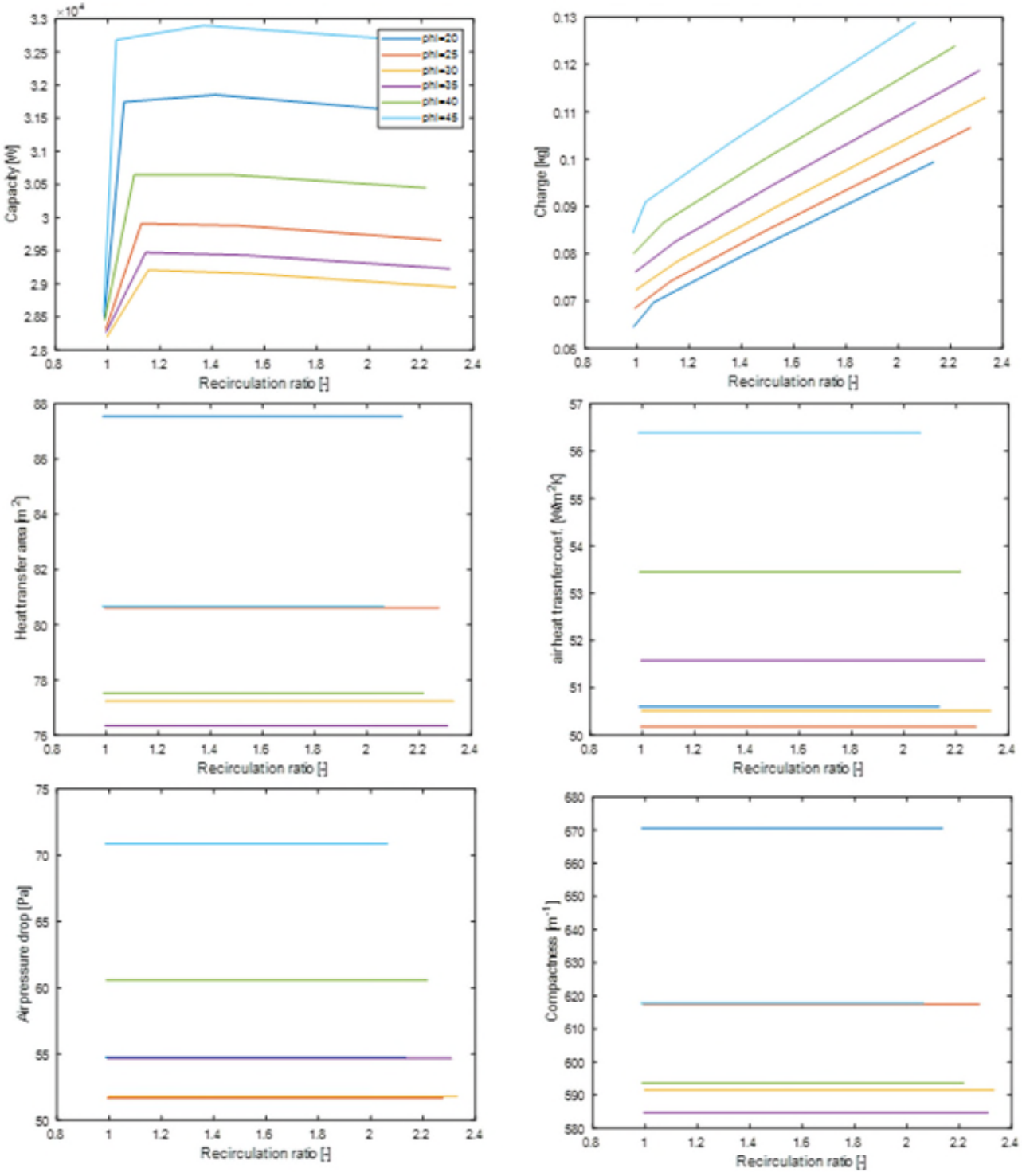


**Figure 78: Heat exchanger design calculations. Four tube banks.**

## 5.4. Summary

The simulations revealed that the bottom-fed evaporators performed the best considering the reductions in recirculation ratios and imposed airflow maldistribution. The crossover tube circuiting resulted in high cooling capacities at all imposed airflow maldistribution and recirculation ratios. The side-fed evaporators revealed some difficulties to handle the balancing of the refrigerant flow distribution, especially as the recirculation ratio decreased and turned out to be vulnerable to the imposed airflow maldistribution here too. Moreover, the size of the inlet header orifices appears to be a crucial point for balancing the liquid column in vertical inlet headers for side-fed evaporators.

The multi-objective optimization showed that a large reduction of refrigerant charge is possible by considering solely the recirculation ratio. If a further reduction of charge is favoured, a simultaneous reduction of the tube diameter as well as an increase of tube circuits are necessary, and it is even possible with a decreased heat exchanger size and volume. Furthermore, the gas and liquid velocities at the outlet of the evaporator do not raise concerns about possible oil retention or weak two-phase heat transfer.

The microchannel evaporator was simulated and build according to available practical production methods and most efficient simulated design.

# 6. Testing of concepts in the laboratory

## 6.1. Introduction

There were conducted tests on all the three concepts that were developed in the project, i.e., CCR (Controlled Circulation Ratio), WDX (Wet Direct Expansion) and micro channel tests. In this part, some of the conducted tests are described.

## 6.2. CCR tests

### 6.2.1. Introduction

To verify the CCR concept, a series of test was conducted. The detailed description of all the tests can be found in a separate document "P2005662-FARS-CCR tests-Rev00". In this chapter, the overall results of the tests are assembled.

The main purpose of the CCR tests were to test the new type of sensor developed by Danfoss in the project to be able to control the circulation rate (NC) and to test a new design of the main types of evaporators, i.e., bottom-fed and side-fed designed in the project and described under section 4.2.1.

The sensor controls the circulation rate of ammonia refrigerant through the evaporator. Tests are lined up to measure the capacity, distribution in each pass, and the charge of the evaporator for the new evaporator design and to compare those to the state-of-the-art design. The primary goal is to verify that the sensor can be used to control the circulation rate in an evaporator.

Another goal is to test a new evaporator design and compare it to state-of-the-art design tested in a commercial project for Danfoss (674503-Danfoss Low Charge Ammonia LCA) where three types of evaporators (bottom-, side- and top-fed) were tested for various circulation rates (1,1 to 5) at two temperature levels -10 °C and -30 °C). These tests showed lots of maldistribution in the circuits of the evaporator, and when the circulation rate came beneath 2, the capacity of the evaporator started to fall.

23 tests were conducted divided into three main test groups:

- **Test group 1 – Evaporator liquid charge:** Was conducted to establish the method of how to measure the charge in the evaporator.
- **Test group 2 – Capacity, liquid hold up and CCR signal:** Was conducted to find the lowest circulation number available to run with and to measure the signal to the CCR sensors.
- **Test group 3 – Controlled circulation rate:** This test group contains the test conducted where the sensor was used to control the injection valve to maintain a fixed circulation number.

In this section, the main results of test group 2 and 3 are shown. For a closer description of the other tests, please have a look at the document "P2005662-FARS-CCR tests-Rev00".

### 6.2.2. Test setup

The CCR equipment was built into a test setup at DTI as shown in Figure 79. A more detailed drawing of the test setup is found in Appendix 1. CCR test setup.

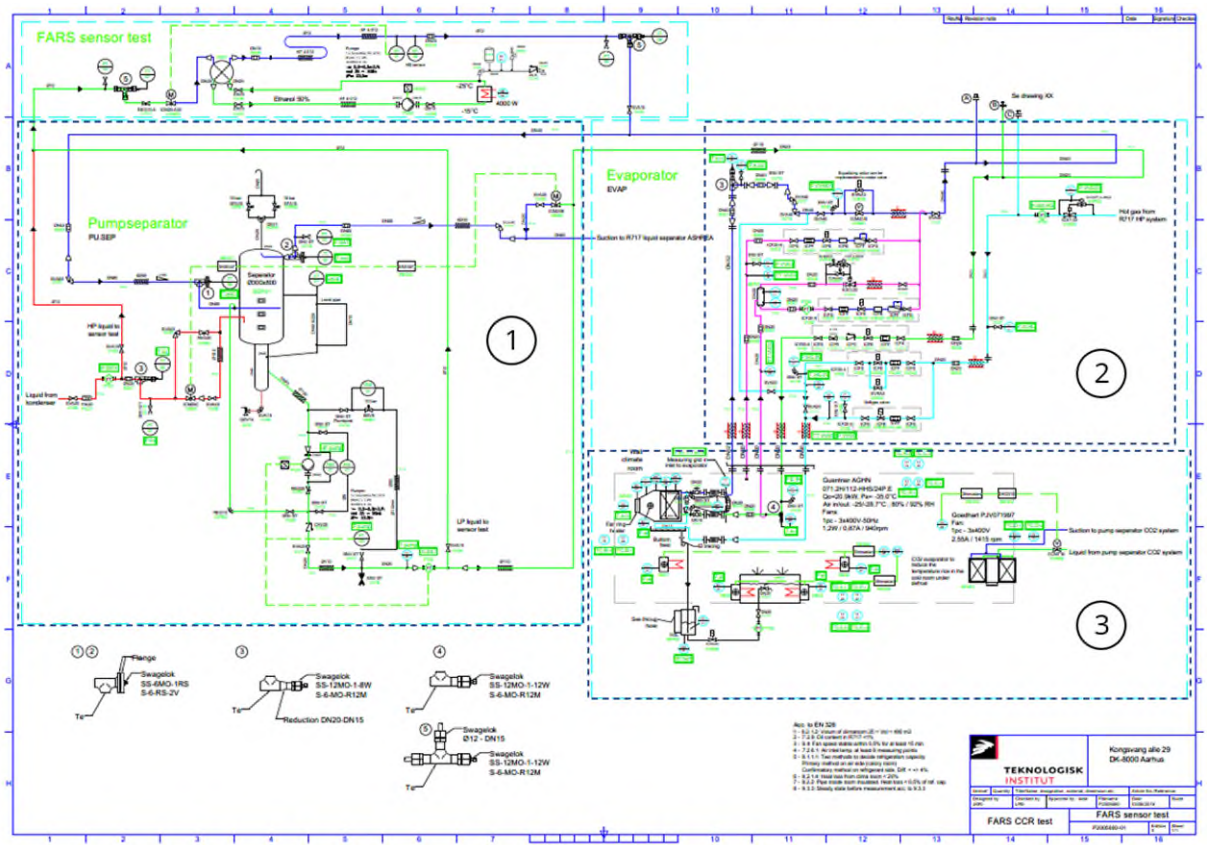


**Figure 79: CCR test setup.**

The bottom-fed cross over evaporator was installed into the laboratory test setup as shown in Figure 79. The test setup is divided in three parts. Part number 3 is the climate chamber where the evaporators to be tested are installed. Part number 2 is the valve stations where the control valves for the evaporator control are placed. The valve stations are placed on top of the climate chamber. The last part, number 1, is the pump separator part where the liquid separator is placed as well as the liquid refrigerant pump to maintain the required flow of refrigerant to the evaporators.

In Figure 80 to the right, the evaporator in the climate chamber is shown. To the right, the valve station on top of the climate chamber is shown.

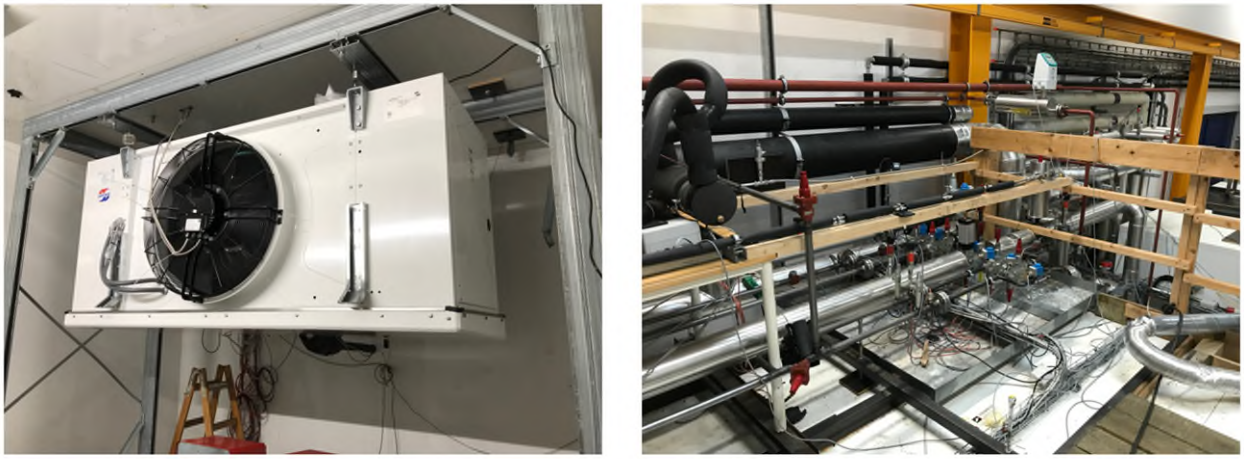

Figure 80: Evaporator to the left and valve station to the right.

In Figure 81 the liquid separator is shown looking from the top of the climate chamber.

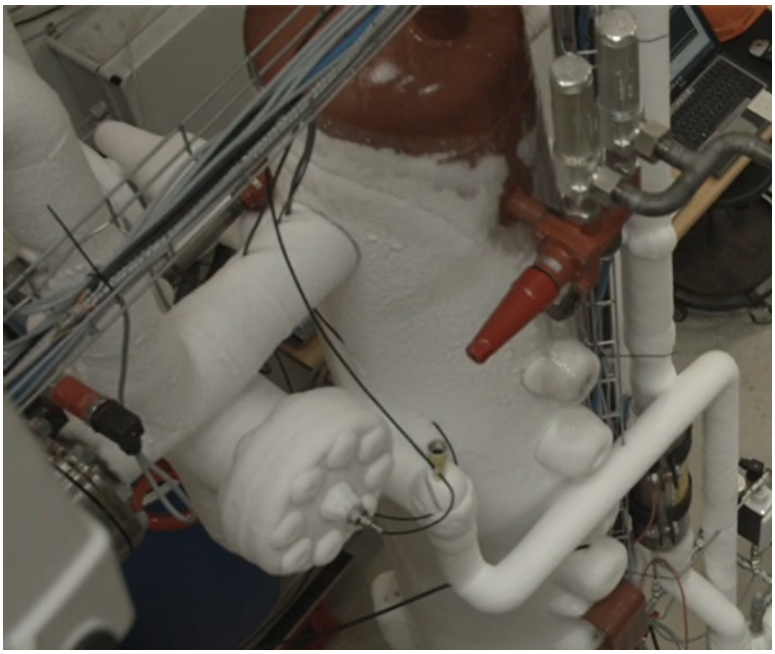

Figure 81: The liquid separator.

### 6.2.3. Main results

In this section, the main results of two of the three test groups are presented.

#### 6.2.3.1. Test group 2 – Capacity, liquid hold up and CCR signal

In this test group, the measurement of the lowest circulation number that is possible to run with without reducing the capacity of the evaporator to much is found. The signal from the heated sensor out of each circuit in the evaporator is also measured to see how this can be used to control the injection valve. These are measured both at design capacity and at part load.

The following main questions are answered through the measurements:

1. What is the lowest circulation ratio we can run with without affecting the capacity to much?
2. What is the change in charge when going from high to the lowest?
3. How is the signal from the CCR sensors and can it be used to control the circulation ratio?
4. Is it necessary to use orifices for the bottom-fed cross over evaporator?

To answer the two first questions, we can have a look at the graph in Figure 82. These measurements show the same trend as measurements for evaporation temperature of -10 °C and entering a temperature difference of 10K.

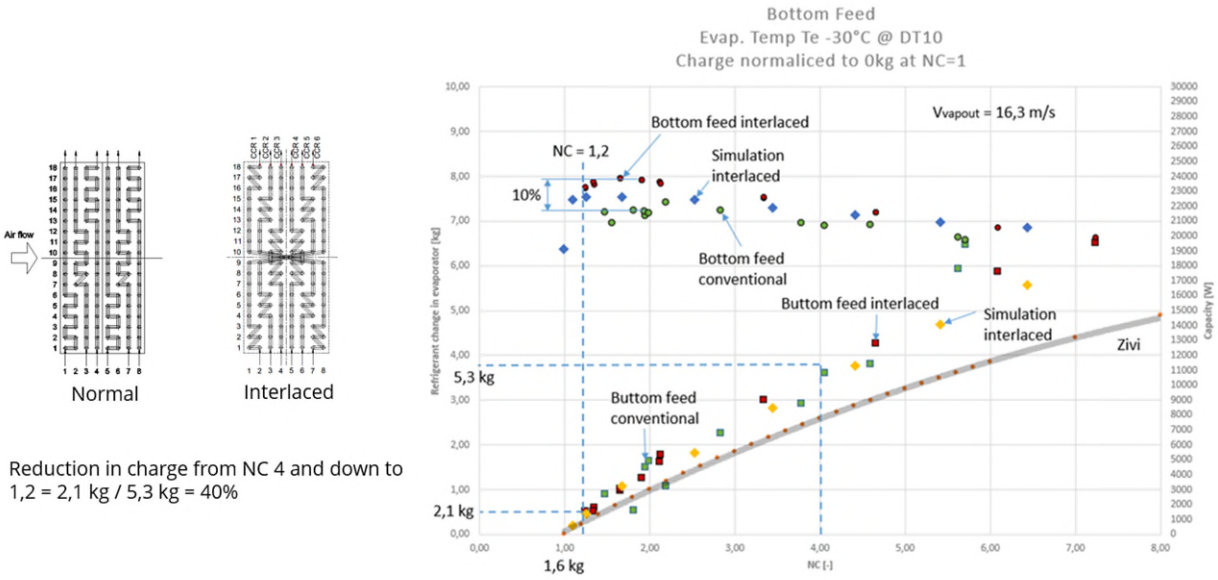


**Figure 82: CCR measurements for evaporation temperature of -30 °C and entering a temperature difference of 10K.**

In the graph, the capacity and charge measurements for the bottom-fed cross over (interlaced) evaporator is shown for an evaporation temperature (Te) of -30 °C and entering temperature difference (ETD) of 10K. These are the conditions that the evaporator is designed for. As can be seen, the normal bottom-feed is still lower in capacity. The capacity for the cross over is around 24 kW when down in around NC of 1.7 where the conventional evaporator is about 10% lower in capacity.

When looking at the lowest NC (circulation number) that can be used without reducing the capacity of the evaporator, it seems to be like the one for Te = -10 °C and ETD = 10K or around 1.2 for the cross over type. For the normal bottom-feed, a lowest value is not found. The capacity is seen to fall very little from NC of 2 to 1. The simulations from DTU seem to correspond quite well with the measurements. The conclusion is that it is possible to run with NC as low as 1.2 when the circulation number is controlled.

Regarding the charge change, it seems that the cross over type has slightly lower change in charge as the NC increases. The DTU simulations correspond well with the

measurements, but the analytical equation integrated from the Zivi void fraction model predicts less changes in charge than shown in measurements.

The change in charge going from NC of 4 down to 1.2 is around 3.0 kg. This corresponds to around a 39 % reduction in charge.

The average gas speed in the outlet pipe from the evaporator is around 16 m/s which is higher than for Te = -10 °C and EDT = 10K because of a lower density of the gas. This should improve the wetting of the pipes' inner surface and thereby the heat transfer coefficient. One would expect a higher capacity. The capacity is more or less the same, and the reason is probably the pressure drop that changes the temperature profile through the circuit.

Looking at the superheated temperatures (SH) for the CCR sensors in Figure 83, they show the same trend as for Te = -10 °C and EDT = 10K.

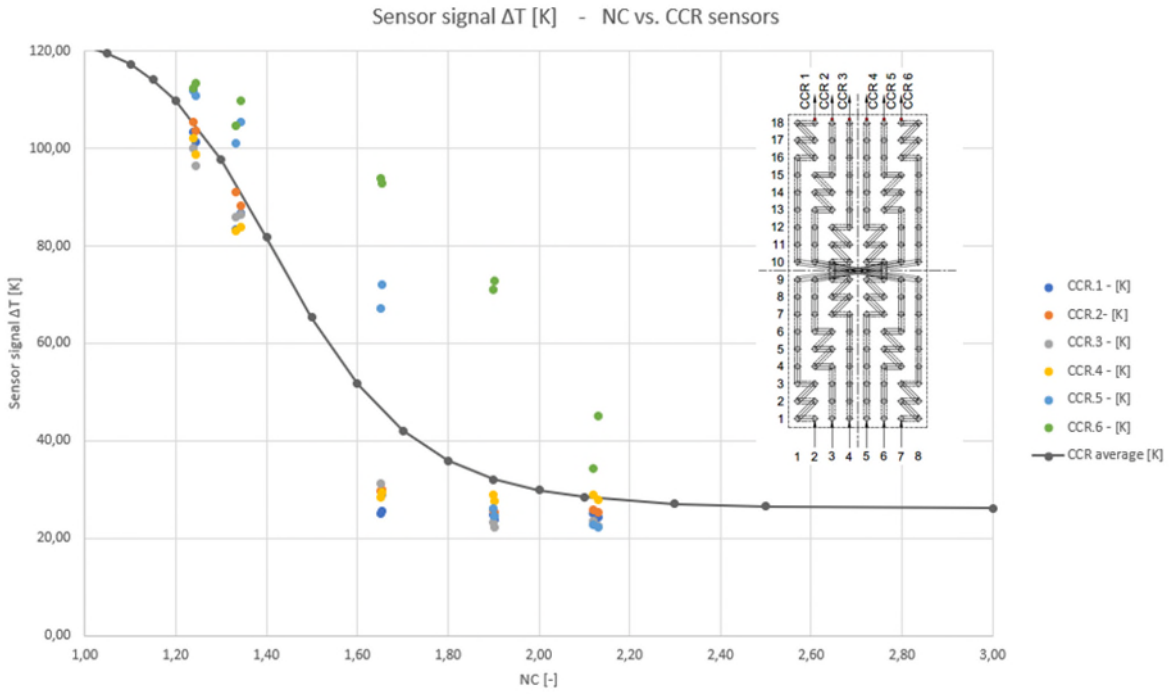


**Figure 83: CCR superheat measurements for evaporation temperature of -30 °C and entering a temperature difference of 10K.**

The SH temperatures in Figure 83 show the maldistribution in the evaporator. It is seen that circuit 6 is the driest one followed by circuit 5. Other circuits are more flooded. The same trend is shown for the case with Te = -10 °C and EDT = 10K, and the SH temperatures are also in the same range. Going from around 30K for NC over 2.2 and up to 115K for close to dry condition. As seen from the graph, there is a signal that can be used through a control algorithm to control the NC to 1.2 as needed.

The observed maldistribution is believed to be because of the skew air flow profile into the evaporator and not because of an uneven refrigerant distribution, and thereby the use of orifices is not considered to help. The test with orifices installed was thereby dropped.

### 6.2.3.2. Test group 3 – Controlled circulation rate

In this test group, the heated sensor was used to control the superheat during a normal icing up of the evaporator. The sensor was placed on the driest circuit, i.e., circuit number 6. The test was run for saturated suction temperature of both -10 °C and -30 °C. Here, the results of Te = -30 °C are shown and a reference to the Te = -10 °C is made.

The question to answer in this test was the following:

1. Is it possible to use the CCR sensor to control the evaporator under normal conditions where icing of the evaporator changes the capacity and thereby the NC?

The accumulated ice on the coil was 60 kg and the fall in capacity during the test period is seen in Figure 84.

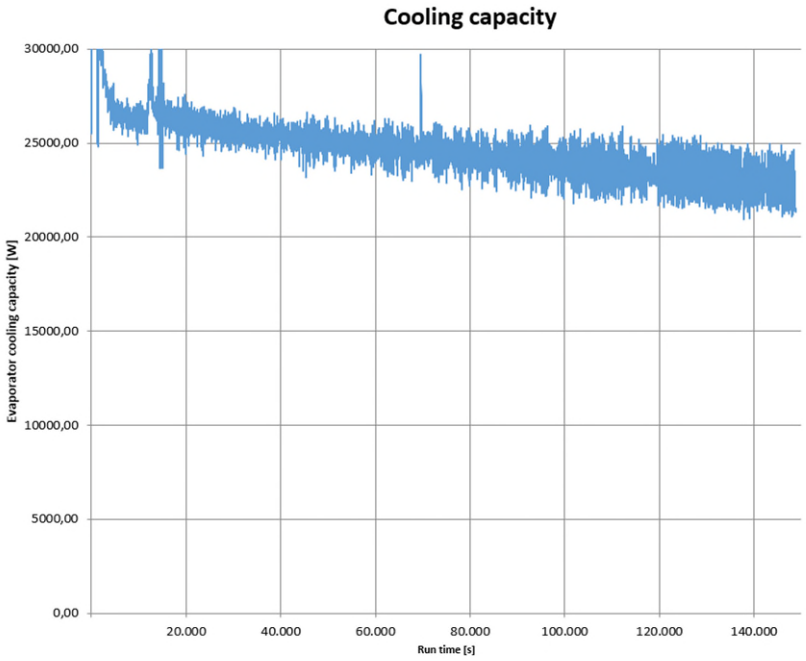


**Figure 84: Fall in capacity during test.**

The capacity of the evaporator dropped from around 26kW down to 23kW which is a drop of 11,5 %. The same trend was also noticed under the Te = -10 °C test.

In Figure 85, the superheat signal from all the CCR sensors is depictured. The controlling sensor was on circuit 6, and the superheat setpoint was set to 70 °C. Figure 85 shows that the controller is able to maintain the setpoint quite well.

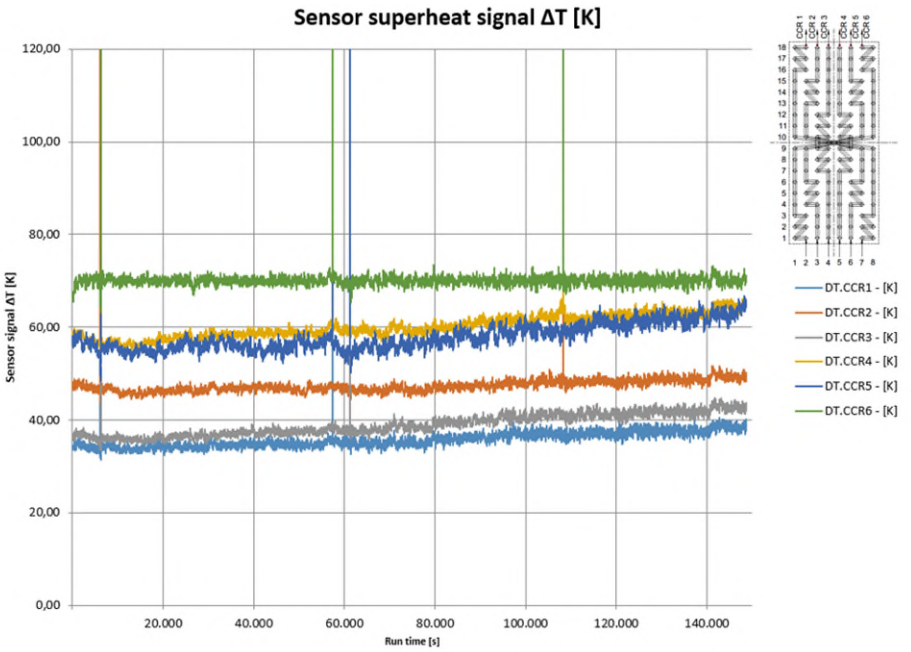


**Figure 85: Superheat signal for all the CCR sensors.**

When looking at the NC throughout the test, as depictured in Figure 86, it is seen that the NC is not constant and rises from around 1.7 to 2.1 throughout the test as the capacity drops. To be able to reach a lower NC, the SH reference should have been higher, or more power should have been used for the heating element.

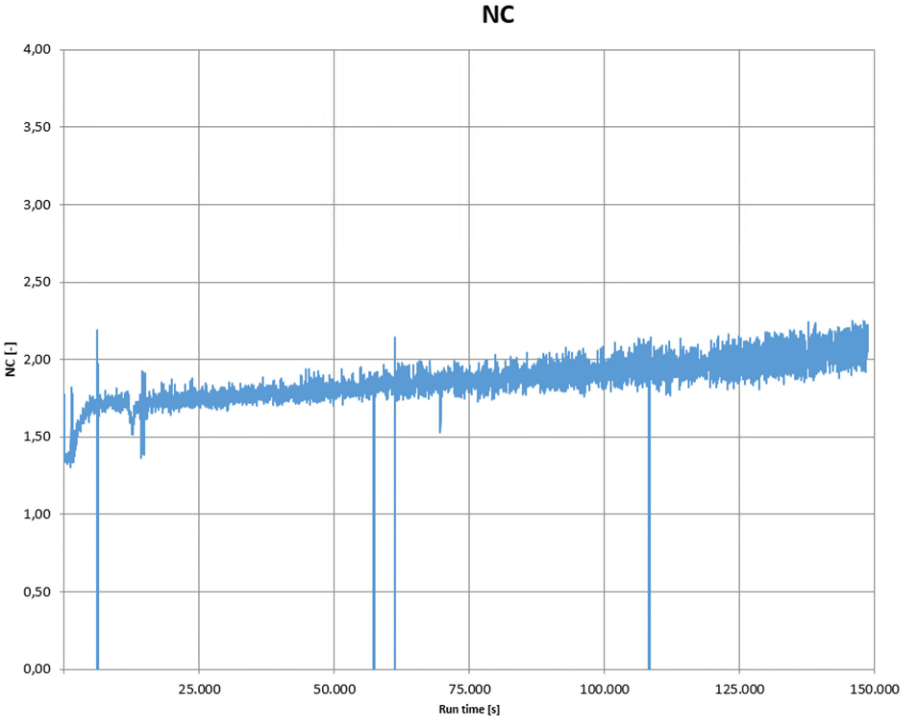


**Figure 86: The circulation number of the evaporator during the test.**

This shows that the SH signal from the CCR sensor 6 is not directly related to the NC. This deviation in NC is not problematic since it is most important to be able to control the NC

around 1.2 to gain the charge benefit, and the increase in charge from the deviation is very small.

The measurements show that it is possible to use the CCR sensor as signal for the controller, and the controller can control the SH signal. The dependency of the NC on the SH is not directly related, and the NC deviates a little from the situation at start when the evaporator is without ice, to when the evaporator is iced up and has dropped in capacity. This deviation is not essential and can be accepted. If the evaporator would run on part load it is not clear where the NC would be for the same SH reference, and there may be a relation that must be considered.

When comparing Te = -10 °C to the results, it is seen that the SH reference must be adjusted if the same NC is required to the running conditions. A correlation for the dependency of evaporation temperature on the required SH reference is needed.

## 6.3. WDX tests

### 6.3.1. Introduction

This part of the test was conducted to test evaporators running with high pressure liquid into the expansion valve and a dry return suction line with as small a superheat in the evaporator as possible. A lot of ideas about how the configuration of the control should be laid out was looked at (see 4.3.1), and the methods validated as most interesting were then tried out in the tests. The simplest solution was to control the evaporator with a simple control solution with as low a suction superheat as possible. The next idea that was tested was to use an external suction superheat heat exchanger (SGHX) to burn off the liquid escaping the evaporator and using the high-pressure liquid as a heat supply. Then a self-controlled method named Zimmerman was tried out. In this method that was originally put forward by Zimmerman, an intermediate vessel was used to control the flow to the evaporator. At last, the evaporator designed for WDX with liquid distributor was connected to the pumped circulated system and tested as a CCR i.e., to control the circulation ratio.

The test was conducted with a saturated suction temperature of both -10 °C and -30 °C with an entering temperature difference (ETD) of 10K for full capacity and 5K for reduced capacity i.e., part load. The evaporator was designed for a saturated suction temperature of -10 °C and an ETD of 10K so the -30 °C conditions were off design point for the evaporator.

First the test series 1 was performed with a ICM liquid injection valve with the smallest orifice available in the Danfoss product assortment. This turned out to be too large, so Danfoss produced a special smaller orifice that was used in series 2 throughout series 10. The valve was still too coarse and hard to control. In series 12, the valve was changed to a pulse modulated AKVA valve that was able to control the flow more exactly. This valve was then used throughout the remaining tests.

Tests were first conducted with manual control of the expansion valve to examine how the system response was and to estimate if a controller would be able to control the signal given in the manual tests. If it was estimated doable for the controller, the control loop was put up and tests were conducted. At last, in series 22 throughout 27, the WDR evaporator used in the previous test with an AKVA liquid injection valve was connected to the pump separator, and the test setup was used to control the evaporator in a pumped circulated system with great success. The temperature signal for the superheat control in these tests was taken from the CCR sensor under development at Danfoss.

### 6.3.2. Test setup

A change was made to the laboratory test setup to be able to run with the WDX (Wet Direct Expansion) solution. This means that the high-pressure liquid directly from the compressor is led to the expansion valve. The wet suction from the evaporator is then led to the suction gas superheater (SGHX), and the liquid is boiled off before entering the suction line as dry gas. This dry gas goes back to the normal suction line to the liquid separator. This means that if liquid escapes the suction gas heat exchanger no harm is done since it will be separated before entering the compressors.

The PI diagram of the test setup is shown in Figure 87 and in larger format in Appendix 2. WDX test setup. It consists of four main parts. The first numbered 1 in the figure is the climate chamber where the evaporator is installed and measured. The climate chamber includes besides the evaporator a heating element to represent a load on the evaporator, a humidifying equipment to humidify the air to produce ice in the evaporator coil, and a measuring equipment to be able to measure the energy flow in and out of the climate chamber.

Above the climate chamber you find the valve stations, numbered 2, consisting of liquid and suction lines and two defrost valve stations where one can be used to test liquid drain hot gas defrost and the other to test pressure controlled hot gas defrost.

The suction gas heat exchanger (SGHX), numbered 3, is connected to the high-pressure liquid coming from the condenser and the wet suction gas coming from the evaporator.

The test setup is connected to a pump separator, numbered 4, where the suction line from the valve station is connected. The high-pressure liquid line from the condenser which feeds the pump separator with liquid ammonia is piped directly to the expansion valve for the evaporator through a solenoid valve. In this way, the test setup can be used for both liquid overfeed systems and direct expansion.

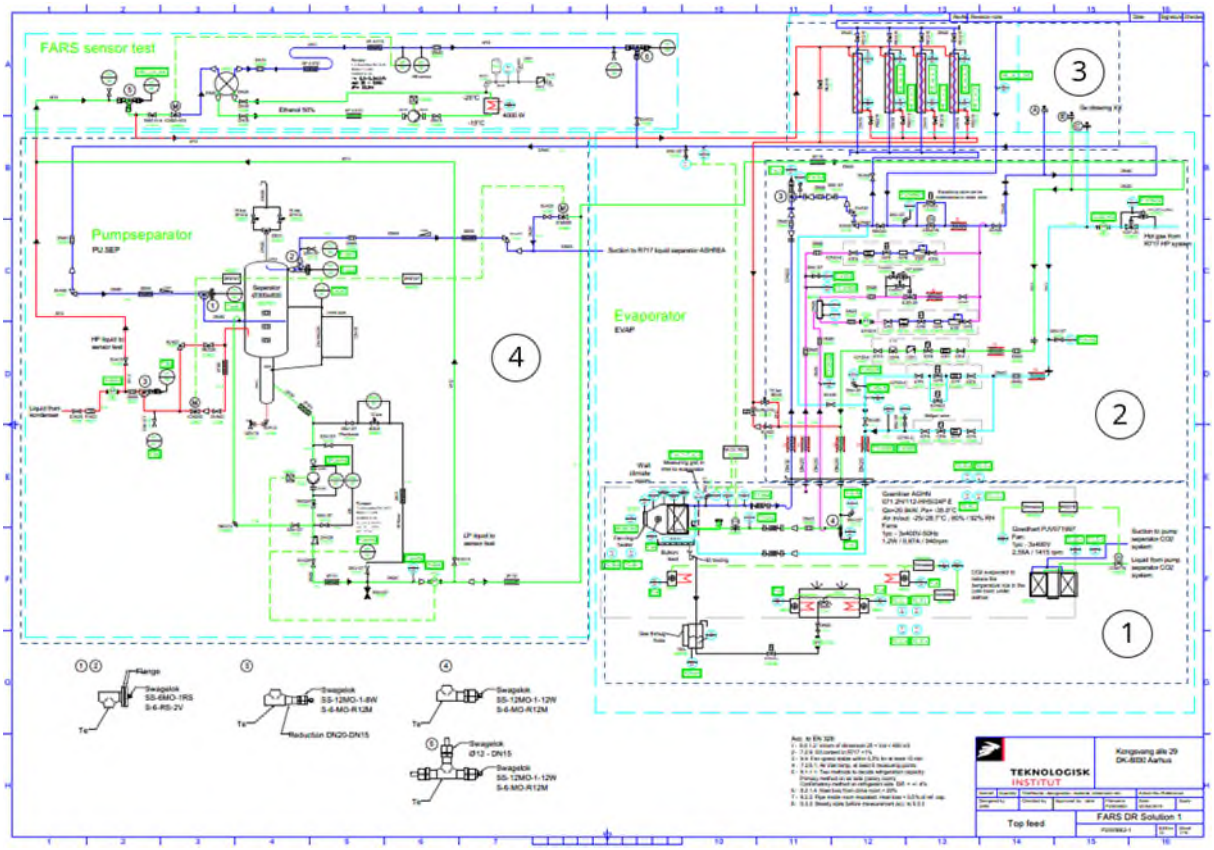


**Figure 87: WDX test setup.**

The evaporator used in the test was a special produced one by Güntner. In Figure 88, the evaporator installation in the climate chamber is shown. On the picture to the left, the air

inlet side is shown with liquid, suction and defrost lines. The picture on the right shows the fan on the air outlet side and the weight cells that the evaporator is hanging in.

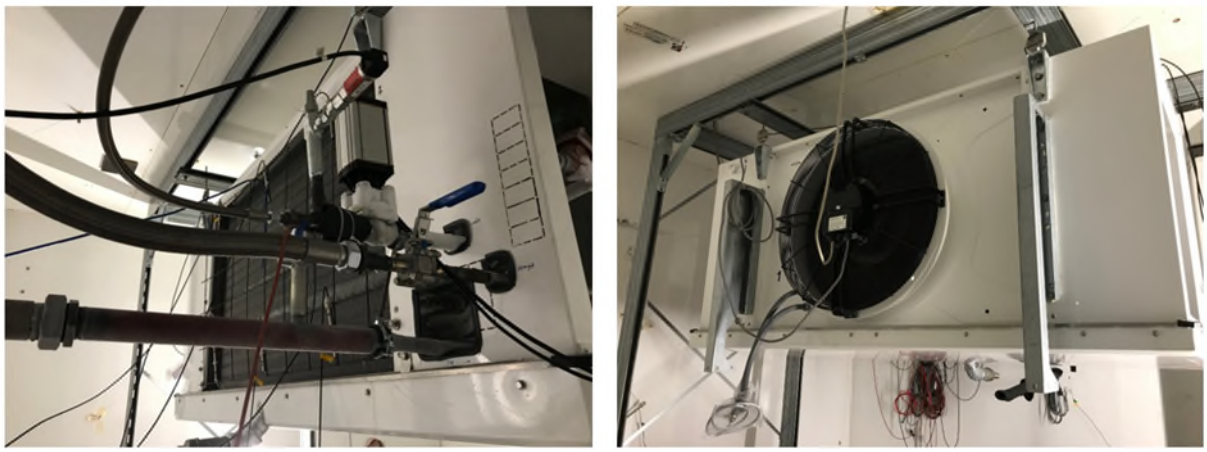

**Figure 88: Güntner WDX evaporator in the climate chamber.**

In Figure 89, a picture from each end of the evaporator is shown. The picture on the left shows the end where the ammonia enters and leaves the evaporator and the picture on the right the opposite end.

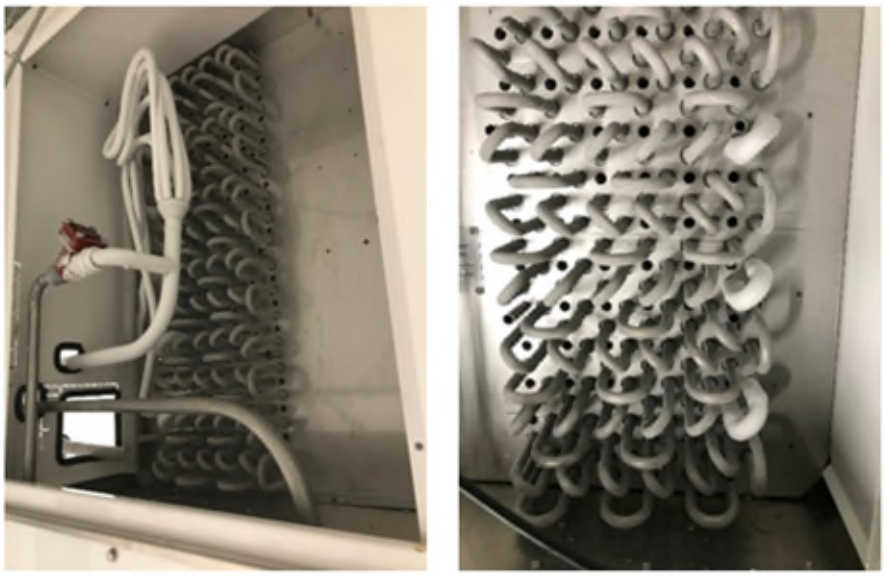

**Figure 89: The ends of the WDX evaporator. To the left the refrigerant inlet.**

The suction gas heat exchanger SGHX (see Figure 90) was made up of four smaller coaxial parallel connected heat exchangers. This was a special built heat exchanger made of aluminum. This was selected instead of using one coaxial heat exchanger since the size of pipes for this was not available, and a commercial coaxial evaporator for ammonia was not found.

Measurements were done on heat exchanger 1 to 3. No sensors were placed on heat exchanger 0.

A control valve was placed on both the liquid and the suction side of the SGHX. The parallel construction has given a lot of challenges since it is extremely difficult to compensate for the maldistribution by adjusting the valves. A small change of the flow in the suction line changes the balance in the SGHX, and maldistribution occurs.


**Figure 90: Suction gas heat exchanger SGHX.**

A better solution would have been to have one coaxial heat exchanger for the total flow to reduce the challenges with maldistribution. The SGHX was used to boil off the liquid exiting the evaporator and returning a dry gas to the suction line.

The first tests conducted were with manual control on the expansion valve to investigate the behavior of the system. To start with, the expansion valve was the smallest ICM valve from Danfoss with ICAD actuator. This valve turned out to be too big. Danfoss constructed a new orifice for the valve to reduce the size and make it possible to run some tests. The valve was still too big and was exchanged to another type called AKVA which is a pulse modulating valve. With the new valve, the control was more successful.

The weight of the evaporator was measured with weight cells to estimate the charge of the evaporator under various running conditions.

On the outlet from the evaporator, six heated sensors were placed to measure the dryness of the suction gas leaving the evaporator. Two other heated sensors were also placed in the common suction line in the bottom and another in the top of the pipe. The intention was to see how the signal from the heated sensors to evaluate how it could be used to control the expansions valve.

A detailed test report "P2005662-FARS-DR tests-Rev01" describing all the test conducted is attached to this rapport, and here in the main rapport only the overall results are presented.

The test started by running with the smallest ICS valve from Danfoss as an expansion valve. In the first series from 1 to 5 the expansion valve was controlled manually, and tests were conducted with and without SGHX for evaporation temperatures of -10 °C and -30 °C. In the series 6 and 7, an automatic control of the expansion valve was done both with and without the SGHX. In the series 8, the Zimmermann method was tested. In the series 9, the influence of the slightly overflooded compared to the superheated is investigated. In the series 10, the maldistribution in the coil was investigated. In the series 11 to 14, a new expansion valve was tested both with and without the SGHX for -10 °C. In the series from 15 to 17, the ALC method for controlling the expansion valve was investigated. In the series 18 to 21, the CCR sensor was used to control the expansion valve for evaporation temperatures of -10 °C and -30 °C – both with and without SGHX. In the series 22 to 24, the liquid inlet to the evaporator was connected to the liquid circulation pump for the flooded system, and the CCR sensors were used to control the circulation number through the evaporator. These tests are a kind of CCR test with the WDX designed evaporator and the same expansion valve as used for the WDX tests. In the series from 25 to 27, the CCR sensor was changed for a normal PT1000 sensor to measure the difference.

### 6.3.3. Main results

In this section, selected tests will be presented. For a full review of the tests, please read the attached document ""P2005662-FARS-DR tests-Rev01"". The selected tests presented here will be:

1. *Series 2-FARS-DR-Med-Sugegasveks:* Manually operated expansion valve with SGHX operating and evaporation temperature of -10 °C.
2. *Series 8-FARS-DR-reg-IHX-Zimmermann:* Here, the method of Zimmermann was investigated.
3. *Series 9-FARS-DR-man-med-og-uden-IHX:* Here, the benefit of running with WDX compared to conventional DX was investigated.
4. *Series 20-FARS.DR-AKV-Uden-Sugegasveksler SH CCR6 -10C Step:* Here, the control was done using the CCR sensor on circuit 6 through a conventional MSS control strategy from Danfoss without the SGHX.
5. *Series 23-FARS.DR-AKV-UdenSHX SH CCR6 -10C Step pumpe:* In this test series, the refrigerant liquid feed into the evaporator was changed from high pressure liquid to low pressure liquid from the liquid circulation pump on the liquid separator. The control was done using the CCR sensor on circuit 6 through a conventional MSS control strategy from Danfoss without the SGHX.

#### 6.3.3.1. Series 2-FARS-DR-Med-Sugegasveks

This test was done to investigate if the evaporator could be controlled by using the superheat after the SGHX (Suction Gas Heat Exchanger) and to see how the signal from the heated sensors looks like and, if it is possible, to use it to control the evaporator. The main questions to answer in the test:

1. Is it possible to use superheat after the SGHX to control the evaporator?
2. Is it possible to use the signal from the heated sensors to control the evaporator?
3. Is it possible to use SGHX to dry out the gas before entering the suction line?
4. What is the lowest circulation rate that can be controlled down to?
5. What is the reduction in charge for different OD?

In this test, a new smaller orifice was installed in the ICM valve, and the flow through the expansion valve was controlled manually. If it is possible to run it manually, it is probably possible to design a control system to handle the control. If it is not possible to run it manually, it will not be possible to control the evaporators automatically.

There were three test runs. The first one where the flow was reduced manually with the expansion valve. The opening degree (OD) of the valve was changed from 24 % down to 15 %. In the second and third run, the opening degree of the valve was increased from 15 % and up to 26 % again to see if there was a consistent signal for both down and up control.

The evaporation temperature was -10 °C, and the temperature in the climate chamber was 0 °C.

***Measurements***

In Figure 91, we can see the calculated superheat out of the evaporator and after the SGHX (orange and blue). The black line is the mass flow rate and is related to the manual opening of the valve. The green line is the saturated suction temperature after the SGHX and represents the suction temperature that the main refrigeration system was adjusted to. On the x axis is the time from start of measurements.

The evaporator is flooded until around 6000 sec. and an OD (opening degree) of 16 %. The superheat out of the SGHX to start with is constant on around 3K. Here, the condition from the SGHX is flooded, and the measured superheat is caused by the maldistribution in the SGHX where some of the heat exchangers are flooded while others are dry. At an OD of around 18 %, it seems that the flooding out of the SGHX is reducing. At an OD of 16 %, the flow from the SGHX seems to be dry but still flooded from the evaporator. By changing the OD from 16 % to 15 %, the evaporator runs dry. It is in this range from 5500 sec. to 6000 sec. where we need to be able to control the evaporator to obtain a dry suction line and a flooded evaporator. This indicates that the valve is still too large and there is a need for a smaller valve.

When going from an OD of 16 % to an OD of 15 %, the mass flow reduces at first as for the previous changes in OD and then ramps down to a lower stable value. Changing the valve from an OD of 16 % to an OD of 15 % changes the flow of the refrigerant from 76 kg/h down to 63 kg/h i.e., 13 kg/h for 1 % change in the OD. The previous changes in OD of 2 % changed the flow from approx. 3 kg/h and down to 9 kg/h for each 2 % change in OD – with the lowest change with the highest OD and with an increasing change when lowering the OD. This gives an extra challenge and shows the need for much finer steps in the valve in the area from 5500 sec. to 6000 sec. to be able to control the evaporator.

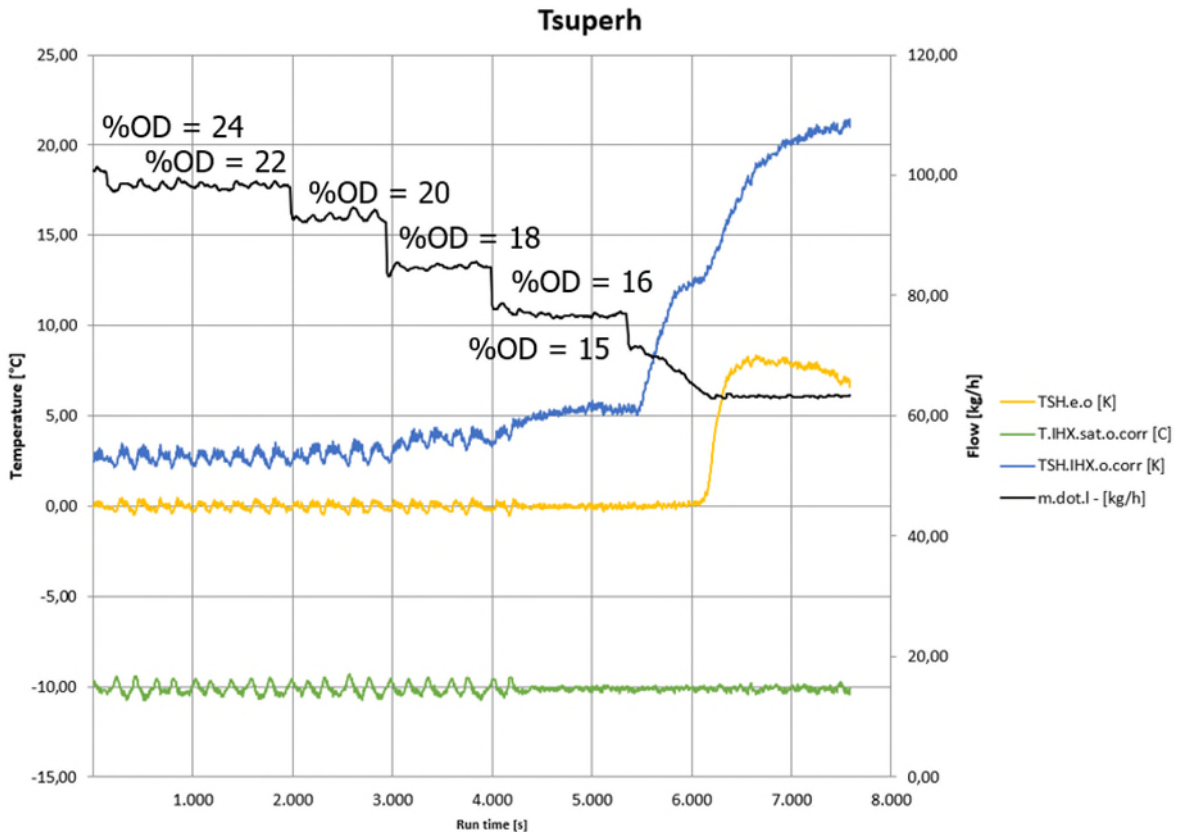


**Figure 91: Temperature measurements after the SGHX (Suction Gas Heat Exchanger).**

The capacity of the evaporator while reducing the OD is shown in Figure 92. Here, it can be seen that the capacity is maintained until the evaporator starts to run dry at around 6000 sec. This indicates that it is possible to reduce the circulation rate through the evaporator significantly without losing capacity. The capacity is rater constant up to around 6000 sec. where it drops to 22500 W (10 %) when the evaporator operates with superheat.

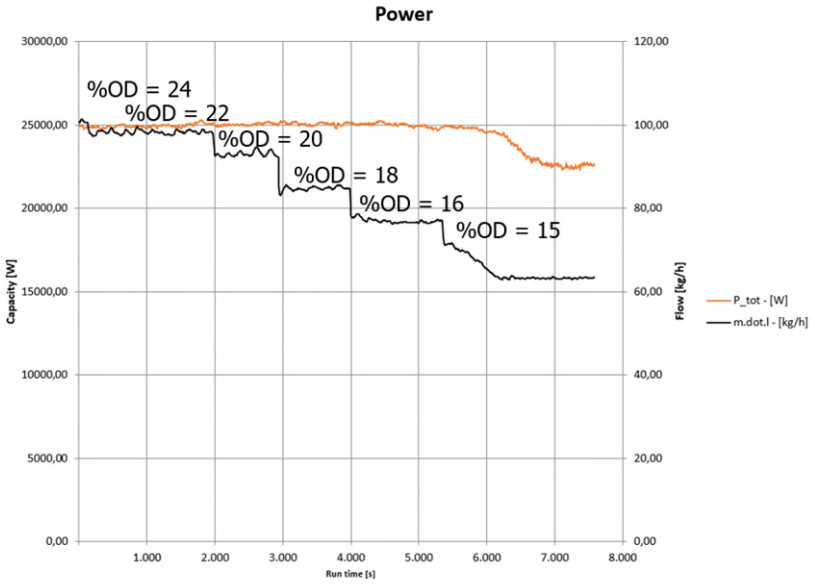


**Figure 92: Capacity.**

In Figure 93, the temperature measurement for the CCR sensors is shown and, to the right, the placements of the sensors. Sensor 1 is placed on the outlet of the top row and then numbered downwards, placed on the outlet of each circuit.

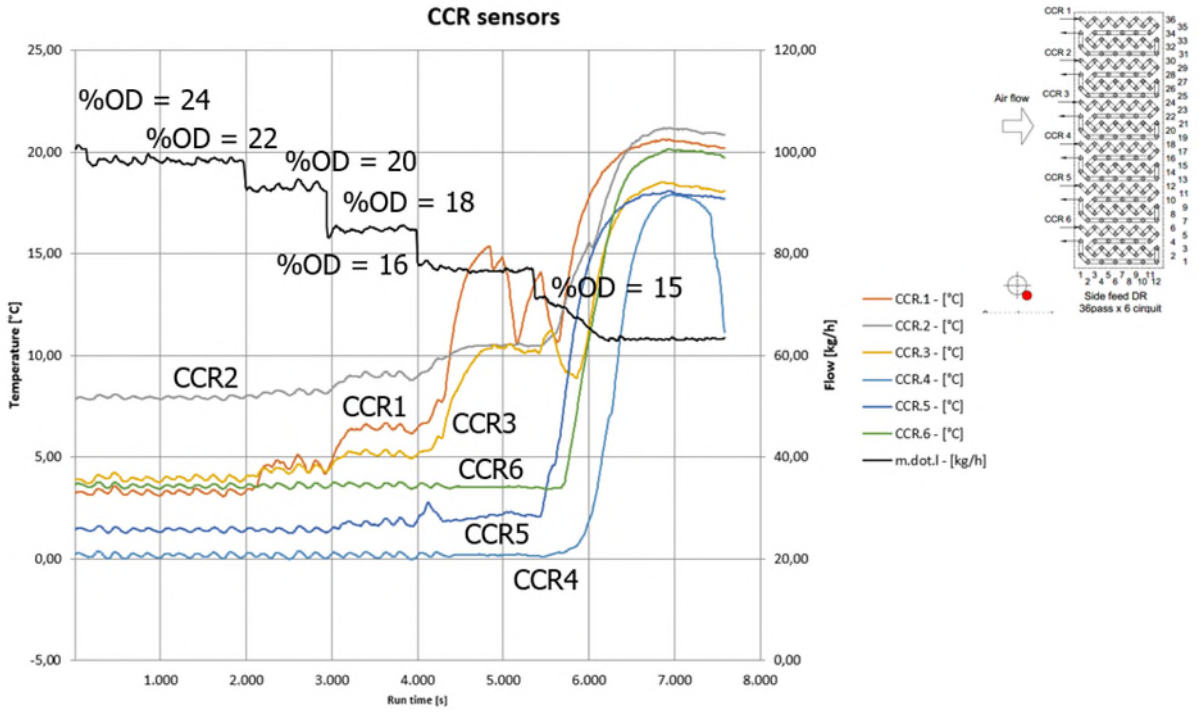


**Figure 93: CCR sensors.**

What can be seen from the graph is that to start with all the circuits are flooded. There is some difference in the temperature that is most likely due to a slightly different placement of the sensors on the pipe and maybe a different face attachment to the pipe. At around 2000 sec., circuit 1 starts to become drier. Then at around 3000 sec., circuit 3 and circuit 2 start to become drier. At around 4000 sec., a step in the temperatures for circuit 1 and circuit 3 appears, and circuit 2 also increases dryness. At 5500 sec. and up to 6000 sec., the other circuits also come into play and all sensors obtain a new and higher temperature above around 6500 sec. This indicates that the CCR sensors give a signal depending on the dryness of the circuit. This signal is dependent on the refrigerant maldistribution of the coil and challenges the selection of the circuit to be used for the control. This must be investigated further. The CCR sensors seem to give a clear indication between a flooded and a dry condition.

The temperature measurements over the SGHX are shown in Figure 94. The black line represents the OD, and the orange represents the saturated suction temperature as before. The SGHX contains four parallel heat exchangers where both high-pressure liquid and the suction gas flow. The heat exchanger furthest to the left in the picture is without measurements, the second from the left is number 1, and the one furthest on the right is number 3. The blue, green and red curves represent the temperature out of heat exchanger 1, 2 and 3, respectively. As can be seen from the measurements, heat exchanger 1 and heat exchanger 3 seem to be flooded and doing something to start with, but number 2 is superheated and ineffective. At around 3000 sec., number 2 starts to be flooded, and

number 3 starts to get superheated. From 5500 sec., they all start to be superheated, and up to 6000 sec., they have increasing superheat. After 6000 sec., when the evaporator starts to be superheated, the superheat from the SGHX starts to stabilize again. These measurements indicate that the parallel circuits in the SGHX cause problems, and if the SGHX had been constructed without the parallel circuits, the SGHX would work better. This would be interesting to investigate.

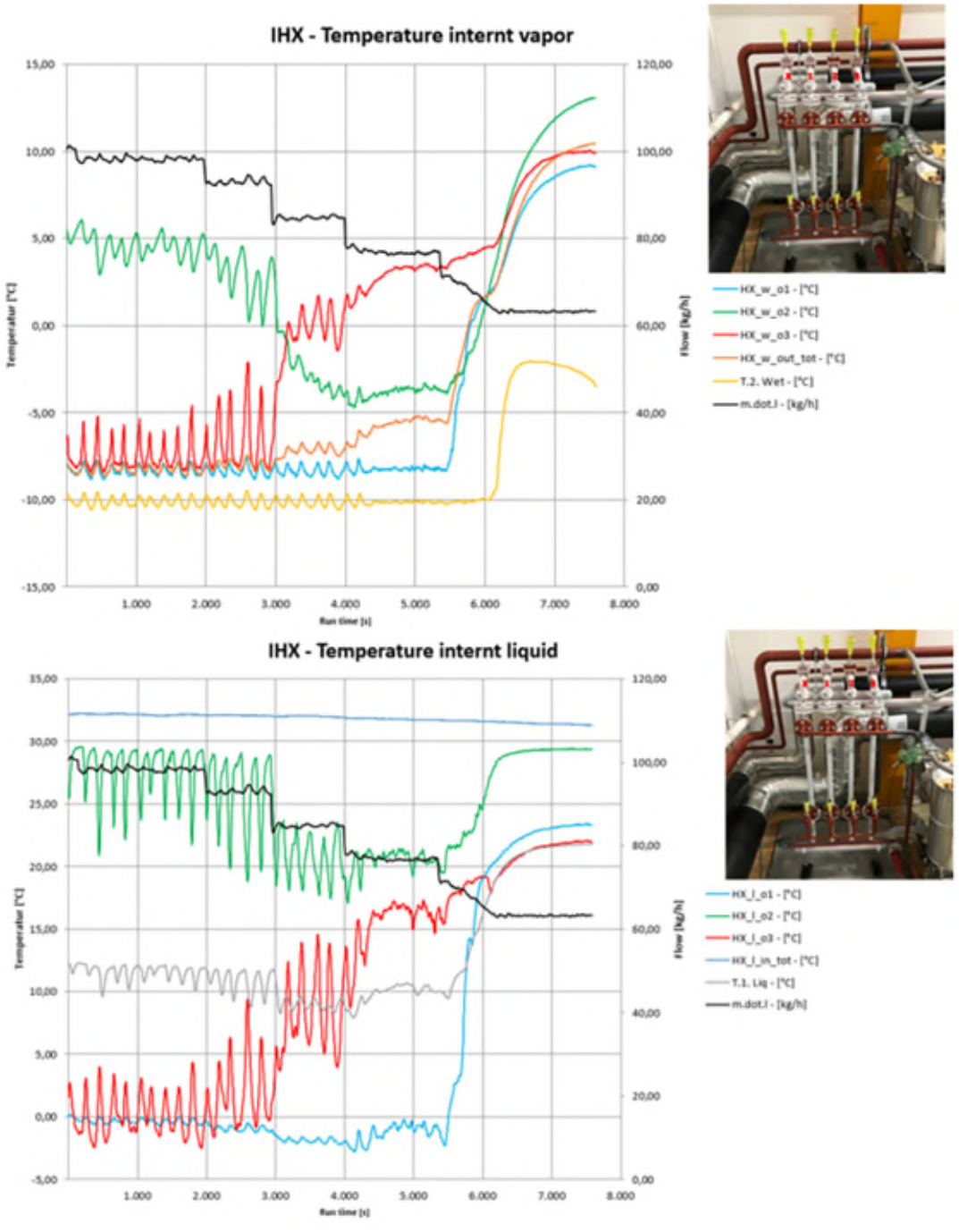


**Figure 94: SGHX temperatures.**

Looking at the lowest circulation rate that it is possible to run with, Figure 92 shows a very stable capacity until the suction gas from the evaporator starts to get superheated. For the

WDX solution it can be concluded that it should be possible to control the circulation rate down to very close to 1 without losing capacity.

The changes in charge can be seen from Figure 95. The circulation number in this test has been rather low ranging from 1.3 and down to superheated gas out of the evaporator. What can be seen is that the charge follows the OD of the valve and thereby the flow through the evaporator and the circulation rate.

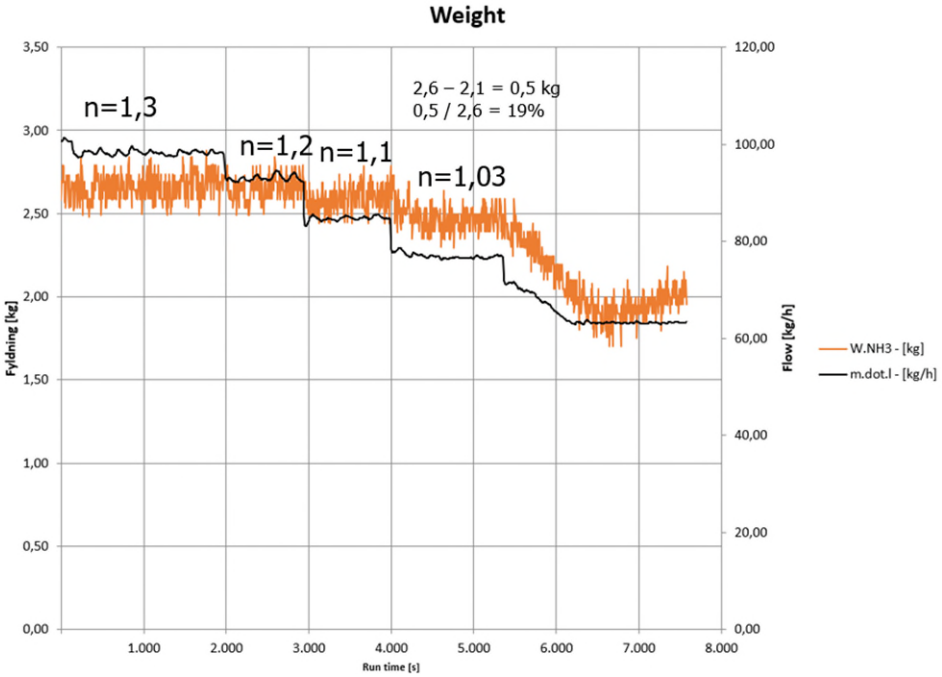


**Figure 95: Changes in charge.**

Going from flooded to superheated gas out of the evaporator reduces the charge the most or by 19 %. On the other hand, to maintain the capacity, the evaporator would also have to be bigger to maintain the capacity, so the reduction will not be as significant as shown in the graph. When going from a circulation rate of 1.3 down to n=1.03, the reduction in charge is about 7 %.

***Conclusion***

The answers to the questions raised in the start of the section are:

1 - It seems that is should be possible to use the superheat after the SGHX if the expansions valve has finer steps per % OD. This could maybe be implemented by having a smaller parallel valve taking care of the fine tuning of the flow. More measurements are needed to verify this.

2 – From measurements it is seen that there is a change in the signal going from flooded to dry. How to apply this signal to the control depends on many factors and there is a need for more measurements.

3 – The problem with the SGHX in the test setup seems to be the maldistribution in the SGHX. This could be eliminated by using another type of heat exchanger without parallel circuits, i.e., coaxial pipe in pipe heat exchanger.

4 – From measurements on this evaporator is seems that it is possible to maintain the capacity down to a very low circulation rate. It depends on the maldistribution of the evaporator how low it is possible to go. More measurements are needed to verify this.

5 – The reduction in charge seems to follow the circulation rate. In this measuring series, the circulation rate had a low value to start with, so the reduction in charge was not that large. The reduction was measured to be 7 %.

### 6.3.3.2. Series 8-FARS-DR-reg-IHX-Zimmermann

This test was made to investigate the idea that came up in the beginning of the project to modify a method proposed by Zimmerman. Here the high-pressure liquid is flashed into the SGHX. This is demonstrated in Figure 96. The green line represents the high-pressure liquid from the condenser expanding to the SGHX through the first motor valve. The second motor valve before the evaporator controls the liquid into the evaporator. In this test, this will be simulated by manually closing a stop valve before the SGHX until a flashing of the gas is represented. Then the refrigerant fed to the evaporator is controlled by the expansion valve.

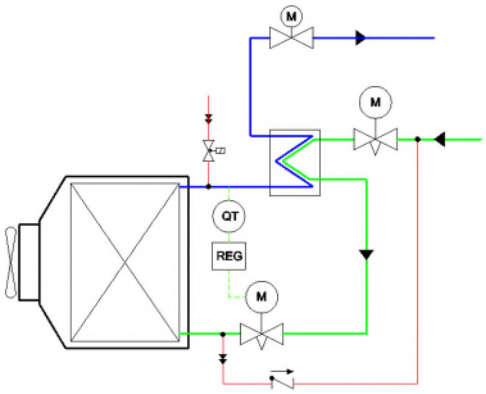


**Figure 96: Zimmerman method.**

The test started out with a high temperature setpoint for the climate chamber and thereby a large capacity on the evaporator. To start with, the expansion valve was 100 % open and was not able to control the SH. The temperature setpoint was gradually reduced until the expansion valve started to close and take over the control of the SH. From there on, the temperature setpoint was reduced.

The question to be answered in this test is the following:

1. Is it possible with normal SH control to control the evaporator after the SGHX by establishing a stable intermediate pressure in the SGHX?

### *Measurements*

As is shown in Figure 97, the expansion valve was 100 % open until the temperature setpoint of the climate chamber was down under 0 °C. This is seen by the fact that the superheat out of the evaporator (TSH.e.o) and out of the SGHX (TSH.IHX.o.corr) is high.

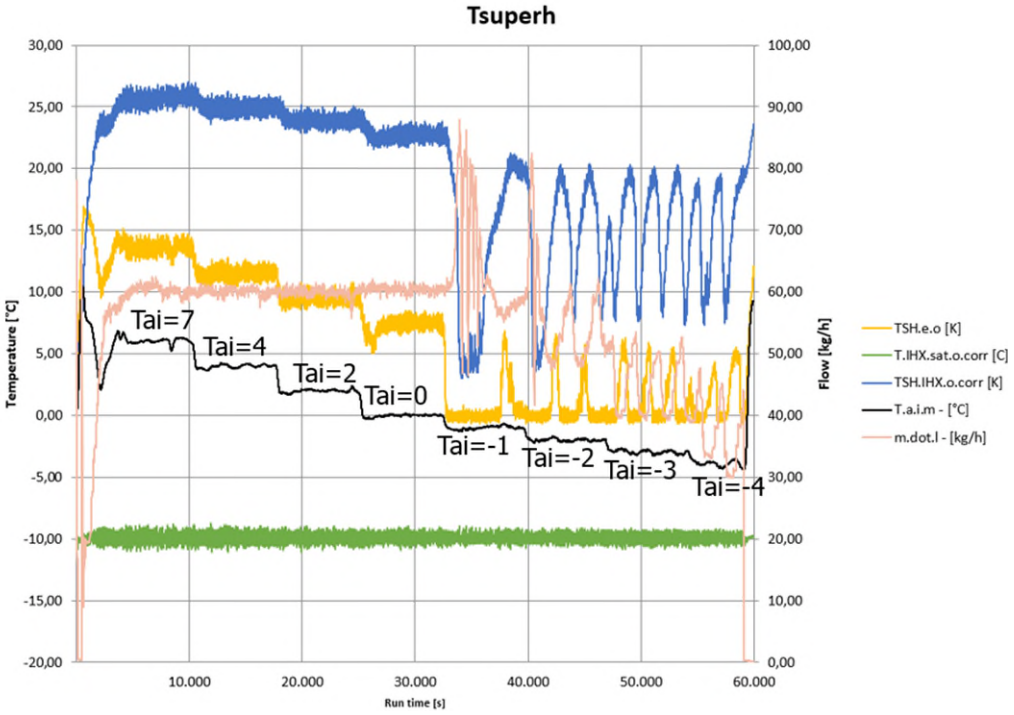


**Figure 97: Temperature measurements.**

The inefficient size of the valve for higher temperatures is, because of the reduced supply pressure that the valve gets in this test, caused by the intermediate pressure in the SGHX.

To investigate the control behaviour of the valve when controlling the SH, the graph in Figure 98 is shown. Here, the measurements from 30000 sec. are shown. In this part, the expansion valve is controlling the SH. As can be seen, the same oscillation occurs as before on the SH control, and it is not possible to obtain stable control.

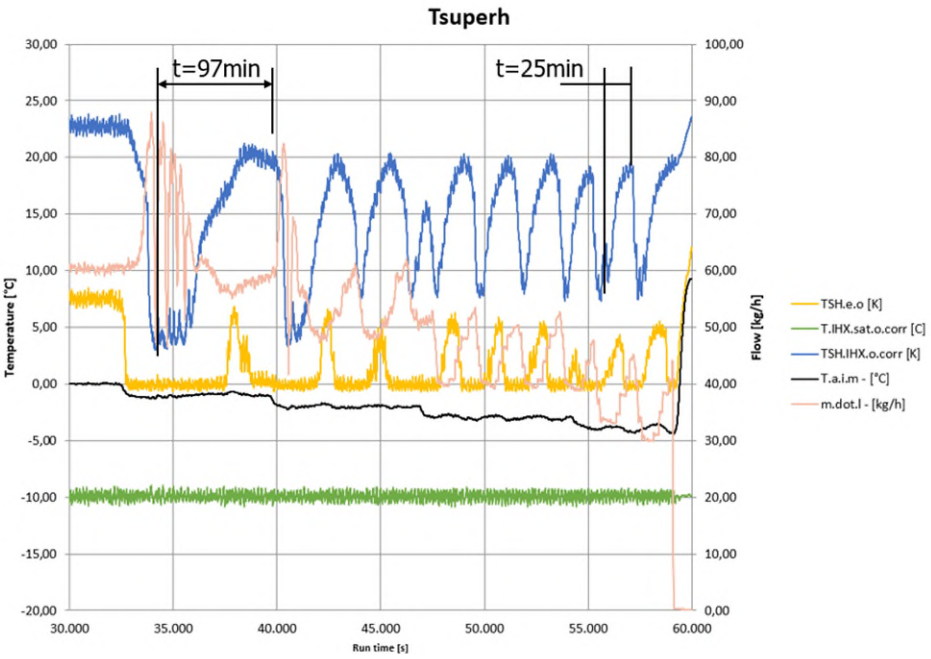


**Figure 98: Temperature measurements from 30000 sec.**

***Conclusion***

The answer to the question raised in the beginning of the section is that it was not possible to get a stable control of the expansion valve by using the modified Zimmerman method.

### 6.3.3.3. Series 9-FARS-DR-man-med-og-uden-IHX

This test series was conducted to verify the savings by running the same evaporator with a normal SH control of 8K against running with a slightly flooded evaporator. This was obtained by raising the suction temperature until the same capacity was reached for the flooded as for the superheated.

The question to answer in this test was:

1. How much can the saturated suction temperature be raised for the same capacity for the evaporator running on 8K SH compared to one running flooded?

The test was conducted with manual adjustment of the expansion valve until the SH of 8K was reached. Then the valve was opened until the evaporator was flooded. Then the saturated suction temperature was increased until the same capacity was measured. This is a measure of the energy savings when running with overflooded evaporators compared to DX.

In the test, the ETD of the selected evaporator is 10K, i.e., the air temperature into the evaporator is 0 °C, and the saturated suction temperature is -10 °C. In this case we can reach the 8K SH in the evaporator. The air cooling through the evaporator is 4K so the leaving temperature difference (LTD) of the air is 6K. An ETD difference of 10K is large and is normally 5K in overflooded installations. In this case the punishment of needing a superheat for the expansion valve is more severe. This extra punishment of needing SH for the evaporator controller compared to flooded is explained in Figure 99. If it is assumed

that the minimum temperature difference between the air and the refrigerant in the evaporator is 1K, and the air stream is to be cooled from 0 °C down to -4 °C, the saturated suction temperature for a flooded evaporator must be -5 °C. For the SH controlled i.e., DX with the same assumption, the highest temperature on the gas out of the evaporator is -1 °C if the flow is pure countercurrent. Then to be able to reach the 8K superheat, the saturated suction temperature must be -9K, i.e., 4K lower than for flooded operation. The assumption of pure countercurrent flow and the same temperature approach between liquid refrigerant and air in the flooded as between refrigerant gas and air in the superheated case is not true, and in real applications the benefit will be larger than here explained.

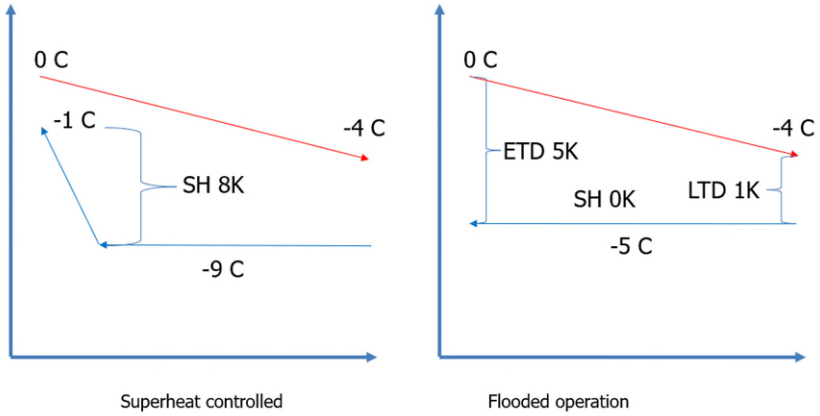


**Figure 99: Superheat driven vs. flooded evaporator.**

***Measurements***

As can be seen in Figure 100, the saturated suction temperature with an SH of 8K was -9,88 °C. When the evaporator was running slightly flooded, the saturated suction temperature was raised to -8,75 °C. This is an increase in saturated suction temperature of 1.13K.

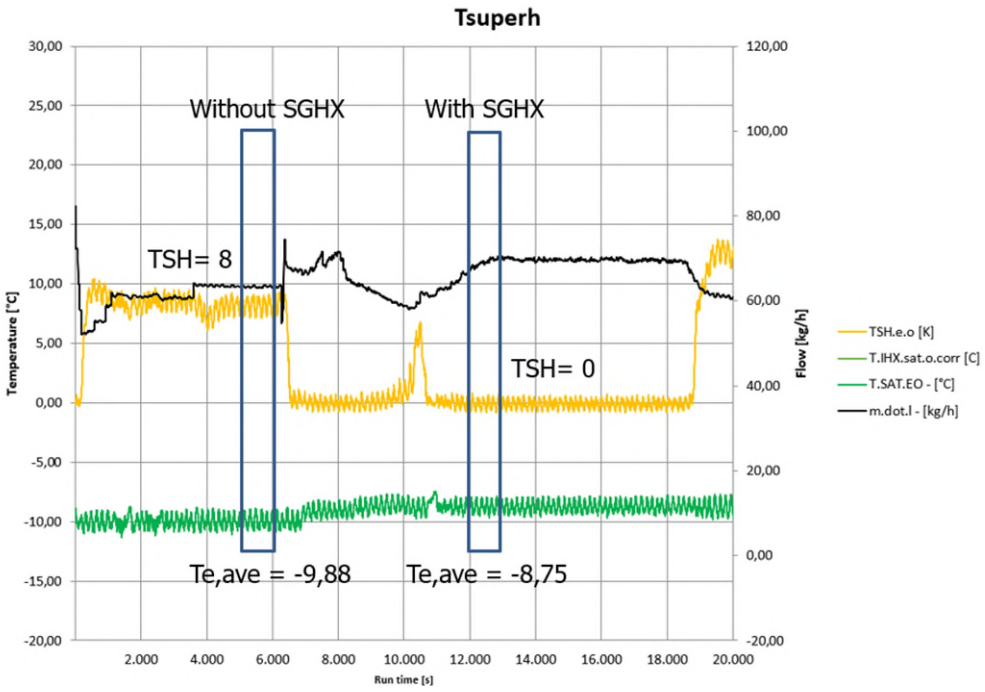


**Figure 100: Temperature measurements.**

When looking at the capacity of the evaporator, the capacity was not exactly the same. The capacity under flooded conditions was slightly higher than 22kW and with an SH of 8K slightly lower than 22kW.

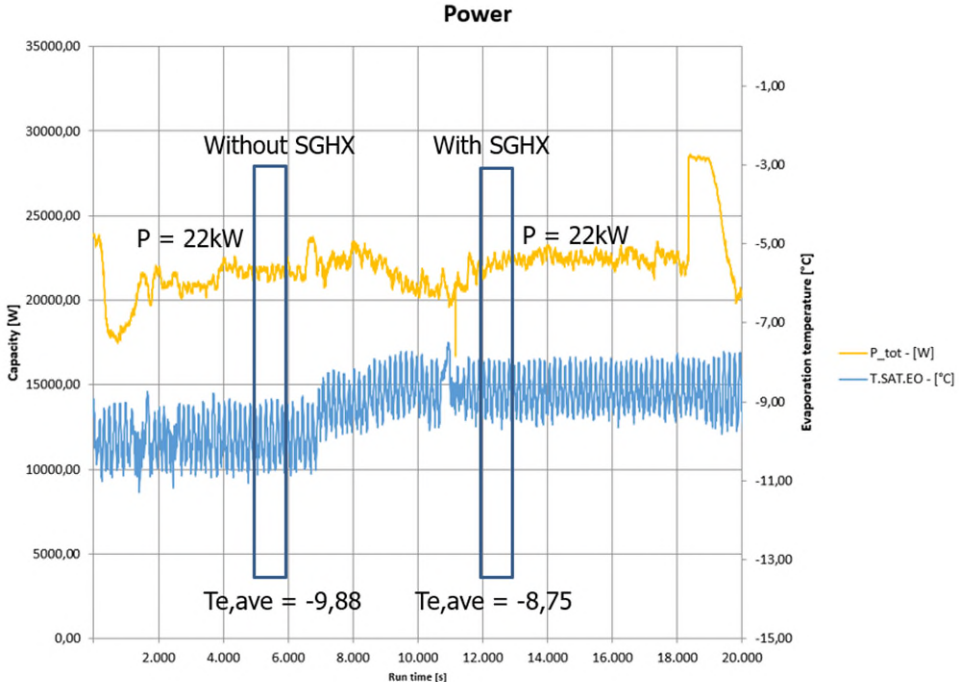


**Figure 101: Capacity of the evaporator.**

To reach the exact same capacity in the test setup is difficult, but if it is possible, the savings in saturated suction temperature would be higher than the 1.13K as mentioned before.

***Conclusion***

To answer the question raised in the beginning of the section, a saving of at least a 1.13K higher saturated suction temperature was measured. By using the rule of thumb that each degree will give a saving in energy of at least 3 to 4 %, one can assume the savings to be from 3.4 % to 4.5 %.

If considering a normal ETD of an overflooded installation of 5K and a required SH of 8K, the reduction of the saturated suction temperature is needed to be able to reach the required SH. In the example explained in Figure 99, the needed extra lowering of the saturated suction temperature to be able to supply the required SH is of 4K. The energy savings in getting the SH out of the evaporator from this alone would be in the range of 12 to 16 % by using the rule of thumbs as before.

By adding these savings, the total estimated savings by running a WDX evaporator or by getting the SH out of the evaporator compared to SH controlled (DX) would be in the range of 5.13K corresponding to from 15.4 % to 20.5 %.

### 6.3.3.4. Series 20-FARS.DR-AKV-Uden-Sugegasveksler SH CCR6 -10C Step

This test was made to see the effect of placing the CCR sensor on the driest circuit of the evaporator. Two test runs were conducted. The first with step in the saturated suction temperature and then step in the fan.

The questions that the test should try to answer were:

1. What is the effect of placing the heated sensor on the driest circuit, i.e., circuit 6?
2. What should the SH reference be for a saturated suction temperature of -10 °C?

***Measurements***

*Test run 1 – Step in saturated suction temperature*

In this test run, the steps in the capacity were implemented by changing the saturated suction temperature. By looking at the temperature measurements in Figure 102, it is seen that the controller will control the SH signal to the reference after steps in the saturated suction temperature. The evaporator seems to be more flooded than when the sensor was placed on the common suction pipe but less flooded than when it was placed on the driest circuit, i.e., number 1 as expected. The less flooding when the sensor is on common suction pipe is probably because of the placement of the sensor and because of a larger diameter of the pipe. The larger diameter participates in a distinct separation of the liquid and gas giving the placement of the sensor a crucial importance.

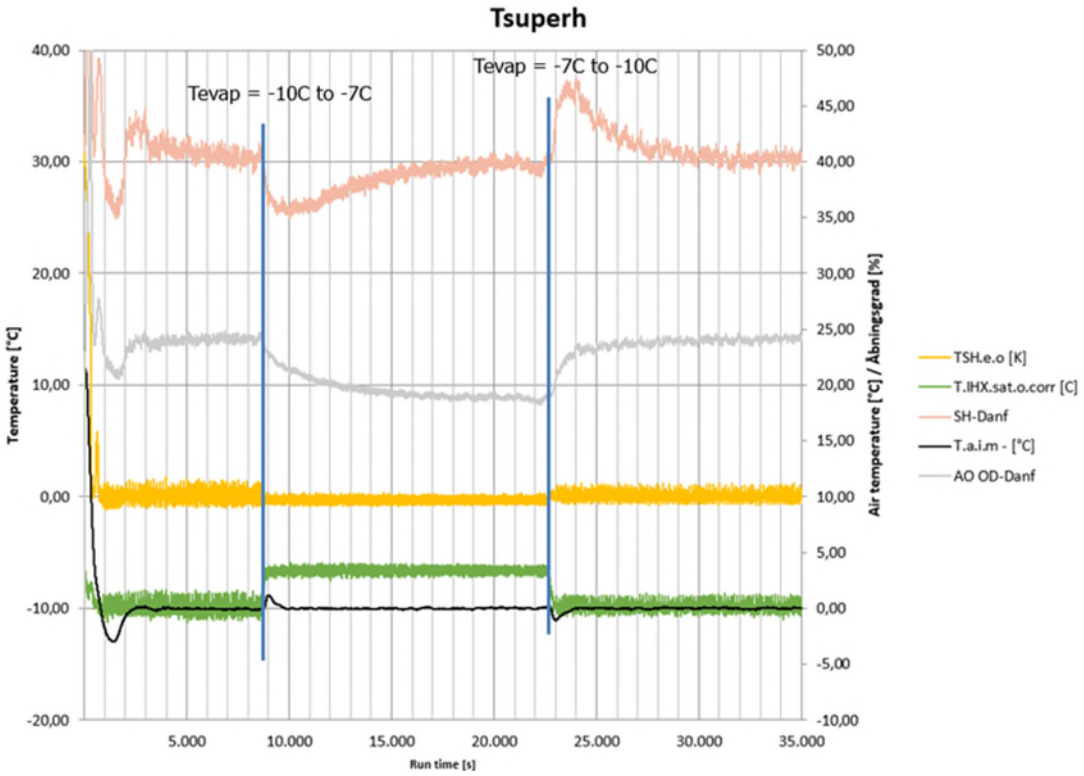


**Figure 102: Temperatures.**

When depicturing the CCR temperature measurements in Figure 103, more distribution is noticed compared to series 19 where the CCR sensor was placed on circuit 1 which is the most wet circuit. Here the circuits 1, 2 and 3 seem to be less flooded and the others more flooded.

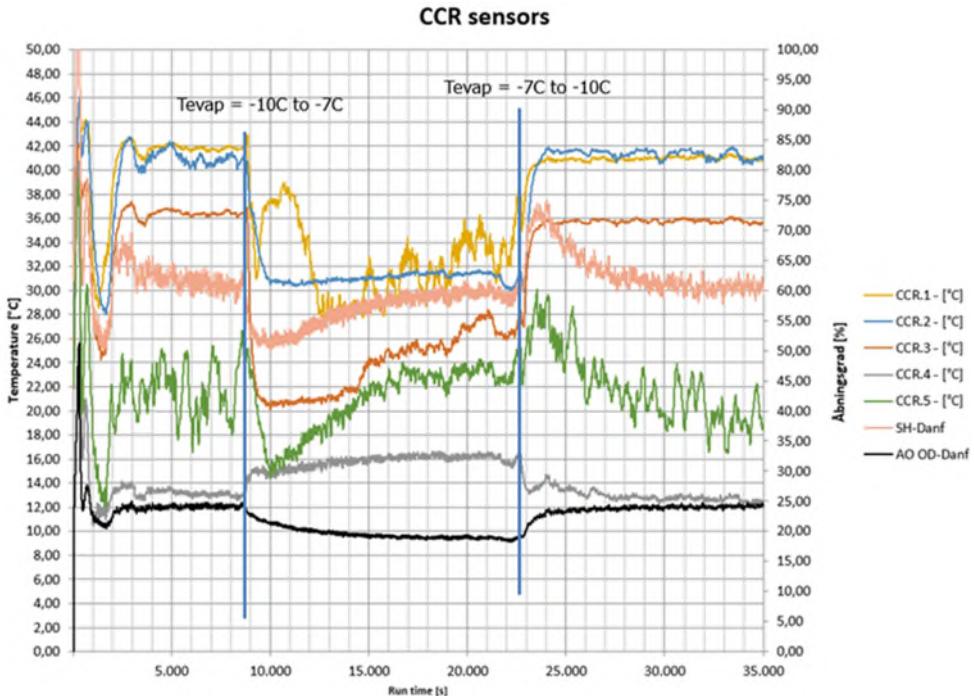


**Figure 103: CCR temperatures.**

Looking at the quality in Figure 104, and comparing to series 19, it is seen that the evaporator is running more dry as expected.

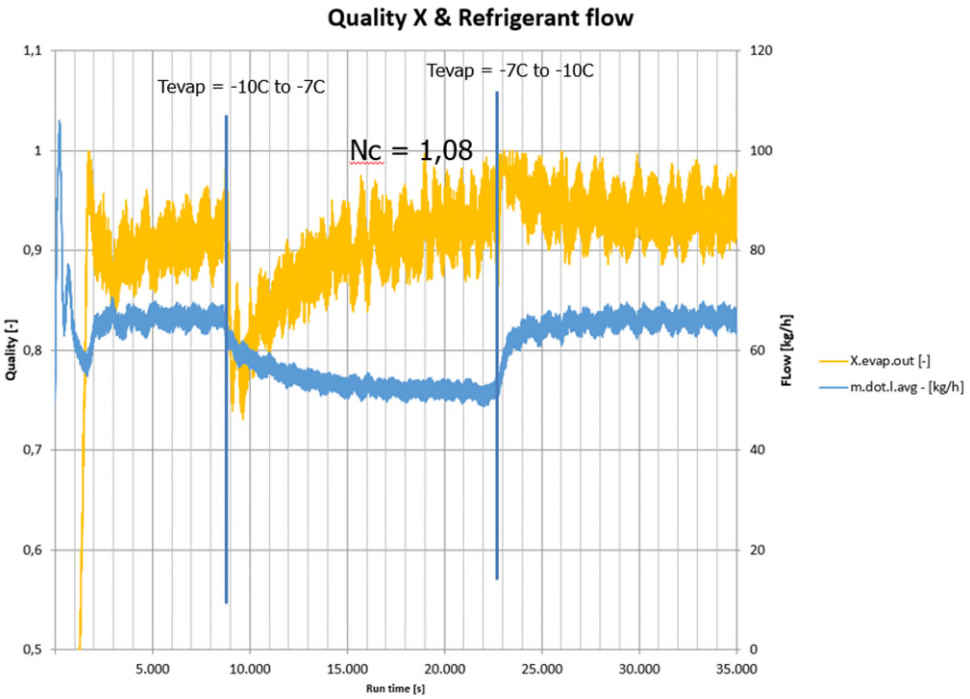


**Figure 104: The quality.**

### *Test run 2 – Step in the fan*

In this test run, the steps in capacity were provoked by changing the fan speed. The fan speed was first reduced and then increased again to see if the evaporator returned to the same conditions as before the change. When looking at the temperature measurements in Figure 105, the controller adjusts the SH to the reference at start-up of the system. Then, when the fan is reduced from 100 % to 50 %, the controller starts to close the expansion valve as it should, and the SH is on its way towards the SH reference.

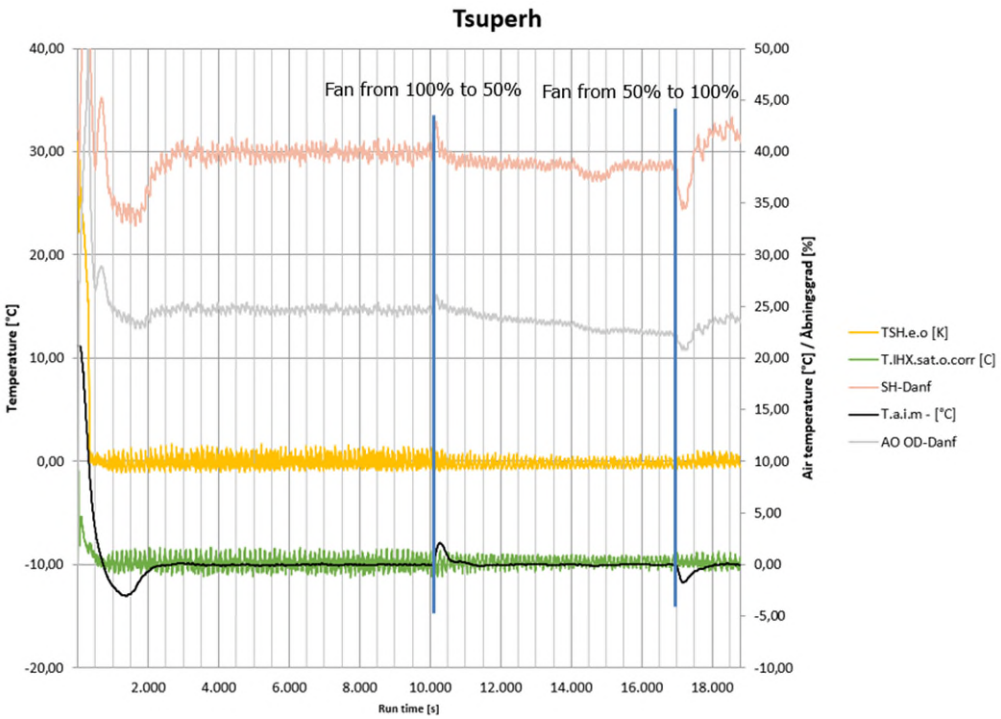


**Figure 105: Temperatures.**

When increasing the fan speed to 100 % again, the controller reacts and opens the valve and compensates for the deviation. By looking at the SH out of the evaporator, it can be seen to be on the limit of flooded for 100 % and more flooded at a lower load on 50 % fan. This can be seen by a larger fluctuation in the measured superheat out of the evaporator (TSH.e.o).

The CCR temperature measurements in Figure 106 show the same where three of the circuits are close to dry while the others are more flooded. After the change in fan speed, the CCR temperatures is lowered to a more stable condition meaning a more flooded condition.

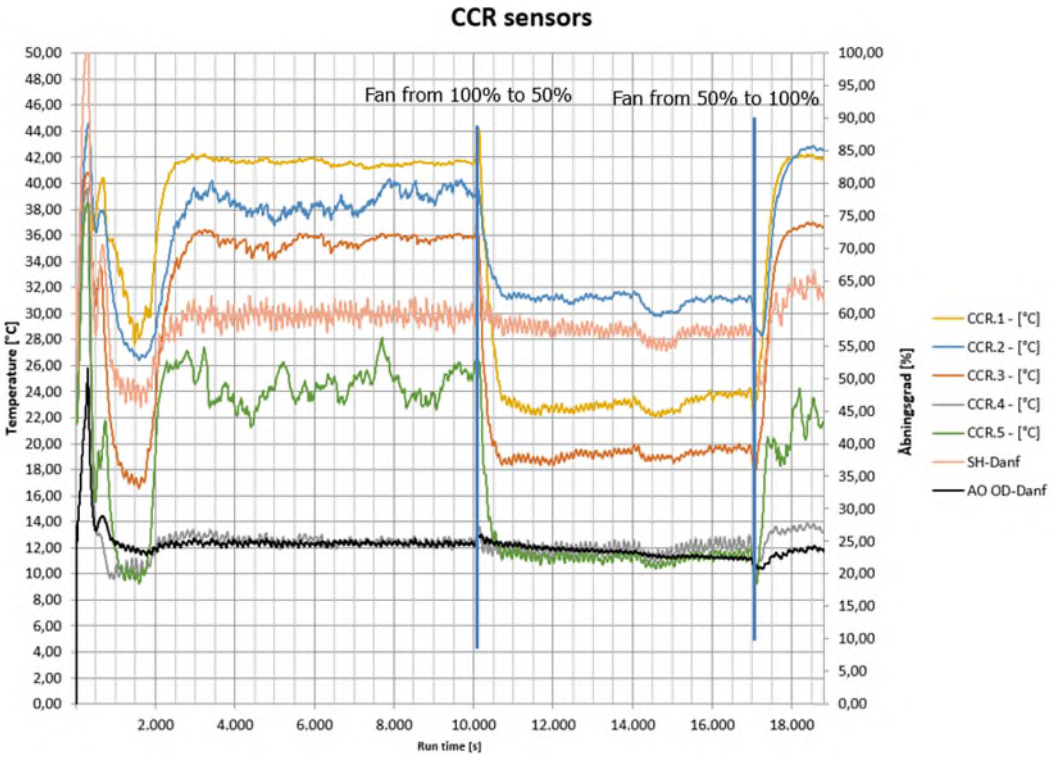


**Figure 106: CCR temperature measurements.**

When looking at the quality out of the evaporator in Figure 107, the same tendency is seen.

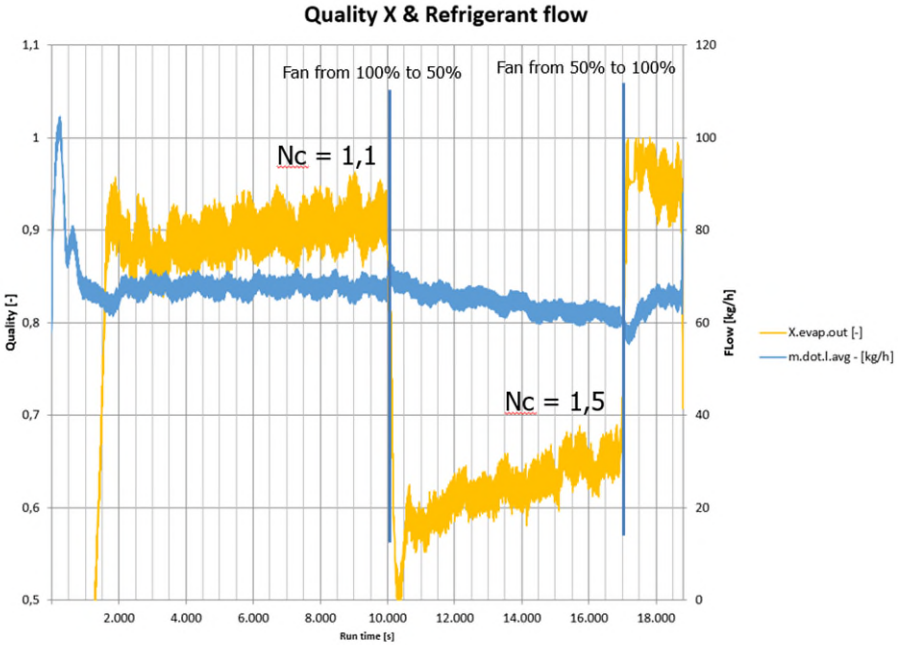


**Figure 107: The quality.**

After the last change in fan speed to 100 %, the quality is reducing and will return to the original state when the SH reaches the SH reference again.

***Conclusion***

The answer to the questions raised in the beginning of the section of the CCR sensor placed on the driest circuit is that the evaporator runs in total more flooded than when the sensor is placed on the most wet circuit.

The SH reference for a saturated suction temperature of -10 °C should be slightly lower than 30K - maybe 25K. This indicates that the SH reference is dependent on the saturated suction temperature.

### 6.3.3.5. Series 23-FARS.DR-AKV-UdenSHX SH CCR6 -10C Step pumpe

During the tests, an idea emerged of trying to use the evaporator designed for WDX for pumped circulation systems. Instead of the high-pressure liquid from the condenser, the expansion valve was connected to the liquid ammonia circulation pump and the valve used to control the circulation ratio.

In this test, the pumped circulation of the WDX evaporator was tested for a saturated suction temperature of -10 °C with the heated censor placed on the driest circuit, i.e., circuit 6. Two test runs were conducted – one with an SH reference of 40K as a starting point, and then the SH reference was lowered to 35K. Steps were conducted by changing the fan speed.

The questions that the test should try to answer were:

1. Is it possible to use CCR and the liquid distributor for liquid overfed systems?
2. What should the SH reference for the -10 °C be?
3. What is the charge of the evaporator during the test?

***Measurements***

*Test run 1 – SH reference 40K*

In this test run, the SH reference was 40K, and a step in the fan was done. At the finish of the test, a pumped down of the evaporator was done to be able to get a reference to the weight measurements. A charge estimation was done.

When looking at the temperatures in Figure 108 on 100 % fan, a superheat is measured out of the evaporator (TSH.e.o). This indicates that the SH reference is too high. When reducing the fan down to 50 %, the controller can adjust the SH to the reference and keep the evaporator flooded.

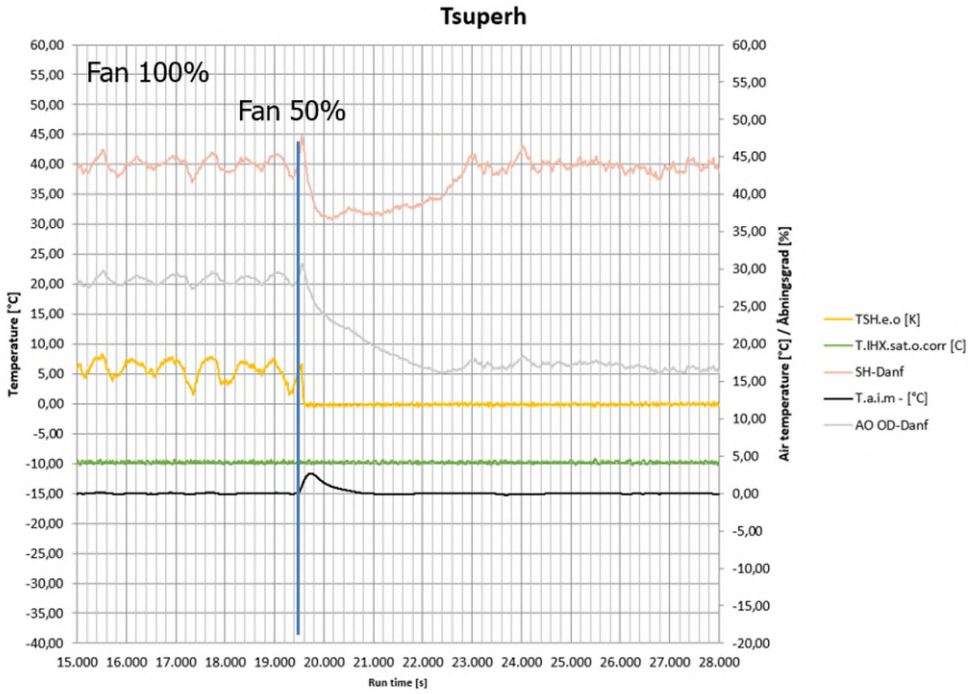


**Figure 108: Temperatures**

The capacity of the evaporator on 100 % fan and a slight superheat is around 22 kW as seen in Figure 109.

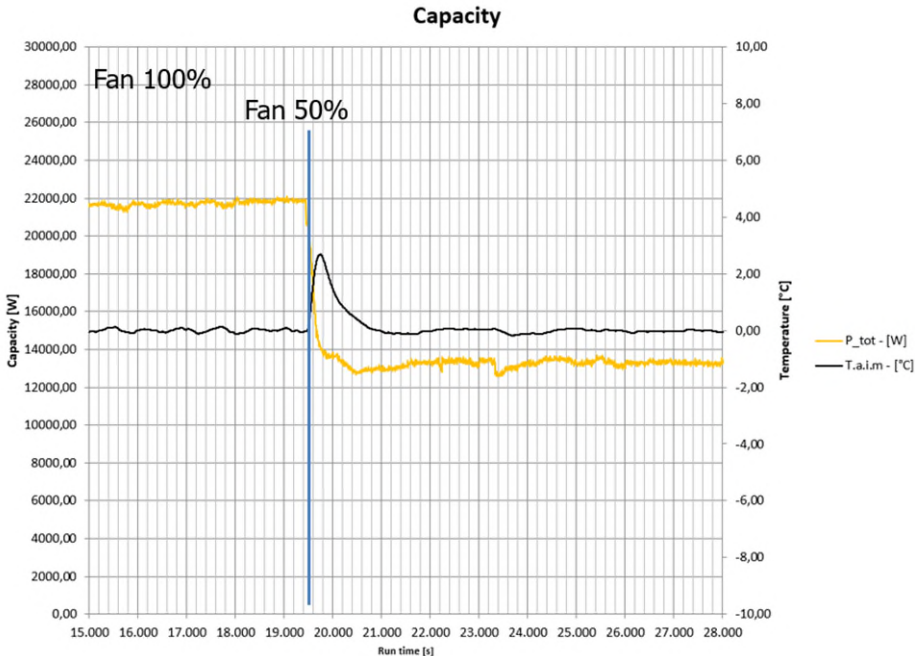


**Figure 109: The capacity**

When looking at the CCR sensor temperatures in Figure 110 it is seen that the temperature fluctuates before the change of fan speed indicating a close to limit between wet and flooded. Right after the change in fan speed, the evaporator gets more into the flooded zone and then retrieves back to the limit when the controller is on the reference.

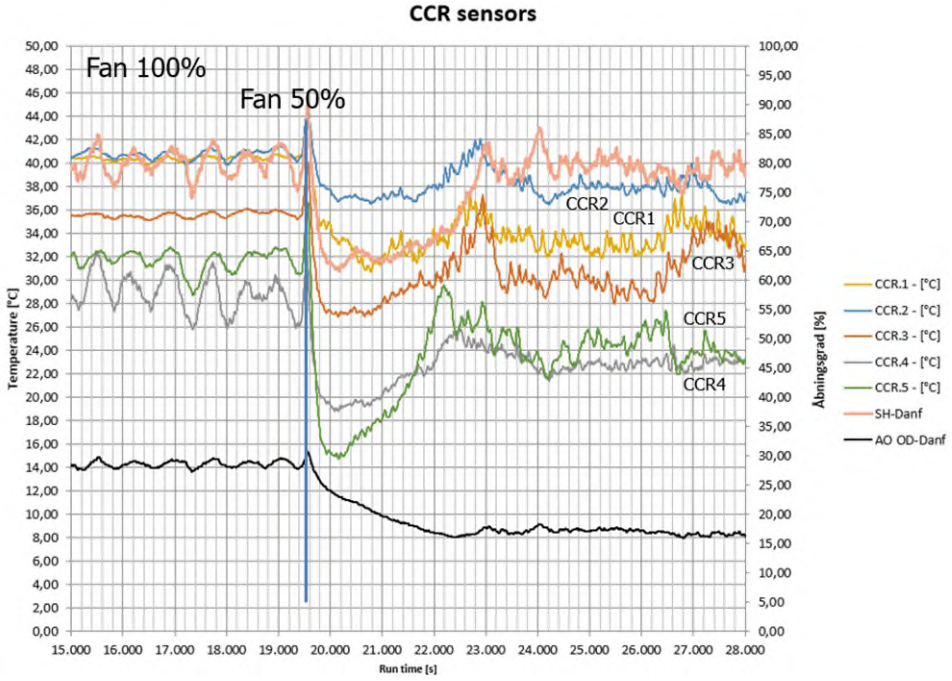


**Figure 110: CCR temperatures.**

The quality in Figure 111, which is calculated from the average of the last 20 measurements, shows that the evaporator is close to the limit between dry and flooded.

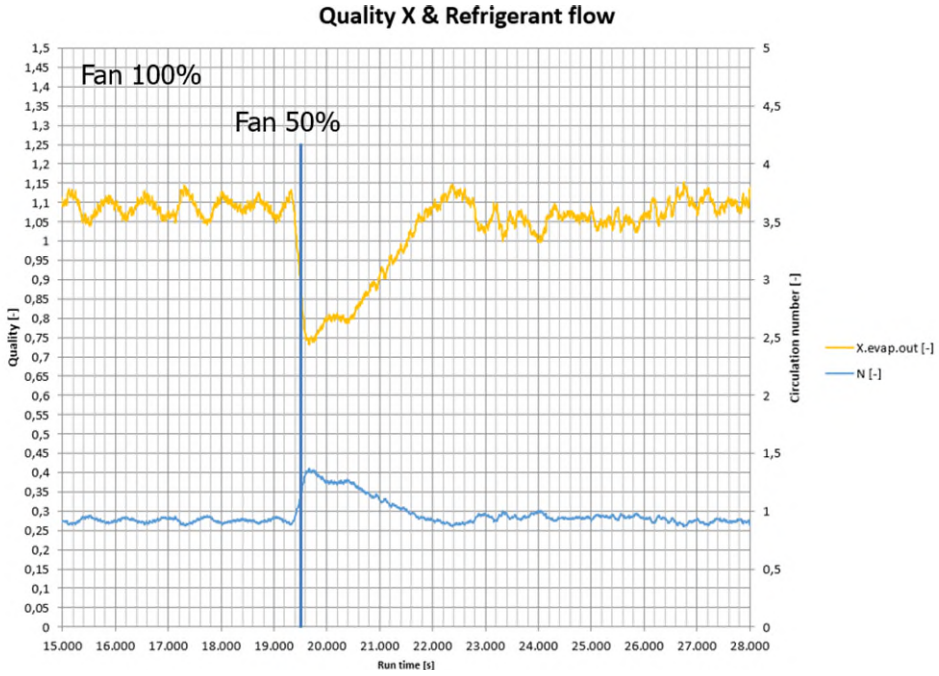


**Figure 111: The quality.**

A pumped down was performed in this test series at the end of measurements to find the weight of the evaporator when all the liquid refrigerant was boiled off. The measurements are shown in Figure 112.

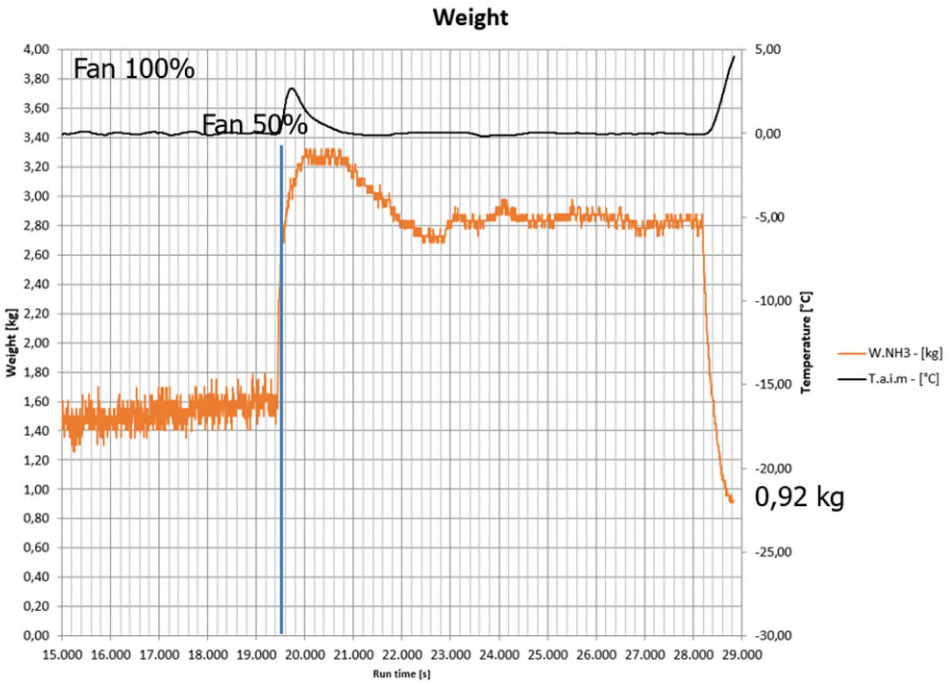


**Figure 112: Weight measurements.**

At the end when all liquid refrigerant was boiled off, the load cells showed 0.92 kg. By subtracting this value from the measurements just before the pumped down, the charge can be found to be 1.9 kg. When the fan was operating at 50 % compared to 100%, the charge increased. This indicates that the refrigerant is backing up in the evaporator during part load. The specific charge of the evaporator at 50 % load of the fan is 0.15 kg/kW.

### *Test run 2 – SH reference 35K*

Here, the same test run was conducted just with an SH reference of 35K. This was expected to give a more wet evaporator.

When looking at the temperatures in Figure 113, the controller can retrieve the SH to the reference after a step in the fan. Another notification is that after the fan is back on 100 %, the evaporator is still flooded. This was expected as the lowering of the SH reference should lead to a more flooded evaporator.

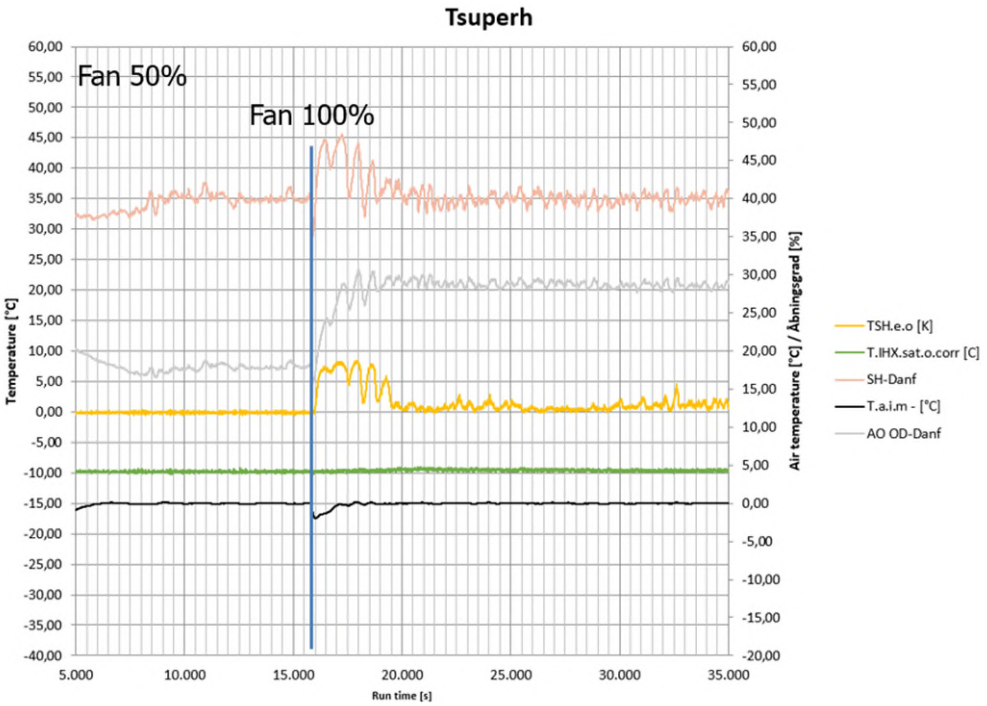


**Figure 113: Temperatures.**

When looking at the capacity in Figure 114 it seems close to the one for test run 1.

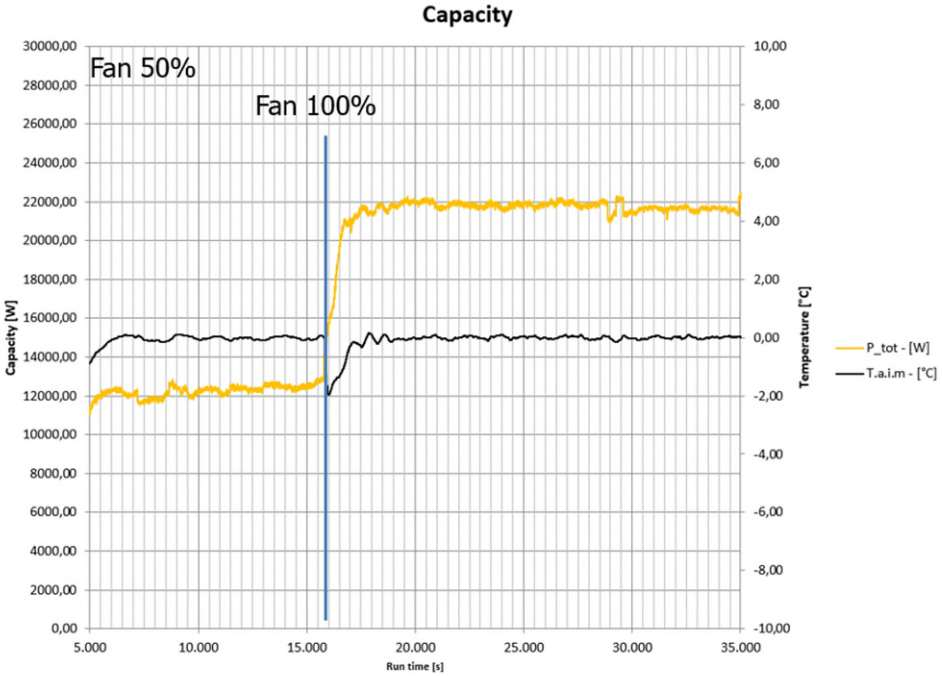


**Figure 114: The capacity.**

When looking at the CCR temperatures, they are fluctuating indicating that the evaporator is close to the limit zone between flooded and dry. Right after the fan is set on 100 %, the evaporator dries out and then returns to the same again.

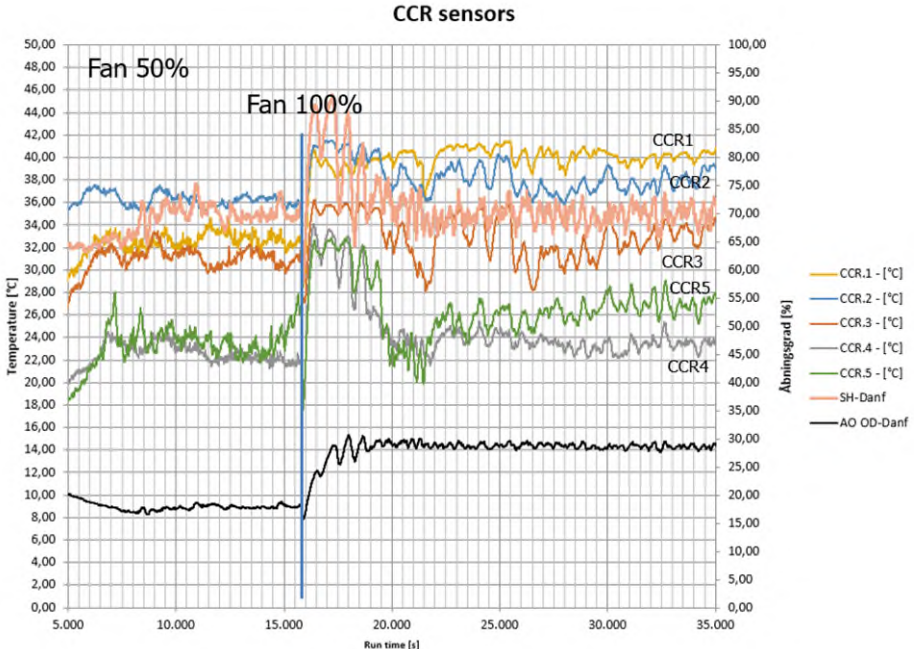


**Figure 115: CCR temperatures.**

The quality in Figure 116 verifies that the evaporator is running more flooded than in test run 1 as expected. To run the evaporator even more wet, the SH reference could be adjusted lower, i.e., maybe to 30K, or the effect on the heated sensor could be increased.

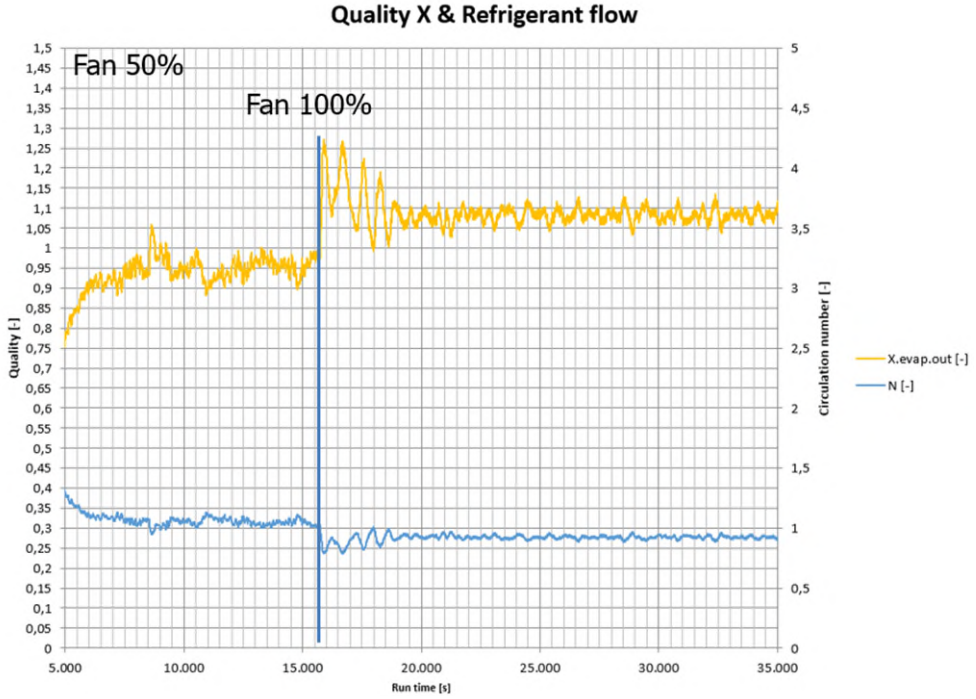


**Figure 116: The quality.**

This shows that there is a connection between the SH reference and the saturated suction temperature and the amount of power to the heating element in the CCR sensor.

At last, a weight measurement was conducted as seen in Figure 117. Here, the weight after pumped down was 0.34 kg. The measured weight on 100 % fan just before pumped down is 1.5 kg. The weight is seen to increase steadily after the fan is turned on to 100 %. This is probably due to the ice build-up on the coil that biases the measurements. The only measuring point that is valid is the one taken directly before the pumped down.

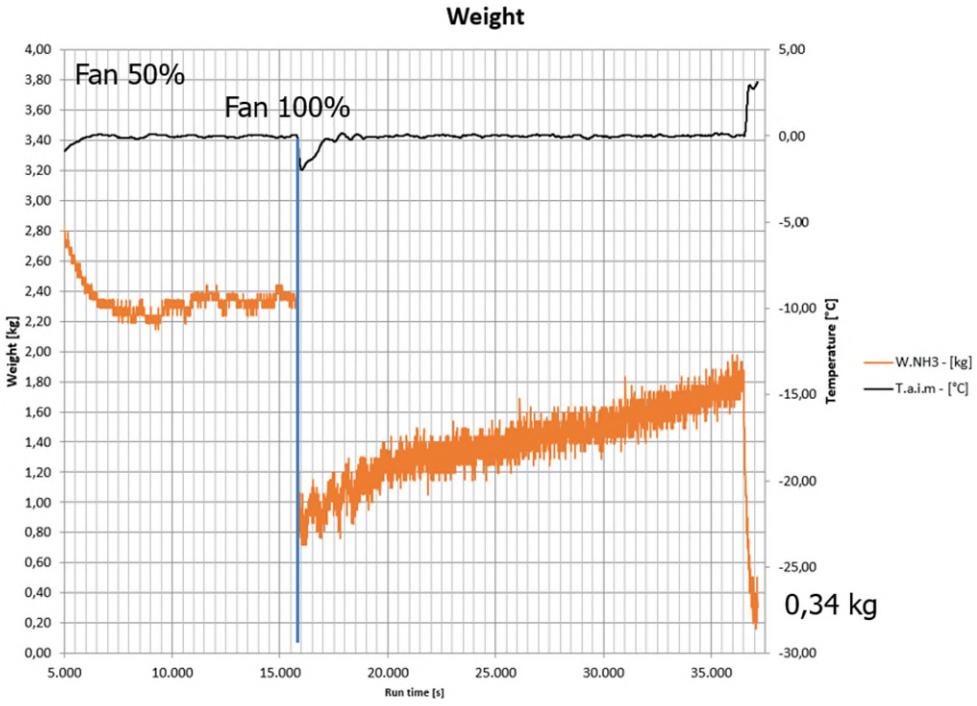


**Figure 117: Weight measurements.**

In test run 1, the weight for 50 % fan was measured to be 1.9 kg. The difference between 100 % and 50 % is a 0.4 kg larger charge when running at 50 %. This is a 21 % increase. The specific charge in the evaporator when the fan is running with a 100 % load is 0.07 kg/kW.

### *Conclusion*

To answer the questions raised in the beginning of the section, it seems to give good results to use the liquid distributor and the side-fed evaporator for the pumped circulated application. The distributor seems to even the maldistribution and increase the controllability of the evaporator.

The SH reference for -10 °C should be somewhat lower than 35K, i.e., maybe around 30K.

It was found that the charge is hard to measure because of ice accumulation in the evaporator coil. The only point that can be verified is the measurement point directly before a pumped down. After pump down, the weight contains both the ice and deviation in the evaporator weight. The measurement showed that the charge at 50 % fan speed was 1.9 kg, and at 100 % fan load, the charge was 1.5 kg. The specific charge of the evaporator was 0.15 kg/kW on 50 % fan speed and 0.07 kg/kW on 100 % fan speed.

### 6.3.4. Summary and conclusions

The suction gas superheater (SGHX) was tested and revealed that the way the SGHX design was unsatisfactory. There wase too much maldistribution in the four parallel sections, and the liquid just flowed the easiest way through the SGHX. A better solution would have been to select a coaxial SGHX.

The measurements also showed the importance of being able to fine adjust the expansion valve. The first valve tested was too coarse, and the influence of each step for the valve was too large. The selected valve must be so small that each step has a small influence on the ammonia mass flow, and the narrow area that the valve must control within includes many steps. This results in a valve with a very small orifice. The disadvantage of such a small orifice is that dirt in the system and oil easily plugs the valve. The valve that gave the best results was a pulse modulating valve where the opening degree was controlled by a frequent open and closing time that can be adjusted to control the valve.

The idea of the modified Zimmerman method was tested, and the test showed that it was not possible to get a stable control of the evaporator using this method.

A test was conducted to measure the benefit of using an overheated control strategy (DX) versus a slightly overflooded. The estimated savings were from 15.4 to 20,5 %. This is without the losses that comes from a riser leading the suction gas from the evaporator up to the common suction line and long wet suction pipes back to the pumped separator, so the estimated savings would be higher.

A control loop to test the automatic control of the evaporator was set up and consisted of the new heated sensor connected to a modified controller running with fixed SH. The expansion valve was chosen as a pulse modulation valve of type AKVA from Danfoss. With the heated sensor placed on the driest circuit it was possible to control the SH signal after a step in both evaporation temperature and fan speed. The measurements also showed that the SH reference had to be adjusted according to the saturated suction temperature.

Tests were conducted where the liquid inlet to the evaporator was connected to the pumped circulated system. This was done to investigate if the specially designed evaporator for WDX with venturi liquid distributor could also be used for liquid overfeed control. It turned out to work well and it was possible to control the circulation ratio close to the border between dry and overflooded.

## 6.4. Micro channel tests

### 6.4.1. Introduction

The purpose of the tests for the micro channel evaporator was to evaluate a new design (explained in section 4.4) and compare it to simulations and a conventional evaporator design as tested under the CCR test. The main topics are:

1. What is the areal reduction compared to conventional evaporators for the same capacity?
2. What is the reduction in charge compared to conventional evaporators?
3. How is the defrosting compared to conventional evaporators?

The micro channel evaporator was designed to give the same capacity as the conventional evaporator, and the purpose of the test is to verify the design and measure the capacity and the charge for various circulation numbers.

One of the concerns regarding micro channel evaporators is the defrost. A test to compare the water drainage and defrosting time was conducted. It is assumed that the defrosting time is much shorter since the micro channel is very compact and all aluminium. But the somewhat lower heat transfer area will allow for a less amount of ice build-up and is thereby expected to need defrosting more frequently. The optimization of the defrosting is thereby very important to reduce the total defrosting time of the coil. The test is conducted to reveal the amount of ice that can be allowed to build op on the surface, the defrosting time, and the water drainage from the coil during defrost.

### 6.4.2. Test setup

The P&ID drawing of the test setup is shown in Figure 118. The micro channel evaporator is connected to the small ammonia pump separator. The existing valve stations are used, and the evaporator is connected to the low-pressure liquid, suction and defrost pipelines. The evaporator has two coils and thereby the liquid from the refrigeration pump is divided in two in front of the evaporator and connected through AKVA valves to the coils.

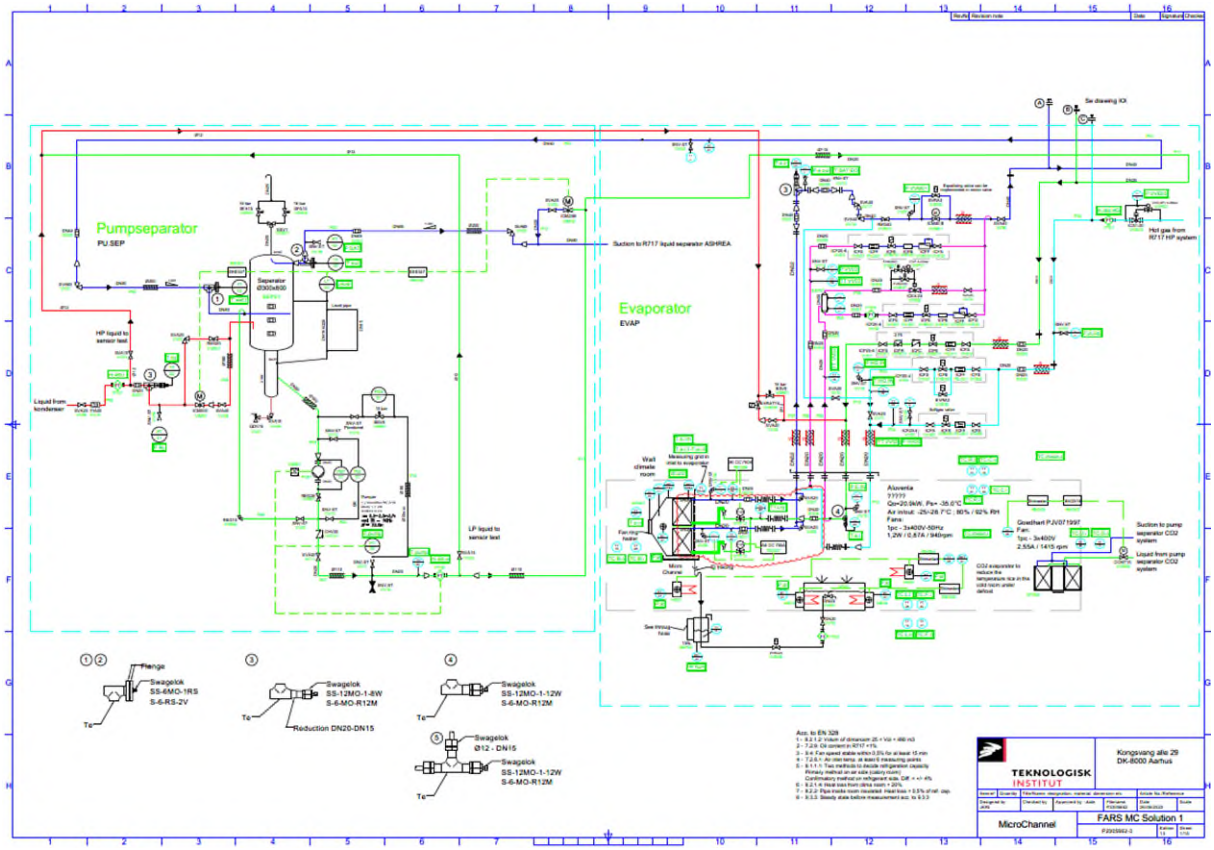


**Figure 118: Micro channel test setup.**

The AKVA valves are used to control the liquid flow to each section in the evaporator. The main liquid valve is kept open during normal running conditions. When performing defrost, the AKVA valves are fully opened, and the main liquid valve is closed. In this way, the condensed defrost liquid from the coil is lead through the AKVA valves on its way to the defrost valve station which is used during defrost.

### 6.4.3. Main results

The several tests that were conducted can be divided into three test groups. The first was where different types of micro channel profiles and fins were tested for water drain ability. The second group consisted of tests to measure the capacity and the charge of the coil and to compare to the traditional fin and tube. The third group contained a group where the coil was iced up subsequent defrosting. Under this chapter the last two groups will be replicated:

1. *Series 3 - FARS—30 op_ned:* Manually operated expansion valve with evaporation temperature of -30 °C.
2. *Series 6 – FARS Afrimning – lav rate:* Here, the evaporator is first iced-up and then defrosted.

To get the more detailed description of all the tests for the micro channel, please look into document "P2005662-FARS-Microchannel tests-Rev00" which is a part of the report.

### 6.4.3.1. Series 3 - FARS—30 op_ned

In this part of the tests, the capacity and charge are measured for manual adjustment of the injection valve. When each capacity measuring point is done, the liquid flow into the evaporator is cut off, and the evaporator is left to dry out to be able to estimate the dry weight for each measuring point. This is done to exclude the influence of ice build-up and other factors on the coil.

The questions to answer in this test are the following:

1. What is the lowest circulation rate possible without reducing the capacity?
2. How is capacity and charge compared to earlier measurements with state-of-the-art bottom feed fin and tube evaporator?
3. Can the evaporator run on a -30 °C evaporation temperature?

***Measurements***

In this test series, three test runs were conducted. One where the refrigerant flow was reduced by closing the injection valve manually, then a test run where the refrigerant flow was increased by opening the valve, and at last by closing the valve again to repeat the first test run. The results are pictured in Figure 119 together with a traditional bottom-fed evaporator (TR) measured in an earlier project.

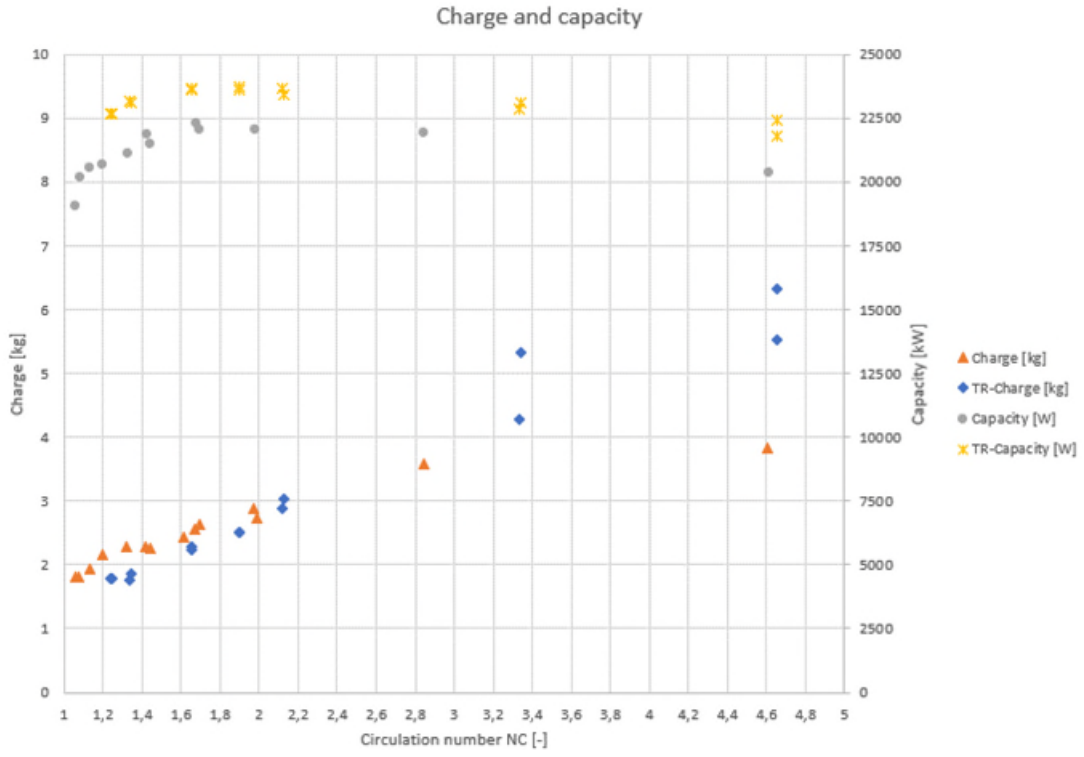


**Figure 119: Comparison between fin and tube and the micro channel designed in the project.**

***Conclusion***

The answer to the questions lined up in the beginning of this section is that the capacity vs. circulation ratio curve is lower for the micro channel compared to the earlier measurements on the fin and tube evaporator – even if the heat transfer area is slightly larger. The heat transfer area for the micro channel is 77 $m^2$, but for the traditional bottom-feed it was 84 $m^2$. This is a reduction in the area of around 8 %.

When looking at the circulation ratio in Figure 119, the same conclusion can be drawn as for fin and tube evaporators, i.e., that the capacity maximizes at a NC of 1.7 and that the evaporator could be controlled down to 1.2 without severe capacity reduction.

The charge vs. circulation ratio curve shows a different and more flat progress and surprisingly large charge. This is caused by the nonoptimal design where one liquid header runs along each plate for the liquid distribution. These headers include a large part of the charge and should be redesigned in the final design to reduce the charge considerably.

The tests show a positive result and indicate that a mirco channel evaporator can work as an evaporator for freezing temperatures down to -30 °C.

### 6.4.3.2. Series 6 – FARS Afrimning – lav rate

In this test series, the micro channel evaporator was function tested. The test consists of a frosting up of the coil and then subsequent defrosting of the coil.

Humidity is added to the room to simulate the icing up of the evaporator. The weight on the evaporator is measured, and the ice build-up is recorded by weight measurements and by taking one photo every 10 minutes of the evaporator surface. During defrosting, photos are taken for every 10 seconds to record the drainage of the micro channel profiles. The measurements will be compared to measurements done in the ELFORSK project number 347-030 about optimization of hot gas defrosting in industrial refrigeration systems. A comparison is made to drain controlled defrosting with bottom-fed evaporator with an ice accumulation of around 25 kg as is found in test "DDV 3. Forsøg – tømmeafrimning – ca 29 kg is" with data file 470 for ice build-up and data file 471 for the following defrosting.

For the ice build-up, the same running conditions as in previous test are used with the lowest circulation number possible before capacity reduction is too severe. The different times in the defrosting cycle must be optimized. These times are the emptying time, the soft defrosting, the normal defrosting, the equalizing time, and the droplet freezing time.

The questions to answer in this test were:

1. How is the ice accumulation on the coil?
2. What is the necessary defrosting time?
3. How is the defrosting of the micro channel compared to the state-of-the-art bottom-fed evaporator from "DDV 3. Forsøg – tømmeafrimning – ca 29 kg is"?

## *Measurements*

### *Icing up of the coil*

During the test, the temperature of the water in the humidifier was adjusted to try to reach a sensible ice build-up of the coil. The test was running for 55 hours. In Figure 120, the capacity and refrigerant flow are shown during the icing up of the coil.

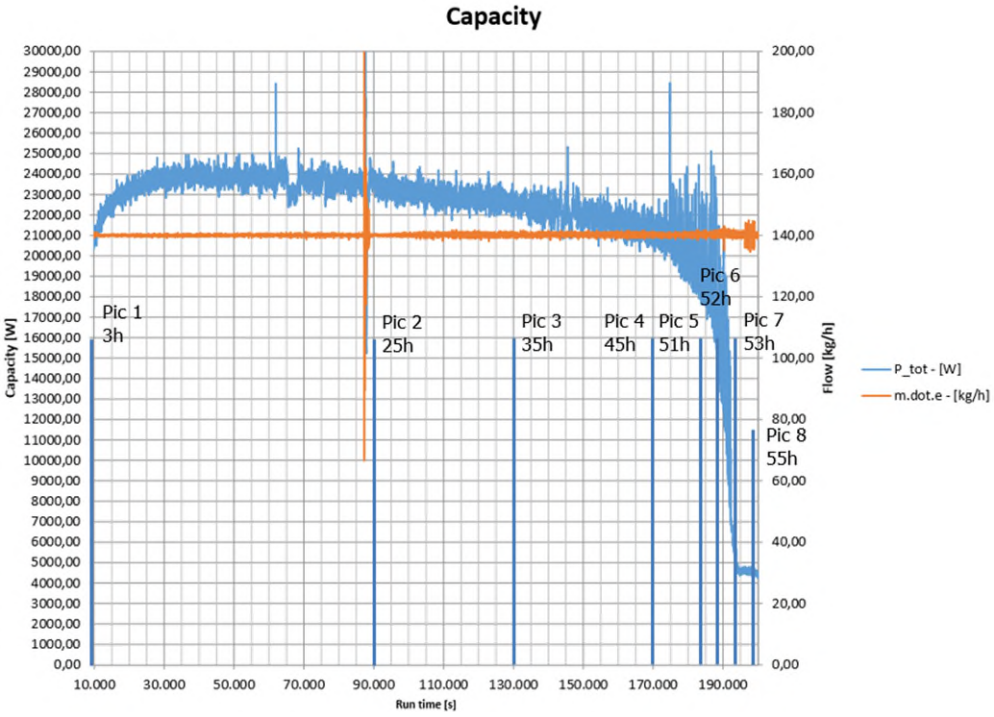


**Figure 120: Capacity change and refrigerant flow to coil during icing up of the coil.**

We experienced a small amount of air leaking into the ammonia circuit in the test setup until 90.000 sec., as can be seen from Figure 121. Here, the saturated suction temperature (T.e.o) raises from -30 °C to around -27,5 °C due to air accumulation in the ammonia cascade plate heat exchanger. Then, at around 90.000 sec., the air is purged, and a stable saturated suction pressure is maintained. As can be seen from Figure 120, the capacity is steadily reducing as ice is accumulated on the coil until around 170.000 sec. where the surface of the coil is closing by ice and the capacity drops rapidly.

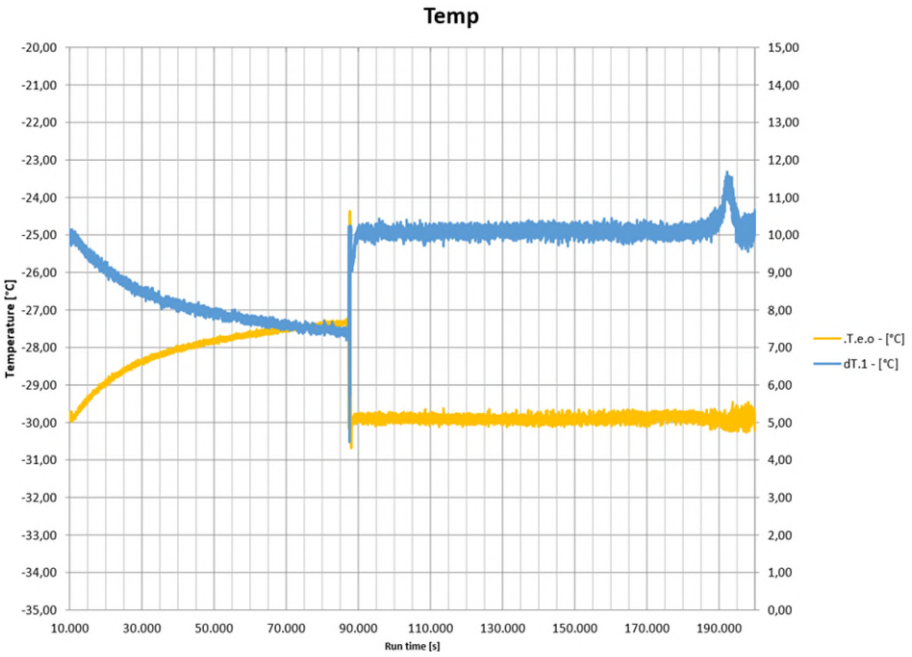


**Figure 121: Saturated suction temperature and air entering temperature difference of the coil.**

Pictures of the icing up of the coil related to Figure 120 are shown in Figure 122 and Figure 123.

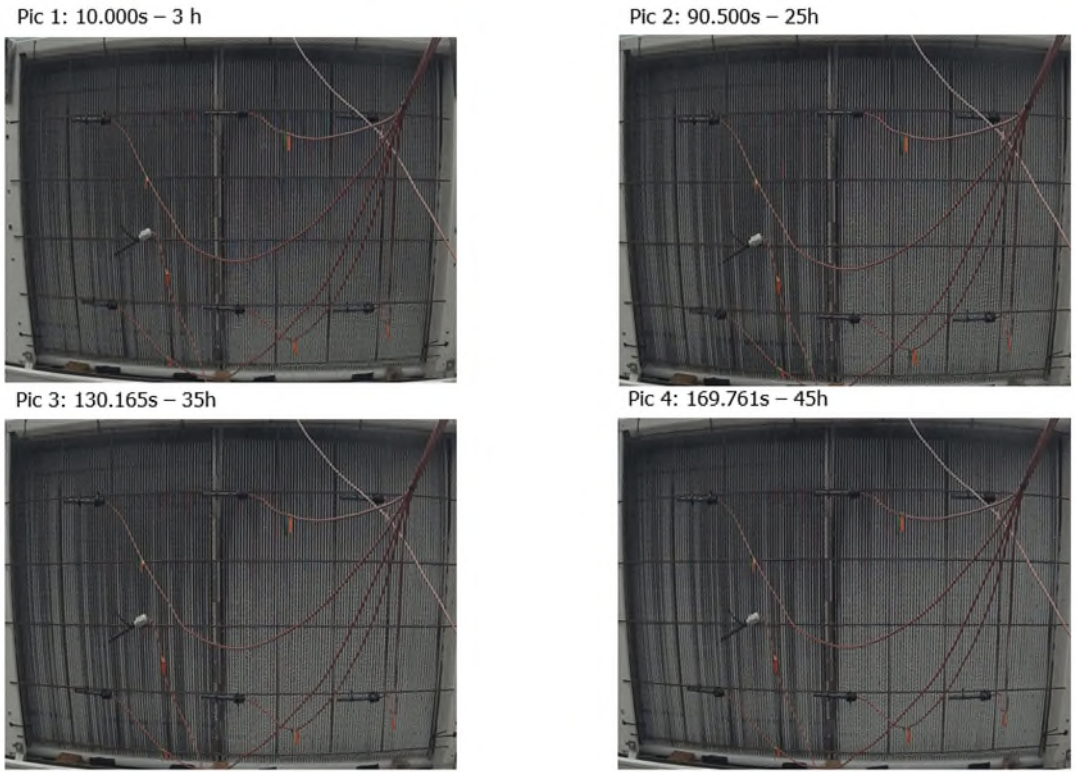


**Figure 122: Icing up of evaporator from 3h to 45h.**

From the first picture in Figure 122 to picture number two there are 22 hours and thereafter 10 hours between the pictures. More ice accumulation is seen on the right coil sections

which indicates more refrigerant flow to this side of the evaporator. The left side is showing a slower and more uneven ice accumulation which indicates a lack of refrigerant flow. The refrigerant to each micro channel plate section was individually controlled which made it difficult to adjust the same flow to all the sections.

In Figure 123, there is one hour between the first three pictures and then two hours between the third and the fourth picture.

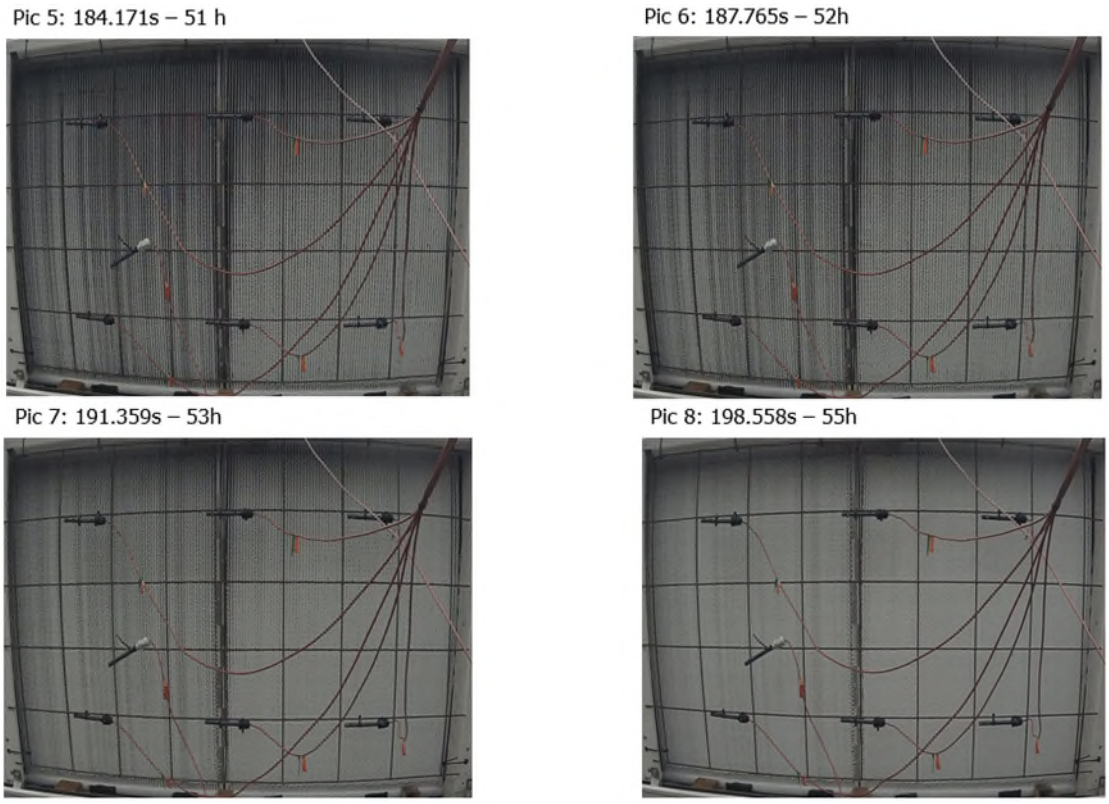


**Figure 123: Icing up of evaporator from 51h to 55h.**

In Figure 122, there is a relatively slow icing up of the coil for the majority of the time, and then in Figure 123, there is a relatively quick blocking of the coil during the last few hours.

### *Defrosting of the coil*

In Figure 124, the hot gas flow to the micro channel evaporator is shown together with the weight of the water barrel containing the water coming from the defrost. The increase in the barrel weight indicates the water return from the defrosting coil. As can be seen from the figure, the hot gas starts to enter the coil at 325.100 sec. marked as 0 min. of defrosting. The hot gas flow peaks shortly after the defrosting starts and subsequently drops as the ice is melted on the coil. At last, when the coil is free of ice, the hot gas flow stabilises on a constant value representing the load by natural convection to the climate chamber.

The amount of ice accumulated on the coil is 17.6 kg, and the duration of the defrosting is 3.7 min.

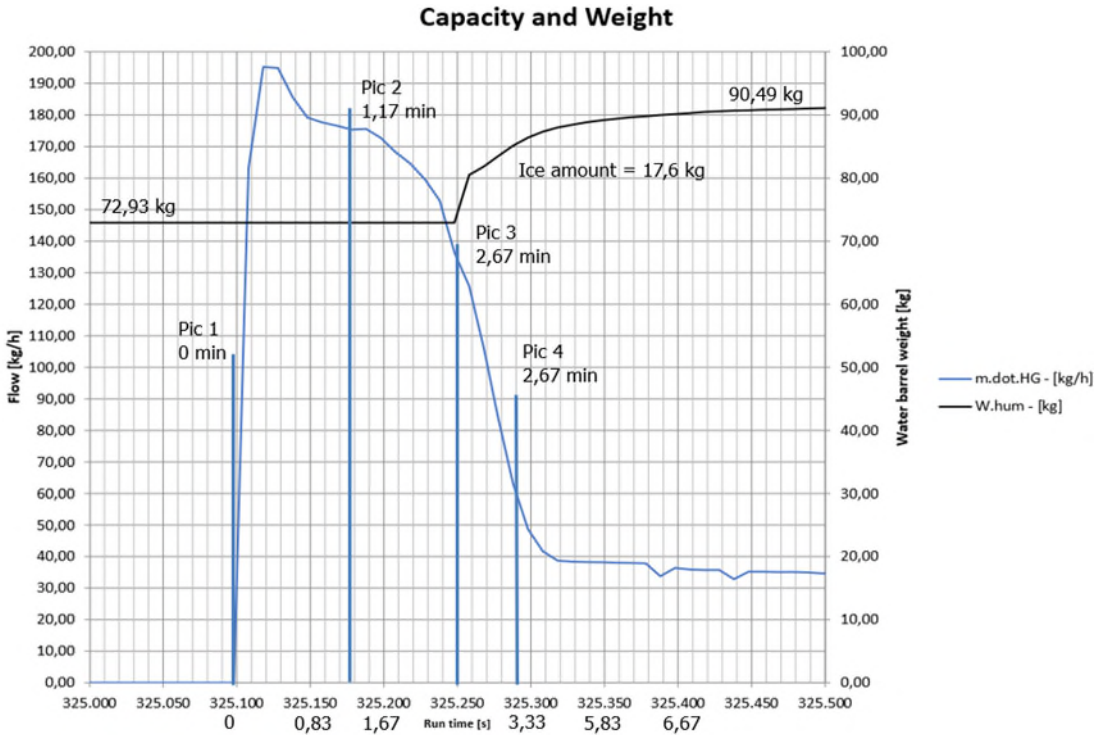


**Figure 124: Defrosting of the micro channel coil.**

In Figure 125, pictures are taken from the coil air entrance side during defrosting. The time for the pictures is marked with a blue line in Figure 124.

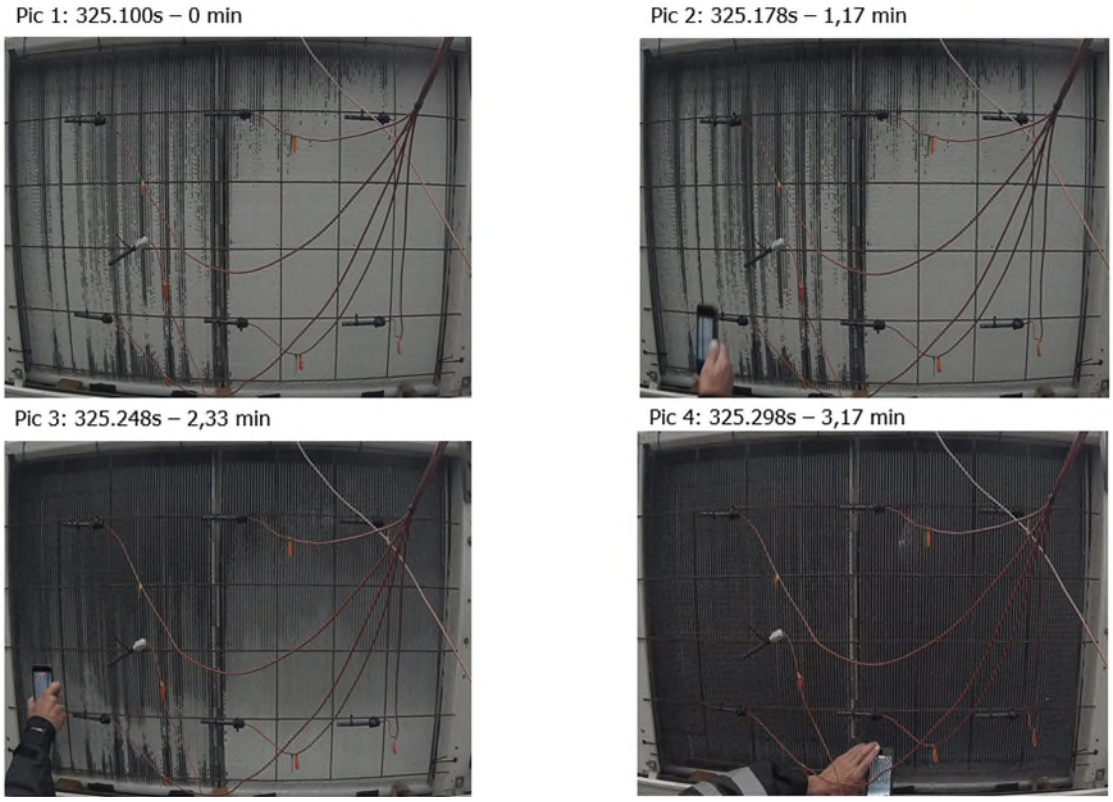


**Figure 125: Pictures of the front of the micro channel evaporator during defrosting.**

In Figure 126, the defrost capacity and used energy is depictured during the defrosting.

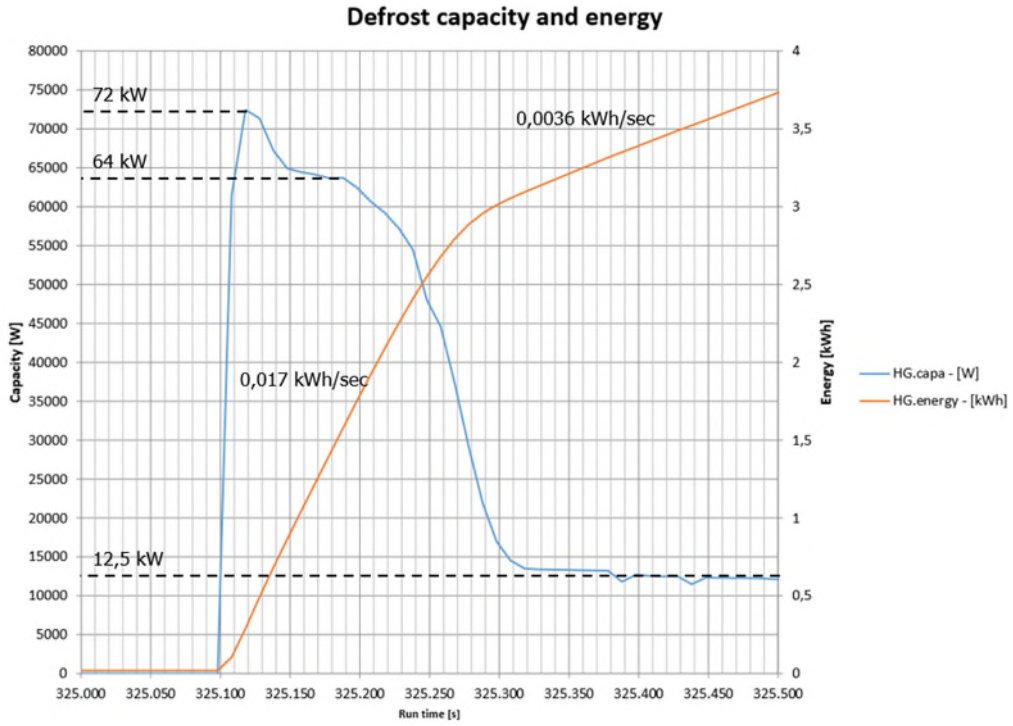


**Figure 126: Defrost capacity and energy.**

Some relevant rules of thumb can be withdrawn from the measurements. Firstly, the required capacity at the beginning of the defrosting is 72 kW for this coil that delivers 24 kW. This means that the defrost capacity ratio for the coil is 3, i.e., we need three coils in defrost to be able to supply the maximum defrost demand. When the start peak is over, the needed ratio drops to around 2.7. When the ice is melted from the coil, the capacity evens out on around 12.5 kW which represents the loss caused by natural recirculation of air though the evaporator. This energy goes back into the climate chamber. This means that the load returned to the climate chamber caused by defrosting is around half of the cooling capacity of the coil.

Another thing to notice is that the energy used for defrosting is near linear when there is ice on the coil and when the ice is gone the slope of the curve changes as given in the Figure 126.

In Figure 127, a comparison between the new micro channel and a traditional bottom-fed evaporator (BF) is done. This comparison is hard to do since the amount of ice is not the same. For the micro channel, the accumulated ice is 17 kg, and for the bottom-fed the accumulated ice amount is 26 kg. The defrosting time for the micro channel is 3.8 min. and for the BF it is 7.5 min. The increase in ice amount from the micro channel to the BF is 53 %, and the corresponding increase in defrosting time is 97 %. This could be an indication of a shorter defrosting time with the micro channel, but this must be investigated further before such conclusions can be drawn.

When comparing the capacity for the bottom-fed in Figure 128 and the micro channel in Figure 120, it is seen that the micro channel evaporator has a maximum capacity of around 24 kW where the bottom-fed has around 22 kW. This is an increase in capacity of around 9 % still with a smaller heat transfer area. The heat transfer area for the micro channel is 77 $m^2$, but for the traditional bottom-feed it was 84 $m^2$. This is a reduction in the area of around 8 %.

The micro channel evaporator was built into the same casing as the bottom-fed and had thereby the same face areal. The only difference in the size of the coil was the depth. The bottom-fed has a dept of 400 mm while the micro channel has a dept of 125 mm or a reduction of 69 %, even though the micro channel has 8 % less heat transfer areal. This indicates how compact the micro channel heat exchanger is. This, of course, influences the amount of ice available to be accumulated on the surface but could be compensated by a shorter defrosting time and more frequent defrosts. On the other hand, if the micro channel would utilize the full depth, more distance between the fins could be used which would allow more ice accumulation.

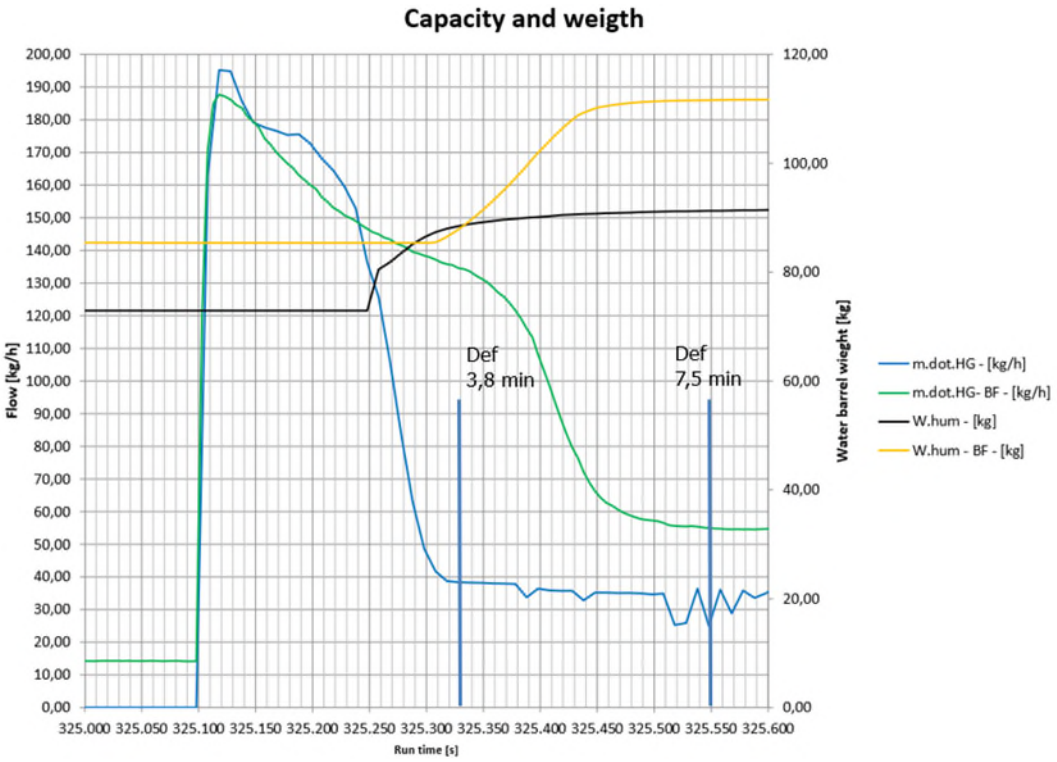


**Figure 127: Capacity and weight comparison between micro channel and bottom-feed (BF).**

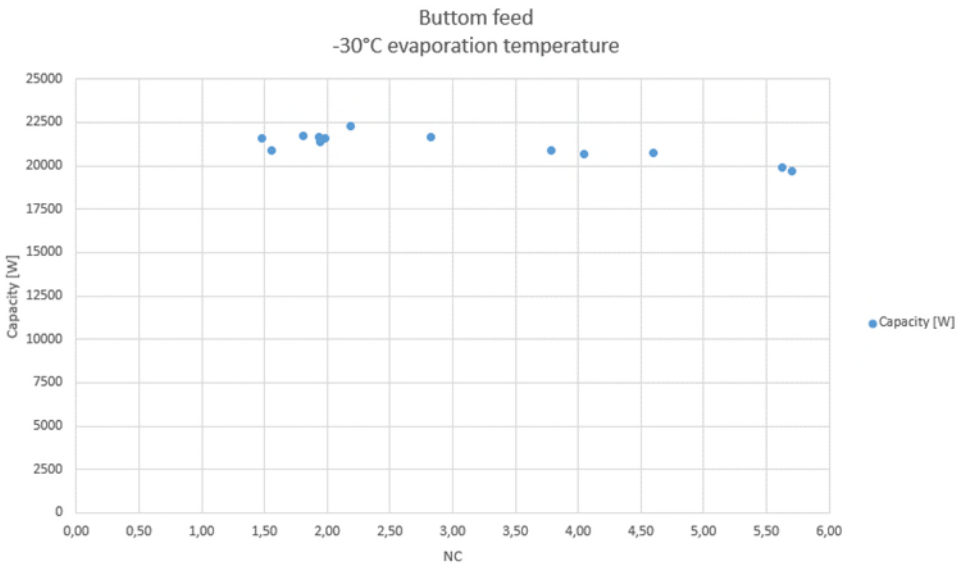


**Figure 128: Normal state-of-the-art bottom-fed evaporator.**

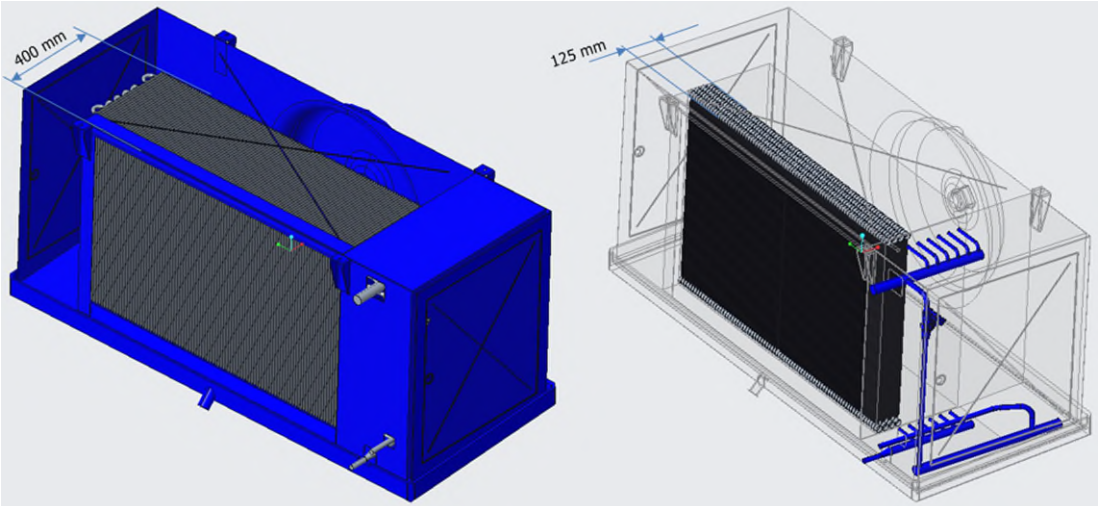


**Figure 129: Bottom-feed to the left and micro channel to the right.**

***Conclusion***

To answer the questions lined up at the beginning, the amount of ice that the coil could accumulate was 17 kg before the evaporator face was closed off with ice and closed for the air flow. The bottom-fed evaporator was able to accumulate up to 70 kg ice. This would require larger fin spacing for the micro channel to be able to have a longer running time between defrost. There is, on the other hand, an indication of a shorter defrosting time that could compensate for the more frequent defrosting. The ice formation on the right coil was even but the left coil had lower coverage that the right one because of maldistribution of refrigerant to the right coil.

The defrosting time for the micro channel coil was around 3.8 min., and the defrosting was successful. The water drained smoothly from the fins and micro channel profiles.

There was a vague hint of a shorter defrosting time for the micro channel compared to the BF but this needs further investigation.

The micro channel evaporator used much less space than the bottom-fed and still showed a higher capacity. This affects the ice amount capable of accumulating on the surface. This could be compensated for by more frequent defrosting.

### 6.4.4. Summary and conclusions

The test setup for the micro channel tests was build according to the drawing in "Figure 118" and the data acquisition system installed and was followed up by six tests. The tests can be divided into two groups. First, a test with manual control of the expansion valve was conducted to find the capacity and charge dependent of the circulation ratio. The second group were tests concerning defrosting of the micro channel.

The first test group showed a positive result and indicates that an mirco channel evaporator can work as an evaporator for freezing temperatures down to -30 °C. The charge measurements showed a need for a redesign of the headers to lower the charge.

The second test group showed that the defrost was not a problem and that the water flowed freely from the surface. The lower ice accumulation because of more compact design could give problems when running the evaporator but shorter defrost time could compensate for this.

# 7. Field tests

## 7.1. Introduction

The purpose of the tests in Brædstrup was to verify the laboratory measurements in a real-life situation. The evaporator is air-cooled connected to a heat pump delivering the heat to the district heating. In the test, the liquid injection valve is controlled by a Danfoss controller to maintain the circulation number (NC) close to optimum. To compare evaporators with and without controlled liquid injection valve, measurements are done on two side by side evaporators where the one has the new controlled liquid injection valves, and the other has the more conventional non-controlled manual adjusted valve.

## 7.2. Test setup

The layout of the plant is shown in Figure 130. The evaporators that are included in the tests are marked with a square as 15 and 16. Evaporator 15 is a reference evaporator, and evaporator 16 is the one where the control of the liquid injection valves is performed. The test setup has 49 different measuring points, including temperature, flow, pressure, differential pressure, weight, and humidity sensors. There are two different types of temperature sensors; thermocouples type T (called TC) and PT1000 (called TT). The pressure sensors are type AKS32 (called PT), and the differential pressure sensors are type EJA110A (called DPT). The flow sensors are from Siemens of type FCS300 (referred to as FT), and the clamp-on flow sensor is from Siemens of type FUS1010. The weight sensor consists of six measuring points that support each corner of an evaporator and two in the middle and are subsequently added together into one weight (called WT). The humidity sensors are type S RPFF-I (called RH%), and finally there is the differential pressure sensor on the fan which is type S 7111-I (called DP_fan). All the different measuring points are logged every 15 seconds.

The location of the various measuring points can be seen in Figure 131 and Figure 132. Here, various calculated values are also illustrated, such as evaporation temperatures based on the respective pressures and a conversion for the clamp-on flow meter.

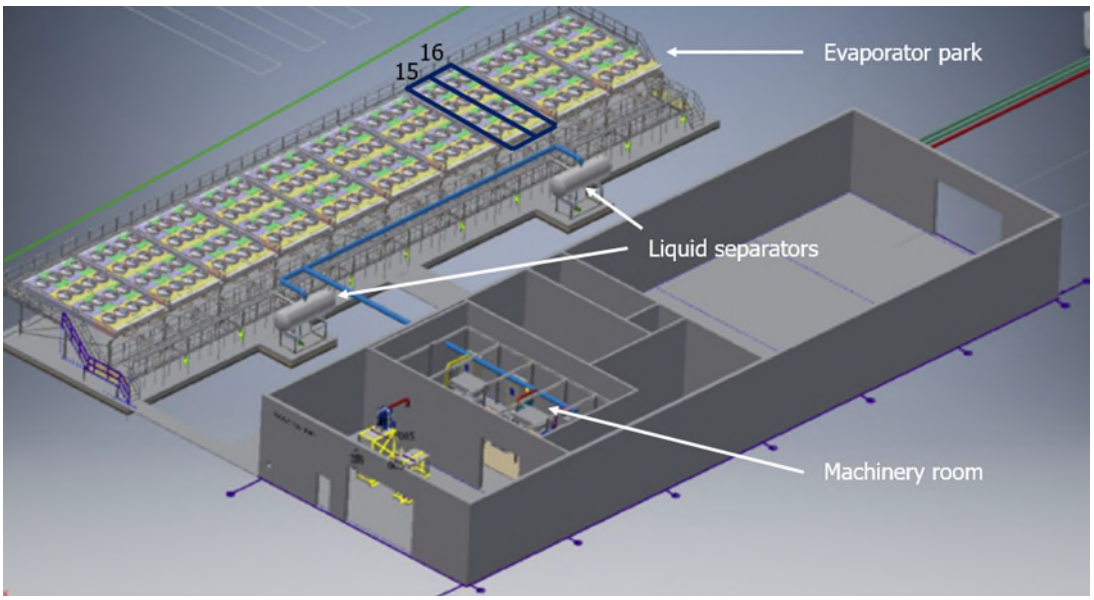


**Figure 130: The Brædstrup layout. Evaporators in the test are marked 15 and 16.**

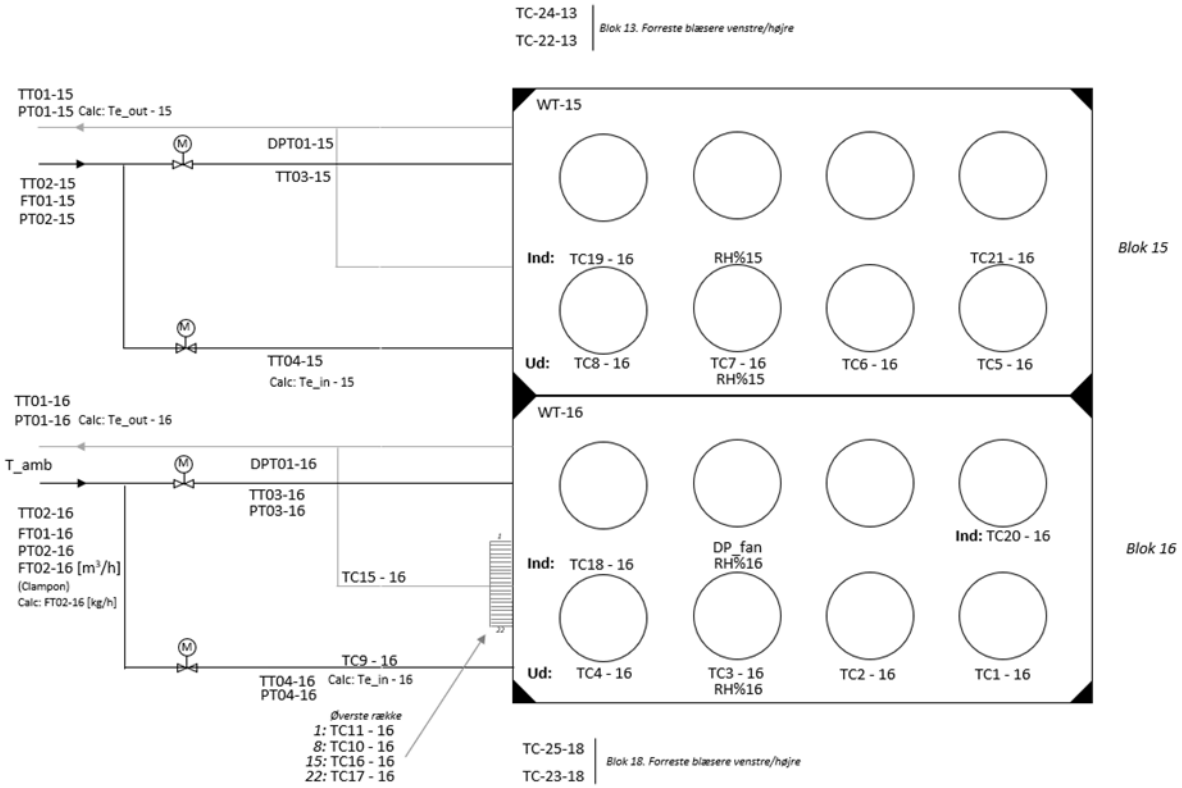


**Figure 131: Illustration of the different measuring points on evaporators 15 and 16.**

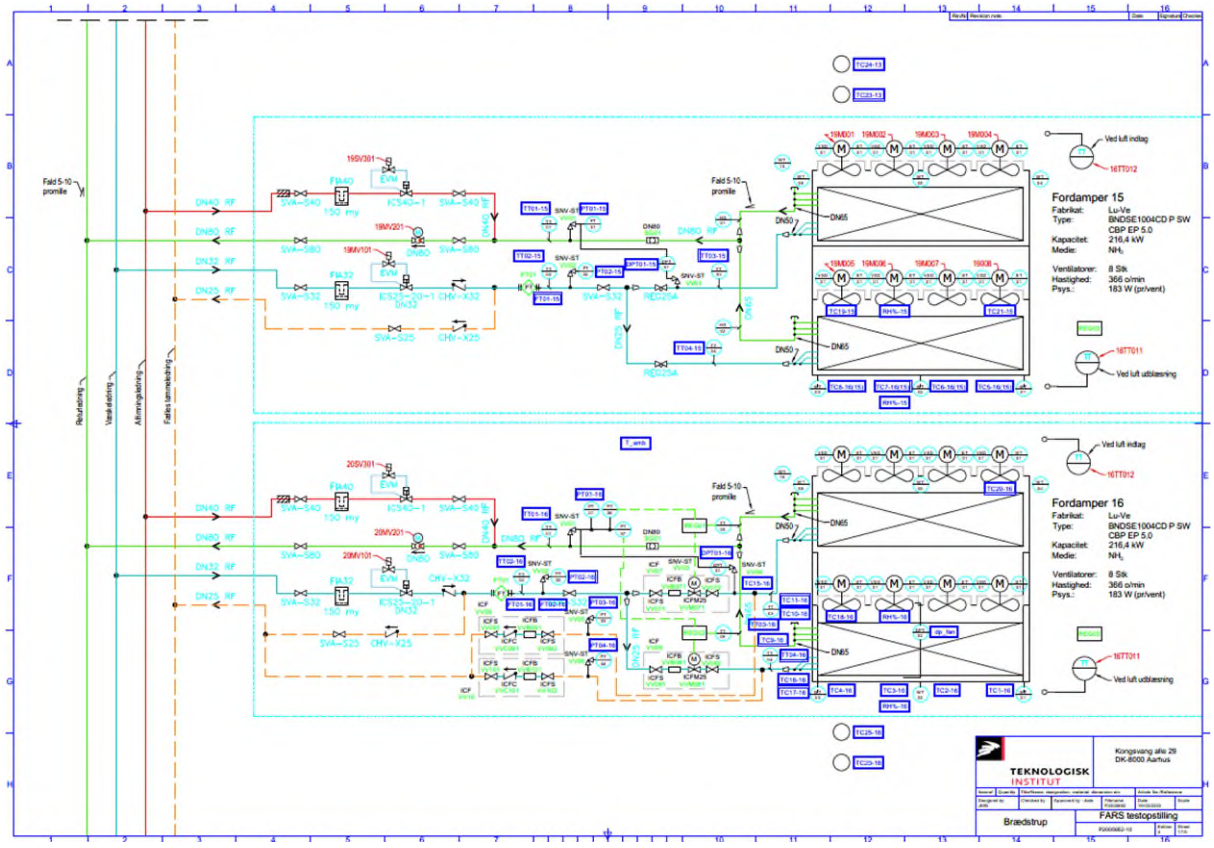


**Figure 132: Brædstrup test setup.**

Photos of the evaporator park and locations for the various measuring points can be seen in the following figures.

**Figure 133: The evaporator park.**

**Figure 134: Load cells.**

**Figure 135: Measuring box, air temperature sensor and temperature sensors on pipes.**

## 7.3. Main results

The conducted field tests were three, and the purpose was to compare the data from the laboratory tests with measurements in a real application. The conducted tests were:

1. *Serie 0 - Verificering af måleudstyr*: Test where the sensors in the test setup are verified and checked to see if the measurements are acceptable.
2. *Serie 1 - The change in the evaporator before and after the change in circuit:* Test to verify the design changes.
3. *Serie 2 - Capacity vs. NC:* Test where the liquid injection into the evaporators is gradually reduced and the charge and capacity are measured to find the lowest circulation ratio without effecting the capacity to much.
4. *Serie 3 - Controlling the NC by using MSS:* Test where an automatic control of the injection valve using a normal superheat controller with a very low superheat adjustment is used.

The third and fourth tests are represented here, and for a detailed description of all the tests, please see "P2005662-FARS-Brædstrup tests results-Rev01".

### 7.3.1. Serie 2 – Capacity vs. NC

This test is conducted by reducing the opening degree of the liquid valve to change the circulation number (NC) from high NC down to low NC. This test is done to evaluate the possibility to control the NC for the evaporator and how much charge can be saved by doing that. The test was conducted on 14-12-2020 and on evaporator 16.

The question to answer in this test was the following:

1. Is there a minimum circulation number?

#### *Measurements*

The test is based on manual changes of the refrigerant flow. The associated measured flow can be seen in Figure 136. The mass flow as a function of the circulation ratio can be seen

in Figure 137. And finally, the capacity as a function of the circulation ratio can be seen in Figure 138.

The capacity was calculated from the air side by using the pressure drop over the coil and fan curve to estimate the air flow and measurements on temperature and humidity. These measurements are inaccurate and fluctuate a lot but can be used for comparison.

The result is based on 499 data points over 120 minutes. It can immediately be concluded that the circulation ratio should be between 1 and 2 to maximize the efficiency of the evaporator, which corresponds to a flow of between 1000 and 2000 kg/h.

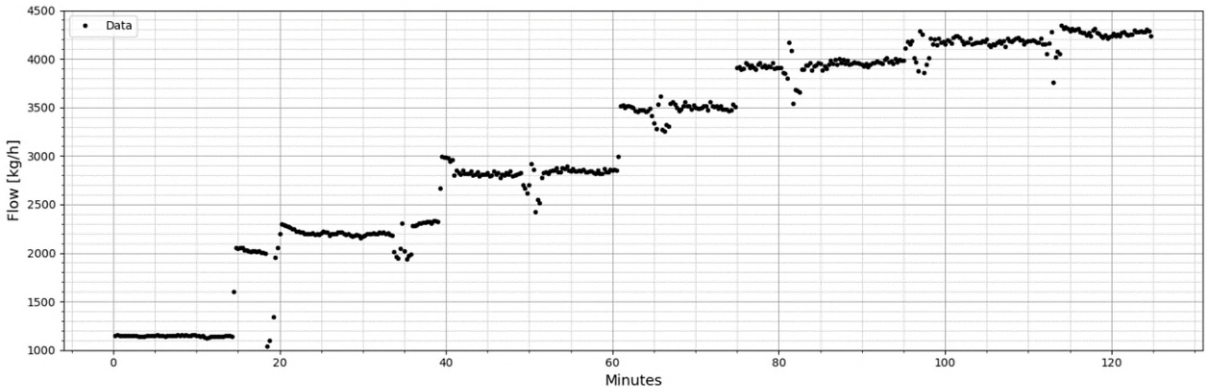


**Figure 136: Flow regulated.**

The flow that was adjusted is seen from Figure 136. The corresponding circulation numbers are shown in Figure 137, and the capacity of the evaporator is shown in Figure 138.

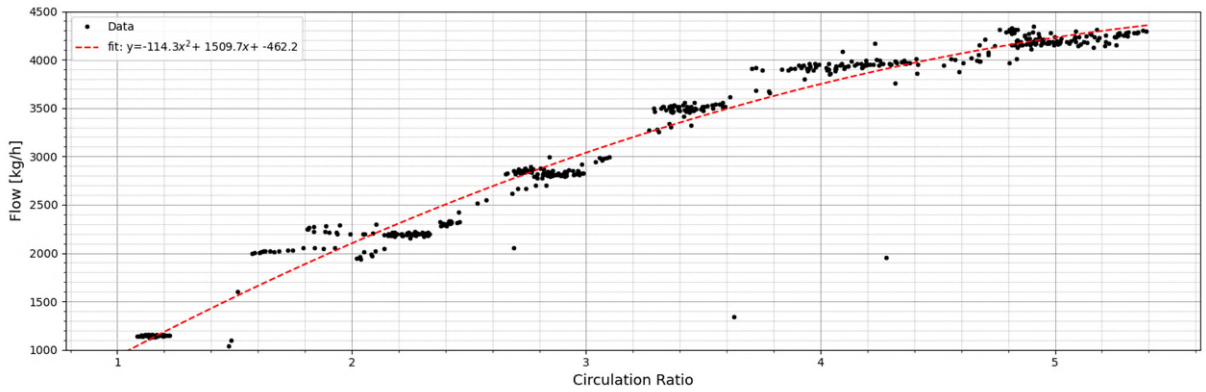


**Figure 137: Flow as function of circulation ratio.**

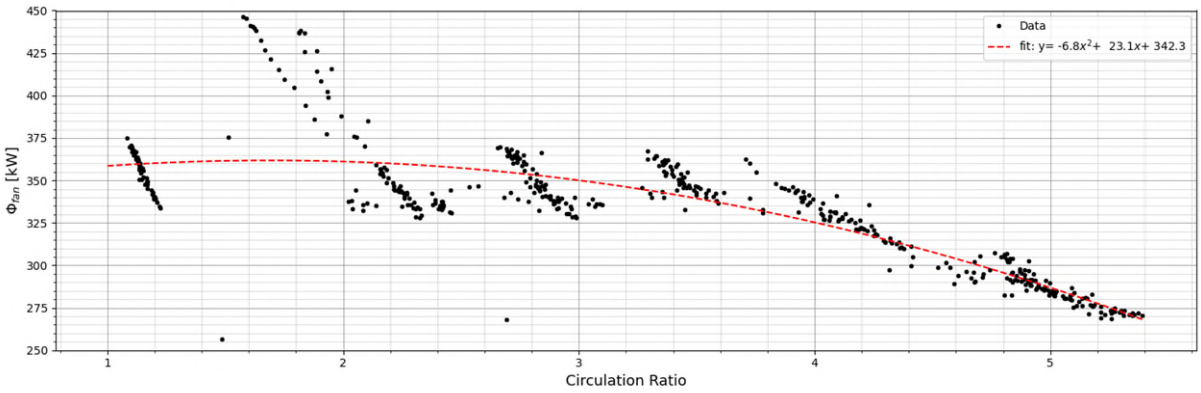


**Figure 138: Capacity as function of circulation ratio.**

As can be seen from Figure 138, the adjustment of the circulation number down to 1.2 and up to 3 will not harm the capacity of the evaporator and thereby the preferred control value for the controlled circulation ratio should be adjusted to around 1.2.

***Conclusions***

The answer to the question laid out in the beginning of the test is that measurements show that the circulation number for the evaporators should be in the rage from 1.2 to 3. To minimize the charge, the circulation number should be controlled between 1.2 and 1.5.

### 7.3.2. Serie3 – Controlling the NC by using MSS

In this test, the manual control valves on both coils for evaporator 16 are replaced with AKVA valves. The valves are connected to the EKE400 controller, and the controlling method chosen is MSS (Minimum Stable Superheat).

The temperature sensor for the controller is placed on the driest circuit and then the superheat (SH) reference is adjusted to SHmin/SHmax 2/2K, i.e., the superheat is a static superheat on 2K which is the lowest available adjustment in the standard controller.

The refrigerant flow for the reference evaporator 15 is adjusted to reflect the variation in the design circulation number from 2 to the maximum with a full open valve.

The questions to answer in this test were the following:

1. Is it possible to control the NC for the evaporator by using a normal MSS control method?
2. What is the accuracy of the method on the NC?
3. How much reduction in charge is possible compared to uncontrolled evaporator?

***Measurements***

A measurement for evaporator 15 with manual controlled liquid injection valves and for evaporator 16 with automatically controlled liquid injection valve is shown in Figure 139. Here the flow is shown as well as the calculated circulation number.

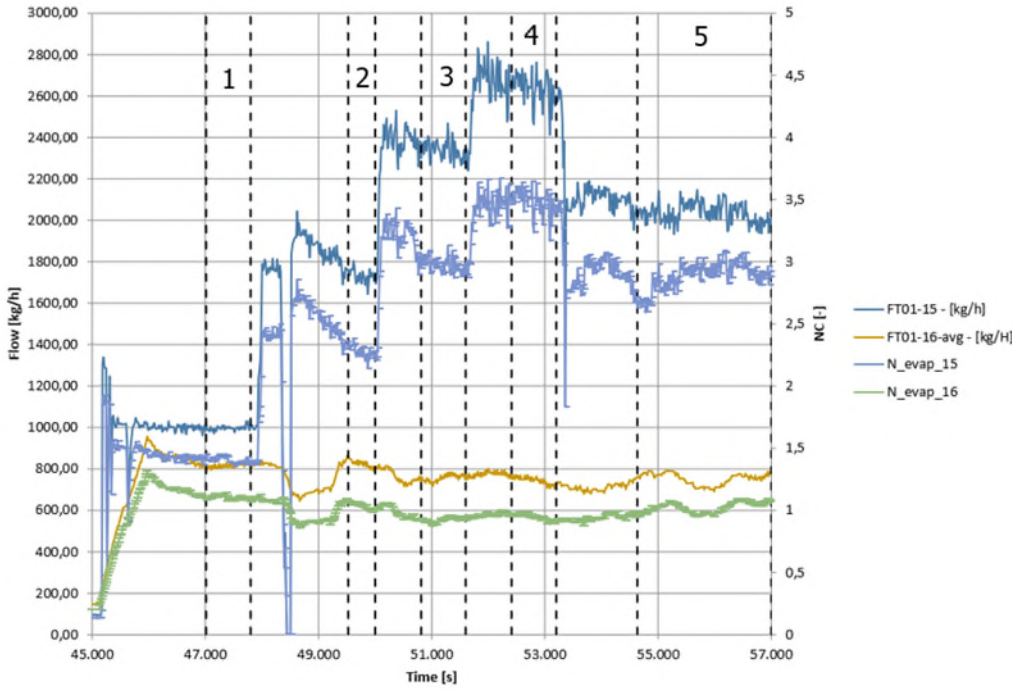


**Figure 139: Measured flow and calculated circulation numbers.**

As the flow is increased in evaporator 15, the circulation number increases. For the controlled evaporator 16, the flow is around 800 kg/h and fluctuates a little. The circulation number for evaporator 16 is swinging around 1, and sometimes the evaporator is slightly superheated and at other occasions it is slightly flooded. In this graph, the average charge value and flow are calculated in between the dotted lines marked at 1 to 5. These points are then depictured in Figure 140 as charge and circulation number vs. refrigerant flow.

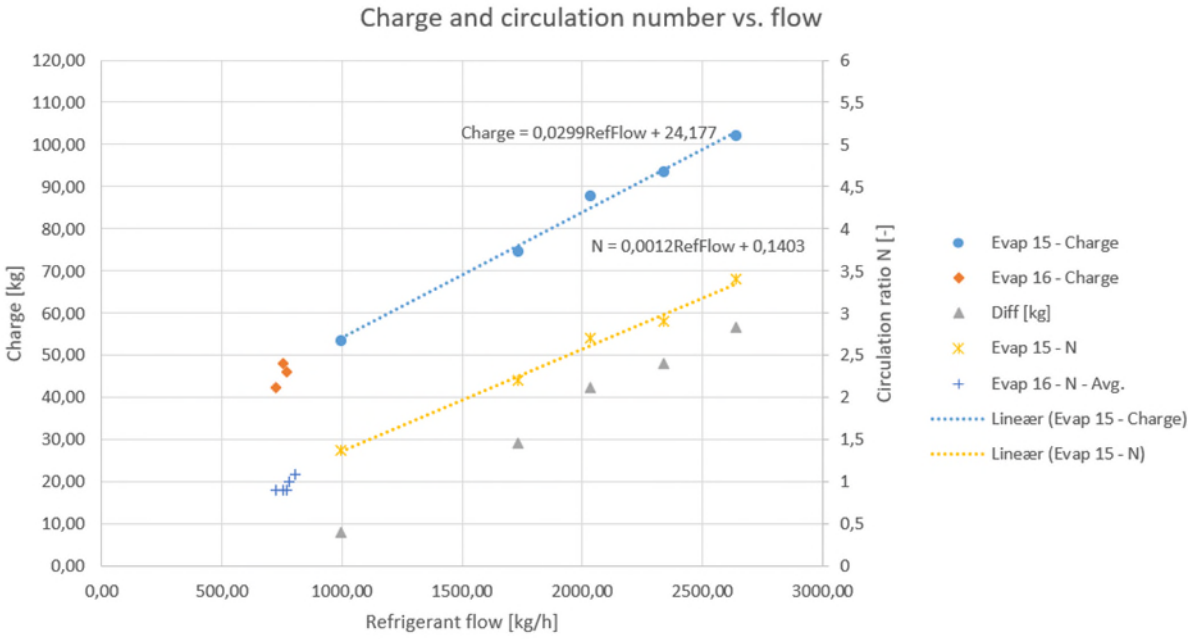


**Figure 140: Charge and circulation number for evaporator 15 and 16.**

Rearranging these numbers to display charge vs. circulation number is depictured in Figure 141.

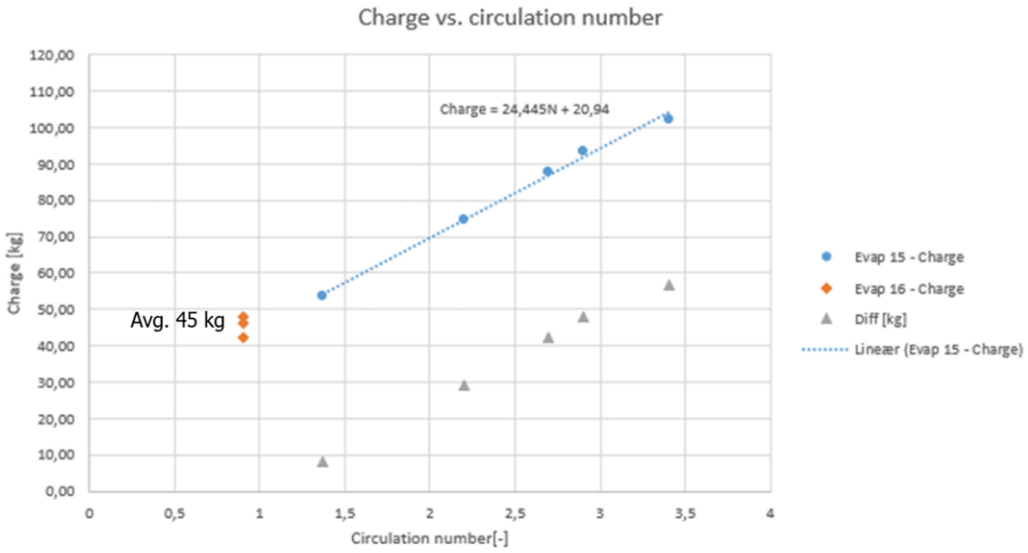


**Figure 141: Charge vs. circulation number.**

In Figure 141, the charge for the superheat-controlled evaporator 16 is in average 45 kg. For the manually controlled evaporator 15, the charge is seen to follow a straight line that points to the charge for evaporator 16. If the circulation number for the uncontrolled system is designed to 3 and is estimated, on average, to run on around 4 because of ice accumulation and lower capacity of the evaporator, the charge would be 119 kg calculated by using the equation in the graph. By controlling the circulation number to 1.2, the charge would be 50 kg constant all the time, and the savings in charge would be 68 kg per evaporator. For the installation at the side with 20 evaporators, the savings in charge would be 1360 kg ammonia.

To estimate the difference in capacity between the evaporator controlled by MMS, i.e., evaporator 16, and the manual controlled evaporator 15, the leaving temperature difference is shown in Figure 142.

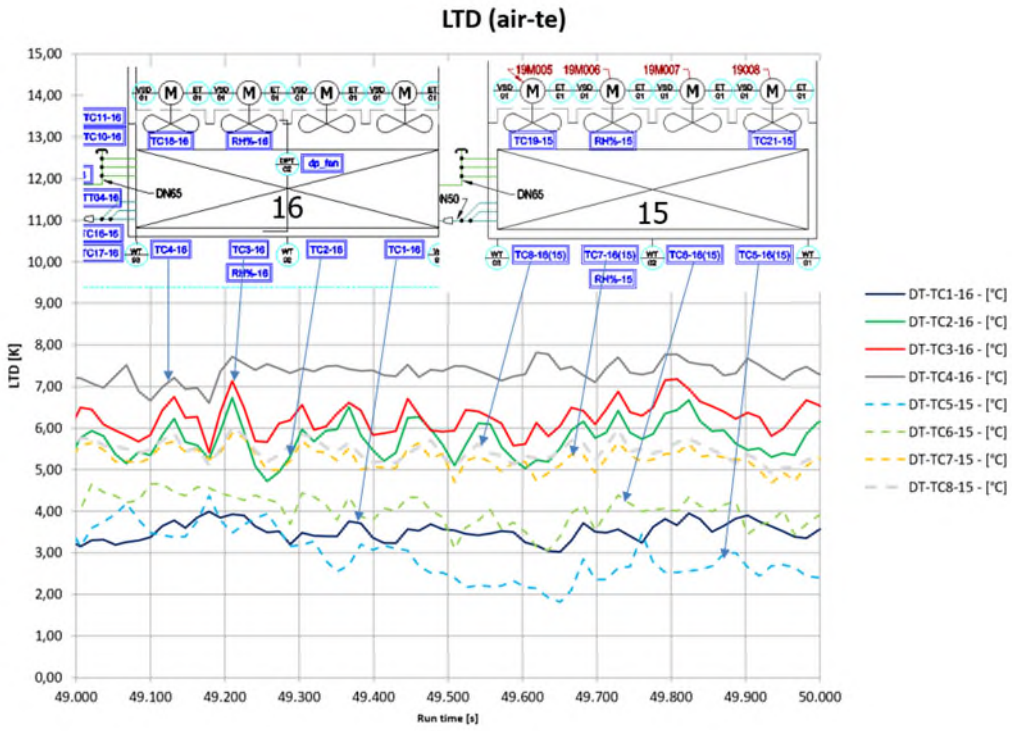


**Figure 142: Leaving temperature difference, i.e., air temperature out of coil minus saturated suction temperature of the coil.**

The graph is made for a circulation number of 3 for evaporator 15. The LTD for the uncontrolled evaporator 15 on circulation number 3 is seen to be lower than for evaporator 16 indicating a higher efficiency of evaporator 15. This is what is expected since the controlled evaporator 16 is around 1 in circulation number which indicates that some of the circuits are with superheat and others are slightly flooded. This picture is expected to even out when we can run evaporator 16 on an optimal circulation number of 1.2 to 1.5 with the new sensor.

There is a significant fall in LTD from the evaporator end near the valve station to the end farthest from the valve station for both evaporators. This is an indication of a considerable recirculation of air from outlet to inlet at the end furthest from the valve station. This is true for both evaporators.

### *Conclusions*

The answer to the questions laid out in start of the test is that measurement shows that it is possible to control the evaporator by choosing the circuit with highest superheat and place the temperature sensor on that circuit. In this case, the maldistribution in the coil will ensure that the coil is very close to be flooded in average. As can be seen in Figure 139, the circulation number for the evaporator 16 is close to 1 and is swinging slightly around that number.

The MSS seems to be able to control the circulation number stable around 1. The new sensor technology will be able to keep the circulation number on the other side of 1, i.e., slightly overflooded.

The estimated savings in charge are around 68 kg ammonia per evaporator. That is a reduction from 119 kg down to 50 kg or a reduction of 58 %.

It is seen that the controlled evaporator 16 has lower efficiency than the uncontrolled evaporator 15 because of the MSS superheat control method and it is estimated to even out when the new sensor can control the circulation number to the most optimal circulation number of 1.2 to 1.5.

## 7.4. Summary and conclusions

A test setup was developed, and a data acquisition system was installed on a heat pump application in Brædstrup. Two out of 20 evaporators were selected for the test. One as a reference and the other with installed control valve. The control strategy was to use fixed SH on 2K placed on the driest circuit in the evaporator.

It was found through measurements that the minimum circulation ratio for the evaporator did correspond to what was found in the laboratory tests. The circulation number should be controlled between 1.2 and 1.5.

It was shown that it was possible to control the circulation ratio close to 1 with a reduction in charge of 68 kg for each evaporator or a charge reduction of 58 %.

# 8. Conclusion

The aim of the project, to investigate and develop solutions for future industrial ammonia systems has been fulfilled, and products are being developed that will hit the market shortly.

In the beginning of the project, the requirements on how the future industrial ammonia systems could look like and what elements to investigate where laid out. It became clear that there are just a few available low charge solutions for new system designs, and the vast majority of already operating systems could not implement this technology into their systems without a high economical cost. These low charge solutions relay on a very specific system design owned by the respective companies. These solutions include special designed evaporators, ammonia liquid distributors not commercially available, and a control strategy not readily available in the market. It became clear that to be able to make a difference the solution must consist of commercially available components for both new designs and for retrofit of older systems that will be in operation for the next 30 years.

Three concepts were lined up, developed, and tested. The first concept was the so-called control circulation ratio (CCR) and it was considered to be used as a retrofit for older systems and for extensions to new plants. In this part of the project, a new type of sensor, the so-called heated sensor, and a control strategy was developed to be able to control the circulation ratio. A new type of an interlaced bottom feed evaporator and a side-fed evaporator was designed and built. The concept was installed in a test setup and tested. The result is a new sensor and control strategy that can control the circulation ratio between 1.2 to 2 and a new type of evaporators specially designed for low circulation numbers.

The second concept was the wet direct expansion (WDR) and was aimed at new system designs and at extensions to existing systems. Here, the same heated sensor was further developed to be able to run on WDX evaporators. A new type of WDX evaporator was designed and built. The concept was installed in a climate chamber and tested. The result is a new type of heated sensor and a control strategy that can control the circulation ratio to between 1.0 and up to 1.5 and a new type of evaporators specific designed for WDX.

The third concept was a micro channel evaporator designed as an evaporator product of the future. The aim of the project was to investigate how the micro channel profiles could be used for evaporators to lower the charge, increase the efficiency, and reduce the footprint. Micro channel has been used for condensers for other refrigerants than ammonia with great success. The concern was the liquid distribution and the defrosting of the fins. A specially designed micro channel profile was used to enhance the water drainage. The tests showed a positive result and indicated that a micro channel evaporator can work as an evaporator for freezing temperatures down to -30 °C. The charge measurements showed a need for a redesign of the headers to lower the charge. The second test group showed that the defrosting was not a problem, that the water flowed freely from the surface, and that the defrosting time seemed shorter than for conventional fin and tube evaporators.

A field test for the CCR part was designed and installed on a heat pump installation in Brædstrup. Here, two evaporators out of 20 were used for the test. One evaporator as

reference with a conventional solution, and the other with controlled expansion valves to control the liquid circulation through the evaporator. The test showed that a circulation number of 1.2 to 1.5 could be used and that this would save around 58 % of the charge compared to running with a circulation ratio of 4.

The solution designed in the project is now being made market ready and is expected to hit the market soon.

# 9. References


[1] F. Bühler, T.-V. Nguyen, and B. Elmegaard, "Energy and exergy analyses of the Danish industry sector," Appl. Energy, vol. 184, pp. 1447–1459, 2016.

[2] K. Wang, F. Cao, S. Wang, and Z. Xing, "Investigation of the performance of a high-temperature heat pump using parallel cycles with serial heating on the water side," Int. J. Refrig., vol. 33, no. 6, pp. 1142–1151, 2010.

[3] F. Fraß, R. Hofmann, K.P., 2015. Principles of Finned-Tube Heat Exchanger Design for Enhanced Heat Transfer, 2nd ed. WSEAS Press.

[4] Granryd, E., Kungliga Tekniska högskolan. Institutionen för energiteknik, KTH Industrial Engineering and Management, Royal Institute of Technology, K.D. of E.T., 2009. Refrigerating engineering. Royal Institute of Technology, KTH, Department of Energy Technology, Division of Applied Thermodynamics and Refrigeration.

[5] Kaminski, S. Groß, U., 2000. "Luftseitiger Wärmeübergang und Druckverlust in Lamellenrohr-Wärmeübertragern". Ki Luft- und Kaeltetechnik 36, 13–18.

[6] Kristófersson, J., Vestergaard, N.P., Skovrup, M., Reinholdt, L., 2017. "Ammonia charge reduction potential in recirculating systems – Calculations", in: IIR Ammonia Refrigeration Conference. Ohrid, Macedonia, pp. 80–87. https://doi.org/10.18462/iir.nh3-co2.2017.0005

[7] Kærn, M.R., 2011. "Analysis of flow maldistribution in fin-and-tube evaporators for residential air-conditioning systems". Phd thesis, Technical University of Denmark, Department of Mechanical Engineering, Kgs. Lyngby, Denmark.

[8] Kærn, M.R., Markussen, W.B., Kristofersson, J., 2019. "Multi-objective optimization of low charge liquid overfeed ammonia evaporators for industrial refrigeration", in: 8th Conference on Ammonia and CO2 Refrigeration Technology. Ohrid, Macedonia, pp. 86–93.

[9] Kærn, M.R., Markussen, W.B., Kristófersson, J., 2020. "Numerical analysis of flow maldistribution in large-scale liquid overfed finned-tube ammonia evaporators"., in: 14th IIR-Gustav Lorentzen Conference on Natural Refrigerants. International Institute of Refrigeration, Kyoto, Japan, pp. 251–256.

[10] Rogié, B., Markussen, W.B., Kærn, M.R., 2020. "Numerical investigation of fin geometry on the air-side heat transfer and pressure drop characteristics of heat exchangers using in-line rectangular microchannels", in: 33rd International Conference on Efficiency, Cost, Optimization, Simulation and Environmental Impact of Energy Systems. p. 12.

[11] Rogie, B., Markussen, W.B., Walther, J.H., Kærn, M.R., 2019. "Numerical investigation of air-side heat transfer and pressure drop characteristics of a new triangular finned microchannel evaporator with water drainage slits". Fluids 4. https://doi.org/10.3390/fluids4040205

[12] Shah, R.K., Sekulic, D.P., 2003. "Fundamentals of heat exchanger design". John Wiley & Sons, Hoboken, New Jersey, USA.

[13] Webb, R.L., Kim, N., 2005. "Principles of Enhanced Heat Transfer", 2nd ed. CRC Press.

[14] Bruce I. Nelson. DX "Ammonia Piping Handbook", 4th edition.

[15] Bruce I. Nelson. "Refrigeration, Politics, and "The Donald Effect"". Ecolibrium, July 2017

[16] Welch, J. "DX Evaporator Installation - Final Projekt Report". http://www.colmaccoil.com/literature/technical-bulletins.aspx

[17] Bruce I. Nelson. "ADX Ammonia System Evacuation". http://www.colmaccoil.com/literature/technical-bulletins.aspx

[18] Bruce I. Nelson - Coilmac Coil & Rick Watters - AMS Mechanical Systems. "Low Charge ADX Ammonia". Global Cold Chain EXPO, June 13-15, 2017, Chicago, IL, West Hall, Mccormick Place

[19] Kuba Kaltetechnic GmbH. "EP0588069 (A1) - Apparatus for dividing a stream og liquid". European Patent Office

[20] Stefan Jensen, Scantec. "WO 2017/161425 A1 - Defrost systems". http://www.google.com/patents/WO2017161425A1?cl=en

[21] Frank Ellefsen. "LPEV - Liquid Pump Expansion Valve". Risø, 1993

[22] Dermot Cotter. "Improvements of the Heat Transfer Performance of an Ammonia Air Cooler". Faculty of Engineering, Sience and Build Environment, Department of Urban Engineering, London South Bank Univeristy, 2009

[23] Bruce I. Nelson. "Refrigerant Distributor". Unitet States Patent Application Publication

[24] Michael Elstrøm. "Capacitive Sensors Measuring the Vapour Quality, Phase of the refrigerant and Ice thickness for Optimized evaporator performance". 13th IIR Gustav Lorentzen Conference, Valencia, 2018

[25] Michael Elstrøm. "Low Charge Ammonia DX System Controlled by HBX Vapor Quality Sensors". EUDP project, 2017

[26] Michael Elstrøm. "New Refrigerant Quality Measurement and Demand Defrost Methods". IIAR 2017

[27] J. Alberto Dopazo, Jose Fernandez-Seara. "Experimental evaluation of an ejector as liquid re-circulator in an overfeed NH3 system with a plate evaporator". International Journal of Refrigeration 34 (1676-1683)

[28] Torbjørn Olsen. "LPR Systemer - Noe erfaringer om hva det er egnet til og hvor begrensningerne er". Norsk Kjøleteknisk Møte - 12-13 April 2018

[30] Massimiliano Dall´Armellina. "Energy Efficiency with Natural Refrigerants". Norsk Kjøleteknisk Møte - 12-13 April 2018

[31] Eric Gestenberger. "Natural working fluids Ammonia - Experimental investigation of tube-fin heat exchangers". Norsk Kjøleteknisk Møte - 12-13 April 2018

[32] Nawaf F. Aljuwayhel, Dougles T. Reindl, Sanford A. Klein, Gregory F. Nellis. "Simple method to improve the performance of industrial evaporators under frosting conditions". International Refrigeration and Air Conditioning Conference at Purdue, July 17-20, 2006

[32] Eric Granryd. "Optimum Cirquit Tube Length and Pressure Drop of the Refrigerant Side of Evaporators". International Refrigeration and Air Conditioning Conference, Paper 143, 1992

[33] Stefan Jensen, Scantec. "Dry Expansion Feed in Dual Stage Ammonia Pants - Operating Experiences form a Large Refrigerated Distribution Centre". 2006 IIAR Ammonia Refrigeration Conference & Exhibition, Reno, Nevada, 2006

[34] Rob Lamb, Scantec. "HFC Phase Down - Low Charge Ammonia Refrigeration Insurgency". Web article

[35] H. Toral. "A study of the hot-wire anemometer void fraction in two phase flow". J. Phys. E. Sci. Instrum, Vol 14, 1981

[36] Sefan Jensen. "Extended Surface Air Coolers for Industrial Plants - the Contractors Perspective". 2009 IIAR Ammonia Refrigeration Conference & Exhibition, Dallas Texas

[37] Bruce I Nelson. "The stainless advantage - Using stainless steel tube/aluminium fin construction in ammonia evaporators". http://www.colmaccoil.com/literature/technical-bulletins.aspx

[38] Bruce I Nelson. "The aluminium advantage - Comparing aluminium vs. galvanised steel ammonia evaporators". http://www.colmaccoil.com/literature/technical-bulletins.aspx

[39] Stefan Jensen, Scantec. "Centrale kølenalæg med lav NH3 fyldning". Kulde og Varmepumper, Nr. 4, 2018

[40] Evapco INC. "Evaporator liquid preheater for reducing refrigerant charge". Patent application WO 2016/004257 A1

[41] Anthony F. Hoesel. "Refrigerant Distributor". Patent application US2063380

[42] Michael Garry. "The Chicaco-area operator invested in a low-charge DX system configured to use less than 10000 lbs for both low and medium temperatures". Shecco, 2018

[43] Stefan S. Jensen. "Low Charge NH3 - From China to Australia". ATMOsphere Australia - Sydney - 7 May 2018

[44] Terry L. Chapp. "Low Ammonia Charge Refrigeration System for Cold Storage". International Association of Refrigerated Warehouses / International Association for Cold Storage Construction

[45] Niels P. Vestergaard. "Charge reduction in pump circulating ammonia systems". 8th IIR conference, Ammonia and CO2 Refrigeration Technologies, Ohrid 2019

[46] Dr Jackson B. Marcinichen and Prof. John R. Thome. "Prediction of Void Fraction and Pressure drop in Vertical Ammonia Risers". IIAR 2019 Industrial Technical Paper #8

[47] K. M. Traeger, P. S. Hrnjak. "Charge Minimization of Microchannel Heat Exchangers". ACRC Project #179 Charge Minimization of Small Systems

[48] Brice Rogie, Martin Ryhl Kærn, Wiebke Brix Markusen. "Air-side heat transfer and pressure drop characteristics of a new triangular finned microchannel evaporator with water drainage slits". 2019

[49] Schecco. "World guide to low charge ammonia". Internet, 2019

[50] Ole Ploug, Bjorn Vestergaard. "New microchannel profile for evaporators and for refrigeration condensers". 4th international conference on AI HX Tech for HVACR, 2015

[51] Melkamu A. Woldesemayat, Afshin J. Ghajar. "Comparision of void fraction correlations for different flow patterns in horizontal and upward inclined pipes". International Journal of Multiphase Flow 33 (2207) (347-370), 2006

[52] Hongliang Qian, Pega Hrnjak. "Mass measurement based calibration of a capacitive sensor to measure void fraction for R134a in smooth tubes". 2019 Elsevier

[53] Franz Summer. "Influence of heat exchanger design on dehumidification and frost formation". https://www.guentner.eu/know-how/technical-articles/

[54] Trevor Hegg, Kurt Liebendorfer, Don Hamilton, Jake Denison. "Low Charge Ammonia Packed Refrigeration Systems: Achieving Ultra-Reliable Operation". 8th IIR conference, Ammonia and CO2 Refrigeration Technologies, Ohrid 2019

[55] Stefan Jensen, Scantec. "Operating Experiences with NH3 Dry Expansion Systems Servicing Refrigerated Distribution Centers". Technical Papers 37th Annual Meeting, International Institute of Ammonia Refrigeration, March 22-25, 2015

[56] A. Person. "The road ahead for ammonia and carbon dioxide refrigerants". 8th IIR conference, Ammonia and CO2 Refrigeration Technologies, Ohrid 2019

[57] Pega Hrnjak. "Packaged ammonia refrigeration units continuously improve - How to measure and present performance?". 8th IIR conference, Ammonia and CO2 Refrigeration Technologies, Ohrid 2019

# Appendix 1. CCR test setup

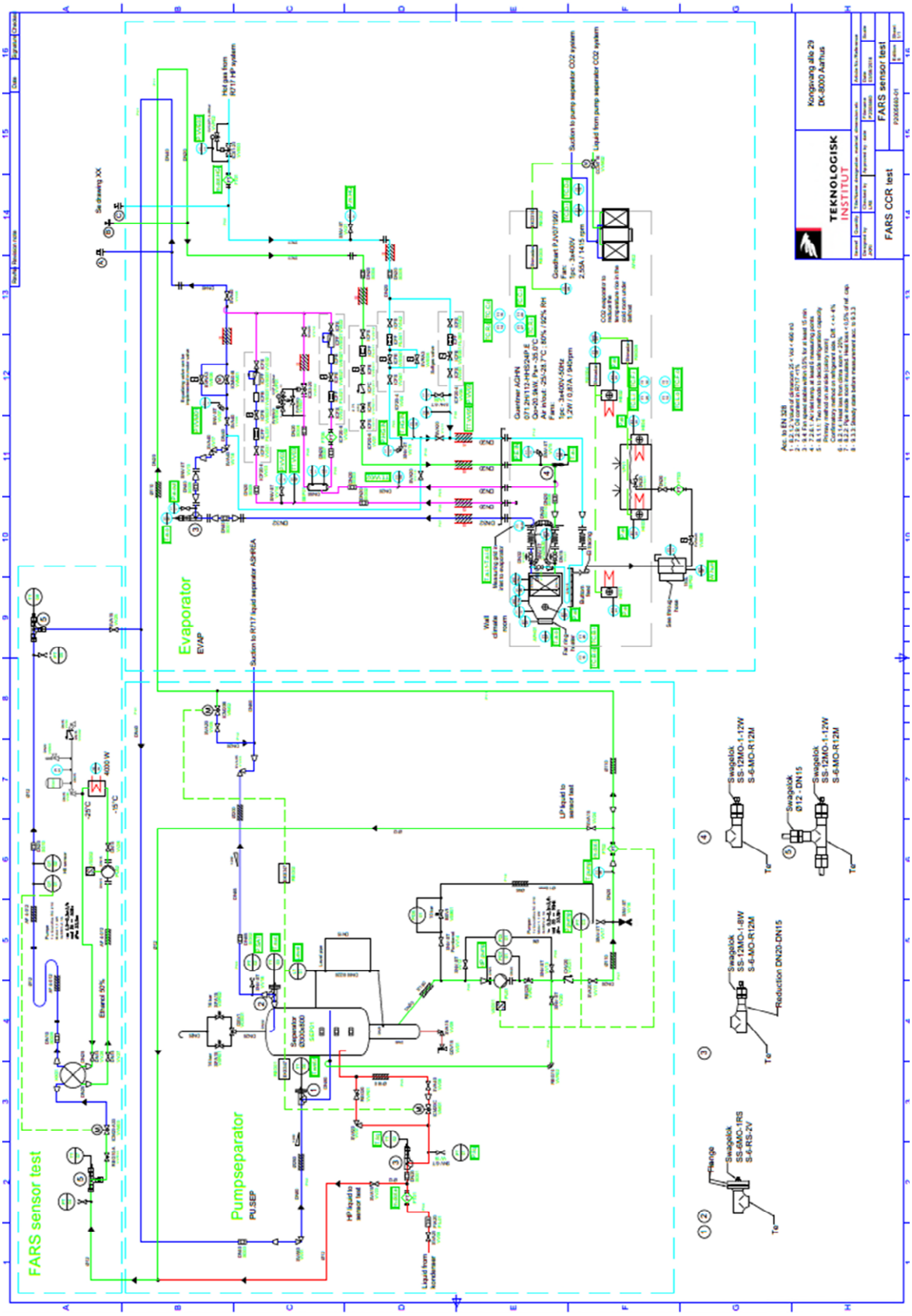

# Appendix 2. WDX test setup

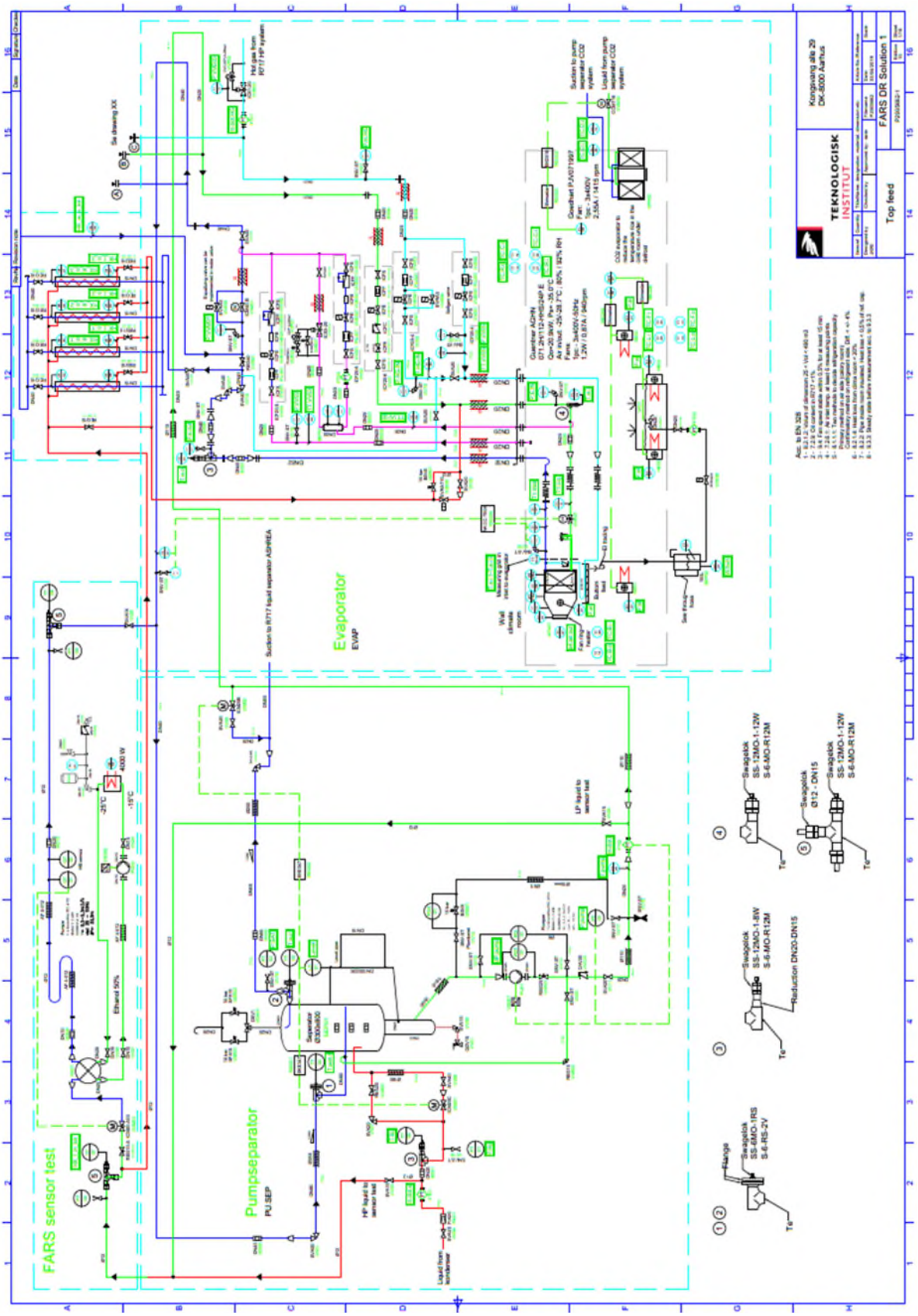

# Appendix 3. Micro Channel test setup